2012, VOL 31

Torsten Lange

Tracing Flow and Salinization Processes at selected Locations of Israel and the West Bank – the Judea Group Aquifer and the Shallow Aquifer of Jericho

153 pages, 69 figures, 21 tables, 228 references

Impressum

Die vorliegende Arbeit ist die Originalfassung der von der Fakultät für Geowissenschaften, Geotechnik und Bergbau der Technischen Universität Bergakademie Freiberg genehmigten Dissertation "Tracing Flow and Salinization Processes at selected Locations of Israel and the West Bank – the Judea Group Aquifer and the Shallow Aquifer of Jericho" zur Erlangung des akademischen Grades Doktor der Naturwissenschaften (Dr. rer. nat.), vorgelegt von Herrn Dipl.-Geologe Torsten Lange.

Tag der Einreichung: 10.06.2011
Tag der Verteidigung: 17.10.2011

Gutachter:
Prof. Dr. Broder Merkel, TU Bergakademie Freiberg Prof. Dr. Martin Sauter, Georg-August-Universität Göttingen Dr. Stephan Weise, Helmholtz-Zentrum für Umweltforschung, Halle

Anschrift des Autors:
Dr. Torsten Lange
Pfalz-Grona-Breite 12
37081 Göttingen

Kurzfassung

Semiaride und aride Gebiete stellen aufgrund des niedrigen oder ungünstig verteilten Niederschlagsdargebots eine besondere Herausforderung bezüglich Erkundung, Bereitstellung, nachhaltiger Nutzung und Schutz sich neu bildender, aber auch fossiler Wasserressourcen dar. Abgesehen von wenigen natürlichen oder künstlich angelegten Oberflächenreservoiren ist der poröse Untergrund dabei gleichzeitig Hauptspeicher und Transportmedium für Wasser und bietet einen Schutz gegen Verdunstung und bis zu einem gewissen Grade gegen oberflächig einwirkende Verunreinigungen. Diese Situation ist charakteristisch für den Nahen Osten und damit für die im Rahmen der vorliegenden Arbeit beschriebenen Teiluntersuchungsgebiete, die sich in Israel und der West Bank befinden. Die Arbeit behandelt drei Hauptthemen.

Einerseits geht sie auf die Charakterisierung der Jungwasseranteile im Abfluß vier bedeutender Quellen des Wadi Qilts und Jerichos sowie in beprobten tiefen Brunnen dreier wichtiger Brunnenfelder ein. Alle diese Objekte entwässern bzw. entnehmen Wasser aus dem Oberen oder Unteren Judea Group Aquifer. Mit ca. 750 m Mächtigkeit stellt dieser eines der bedeutensten Grundwasserreservoire der Region dar und besteht hauptsächlich aus unterschiedlich stark verkarsteten und gestörten Kalkstein- und Dolomitformationen, welche zwischen dem Senon und Eozän in Form einer in sich weiter gegliederten, beidseitig abtauchenden Doppelantiklinalstruktur herausgehoben wurde (Hebron und Ramallah bzw. Judea und Samaria Mountains). Die Grundwasserneubildung ist beschränkt auf die Zeit zwischen Oktober und April sowie auf die Kammlagen des Gebirges, wo die sonst bedeckten Schichten des Aquifers ausstreichen. Es wurde eine Strategie entwickelt, die eingesetzten Tracer auf ähnliche Weise mit Hilfe von Lumped Parameter-Modellen für alle Lokationen zu interpretieren und somit eine Vergleichbarkeit zu gewährleisten.

Andererseits untersucht die Arbeit Versalzungsprozesse im Shallow Aquifer von Jericho und deren Abgrenzung untereinander. Mögliche Hauptquellen der Versalzung sind durch überhöhte Grundwasserentnahme verstärke Zuflüsse von Solen, die Lösung von Salzen aus der Lisan-Formation oder Formationswässer der Lisan-Formation, welche die Ablagerungen des Lisan-Sees, des Pleistozänen Vorgängers des heutigen Toten Meeres, repräsentieren. Eine Unterscheidung der Mechanismen hat dabei durchaus Bedeutung für die Festlegung geeigneter Gegenmaßnahmen. Demzufolge werden die ermittelten, aber auch weitere, potentielle hydrochemische Hauptindikatoren und Tracer benannt. Unsicherheiten sowohl hinsichtlich der Aufstellung einer Wasserbilanz, als auch einer unzureichend bekannten Geologie für das sehr kleinräumige Gebiet von Jericho werden diskutiert.

Aufgrund der begrenzten Interpretierbarkeit der gemessenen Helium-Proben im Kluft- und Karstaquifer der kretazischen Judea Group wird mittels einer Sensitivitätsanalyse die Abhängigkeit der ^{4}He-Akkumulation im Grundwasser eines idealisierten dual-permeablen Aquifers bezüglich des Verhältnisses der ^{4}He-Fracht und der Systemantwortzeit zu den variierten Parametern (hydraulische Gradienten und Leitfähigkeiten, Dispersivitäten und Porositäten) untersucht. Obwohl keine Systemvariable im eigentlichen Sinne, erweist sich die Systemantwortzeit als wichtig für die Interpretation der He-Konzentration im Grundwasser nicht-stationärer Systeme. Zur visuellen Aufbereitung der Sensitivitäten wird eine leicht interpretierbare Darstellungsweise eingeführt.

Abstract

Due to the low amount or unfavorable annual distribution of precipitation the exploration, allocation, sustainable exploitation, and protection of replenishable as well as fossil water resources are challanging tasks in semiarid and arid regions. Beside a few natural or artificial surface water reservoirs the porous underground at the same time is the largest storage and transport medium for water and provides protection against evaporation and to a certain degree against surficial introduction of contaminants. This situation is characteristic for the Near East and thus for the selected investigation areas, that are located in Israel and the West Bank, and that are subject of the conducted partail studies that are presented. The work focuses on three main subjects.

On the one hand, it deals with the characterization of the young groundwater components of the discharge of four major springs of Wadi Qilt and Jericho, as well as of sampled deep wells of three important well fields. All of these objects discharge or abstract water from the Upper and Lower Judea Group Aquifer. With a thickness of about 750 m it is one of the most important groundwater reservoirs of the region and comprises mainly to varying degrees karstified and fractured limestones and dolomites. These formations underwent uplift during Senonian to Eocenian times forming a pair of double-plunging anticlinal structures (Hebron and Ramallah or Judea and Samaria Mountains, respectively) that are again subdivided into minor anticlines and synclines. The groundwater replenishment is restricted to the winter season between October and April, and to the crestal area of the mountains, where the otherwise covered aquifer rocks crop out. A strategy was developed to interpret the applied tracers for all locations in a similar way using a lumped parameter approach, which enables a direct comparison.

On the other hand, the work investigates salinization processes in the Shallow Aquifer of Jericho and their discrimination. Potential sources for salinization are remnant brines that are activated to flow into the range of well extraction due to groundwater overexploitation, dissolution of salts or formation waters from the Lisan formation. These layers represent the sediments of Lake Lisan, the Pleistocene precursor of the Dead Sea. A discrimination of the salinization mechanisms is important to develop reasonable measures to limit or lower the salt concentration in the affected wells. Consequently, the relevant measured but also potential main hydrochemical indicators and isotope tracers are identified. The large uncertainties with respect to the establishment of a well-founded water balance and to the insufficient knowledge about the geology of the small-scale area of Jericho are discussed.

Because the interpretation of the measured helium samples from the fractured and karstified aquifer of the Cretaceous Judea Group is limited, the dependencies of the ^{4}He accumulation in groundwater in an idealized dual-continuum aquifer are investigated with respect to the relation of the ^{4}He mass fluxes and the system response time to the varied parameters (groundwater head gradient, hydraulic conductivities, dispersivities, porosities) by means of a sensitivity analysis. Although the system response time is not a system variable as such it clearly turned out that knowledge about it may be an important information for the interpretation of He concentrations in groundwaters of non-stationary systems. To enhance the visual post-processing of the parameter sensitivity analysis an easily interpretable way of data presentation is introduced.

Contents

List of Figures

List of Tables

1 Introduction

The distribution of water resources in the Near East is very heterogenic. Transitions between areas of surplus, balanced or distinct water scarcity characteristics may happen over very short distances. In general semi-arid to arid conditions dominate this region. Naturally, this is the effect mainly of the geographical position in the Eastern Mediterranean region, the distance to the Mediterranean Sea itself, the versatile topographic shape, and the large-scale weather pattern, as well. Special features like the saline Dead Sea in the Jordan Valley or the residing brines in its neighbouring aquifers may negatively affect the fresh groundwater sources in the sourroundings if conditions change, be it climatically or antropogenically induced.

Additionally, the regional water stress is accompanied by further stress factors due to a currently difficult socio-economical situation especially in the West Bank, the general and predicted increase in the population figures, the domestic and industrial water demand, and the potential or planned future development in each country, as well as political dissent among the riparien states of the Jordan river. The latter even lead to military actions several times in the past and potentially may do in the future. Water issues therefore were part of several negotiations between the neighbouring states. This in turn increased demands for a scientifically foundated evaluation of the existing and available water resources of which groundwater is among the most important.

As a result numerous studies and development projects that adressed most aspects related to water issues were conducted over the last decades in the Near East region, where German organizations like the Federal Ministry of Education and Research (BMBF), the German Research Foundation (DFG), the Federal Institute for Geosciences and Natural Resources (BGR), or the different suborganisations of the Deutsche Gesellschaft für Internationale Zusammenarbeit (GIZ) GmbH were continuously involved. In the course of these projects and due to the increasing stresses on the water resources the countries of the area increased their efforts to develope national, regional, and lower-scale water master plans as adequate measures to respond to these challenges.

The conducted work that is subject of this thesis, is part of the attained results of the BMBF-funded joined German-Israeli-Palestinian Project "Groundwater Availabily and the Fate of Pestizide Input" (GAPI). While Part I of the project generally adressed subjects like sources and the availability of groundwater and its characterization by means of hydrochemical and tracer methods, Part II focused on the fate of pestizides in the soil as well as on the applicability of different waste water sources in agriculture. Each of the two parts were subdivided to further packages that were carried under the responsibility of the individual working groups at the Center for Environmental Research in Leipzig and Halle, Germany, the Hebrew University in Jerusalem, Israel, and the Al Quds University in Abu Dis, Palestine.

The presented work comprises the results from a working package within Part I, that on the one hand aimed to characterize the groundwater sources of the Mountain (Judea Group) aquifer with respect to their age structure and in turn to their potential vulnerability. This aquifer represents a thick Creataceous, Albian to Turonian carbonate sequence, is one of the most important groundwater reservoirs for Israel and Palestine, and exploited by numerous deep wells. On the other hand the thesis focuses on salinization mechanisms in the unconsolidated aquifer of the Jericho area, which is located in the Jordan Valley, northeast of the Dead Sea.

2 Geological and hydrogeological background

2.1 Geological formation of the area

The development of the present hydro-geological structures in Israel (with exception of the Sinai) and Palestine is related to the time between the initial Late Permian "submergence" of the Late Paleozoic Helez Geanticline after a period of updoming and removal of its sedimentary load during the Late Carboniferous - Early Permian [220] and today. As the updoming of several of such geanticlines in North Africa and its Arabian extension correlates to the Variscan orogeny in Europe this major geanticline was termed Hercynian Geanticline of Helez [97]. Where until then marin ingressions onto the Arabo-Nubian platform have been derived from the Paleotethyan margin in the N a dramatic change in the tectonic setting led to a tilting of the whole area towards the present Mediterranean coast caused by the onset of rifting in Scythian-Anisian time, Early Triassic [79].

Three major tectonic stages subdivide the Mesozoic era (Figure 2.1):

Local differential movements mark the first, extensional stage lasting from Scythian to Pliensbachian, Early Liassic that is charactarised by a syn-sedimentary, generally rapid subsidence of local troughs due to differential movements and block tilting along NE-SW to NNE-SSW directed listric-normal faults causing small-scale changes in facies and in thickness. Higher magmatic and volcanic activity mark the end of the initial rifting phase in the area and consequently the end of the first stage. A major representative of that volcanic activity is the more than 2000 m thick Asher volcanic sequence in northeastern Israel, deposited in a rift-like deep trough [96].

The formation of a passive margin, the second stage, contrasts the now practically terminated stage of local differential movements by the development of a dominating wedge of uniform shallow marine sequences with occasional continental interfingering upon a narrow, as a whole towards the present Eastern Mediterranean coast subsiding or tilting area. Thus, a carbonate platform is constructed along this downwarping shelf belt, which is limited to the Neotethyan Ocean floor by a step edge of 1500 to 2000 m and to the stable shelf domain, where subsidence rates remain moderate [79]. In the focused area of this study undisturbed sedimentation of platform carbonates prevail until the Early Conjacian with a general transgressive trend [129] as well as interfingering with the more distal and impervious, marly Talme-Yaffe Group in the west and occasionally with the clastic Kurnub type sedimentation on the Arabo-Nubian craton in the south and east [75]. The majority

of the accumulated sediments of the second stage belong to the Judea Group, a sequence mainly built up of limestones and dolomites that after the marine regression of sea water were karstified to varying degrees. An exception from the rule of a continous high sea level represents the uppermost parts of the section, where high-energy up to sublitoral levels are widespread in the Judea Mountains and elsewhere [42], and a subaerial event extending from south of the Ramon region to the Galilee in the north with no relation to the Syrian Arc folding enabled in Central Israel a karstic relief to develope, shallow braided rivers to prograde and a humbled pedogenisis [181]. To summerize, the second stage is connected to the proceeding opening and extension of the Neotethyan Ocean which culminates during the Early Cretaceous [184] and decelerates during Late Cretaceous.
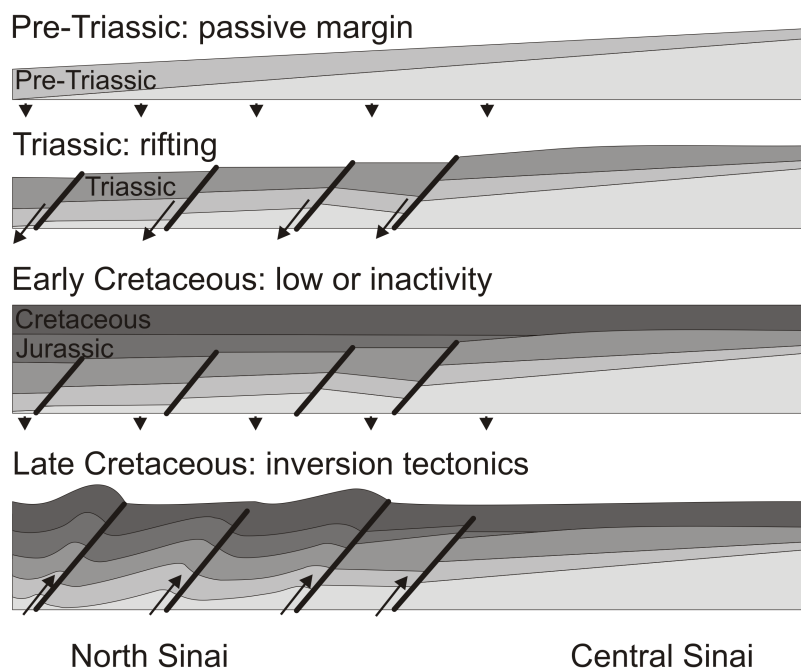
Figure 2.1: General tectonical development from Pre-Triassic passive margin stage to the Late Cretaceous inversion stage according to [150]. Although the figure schematically depicts the Mesozoic tectonic and sedimentary evolution of North and Central Sinai, it is very similar to that of Israel and Palestine, for which the situation in North Sinai more closely corresponds.

The onset of the closure of the Neotethyan Ocean heralds the third and last Mesozoic tectonic stage in the Late Cretaceous [129], when the Early Mesozoic normal faults are reactivated as reverse faults, leading to the establishment of the NNE directed, double plunging Hebron and Ramallah monocline structures as part of the higher-ranking Syrian Arc structure, which extends from northern Egypt in the southwest to Syria in the northeast. The strainfield responsible for the folding lasts throughout the Senonian until the Eocene [170], which comprises the time of the depostion of the Mount Scopus Group, except for the Eocene. Eocene to Neogene

sedimention was exposed to erosion as happened to the Judea Group section in the crestal zone or was subjected to on-lapping at the flanks of the major monoclines [75].

The Ha'Shefela syncline with the eponymos foothills inhabit the downthrusted block west of the steep monoclinal flexure and is subjected to intensiv groundwater exploitation from the Upper Judea Group Aquifer. But also the well fields in the Eastern Aquifer Basin produce groundwater from those synclinal, hydrological accumulation structures, caused by undulations, subfolds, grabens, or fault barriers within the internal structure of the major monoclines. [29] conceptually takes this up and by building a groundwater flow model that considers such structurally determinated groundwater pathways came to a river-like flow pattern particularly in the Upper Aquifer.

The second main regional structure of major importance concerning the Jericho area is the Dead Sea transform fault structure (DSTFS), which joins the divergent plate boundary along the Red Sea with the zone of plate convergence along the Alpine orogenic belt in Turkey where it junctionally meets the East Anatolian Fault Zone and the Aslantas - Kyrenia-Misis Fault Zone [175]. The overall amount of left-lateral motion since the Early Miocene ($\approx$20 Ma) has been estimated to 105 km [76] though it is devided into two phases of relative motion. 65 km are supposed to be assigned to the Miocene, whereas the rest falls into Pliocene to Holocene times. The first phase is characterised by a more or less straight fault line with insignificant morphotectonic features and it tectonically correlates to the closure of the Bitlis Ocean in Southern Turkey. Due to the stronger compressional character the DSTFS became a system dominated by step faults resulting in transpression and pressure releasing features, by strain releasing bands and rhomb-shape grabens (e.g. [167], [168]) for which the Dead Sea basin is the regional "locus typicus". Throughout the Neogene-Quarternary several lakes and marine incursions have left a thick sediment succession of which the Pleistocene Samra and Lisan lakustrine sections as well as the Wadi fan deposits comprise the Pleistocene-Holocene Shallow Aquifer around Jericho [27], [28]. Whereas the Samra Formation is mainly characterised by clastic units, alternating thin layers derived from chemical precipitation and fine clay detritus, which are occasionally disrupted by intercalations of gravel bars comprise the Lisan lake deposits. Most of the groundwater production depends on the mentioned gravel bars and the Samra Formation, which exhibit higher hydraulic conductivities.

In Figure 2.2 a stratigraphic table valid for all local study sites is presented. It includes the Palestinian as well as Israeli nomenklatura and a general hydrogeological characterisation of the geological units. In this thesis the Israeli nomenklatura is applied in most cases as it resolves the geological succession more finely.

2.2 Selection and hydrogeology of the study sites

The potential target areas for the project before its practical implementation comprised the Hebron and Ramallah or Judea and Samaria Mountains, respectively as well as their

System	Series	Israeli Group	Israeli Formation	Palestinian Group	Palestinian Formation	Hydrogeological Unit	Thickness [m]
Quaternary	Holocene	Kurka	Alluvium	Recent	Alluvium		
Quaternary	Holocene	Kurka	River gravel	Recent	Gravel		
Quaternary	Pleistocene	Dead Sea	Lisan	Lisan	Lisan		
Neogene	Pliocene-Miocene	Saqia	Bit Nir and Ziqlag	Beida	Beida		
Paleogene	Eocene	Avedat	Zora		Reef nummulitic limestone	locally variating	
Paleogene	Eocene	Avedat	Zora		Nummulitic limestone	locally variating	
Paleogene	Paleocene	Mount Scopus	Taqiye	Belqa	Khan Al Ahmar and Zerqa		
Senonian	Maastrichtian / Campanian / Santonian	Mount Scopus	Ghareb	Belqa	Amman and Abu Dis	Aquiclude	100-400
			Mishash				
			Menua				
Cretaceous	Turonian	Judea	Bina	Ajlun	Jerusalem	Aquifer	90-100
Cretaceous	Cenomanian	Judea	Weradim	Ajlun	Upper Bethlehem	Aquifer / Aquiclude	90-100
			Kefar Shaul		Lower Bethlehem	Aquitard	30-40
			Amminadav		Hebron	Aquifer	110-140
			Moza		Yatta	Aquiclude	10-15
			Bet Meir		Yatta	Aquitard	120-140
			Kesalon		Upper Beit Kahil	Aquifer	30
			Soreq		Lower Beit Kahil	Aquitard	110-170
			Givat Ye'arim		Lower Beit Kahil	Aquifer	20-40
			Kefira			Aquitard	160-180
Cretaceous	Albian	Judea	Qatana	Kurnub	Kobar	Aquiclude	

Figure 2.2: Stratigraphic table for the study area, modified after [207].

vicinity. Due to the actual conditions especially in the West Bank area the sites were to be selected according to the following considerations:

- The sites should possess typical characteristics, for example with regard to aquifer hydraulics, structural position, thickness of the unsaturated zone, or confined or unconfind conditions.

- All wells should be repeatedly accessible.

- With respect to the frame of the joined German-Israeli-Palestinian project the sites should be located both, in the Western (Yarkon-Taninim) as well as the Eastern groundwater basins.

In assessing these requirements the Agur, Herodion, and Ein Samia well fields were selected in the beginning. Later the Jericho area was added to the list to use mutual synergy effects in conjunction with another group of the German-Israeli-Jordanian-Palestinian Joint Research Program (GIJP) that already worked and made practical experiences there [121]. The 4 locations differ in several aspects: transmissivities, stratigraphic level of abstraction, thickness of the unsaturated zone, confined or unconfined, recharge mechanism. Table 2.1 holds the main charecteristics of the study sites. Beside some facial

Table 2.1: Average characteristics of the selected sites (med – medium, LA/UA – Lower/Upper Judea Group Aquifer, SF – Samra formation/facies, syn – syncline, unconsol – unconsolidated sediments, UC/C – unconfined/confined, R – "roofed" or covered aquifer, N.A. – not available, P – precipitation, RO – runoff, MA – Mountain aquifer, SP – springs, AR – agricultural return flow).

characteristics	Agur	Jericho	Herodion	Ein Samia
elevation [masl]	200..400	$\approx$ -250	600..700	$\approx$ 425
hydraulic conductivity	med..very high	low..high	low..med	med..high
abstraction from unit	UA	SF	LA/UA	LA/UA
geological structure	syn	unconsol	syn	graben
thickness of unsaturated zone [m]	N.A.	20..100	>250	$\approx$60
unconfined/ confined	UC/C	UC	R/C	UC/C
recharge type	P	RO/MA/SP/AR	P	P

differences in the formations of the Judea Group it can be generalized, that higher transmissivities in the subaquifers reflect a higher karst porosity. For instants, a very sharp

contrast in hydraulic conductivities can be found across the transition zone from the montains with high head gradients to the western foothill region (Ha'Shefala) with very low head gradients. A reevaluation of the published tracer data of four major springs in Wadi Qilt from [101], [127], [125], [128], and [121] were additionally included in this work. Figure 2.3 specifies the individual locations.

2.2.1 Jericho area

Groundwater salinization is common in many places of the lower Jordan Valley. Jericho, located on its western side (Figure 2.3) at about -250 m asl, some 10 km NW of the Dead Sea and about 30 km E of Jerusalem shares this characteristic. The study area (Figure 2.4) is limited:

1. by the easternmost wells,

2. in the west by the border fault, which separates the Cretaceous carbonate aquifer from the Quaternary basin fill of the Jordan Valley,

3. and to the north and south by Wadi Nueima and Wadi Qilt, respectively.

There are a few wells located on the southern side of Wadi Qilt, however. Except for the local springs that discharge the Cretaceous Judea Group Aquifer (Mountain aquifer) the utilised groundwaters in the Jericho area are pumped from the Plio-Pleistocene to Holocene Samra and Lisan Formations. Because this section usually is referred to as Shallow Aquifer, the term is used also in this work. The climate in general is hot and dry and the potential evaporation flux exceeds the amount of precipitation (150 mm/yr) by manifold [205]. If there was no additional groundwater inflow into the local aquifer and no contribution from the various local perennial springs the private farmers and cooperativs of Jericho could not maintain the scale of productive agriculture.

The Jericho area – a socio-economic perspective:

Due to the favourable conditions in the rain shadow of the mountains, which are provided by the springs that possess a perennial freshwater discharge like Ein Sultan, the site of Jericho has been intermittently settled since the Pre-Pottery Neolithic A, around 10000 B.P. [24]. It is located along with other similar early settlements in the Dead Sea rift valley. The latter is an element of the Dead Sea Transform system extending from the Red Sea to the compressional plate boundary of the Alpine orogenic belt in Turkey and represents a natural route for north-south movement since ancient history. Agriculture has been practiced in the area since then. The original historical open canal system to transfer spring water to remote plots in the Jericho area has been extended and improved by concrete open canals starting in the 1920's under the British Mandate. To further encourage agricultural production in the Jordan Valley, the Hashemite Kingdom of Jordan initiated various well drilling programs, e.g. around Jericho. Between the 1950's and 1967 around 80 wells have been drilled into the Shallow Pleistocene-Holocene aquifer of the Jericho area causing on the one hand a remarkable improvement of the traditional mode of
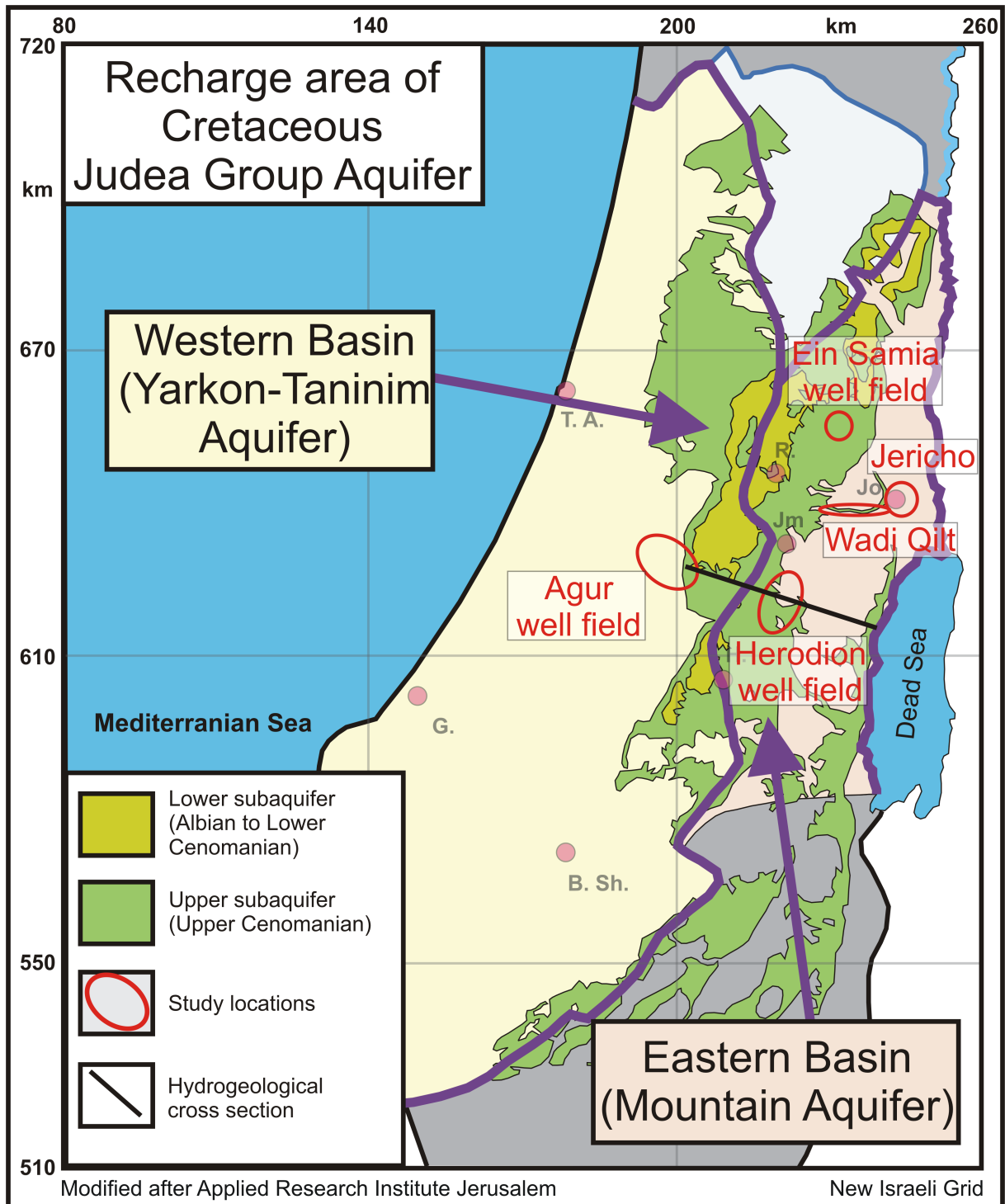
Figure 2.3: Location of the study areas and distribution of the outcropping recharge zones for the Judea Group Aquifer. The locations of the cities of Tel Aviv, Gaza, Beer Sheva, Ramallah, Jerusalem, and Jericho are indicated by red dots and T.A., G., B. Sh., R., Jm, and Jo, respectively.
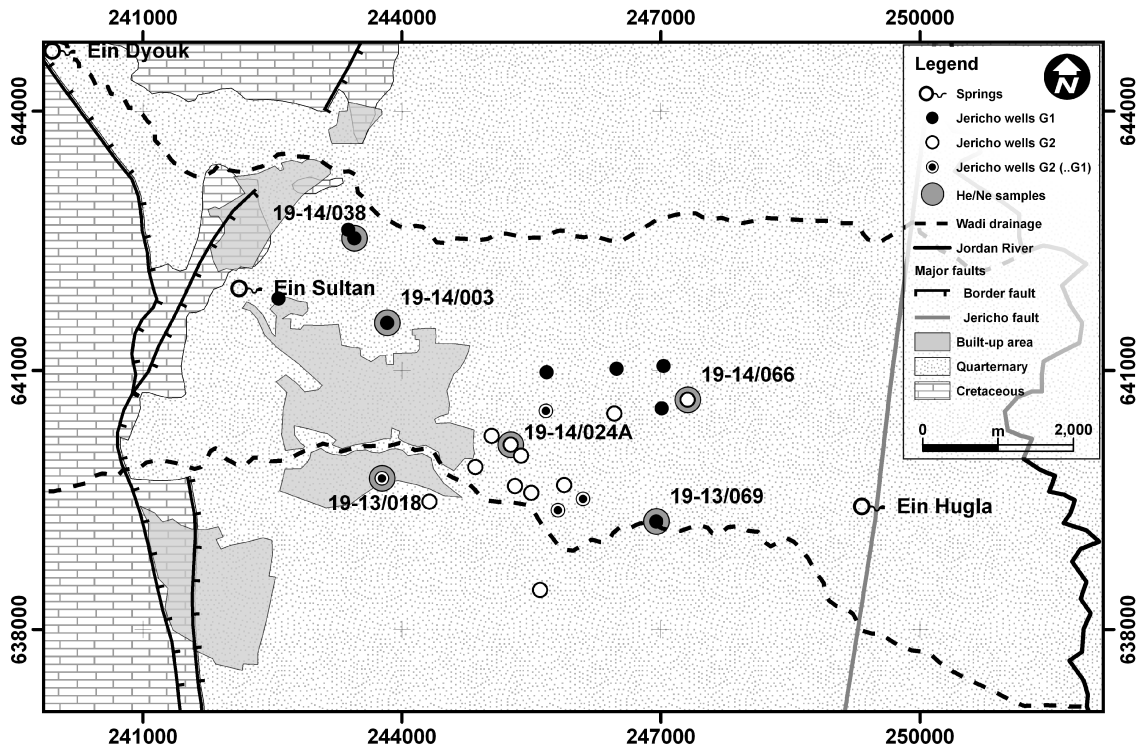
Figure 2.4: Geological outline map of the Jericho area with the locations of the investigated wells and springs. The symbols indicate a grouping based on the hydrochemistry of the well samples and whether the well also was sampled for helium and neon (section 5.1). The coordinate system is New Israeli Grid.

agriculture while extending the area of cultivated land. On the other hand the cultivation of vegetables and fruits with high water demand like bananas and citrus fruits was made feasible on a much larger scale - even for export. However, these crops consumed much of the additional water that was provided by the new groundwater wells.

During the last decades it became very difficult to maintain the high level of agricultural production. Decreasing groundwater levels were accompanied by a general increase in the groundwater salinity of the Shallow Aquifer. It is clear, that in political unstable areas like in the West Bank, this may seriously affect the agri-economic development of the Jericho area. For example, at the easternmost agricultural plots salt tolerable plants like maize are nowadays the only crops, which can be cultivated. Also high levels of nitrate and locally increasing in bacterial counts may endanger health of consumers. Additionally, the town of Jericho experienced an increase in the population figure from an estimated 12,000 in 1980 to an estimated 25,000 people in 2003. Without any appropriate wastewater treatment facilities it relies solely on cesspits and a private sector controlled disposal, which has to be seen in the light of the difficult political and economical situation. The investigations conducted in the Jericho area continue recent efforts, e.g. by [141], [121], and [120] to understand the processes that lead to the deterioration of the Shallow Aquifer

groundwaters.

Geological setting:

Of local importance as aquifers are the Plio-Pleistocene Samra and Lisan Formations that belong to the Dead Sea Group, the Miocene to recent sedimentary fill of a subdivided system of graben basins within the Dead Sea – Jordan Valley that are related to the Dead Sea Transform system. The Jericho fault (Figure 2.4) is one active local branch of that transform fault system. Samra and Lisan Formations have been extensively described e.g. by [27] and [28]. In the west of the study area these sediments are separated from the Cretaceous rocks, which are the limestone and dolomite formations with highly contrasting hydraulic conductivities due to karstification and the confining Senonian chalks that cover much of the Hebron and Ramallah Mountains (Judea and Samaria Mountains). In the crestal zone of the Hebron (Judea) Mountains the outcropping Mountain aquifer limestone and dolomite strata represent the most important recharge area for both, Israel and the West Bank. Simultaneously the crestal zone acts as surface as well as groundwater divide between the Western and the Eastern Groundwater Basins (Figure 2.3), although the groundwater devide is located a few kilometers west of the surface water devide, due to the asymmetric shape of the major anticlinal structures.

The age of the top of the Lisan formation is determined to be between 18,000 to 15,000 B.P. (e.g. [116], [195], [130]). With the retreat of the saline Lake Lisan, the precursor of the current Dead Sea, the local hydrography reshaped to its present state due to the development of the erosive Jordan River and the incision of Wadi Qilt and Wadi Nueima into their own fan deposits as well as into the Lisan and Samra formations. The local record of the Samra formation comprises calcitic lutites, arenites, and conglomerates partly showing cross bedding and ripple marks. The sequence was deposited in an interfacing fluviatile-lacustrine environment [28]. With closer distances to the border fault west of Jericho, which separates the basin fill from the consolidated Cretaceous rocks of the Hebron (Judea) Mountains, fan deposits gain in importance. Whereas more to the east of the Jordan Valley Lisan formation overlays Samra formation, a "Samra-like" lithofacies prevails even through Lisan times where the wadis cross the border fault and continued to build up sedimentary fans and flood plains according to the lake level fluctuations. Similar sedimentation modes proceeded in Holocene times. Such fan and floodplain layers are the source of the rich arid brown soils of Jericho ([28], [15]). However, the Lisan lake level had been relatively stable for much time of its existence around -290 to -270 m asl [195], which is the ground level range for about half of the Jericho agricultural wells. Depending on the basin geometry of Lake Lisan in the Jericho area, the thickness of Lake Lisan sediments therefore may vary broadly. Particularly in marginal areas of the former lake, calciclastics with varying particle sizes, beach ridges, and channels occasionally intercalate. A schematic geological cross section is provided in Figure 2.5. Because of its importance as a potential contributor to groundwater salinization, the geology and geochemistry of the Lisan Formation sediments are described seperately following the next paragraph.

Water sources:
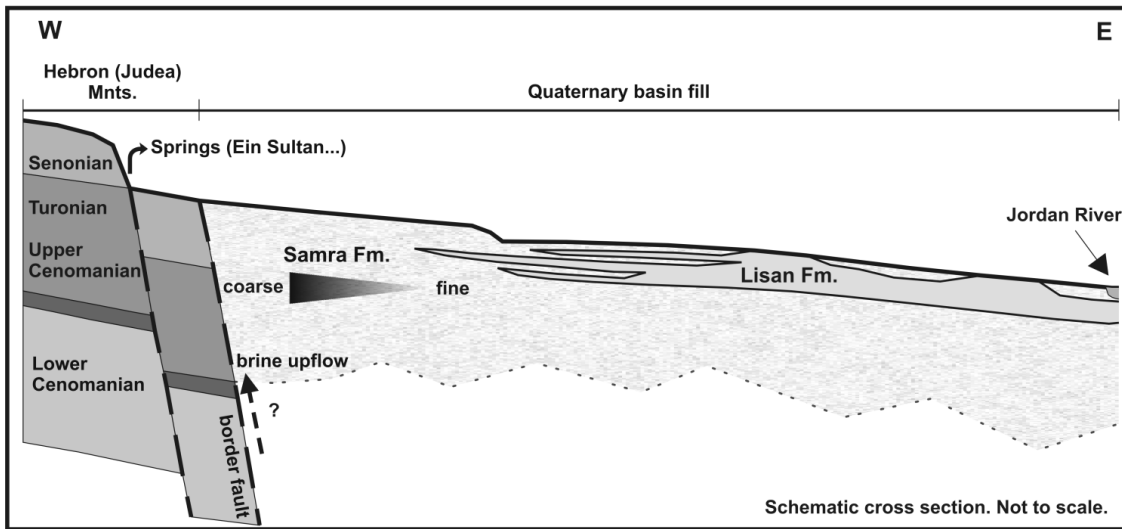
Figure 2.5: Schematic geological cross-section for the Jericho.

The groundwater regime in the Jericho area is highly unsteady, which is reflected by large seasonal variations in the hydraulic head distribution. Increasing abtraction rates due the operation of numerous wells since the 1950s amplify the natural strength of oscillation beween spring and autumn. According to [222] seasonal variations in pressure head can reach about 20 m, when the amount and intensity of rain is as high as in 1991/1992, an unsual wet winter in the whole region. Salinization phenomena that are observed in many agricultural wells of Jericho might be attributed to brine admixture, to dissolution of remnant salts in the Lisan formation, as well as to agricultural return flow in connection with the high evaporation rates. Infiltration by precipitation is assumed to steadily equal zero. For the area of Deir Alla, in the middle part of the Jordan Valley with comparable overall conditions but a higher average annual precipitation of   250 mm, [227] determined infiltration rates below 1 mm/y. The known freshwater sources in and around the Jericho area are derived from springs northwest of Jericho (Ein Dyouk, Ein Nueima, Ein Sultan - average annual discharge $\approx$13.5 mil. m^3), springs in the upper Wadi Qilt (Ein Fara, Al Fawwar, Ein Qilt - average annual discharge $\approx$7.4 mil. m^3), as well as surface runoff from Wadi Qilt and Wadi Nueima accompanying heavy rain events in the respective mountainous catchments during the rainy season [135]. Most of the mentioned springs are connected to a more or less developed karstic network; some localities are related to permeability barriers caused by faults. All of them discharge the Cenomanian-Turonian section of the Mountain aquifer. Although mountain runoff is assumed to represent a significant amount of the total annual recharge, estimates of its long-term annual proportion are uncertain, because the timing and location of runoff generation in the mountains due to intensive rain events can not be predicted and only measured with much efforts on time when it enters the Jordan Valley. [135] and [121] estimated $\approx$2 and $\approx$9 mil. m^3 per year, respectively. Efforts have been undertaken from the 1960s on ([177], [111]) to measure and estimate runoff volumes. But only recently these efforts go in the direction of a simultaneous monitoring of both, runoff and rainfall

distribution in order to derive reliable estimations of the annual runoff that may reach the Jordan Valley. An example is the study of [185] for Wadi Fara, upstream of Wadi Qilt.

However, the main contribution for domestic and irrigation purposes in the actual study area is derived from Ein Sultan spring (also known as Elisha). Until early 2006 the spring water was distributed through a concrete and earth embankment supported open canal system directly to the water right holding farmers. Because water allocation was controlled by an inflexible scheme of opening and closing of water gates, most of the farmers used open pools or ponds to buffer momentary inapplicable amounts of their share as well as pumped groundwater, making the water vulnerable to the high potential evaporation but to greater extent to seepage. It may be noted, that the individual water shares were determined based on time durations of flow through the water gates, specifically at an hourly basis. Consequently that kind of distribution procedure failed to be reproducible since the water shares did not necessarily coincide with a specific volume. The flow rate considerably dropped along the canal branches from the spring outlet in the northwest downstream to the east. The reasons were the sequentially organised water diversion but also seepage losses from the canal [8]. Different numbers exist about the total amount of spring water lost before application. A probably resonable estimate of the loss, based on calculations by the latter author and on findings of the International Fund for Agricultural Development (IFAD) [108], which mentions a survey conducted by the Palestinian Water Authority (PWA), sums up to about 30 %, whereas the annual discharge of Ein Sultan is about 5 mil. m^3. Approximately 1.4 mil. m^3 were diverted for domestic purposes annually (as of 2006). With respect to the groundwater balance a major part of the above-mentioned seepage might be accounted rather to be a gain then a total loss. But also the Jericho municipal tap water network is heavily affected by leakage. According to [16] losses amount to $\approx$65 %. However, either the estimated value was to high or the loss significantly droped until 2009 to a value of $\approx$23.7 % [161]. As of 2009, the total amount of water passing the domestic network amounts to $\approx$2.5 mil. m^3 [161]. The real amount of irrigation return flow remains speculative and is assumed to be considerably below 10 %, perhaps as low as about 2 % of the applied water [121]. In 2006 the old canal system was completely replaced by a pressurised pipe system that was funded by the IFAD. This turned the water allocation scheme from time to volume based. Thus the farmers are not dependent on their storage facilities anymore. However, it should be interesting to observe whether this 're-setting' will rather complicate or enlighten the understanding of the Jericho shallow groundwater system in future. Possible fluxes of fresh groundwater (e.g. [29], [92]) and of trapped ancient brines from west to east across the border fault have always been a matter of debate. Brines were discovered in the 1970's in groundwater wells on the western side of the border fault across from Jericho. In general the border fault west of Jericho is considered to be impervious [88], because the Senonian impermeable chalks were down-faulted against the high permeable Cenomanian-Turonian section of the Mountain aquifer. On the other hand [225] showed that under similar geological conditions seeping along the Dead Sea is likely to occur.

Geochemistry of Lisan Formation:

It already has been mentioned that the salinity of Lake Lisan was high. However, it was much lower than that of the current Dead Sea. Laminated authigenic white aragonitic chalk, dark detrital layers and gypsum layers constitute main parts of the Lisan Formation. The aragonite layers are authigenic chemical precipitates whereas the non-calcic silt and clay fraction is imported from remote areas by wind as it is described also for the current Dead Sea detritus [188]. However, it is commonly observed that microorganisms can mediate the formation of calcium carbonate seed crystals (e.g. [124], [174], [119], [163]), which would be in agreement with the fact that Lake Lisan aragonite has been precipitated directly from the surface water of Lake Lisan [196]. Generally Mg/Ca ratios > 3.5 favour aragonite precipitation [134], ratios < 2 promote the formation of Mg-calcites or calcites. After the final decline of the lake level, the aragonite was preserved owing to the arid conditions in the Jordan Valley and the high Mg/Ca ratio of interstitial soluble salts which were precipitated from the pore water [115]. Indeed aragonite would recrystallize or transform in any solution having low salinity and low Mg concentrations as has been demonstrated by [115] and [114]. Because compared to calcite, aragonite is able to incorporate relative high amounts of Sr, the transformation of aragonite to calcite in turn should release relevant amounts of Sr. From Lisan sections in the Perazim Valley SE of the Dead Sea, [196] derived two precipitation mechanisms for gypsum, which at the respective location forms distinct layers of up to 70 cm, thin laminae or authigenic crystals, which are disseminated mainly in the detrital laminae, but also in the aragonite laminae throughout the Lisan Formation. [130] showed that those authigenic crystals are of secondary nature since they penetrate the original lamination starting to grow from the detrital laminae into the aragonitic laminae. They also observed that organic matter is associated with the crystals. analysed δ^{34}S for the two groups of gypsum revealing values between 18 to 28 ‰ for the distinct bulky gypsum layers and -26 to -1 ‰ for laminated and disseminated gypsum. This is indicative for the oxidation of sulfidic compounds as suggested by the latter authors who related those processes to the final recession of Lake Lisan. The recession is believed to have caused the oxidation of the reduced pore water and solid matter, respectively. Indeed, [208] could not find any sulfide minerals nor have such been described anywhere. The high δ^{34}S values prevailing in the bulky gypsum layers can be explained by the divergent path that is responsible for their deposition. These layers have been precipitated due to overturns of Lake Lisan, which are generally associated with a dropping level, i.e. limited freshwater input. Just these overturn events enabled the precipitation of such gypsum layers and bulky beds since the sulfate ions were locked in the less saline surface water layer, which continuously lost all Ca through the precipitation of aragonite. On the other hand the deep brine water layer was anoxic and hosted a major calcium pool owing its existence to a previous development starting with the desiccation of the Sedom lagoon and the exchange of sodium against calcium in the Cretaceous limestones [193]. However, [196] mentioned that considering the sulfate balance, the amount of gypsum found as layers and bulky beds is three times less than expected based on the estimated sulfate input. This information is helpful for the understanding of the sulfur isotope signature of the later discussed groundwater samples.

2.2.2 Agur well field

The Agur well field is located east of Tell es-Safi, the Bronze Age biblical city of Gath, alongside Nahal Ha'Elah (or Wadi es-Sant) (cf. Figure 2.6). The arrangement of the wells is approximately westnorthwest-eastsoutheast and spans between south of Bet Shemesh in the east (Agur 7) and north of the village of Agur in the west (Agur 1 and Agur 2) [190]. While passing the Shefela hills, which approximately extend from Beer Sheva to the city of Lod [187] the Wadi is one of the valleys that connects the coastal plain with the mountain ranges that otherwise are separeted by the foothills. The average amount of precipitation that reaches the Shefela hill country is about 500 mm/yr (e.g. [89]). It increases towards the recharge zone in the mountains to approximately 650 mm.
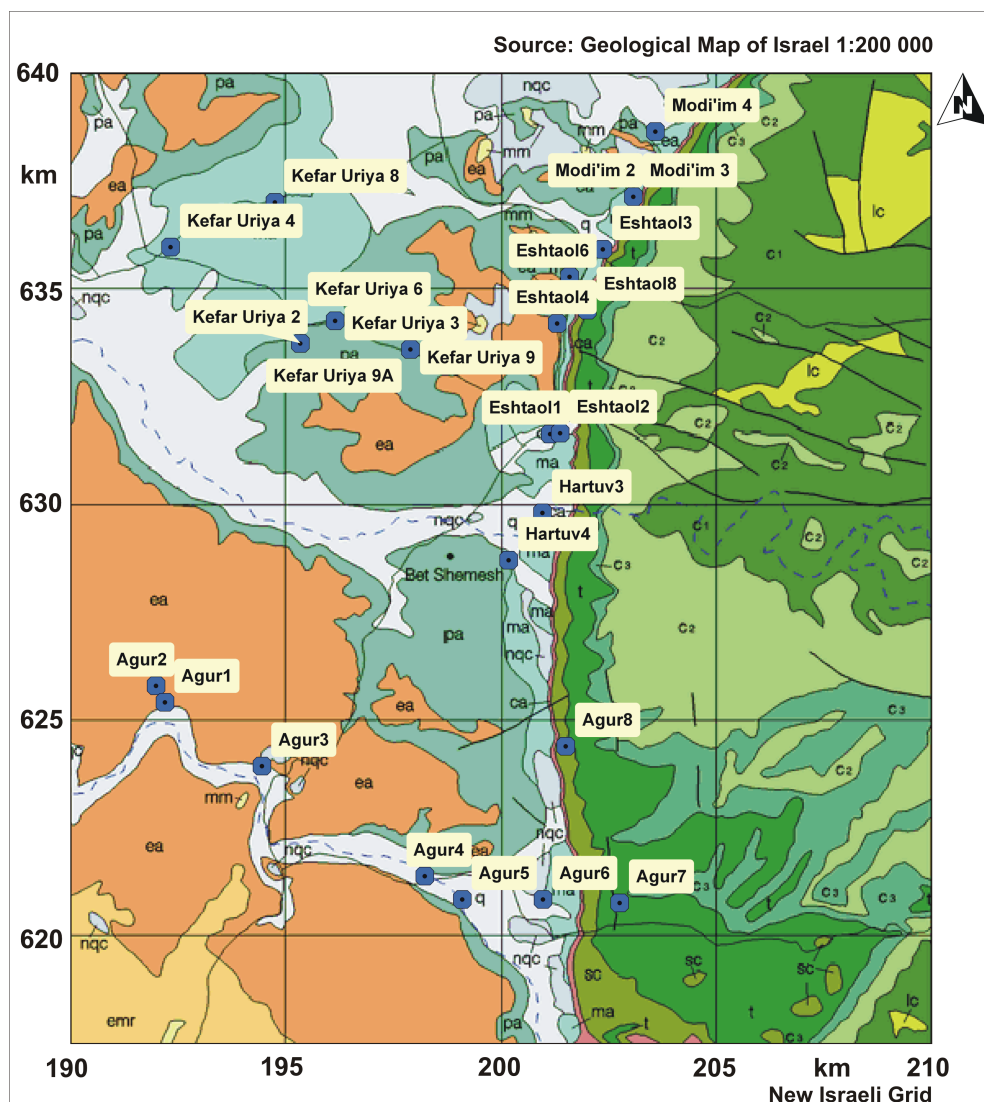
Figure 2.6: Geological map [190] and well locations for the Agur well field and its closer vicinity (geological legend in Figure 2.13).

15
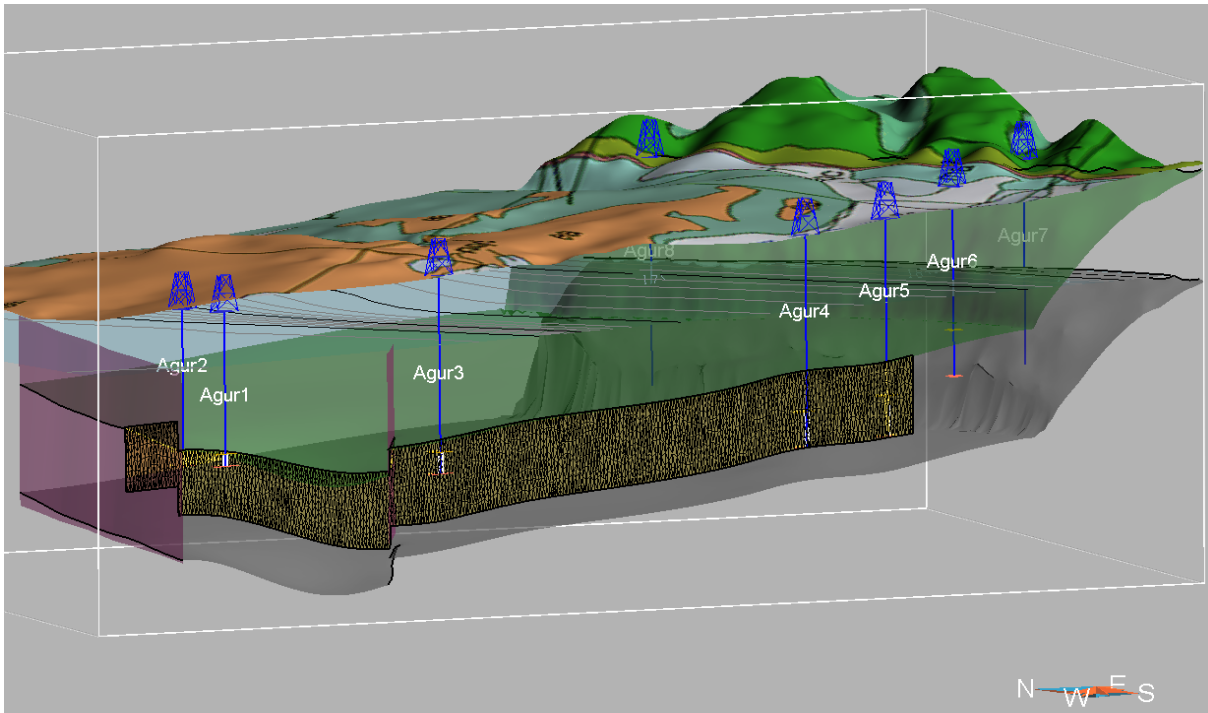
Figure 2.7: Approximately 15 km westnorthwest-eastsoutheast directed cross section through a 3D geological model showing the Judea Group Aquifer in the Agur area limited at the base by the lower, gray and at the top by the upper green layer [74]. To the east the Judea Mountains raises. Vertical surfaces of mangenta color represent major faults that offset the aquifer. A cross section through the Upper subaquifer marked by its yellow color and a triangulated mesh runs approximately between the wells of Agur 5 and Agur 2. The geometry of this surface was used to conduct a parameter sensitivity analysis with respect to the helium accumulation in groundwater, which is discussed in section 4.5 and section 5.4. The flat blueish surface with isolines represents the approximate groundwater elevation head distribution according to [98]. The top layer refers to the terrain surface and is draped by a geological map [190].

Some major geological characteristics descriminate the area from the other three sites:

- Thick sequences of mainly non- or low-permeable marls and chalks of Senonian to Eocene age – in part bituminous – cover the west-dipping Judea Group Aquifer west of Agur 7, the most eastern well;

- Confined conditions for both, the Lower and the Upper Judea Group Aquifer prevail somewhere west of Agur 7 (Figure 2.7).

- Parts of the sequences that cover the aquifer are continuously or temporarily – partially or fully water saturated, and may locally contain varying concentrations of water soluble minerals or residual brine pore water, and thus may contribute to

the salinization that is observed to increase from east to west not only in the Agur well field.

- the hydraulic conductivities of the Judea Group Aquifer in the lowlands of the Western basin, apart from the mountains is generally high ($\approx 10^2$m/day and higher) due to a higher degree of karstification, which is refered to be a paleokarstic development in times when the global or Mediterranian sea level had droped considerably (e.g. [77], [23]).

The source of salinization in the Ha'Shefela area that was mentionend above has been discussed by many authors. A final, generally accepted explanation, however, has not been agreed upon yet due to the existance of syncline and anticline structures, large fault displacements, and a number of possible paths such as local or remote, downward seeping or upward flow [94], [110], [82], [20], [140], or [77].

2.2.3 Herodion well field

The sampled wells of the Herodion well field belong to the Eastern aquifer basin (Figure 2.3) and were drilled into the Herodion (also Beit Sahour) syncline structure about 8 km east of the crest of the main anticlinal structure – the Hebron (also Surif) anticline – in the southern West Bank. Its high potential yield was already recognized in 1963 [177] and developed since than. Herodion 1, Herodion 2, and Herodion 3 were drilled alongside a fault that has a displacement of between 50 and 100 m [74]. From all study sites it is the well field with the highest surface elevation. Its north-south extention is approximatly from south of Bethlehem in the north to Beit Fajjar in the south. In the geological outline map for the study area [190] a much larger number of wells is depicted compared to the wells selected for this study, which indicates high aquifer exploitation within the well field Figure 2.10.
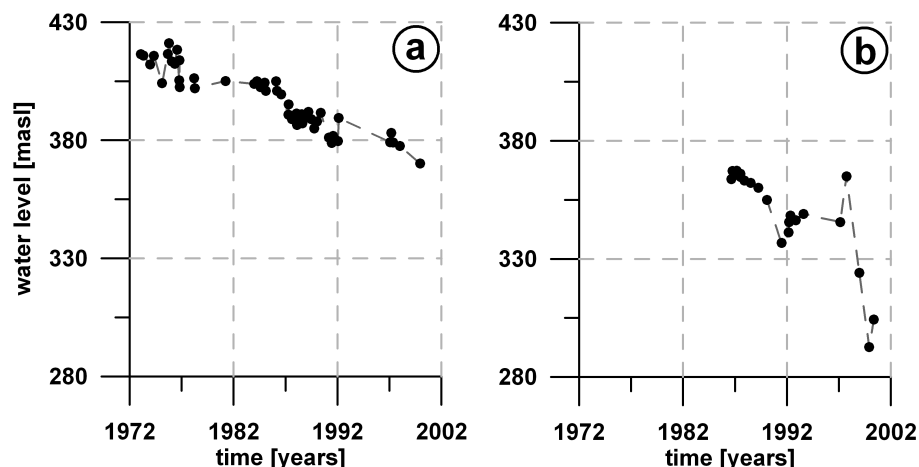
Figure 2.8: Groundwater elevation heads of the wells Herodion 2 (a) and Herodion 4 (b) between 1972 and 2000, taken from [166].
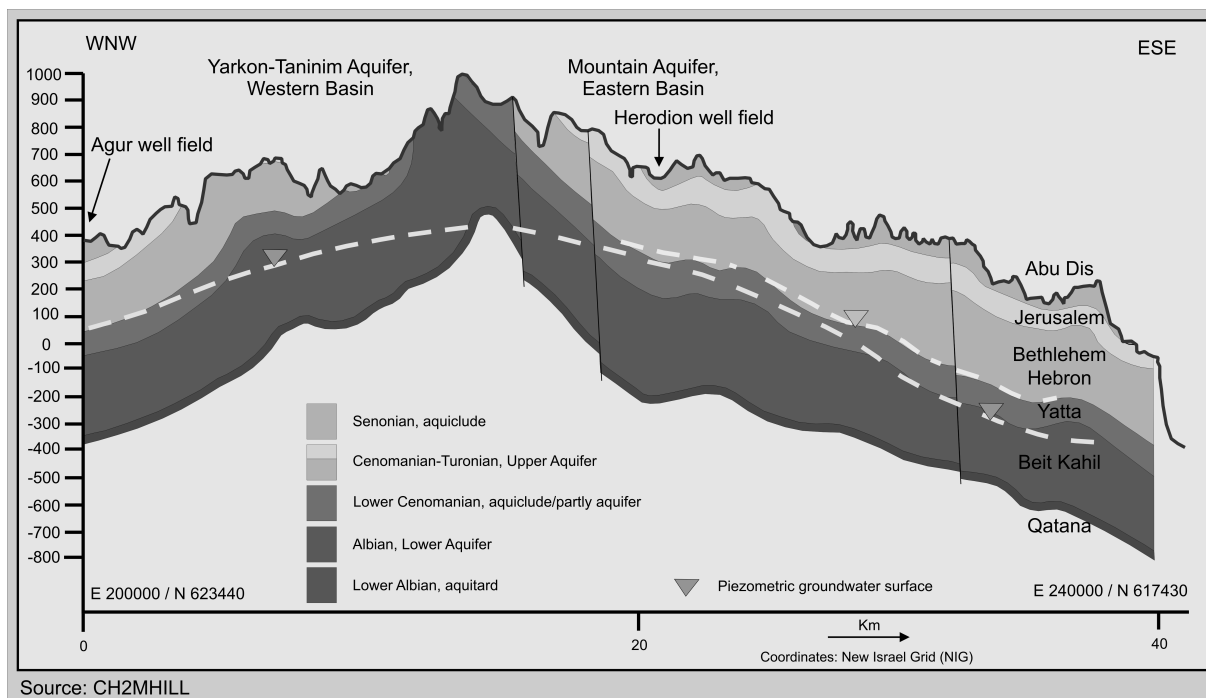
Figure 2.9: General cross section perpendicular to the Hebron Mountain monocline [49]. The geographical location is indicated in Figure 2.3. The formation names are Palestinian.

Actually, this is the main challenge for a proper well field management. Water levels in many of the wells had droped seriously by several tens of meters since they were put in operation Figure 2.8.

By 1995, when the Interim Agreement on the West Bank and the Gaza Strip (Oslo accords) between the State of Israel and the new Palestinian Authorities were achieved this tendency even started to be accelerated. With ratification of the treaty wells were eventually allowed to be drilled and operated by the Palestinian Authorities based on estimations about groundwater availabilities that were adopted for the contract. However, it became obvious that either the negotiated abstraction volumes for both contractual partners were not fully in consistency with a sustainable exploitation of the groundwater resources or the abstracted amounts exceed the safe yield of the catchment of the well field.

Due to the absence of any geogenic salinization source the only thread to the groundwater is anthropogenic pollution, which mainly is related to the release of untreated wastewater into the wadis, poorly protected cesspits, and others. The main paths these effluents take to the groundwater are karstic features like shafts or highly permeable faults and fractures especially if those underwent karstification processes in the phreatic zone. Further, as in other areas the zones of higher conductivity in the southern part of the Eastern Basin are related to synclinal structures ([29], [30], [63], [223]). It is self-evident that those synclinal high conductivity zones especially in the Upper aquifer are connected to a local or distributed network of karst features that reaches groundlevel and is capable to easily
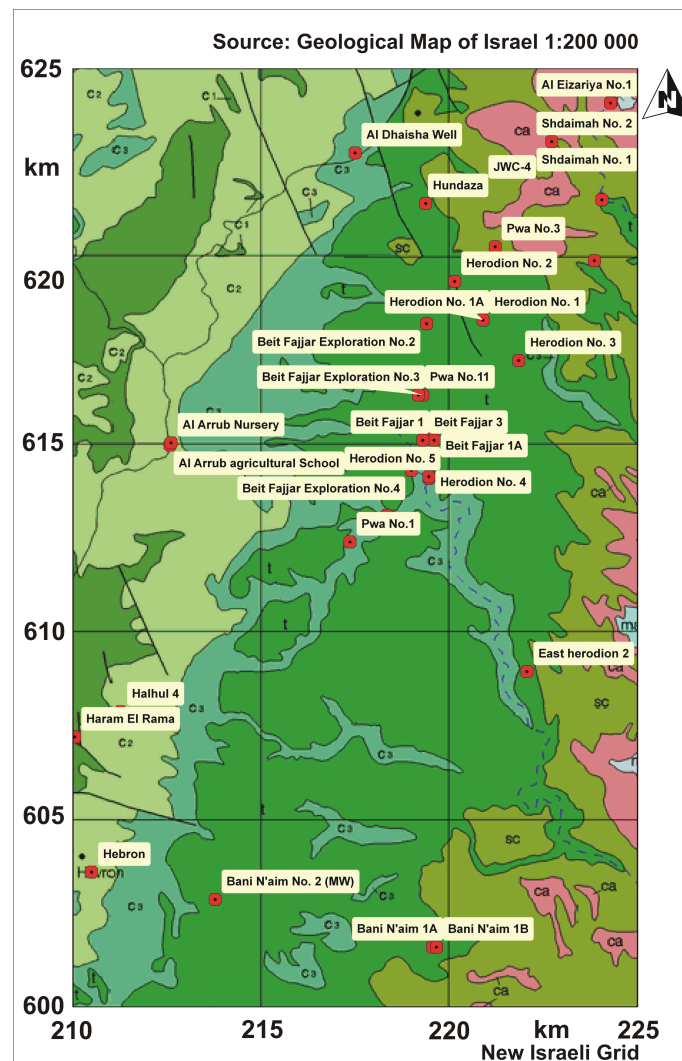
Figure 2.10: Geological map [190] and well locations for the Herodion well field and its close vicinity (geological legend in Figure 2.13).

gather water from rain and runoff events including effluents dumped into wadis, which might already follow the major local fault arrangement that, in turn, could embed important pathways to the mentioned synclinal high conductivity zones. Hydraulic conductivity contrasts between the latter and the anticlinal areas can be very large. According to [63] they may reach two orders of magnitudes (10^{-2} m/day vs. 1m/day), explaining the high head gradients in reach of the anticlinal structures. The example of Shdema 1 obviously supports these considerations, as it was drilled directly into a local syncline structure, and shut down not long after its initial starting, because of high contents in biological (coliform bacteria) and chemical pollutants (oral communications with A. Marei, Al Quds University).

The average annual amount of rain based on data from the Al Arroub Meterorological Station for the period of 1953-2001 is about 600 mm [166]. A hydrogeological east-west

cross-section [49] through the area (compare Figure 2.3 for location) outlines the general situation. Whereas in the Lower aquifer groundwater undergoes confined conditions with a certain distance to the anticlinal crest, phreatic or unconfined conditions below the cover sediments of post-Turonian age prevail in the Upper aquifer. The groundwater level in the Upper aquifer has a strong spatial variation and must not be taken from Figure 2.9 as is, since it is conceptualized.

2.2.4 Ein Samia well field

The Ein Samia well field got its name from a spring that discharges the Upper Cretaceous Aminadav formation next to a fault in Wadi Samia. Remnants of an ancient mill and an aqueduct of Roman and Ottomanian age witness the importance as well as longtime and diverse use of that spring. Wadi Samia is a graben structure belonging to the generally northwest to north-northwest trending Samia fault strip that is of Neogene Age, about 1 to 2 km wide, and stretches between Jericho in the south and the village Beit Ur al-Tahta in the north. However, several other wells were installed along the Samia fault strip (Figure 2.11).

The deep Ein Samia wells were all sank into the graben structure, where groundwater is abstracted from both, the Upper (Ein Samia 2A and 6) and Lower (Ein Samia 3, 4 and 6) aquifers. As indicated, at Ein Samia 6 both aquifers are exploited. The Upper aquifer is assumed to contribute about 2/3 of the overall extraction volume at Ein Samia 6 (oral communication with Jerusalem Water Undertaking company). Although located closely to the other wells the water level of Ein Samia 4 is about 100 m less, which is attributed to a fault running between them and that acts as a hydraulic barrier due to its low permeability. The annual precipitation in the area is about 400 mm.

Although karstic features have been observed by borehole-video logs for instance in Ein Samia 6 hydraulic conductivities and transmissivities seem to be rather moderate. However, hydraulic conductivities are higher by about one order of magnitude in the Upper (≈ 15 m/day) then in the in the Lower aquifer (≈ 2.5 m/day) [11]. In terms of transmissivities this is somehow balanced due to the difference in the saturated thickness of the both subaquifers. Pumping tests at Ein Samia 6 revealed transmissivities of about ≈ 840 and 950 m^2/day for the Lower and Upper aquifer, respectively. As major parts of Soreq formation are comprised of marly limestones it is characterized in general by low conductivities [11]. In turn it further splits up the Lower aquifer into two subaquifers. Kesalon formation is of low thickness (≈ 20 m) but of higher hydraulic conductivity (≈ 8 to 10 m/day) [11].
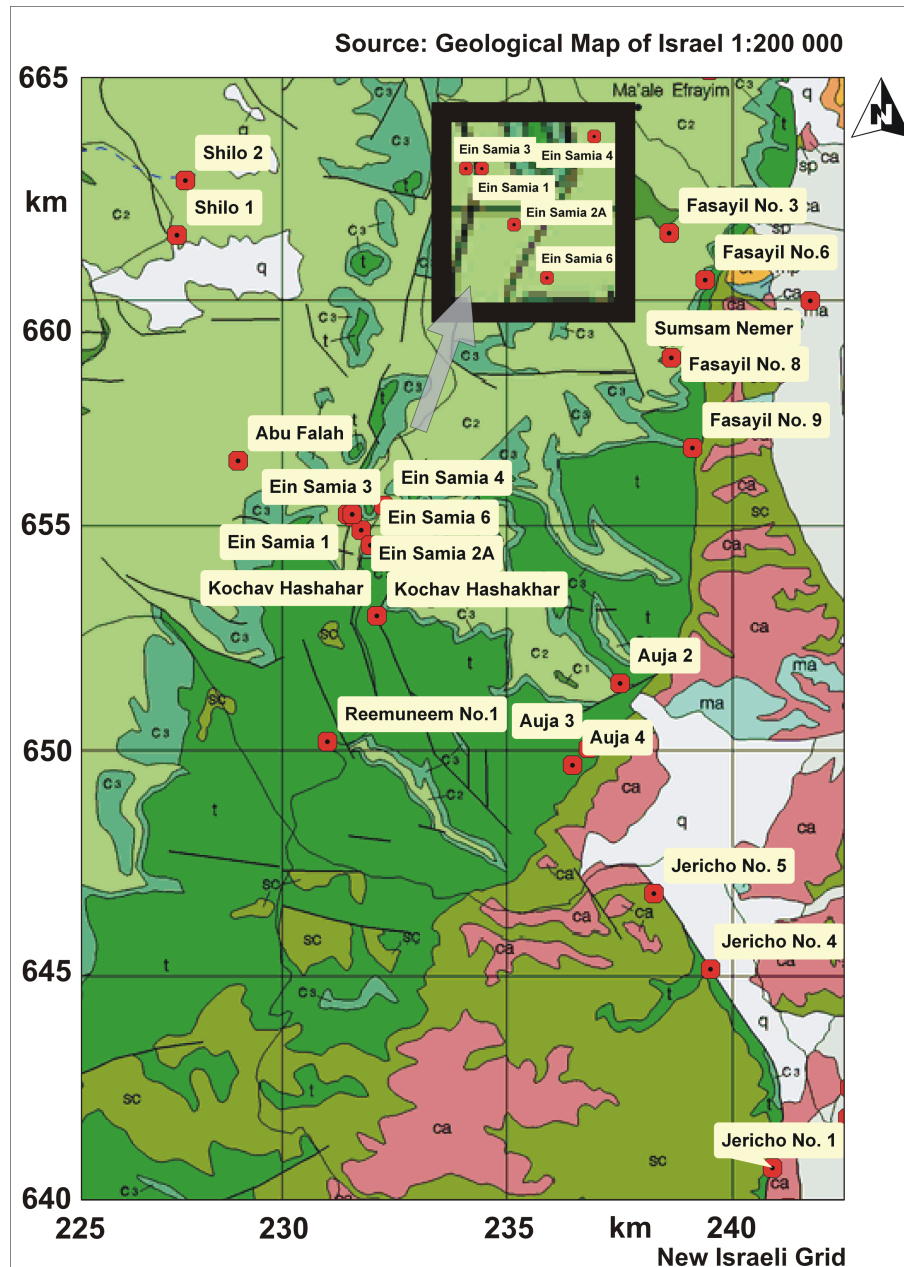
Figure 2.11: Geological map [190] and well locations for the Ein Samia well field and the closer vicinity (geological legend in Figure 2.13). The closer area and the positions of the Ein Samia wells to each other are magnified in the thick, black rectangle.

2.2.5 The Wadi Qilt spring system

As the tracer data of three major Wadi Qilt springs (Fara, Al Fawwar, Ein el Qilt) and one in the northwest of Jericho (Ein el Sultan) were reevaluated in the course of this thesis the important information about the Wadi and the springs is provided. Essential information about the spring of Ein el Sultan that also belongs to this partial study can be taken from subsection 2.2.1. The understanding of the geological as well as hydrogeological characteristics of the Wadi Qilt and its system of springs was improved over time by many studies ([177], [17], [179], [178], [127], [125], [222], [206], and [207]).
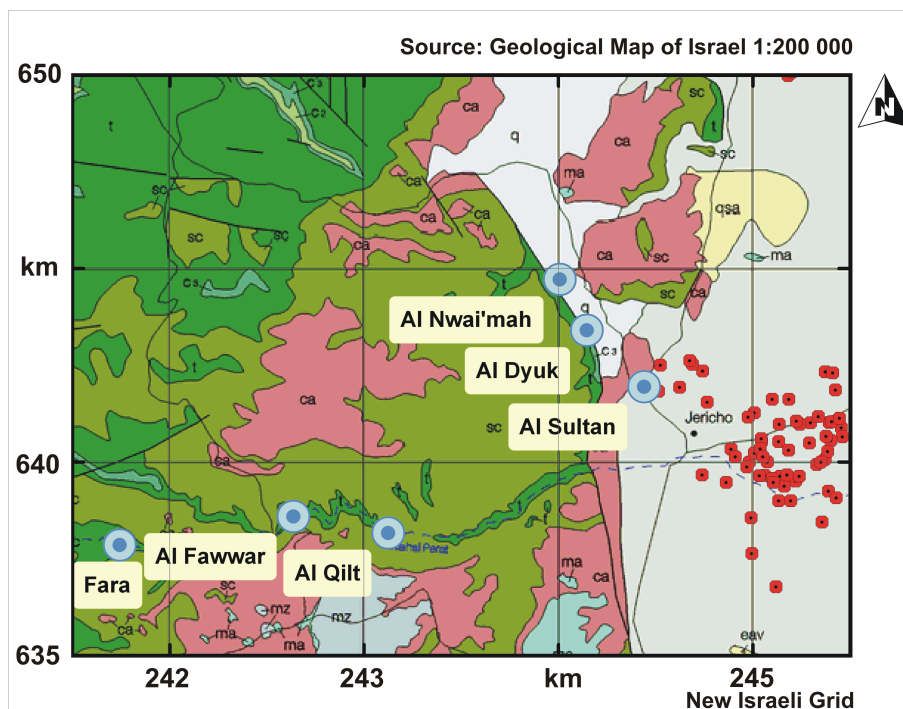
Figure 2.12: Geological map [190] and locations of the major springs of Wadi Qilt and Jericho and unspecified well locations in the Shallow Aquifer in the Jericho area (geological legend in Figure 2.13).

Wadi Qilt and many of its up-stream branches have deeply incised into the east dipping layers of the Mount Scopus Group and of the upper parts of the Judea Group, with the first representing the protective roof for the Upper Judea Group Aquifer. According to [222], [206], [207], and oral communication with Francis Hirsch (formerly at Geological Survey of Israel) the Upper aquifer is again split up by the Kefar Shaul formation – a 30 to 40 m thick section of marls and chalks. For the subaquifer above the Kefar Shaul formation [207] used the term Uppermost aquifer from which all major springs in Wadi Qilt discharge. However, beside the important major aquitard of the Kefar Shaul formation spatially varying facies types are responsible for the formation of locally limited low or non-permeable layers and, in turn, of perched aquifers. Only where the Uppermost aquifer crops out, springs may emerge if the perched groundwater level is high enough. In Wadi Qilt all of the major springs are connected to specific geological structures, and

Table 2.2: Discharge volumes of Ein el Sultan (Jericho) and the main Wadi Qilt springs Fara, Al Fawwar, and Ein el Qilt [160].

spring	mean [m^3]	minimum (year) [m^3]	maximum (year) [m^3]
Fara	778000	376000 (1963)	1371000 (1984)
Al Fawwar	4632000	303000 (1979)	11866000 (1992)
Ein el Qilt + Al Fawwar	6579000	2042000 (1979)	30675000 (1992)
Ein el Sultan	5569000	4998000 (1971)	6085000 (1988)

can be categorized according to that.

The Fara spring discharges up-stream of Wadi Qilt in Wadi Fara at an elevation of 290 masl at the base of Shivta formation. As the underlying Derorim formation is locally developed as a chalk or chalky limestone layer and the spring is connected to the Auja monocline, an important monocline structure in the West Bank, it can be categorized as contact spring [207]. At an elevation of 75 masl the spring Al Fawwar discharges at the junction of Wadi Fara and Wadi Mukhmas. East of the confluence point the conjoined wadi meets Wadi Qilt. Due to its structural relation to a highly permeable fault that is tapped by an ancient karst sinkhole, the spring was refered to as sinkhole karst spring by [207]. Two effects are responsible for the emergence of the spring Ein el Qilt. While approximately 800 m east of the spring the Senonian layers are downfaulted and offset against the Uppermost aquifer, which results in a so-called backwater effect, a set of northwest-southeast striking joints provide the pathway to the discharge location in the wadi. Although the location of Ein el Sultan is in the northwestern part of Jericho, it is also mentioned here, that it is connected to a southwest-northeast trending major normal fault and fed by the Uppermost aquifer, but emerges from the unconsolidated Shallow Aquifer.

The rainfall-discharge relationship is very strong for the Wadi Qilt springs. The variation of the discharge at Al Fawwar and Ein el Qilt between the dry and the rainy season can be very high depending on the amount of rainfall up in the mountains. Whereas in rather dry years the discharge rate may approximately just double it increases by one order of magnitude in very wet years [207]. Base flow conditions at Al Fawwar and Ein el Qilt approximates to less than 50 to 100 L/s. However, it may be noted that shortly after the rainy season Al Fawwar becomes a pulsing spring. Much less variation are characteristic for the Fara spring whose discharge pattern is more continuous with about 25..40 L/s with individual peaks following rainy periods approximately doubling the discharge rate [222].

q	**Allvium** (gravel, sand, clay, loess), *Quarternary*
nqc	**Conglomerates**, *Neogene/Quarternary*
mm	**Ziqlag Fm.** (Limestone, 42-50 m), *Miocene*
eav	**Avedat Group** (Chalk, limestone, chert), *Lower-Middle Eocene*
emr	**Maresha Fm.** (Chalk, 100 m), *Middle Eocene*
ea	**Adulam Fm.** (Chalk, chert, 150-300 m), *Lower-Middle Eocene*
mz	**Hatrurim Fm. - "Mottled Zone"** (Chalk, marl, 130 m), *Metamorphosed Maastrichtian-Miocene*
pa	**Taqiye Fm.** (Marl, clay, chalk, 63-150 m), Paleocene
ma	**Ghareb Fm.** (Chalk, 55-80 m), Maastrichtian
ca	**Mishash Fm.** (Chert, chalk, phosphorite, limestone, 86-126 m), *Campanian*
sc	**Menuha Fm.** (Chalk, marl, chert, sandstone, 82-164 m), *Coniacian-Campania*n
t	**Bina Fm., Derorim, Shivta, Nezer fms.** (Limestone, marl, dolostone, 171-230 m), *Turonian*
C3	**Sakhnin Fm., Weradim Fm., Tamer Fm.** (Dolostone, limestone, 58-160 m), *Cenomanian*
C2	**Bet Meir Fm., Moza, Amminadav, Kefar Shaul fms., Ein Yorke'am, Zafit, Avnon fms.** (Limestone, dolostone, 58-160 m), *Cenomanian*
C1	**Givat Ye'arim Fm., Soreq, Kesalon fms, Hevyon Fm.** (Dolostone, limestone, marl, chalk, chert, 160-227 m), *Albian-Cenomanian*
lc	**Hidra, Rama, Kefira fms.** (Limestone, marl, chalk, sandstone, 670 m), *Albian-Cenomanian*

Figure 2.13: Stratigraphic legend for the geological maps [190].

3 Theory and application of environmental tracers to characterize groundwater flow

Tracers are indicators for physical, chemical, or biological processes that otherwise would be inaccessible for observation. Therefore, the application of any tracer technique is primarily based on:

1. the spatial and temporal distribution of the substance,

2. the rate of tracer transformation to a daughter substance and/or

3. the rate of tracer transport from one position to or from one domain into another.

In turn the above items require a significant good knowledge about the initial conditions of the observed time frame, the systems status (steady state or transient), and the external trends the observed system might be exposed to.

Regarding groundwater flow and transport processes the required initial and boundary conditions for the tracer can be temporal (e.g. lumped parameter approach) or spatio-temporal (distributed models). For example in the case of lumped parameter models according to authors like [153], [137], or [138] just the tracer input function over time, the initial tracer concentration, and the rate of transformation have to be provided, whereas the system itself is treated as a black box. Often, those models are used to estimate one or a very small number of integral model parameters (thus "lumped" parameter models) that characterize the aquifer system. Analogical to this inverse fitting technique more sophisticated inverse modeling approaches are needed for instance to estimate aquifer properties or to find initial spatio-temporal conditions using back tracking procedures (e.g. [151] or [228] in non-porous media). From a conceptual point of view one has to distinct between conservative, partitioning (e.g. [142] for the unsaturated zone or [165] for geothermal reservoirs), and reactive tracers (e.g. [102]). Whereas tritium in groundwater is supposed to be a conservative tracer since it is part of the water molecule, noble gases like helium and neon [67], or radon [66] for example could serve as partitioning tracers with respect to DNAPL contaminations. A more recent development is the use of reactive tracers to characterize geothermal reservoirs by means of organic compounds like phenolic esters (e.g. [155]). However, a tracer may behave differently in different environments like saturated or unsaturated, oxic or unoxic conditions, or no organic versus high organic content in the solid phase (e.g. [55], [57], [56], [91], [54]). Hence, it is important to consider all processes that may have a significant impact on the tracer concentrations and

consequently on the estimation of groundwater ages. Multitracer approaches therefore provide better chances to detect problems with individual tracers and to derive a more comprehensive understanding. The following sections provide the theoretical background for the evaluation of the tracers that where applied in this study.

3.1 Stable isotopes

3.1.1 δ^2H and δ^{18}O

The evaluation of the isotopic distribution of oxygen and hydrogen in water is a powerful tool to understand the characteristic composition of groundwater with respect to provenance, age, as well as physical and chemical processes. While provenance can be suggested by comparing the local signature of groundwater and precipitation with those of other locations, assumptions about the age is generally related to both, documented climatic trends over time and the knowledge about the specific, local environmental conditions that were charactersistic for certain periods in the past. Physical and chemical processes comprise phase transitions, diffusive transport, thermodynamic equilibria, and chemical reactions.

The setting and modification of the oxygene and hydrogene isotopic distribution in water is mainly determined by the temperature, i.e. the energy at the molecular or atomic level that prevails during a fractionation process, for instance the isotope exchange reactions between different substances like water and rock or during the phase transition of water, e.g. between liquid and vapor. The dependence of the isotopic fractionation on temperature is basically the result of the effect of the isotope mass differences for example with respect to bonding strengths or the diffusion coefficient [38]. The isotopic signature of groundwater that was affected by geothermal water-rock interaction and the dissoluted components are thus indicative for the prevailing temperatures in a geothermal system.

Due of the general geological structure and hydraulic conditions in the study area and because there is neither reported nor assumed evidence for relevant isotope exchange related to specific geothermal conditions, the corresponding geothermal processes do not need to be explained here to understand the oxygene and hydrogene isotopic pattern of the sampled groundwaters. Hence, the main fractionation processes involved are the two directions of liquid-vapor phase transition corresponding to the most important natural fractionation processes of evaporation and condensation.

Condensation from clouds during precipitation

The main features of the condensation mechanism in a cloud that experiences rain-out was early predicted by [122] and can be described by the Rayleigh type distillation process [169]. It is based on the assumption of an open system, where the formating water drops at time t are in instantaneous equilibrium with the remaining vapor phase while removed at the same time. This may be expressed in differencial notation ([52], p. 65) or in its

integrated form of Equation 3.2 and Equation 3.3 [105], while Equation 3.1 defines the fractionation factor.

$$\alpha = \frac{R_l}{R_v} \tag{3.1}$$

$$\frac{R_v}{R_{v_0}} = f^{\alpha-1} \tag{3.2}$$

$$\frac{R_l}{R_{v_0}} = \alpha \cdot f^{\alpha-1} \tag{3.3}$$

Refering to Equation 3.1, Equation 3.2, and Equation 3.3 α is the equilibrium fractionation factor between the instantaneous rain-out and the remaining vapor, and R_v, R_l, and R_{v_0} are the isotopic ratios of the remaining vapor, the instantaneous rain-out, and the initial cloud, respectively, and f is the fraction of the residual vapor. The equilibrium fractionation factor is a common expression and relates the isotope ratios of two phases or substances, between which the fractionation process occurs $\alpha_{A-B} = R_A/R_B$.

Evaporation from water reservoirs to the vapor phase

Evaporation is the second main physical process to be discussed. Most of the global precipitation is generated by evaporation from marine but to lower extent also from inland sources, for example from waters of larger lakes. Lake Issyk-Kul in Kyrgyzstan, having an east-west and north-south extention of about 182 and 58 km, respectively, is an extreme example as it is located in Inner Asia far from any marine source and provides large amounts of vapor to the commonly dry air masses, which creates a significant increase in the amount of precipitation from its western side to its eastern side [62].

In most cases the fractionation process during evaporation differs from that of the above described Rayleigh type fractionation between a cloud and its rain-out. The main reason can be refered to the idealized concepts of an open or a closed systems. While evaporation from a liquid water reservoir to air with 100 % humidity would relate to an ideal closed, equilibrated system that fully obeys the equilibrium fractionation factor at the prevailing temperature, evaporation from the same reservoir to air of 0 % humidity would closely relate to the same open system condition like in the Rayleigh type condensation process, because any vapor would be removed immediately. The major difference between the latter case and a Rayleigh type condensation is, that a cloud and an ocean represent a small, finite and a large, infinite reservoir, respectively. In turn, that means that if air humidity is less then 100 % equilibrium conditions between liquid and vapor phase can not be reached and the fractionation process remains incomplete. That kind of non-equilibrium conditions are rather refered to the term kinetic fractionation.

The above described kinetic evaporation effects were first discovered and published by [59] who compared samples from various locations all over the world. He empirically found the most prominent equation for the $\delta^{18}O$-δ^2H relation for global meteoric waters (Equation 3.4) usually denominated as the Global Meteoric Water line (GMWL).

$$\delta^2H = 8 \cdot \delta^{18}O + 10‰ \tag{3.4}$$

The δ-notation represents the deviation of $^{18}O/^{16}O$ and D/H ratios from the V-SMOV standard in ‰ (parts per thousands). While a slope of 8 is characteristic for meteoric waters for the water-vapor equilibrium fractionation between δ^2H and $\delta^{18}O$, the constant shift of 10‰ on the right-hand side of Equation 3.4, is commonly refered to as deuterium excess [65] and defined by Equation 3.5. The d-excess would not exist if equilibrium conditions between the ocean and air prevailed and the function would intersect at δ^2H = 0 and $\delta^{18}O$ = 0. Note, that this intersection corresponds to the V-SMOW/SMOW-signature ((Vienna-) Standard Mean Oceanic Water).

$$d = \delta^2H - 8 \cdot \delta^{18}O. \tag{3.5}$$

Indeed the deuterium excess is the main measure for the strength of the kinetic conditions that prevail during the evaporation process above the ocean. For the precipitation occuring over Israel and the West Bank [81] defined the so-called local Mediterranean Meteoric Water line (MMWL), which is characteristic for the evaporation conditions over the Mediterranean Sea (Equation 3.6).

During the evaporation from water reservoirs, these get enriched in the ^2H and ^{18}O isotopes. Their isotopic signatures plot along straight lines with slopes between 8 and 3.9 for humidities between 100 and 0 % respectively [90].

$$\delta^2H = 8 \cdot \delta^{18}O + 22‰ \tag{3.6}$$

Isotope effects

All isotope effects, which are discussed in the following are connected to the two basic physical processes of evaporation and condensation, which often overlap each other.

Altitude effect The altitude effect has been comprehensively studied by many authors, with a minor selection of [80], [164], and [78]. It is basically an effect of temperature differences between lower and higher altitudes during rain-out. For $\delta^{18}O$ lapse rates between -0.15 to -0.5 ‰/100 m are reported, depending on the initial temperature ([80], [52], [164]). The corresponding δ^2H lapse rates range between -1 and -4 ‰ per 100 m.

Continental effect The continental effect simply refers to the depletion of the clouds due to rain-out while moving from the cost inland.

Temperature effect Lower ambient temperatures increase the fractionation in analogy to the elevation effect. On a global scale this is reflected by the latitude effect with increasing depleation of the precipitation from the equator to the pols.

Amount effect The amount effect is the negative correlation of the precipitation amount and the $\delta^2 H$ and $\delta^{18}O$ values and very pronounced in convective systems, which are characteristic especially in the tropics. Different, overlapping processes related to condensation and evaporation in and below the clouds as well as in the rain drops are involved [173].

3.1.2 ^{3}He and ^{4}He

Helium - a versatile isotope tracer for several types of geo-processes

As a rare and inert gas helium has been already discovered by [9] as a potential isotope tracer for various geo-processes by comparing atmospheric helium with helium from a gas well. Despite the fact that the technique of gas mass spectrometry was in a very early stage of development the measured atmospheric ^{3}He/^{4}He ratio was surprisingly close to the nowadays accepted natural ratio of $1.384 \cdot 10^{-6}$ that often is symbolised using the R_a notation. Already two years later the same authors could varify their previous assumption by extending their measurements to additional gas wells as well as minerals [10]. The major processes that provoke helium accumulation in groundwater are:

- radioactive decay: Predominantly ^{4}He is produced in-situ from uranium and thorium. In the presence of ^{6}Li also ^{3}He can be produced in considerable amounts.

- crustal helium flux: Generally vertical directed to the earths surface, it is actual also a product of mainly uranium and thorium decay in the crust. The continental, crustal signature of the ^{3}He/^{4}He ratio approximates to about $2 \cdot 10^{-8}$ [139].

- mantle derived helium flux: This flux is strongly enriched in ^{3}He compared to the other two major sources. Most of the ^{3}He that is stored in the mantle may be related to a primordial source (^{3}He/^{4}He $> 1 \cdot 10^4$ [152], [159]) but also to the depletion of the mantle with respect to uranium and thorium.

Regarding in-situ ^{4}He production in the aquifer rock Equation 3.7 is a zero-order function that applies according to [14]:

$$J_{He} = \Lambda \frac{\rho_{rock}}{\rho_{water}} (C_{uranium} \cdot P_{uranium} + C_{thorium} \cdot P_{thorium}) \cdot \left(\frac{1 - \theta}{\theta_{eff}} \right) \tag{3.7}$$

where J_{He} is the helium mass flux, Λ is the fraction of the produced He that enters the effective water saturated pore space, ρ the density, $C_{element}$ the elemental mass concentration in the rock, $P_{element}$ the elemental mass production rate and θ the pore volume with

θ_{eff} the effective pore volume.

But also gas stripping from groundwater due to gas producing chemical reactions and gas fluxes from below of an aquifer can effectively reduce the helium concentration and significantly modify the ^{3}He/^{4}He ratio. It is a known phenomenon for instance in the course of denitrification or methanogenesis, where N_2, CH_4, and CO_2 are the most important stripping gases.

However, virtual all groundwater that just infiltrated is oversaturated with respect to air, which is a result of the infiltration process itself. Soils that were unsaturated with respect to water become quickly saturated during stronger infiltration events. During that process air bubbles usually are entrapped and may totally or partially dissolve. While the total dissolution of a certain amount of excess air can be easily substracted from the measured concentrations, partial dissolution of entrapped air as well as partial reequilibration needs to be modeled in order to discriminate the isotope fractions that do or do not belong to the entrapped excess air component. Several models exist to account for partial dissolution and partial reequilibration of noble gases and their isotopes in groundwater [6], [7], [162], [5]. With respect to the case of partial dissolution [7] successfully applied their closed system (CE) model, which assumes an equilibration between groundwater and a not fully dissoluted air gas phase. The second process of partial reequilibration (PR), where the different gas and isotope species reequilibrate according to their individual physical properties like the diffusion coefficient was discovered by [197].

Therefore, it is necessary to check the absolute concentrations as well as the distribution of ^{3}He and ^{4}He in the groundwater samples for the impact from the above described processes. Thereby, it is preferable to use as many as possible noble gas components and isotope species. However, in most cases neon and its isotopes (^{20}Ne, ^{22}Ne) are the most important cross-check reference for air excess because its dry air fraction can be assumed as constant over time, and there is no known process that would introduce significant amounts of ^{20}Ne to groundwater ([61], [12], [73]). In a recent evaluation of noble gas groundwater samples from the Ntane Sandstone aquifer, Botswana [156] found evidence for CE as well as PR with the help of neon.

Helium and neon solubility in groundwater

Usually, the two publications of [218] and [31] are cited as sources for the calculation of the helium solubility in water. While [218] includes a correction term for salinity but lacks validity for other then normal pressure [31] include correction for pressure but not for salinity. The latter was used in the course of this study, because - if moderate - salinity has a low impact on helium solubiliy while compensation for pressure can still be applied. However, for higher salinities and especially for salinities as high as that of the Dead Sea water (see section 5.1) correction is necessary. For that case [219] provides an adjusted solution. Since the amount of ^{4}He exceeds that of ^{3}He by several orders of magnitudes the computable solubilities using the above methods of helium actually renders that of ^{4}He. To account for the solubility isotope fractionation between ^{3}He and ^{4}He [32] is the only available source.

Table 3.1: Parameters to account for different temperatures in Equation 3.10 for helium and neon according to [31].

gas	A_3 [1]	T_1 [K]	mole fraction in air [ppmv]
He	131.42	41.824	5.22
Ne	142.50	41.667	18.00

Equation 3.8 is the general formulation of Henry's law for the partition of a soluble gas between a liquid and the gas phase above:

$$f = Kx \tag{3.8}$$

where f is the fugacity or equilibrium concentration in the liquid, K the temperature dependent equilibrium distribution or Henry coefficient, and x the mole fraction in the gas phase.

[31] developed a universal solubility equation for seven non-polar gases including helium and neon and experimentally found the relation (Equation 3.9) between both, the Henry and the Bunsen coefficients to account for corrections imposed by pressure unequal to 1 atm:

$$\beta = \frac{124.4142 \cdot x \cdot \frac{p_l}{p_0}}{K} \tag{3.9}$$

where β and K are the Bunsen and Henry coefficients, respectively, x the mole fraction of the gas in air, and the ratio of p_l and p_0 is the divergence from normal pressure.

With the definition of the temperature dependent Henry coefficient (Equation 3.10) [31] provided all necessary terms that allow the computation of the air pressure and temperature dependent helium and neon solubility in water:

$$ln\, \frac{1}{K} = A_2 \left(\frac{T_1}{T_l} - 1 \right) + A_3 \left(\frac{T_1}{T_l} - 1 \right)^2 \tag{3.10}$$

where A_3 and A_2 are empirical parameters, with constant $A_2 = 36.855$, and T_l is the local temperature in [K]. The temperature T_1 is derived through therodynamic considerations and is listed together with A_3 and the mole fractions in air in Table 3.1 for helium as well as neon.

Finally, helium dissolution in water is accompanied by He isotope fractionation. With

Table 3.2: Parameters to account for helium fractionation at different temperatures in Equation 3.11 according to [32].

gas	$A_{0,\,frac}$	$A_{1\,frac}$	$A_{2\,frac}$
He	-0.0299645	19.8715	-1833.92

Equation 3.11 [32] provide a functional relation for this process:

$$ln\,\alpha = \Delta A_{0\,frac} + \frac{\Delta A_{1\,frac}}{T_l} + \frac{\Delta A_{2\,frac}}{T_l^2} \tag{3.11}$$

where α is the fractionation factor, $A_{0\,frac}$ to $A_{2\,frac}$ are empirical parameters tabulated in Table 3.2, and T_l is the local temperature in [K].

Due to the small mass differences between the neon isotopes fractionation does not need to be considered in usual situations. In turn, the atmospheric neon isotope ratios are practically equal to that of water in equilibrium with air.

3.2 Radiogenic isotopes

3.2.1 Tritium (^{3}H)

Atmospheric input to surface and groundwater

Tritium ($^3_1$H or T) is introduced to surface water and groundwater primarily by precipitation and air moisture. It relates to different natural and antropogenic sources. Natural production is mainly related to the well known fast neutron reaction:

$$^{14}_{7}\text{N} + n(> 4\,MeV) \rightarrow\, ^{12}_{6}\text{C} + ^{3}_{1}\text{H} \tag{3.12}$$

In a next step the chemical reaction of atmospheric oxygene and tritium isotopes to water molecules is responsible for the introduction of tritium to the hydrological cycle ($\text{T} + \text{H} + \frac{1}{2}\text{O}_2 \rightarrow \text{HTO}$). Tritium production also occures in terrestrial material and in the ocean, but those rates are several orders of magnitudes lower and of no practical interest to normal isotope hydrology applications. The natural distribution of tritiated water is uneven, with the world oceans inventory of about 99 % and the rest stored in both, the hydrosphere and atmosphere. Tritium concentrations in precipitation are exposed to a latitude effect (e.g. [60]) with increasing values from lower to higher latitudes. Early tritium measurements from the 1950s and 1960s [118], [176] suggest undisturbed average tritium concentrations in precipitation at latitudes of Israel of about 5 TU for the pre-bomb era.

Anthropogenic tritium sources include atmospheric test detonations of thermonuclear bombs, nuclear reactors, fuel reprocessing plants, heavy water production facilities, medi-

cal compounds, self-luminous paints and coatings and others. However, the main tritium release ever originated from the atmospheric detonations of thermonuclear bombs mainly from the 1950s to 1963 although the last atmospheric detonation was conducted in 1980 by China. All other sources have a more local impact especially on groundwater itself. In those cases it might lead to misinterpretation of the measured concentrations. Washout of the bomb tritium from the stratosphere in fact is complete at least since about the turn of the millenium. Thus, all tritium in todays precipitation is basically free of bomb tritium. However, locally the natural level can be exceeded due to ground based sources like nuclear reprocessing plants.

For historical reasons the measuring unit is TU with:

$$1 \text{ TU} = 1 \text{ T atom per } 10^{18} \text{ hydrogene atoms} = 0.118 \frac{\text{Bq}}{\text{kg}_{\text{water}}} \tag{3.13}$$

Further, the unstable tritium isotope undergoes nuclear beta transformation:

$$^{3}_{1}\text{H} \rightarrow {}^{3}_{2}\text{He} + \beta^{-} + \overline{\nu}_{\text{e}} \tag{3.14}$$

with a half-life of 12.43 years [209] and an average β^{-} energy of 5.7 keV.

Tritium input function

The utilization of tritium in hydrogeology depends on a local input function of measured tritium concentrations in precipitation. For Israel and the West Bank data from the the Global Network of Isotopes in Precipitation, the GNIP database of the International Atomic Energy Agency (IAEA) can be accessed through the webpage of the IAEA [109]. For the preparation of the input function that has been applied during this study weighted monthly tritium data from the Rehovot meteorological station were selected as they represent the most complete time series. As the whole precipitation over Israel and Palestine happens between September and May and the lumped parameter approach does not allow dry periods the GNIP tritium data were subsequently again weighted on a yearly basis. The resulting input function thus comprised equal monthly tritium values for each individual year. Situated southeast of Tel Aviv the station is in reasonable distance to the study locations, requiring just simple adjustment of the data. The calculated weighted yearly tritium values (Figure 3.1) are multiplied by a self-defined factor of 1.05 to consider the elevated inland position of the study locations. The resulting input function is very similar to that used by [117] for the area of the Soreq cave, northwest of Jerusalem.

3.3 Chemical tracers

3.3.1 Chlorofluorocarbons, SF$_6$

Many efforts during the last decades made available a wider choice of environmental tracers for groundwater age estimation in addition to the existing ones due to new or enhanced analytical techniques. Beside ^{85}Kr/Kr, pharmaceuticals, and other compounds the group
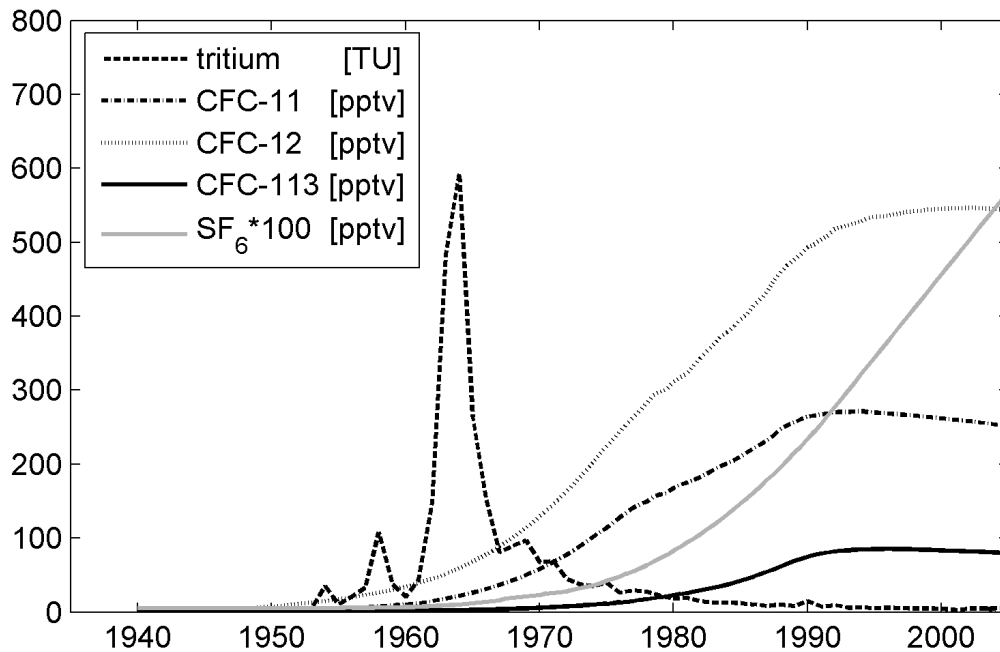
Figure 3.1: Tritium, CFC, and SF_6 input functions used for the evaluation of the measured data from the study locations. While the tritium input function is based on GNIP data [109] of the Bet Dagan meteorological station, the CFC and SF_6 were adopted from [45].

of volatile chlorofluorocarbons (CFCs) and sulphur hexafluoride (SF_6) were increasingly used starting in the 1980s because they combined several important aspects of global and general applicability:

- sufficient high stability in oceanic water, inland surface water, and groundwater,

- monotonically increasing global input function,

- fast advective transport and mixing in the atmosphere.

Meanwhile, however, CFC concentrations in the atmosphere generally decrease after several treaties and agreements about a worldwide and stepwise abandonment starting with the Montreal Protocol in 1987 and an agreed completing in 2030. A possible dangerous depletion of the stratospheric ozon layer by CFCs was first supposed by [148]. Because as halogenated, aliphatic hydrocarbons CFCs are hydrophobic, lipophilic but also very persistent under aerobic conditions. Thus they accumulate in the atmosphere, where due to photodissociation of the CFC compounds a long lasting destructive chlorine cycle is triggered. Nevertheless, some individual countries still possess an increasing CFC production. However, beside that CFC's are obviously quite stable in the oxic environment they are susceptible to degradation depending on the individual compound. Often, it is not sufficiently clear to which extent abiotic or biotic processes are involved

(e.g. [191], [183], [103]). Solid phase sorption of CFC compounds also have been shown to significantly affect apparent ages (e.g. [57], [25]). In contrast to the CFCs SF_6 on the one hand is assumed to be much more persistent even under anaerob conditions and not affected by sorption (e.g. [25]). But on the other hand SF_6 concentrations are much more susceptible to excess air or degassing for instance in the course of denitrification [211]. To some extent the effect of uncertainty of the infiltration temperature on apparent SF_6 ages is better compensated due to the steep rising input function. Thick unsaturated zones as well as a highly varying morphology are additional factors that can hamper the evaluation. However, due to their widespread use in industry or private households CFCs and SF_6 have in common that anthropogenic pollution or a locally differing input function especially in urban and highly industrialied areas [157] can complicate interpretation further if not impeding.

Input functions for CFC-11, CFC-12, CFC-113, and SF_6

In this and in subsection 3.2.1 it was already mentioned that exact input functions for specific locations are unknown in many cases and have to be estimated. This is also true for the CFCs and SF_6 in the area of Israel and the West Bank. However, [144] and [158], for example, showed that most of the CFC emmisions by the mid-1990s happend in the northern hemisphere and especially in the USA, Europe, as well as Japan. Comparisons provided by [158], [104], or [213] additionally point to local enrichment over the assumed atmospheric background concentration affecting the individual compounds differently, thus changing their ratios. Also diurnal, weekly and seasonal cycles are described by these authors. To level out that kind of cycling or irregular peaks [158] suggested gas sampling in soil using it as a low pass filter. In general, the sampling frequency should be high enough to detect relevant interfering events and cycles.

As no local input function is available for the study area the USGS atmospheric CFC and SF_6 mixing ratio data sets for the northern hemisphere were adopted for this study [45]. In Figure 3.1 the atmospheric input functions are plotted together with that of tritium. These data are based on the Chromatographic for Atmospheric Trace Species (CATS) program of the Earth System Research Laboratory of the U.S. National Oceanic & Atmospheric Administration [154].

Solubilities of CFCs and SF_6 are generally low and especially sensitive to temperature. For that reason uncertainty with respect to the temperature at which the system is closed will affect the interpretation of the measurements so much the more as smaller the slope of the input function is. Usually, model uncerianties increase in places where the unsaturated zone is very thick and even more if vertical dispersion is relevant or large like in karstic limestones or dolomites. Also the gas composition above the groundwater table could be different to a certain degree.

As already discussed in subsection 3.1.2 rapid infiltration during stronger rain events may further lead to full or partial dissolution of additional air (excess air) that is entrapped during the infiltration process [100]. However, the sensitivity to others then full

dissolution of excess air was not discussed so far for CFCs or SF_6 in literature.

Parameterized equations for the solubilities of the four compounds can be found in [214], [41], and [43]. The basic equation that applies to all is the modified Henry's law equation according to [217] that was simplified by [214] to

$$C^* = K'x'(P - p_{H_2O}) \tag{3.15}$$

where K' is the partial pressure equilibrium constant, x' the dry air mole fraction of the gas, P the atmospheric pressure, and p_{H_2O} the vapor pressure of water. The range of validity is limited to $P \approx$ atmospheric pressure.

The equilibrium constant (K'), which is a function of temperature and salinity can be similarily calculated for all four compounds. While temperature dependence is determined using the integrated van't Hoff equation, compensation for salinity is maintained by the logarithmic Setchenow salinity term [217], [216]. The general expression of this function is:

$$
\begin{aligned}
ln\,K' = a_1 + a_2 \cdot \left(\frac{100}{T}\right) + a_3 \cdot ln\left(\frac{T}{100}\right) + a_4 \cdot ln\left(\frac{T}{100}\right)^2 ... \\
+ S\left[b_1 + b_2 \cdot \left(\frac{T}{100}\right) + b_3 \cdot \left(\frac{T}{100}\right)^2\right]
\end{aligned}
\tag{3.16}
$$

where T is the temperature [K], and S the salinity [‰]. The fitting parameters for the considered compounds are listed in Table 3.3.

Similar to the equilibrium constant the vapor pressure of water is a function of temperature and pressure. To determine this parameter the temperature-density relation of water and the barometric pressure must be known. Tabulated values for density versus temperature were taken from [64]. For the air pressure the well know barometric formular has to be applied:

$$P_{bar} = P_0 \cdot 1 - \frac{\Delta K \cdot h^{5.255}}{T_0} \tag{3.17}$$

where p_0 and T_0 are the pressure and temperature at sea level, and h the elevation above sea level. The temperature gradient over elevation ΔK can be approximated for average conditions to 0.0065.

Table 3.3: Volumetric fitting constants for the integrated van't Hoff-logarithmic Setchenow equation in Equation 3.16. For the individual compounds some of the subterms are omitted due to sufficient accuracy or due to a better fit. Data obtained from [214], [41], and [43].

Volum. fitting const.	CFC-11 $\mathrm{mol\,L^{-1}\,atm^{-1}}$	CFC-12 $\mathrm{mol\,L^{-1}\,atm^{-1}}$	CFC-113 $\mathrm{mol\,L^{-1}\,atm^{-1}}$	SF$_6$ $\mathrm{mol\,L^{-1}\,atm^{-1}}$
a_1	-134.1536	-122.3246	-134.243	-96.5975
a_2	203.2156	182.5306	203.898	139.883
a_3	56.232	50.5898	54.9583	37.8193
a_4				
b_1	-0.144449	-0.145633	-0.02632	0.0310693
b_2	0.092952	0.092509	0.005874	-0.0356385
b_3	0.0159977	0.0156627		0.00743254

Further, the saturated vapor pressure can be calculated using Equation 3.18 according to [87]:

$$log_{10}\, P_{sat} = -\,7.90298 \cdot \left(\frac{T_s}{T} - 1\right) + \left(5.02808 \cdot log_{10}\frac{T_s}{T}\right)...$$

$$-\,1.3816 \cdot 10^{-7} \cdot \left(10^{11.344\cdot\left(1-\frac{T}{T_s}\right)} - 1\right)... \tag{3.18}$$

$$+\,8.1328 \cdot 10^{-3} \cdot \left(10^{-3.49149\cdot\left(\frac{T_s}{T}-1\right)} - 1\right) + \, log_{10}\, P_{bws}$$

where P_{bws} is the saturated vapor pressure of water at boiling point (1013.246 hPa), T_s the boiling point temperature, and T the absolute temperature [K].

For the last step to derive the final saturated vapor pressure of water, i.e. corrected for atmospheric pressure, Equation 3.19 can be applied according to [19]:

$$P_{sat,\,corr} = P_{sat} \cdot \left(1 + \frac{\frac{M_{H_2O}}{\rho_{H_2O}} \cdot (P_0 - P_{bar})}{R \cdot T}\right) \tag{3.19}$$

where M_{H_2O} is the molar weight of water, ρ_{H_2O} the corrected density of water, and R the ideal gas constant.

In most cases atmospheric pressures and water temperatures have to be estimated and averaged over the investigated area in order to apply for example lumped parameter models. But these are not the only uncertainties that introduce ambiguity to the model interpretation. As has been generally described in the introduction of chapter 3 excess air may significantly affect the tracer concentrations as well. Excess air may enter the system by total or partial dissolution. The impact on the concentration of a tracer is inverse proportional to its solubility. For that reason the SF_6 concentration is by far more sensitive to excess air than the CFCs. To calculate theoretical excess air concentrations Equation 3.20 and Equation 3.21 can be applied:

$$\frac{P_{std} \cdot V_{m,std}}{T_{std}} = \frac{P_l \cdot V_{m,l}}{T_l} \tag{3.20}$$

$$n_i = \frac{x'_i \cdot V_{dry\,air}}{V_{M,P_l}} \tag{3.21}$$

where Equation 3.20 relates the molar volume $V_{m,std}$ at standart conditions to the local conditions with the local pressure P_l and temperature T_l, and the molarity n_i of a species i in Equation 3.21 is the reciprocal product of its dissoluted volume $x'_i \cdot V_{dry\,air}$ with respect to its dry air fraction and the molar volume with respect to 1 L of air. For example, assuming a system closure at an elevation of 400 m and a water temperature of $18\,°C$ excess air of 0.5 mL/L results in excesses for CFC-11, CFC-12, CFC-113, and SF_6 of 0.16%, 0.6%, 0.55%, and 7.8%, respectively. In Figure 3.2 the effect of totally dissolved excess air between 0.05 and 15 mL air/L water on the CFC-113 and SF_6 concentrations is depicted.

Excess especially of SF_6 often can be recognized by comparing tracer ratios and due to expert knowledge about the investigated area. It can, however, not be quantified without a cross-check that is independend from a temporally variable input function. In most cases ^{20}Ne is a suitable cross-check reference for air excess because its dry air fraction can be assumed as constant over time, and there is no known process that would introduce significant amounts of ^{20}Ne to groundwater ([61], [12], [73]).

3.4 Lumped parameter models

Lumped parameter models do not require any spatial discretization as they treat the studied system as a so-called black box. They are common to many branches of natural sciences. The first application to tracer hydrology was conducted by [72], who introduced both, the piston flow as well as the exponential model. Subsequently [153], [133], [137], [138], and others introduced more models and applications. The general functional principle of any of the available lumped parameter models is the calculation of the convoluted theoretical output function for a given measured input function, the specified transfer function, and the required parameters like the mean residence time T_M or the dispersion parameter in case of the dispersion model. In the following the lumped parameter models
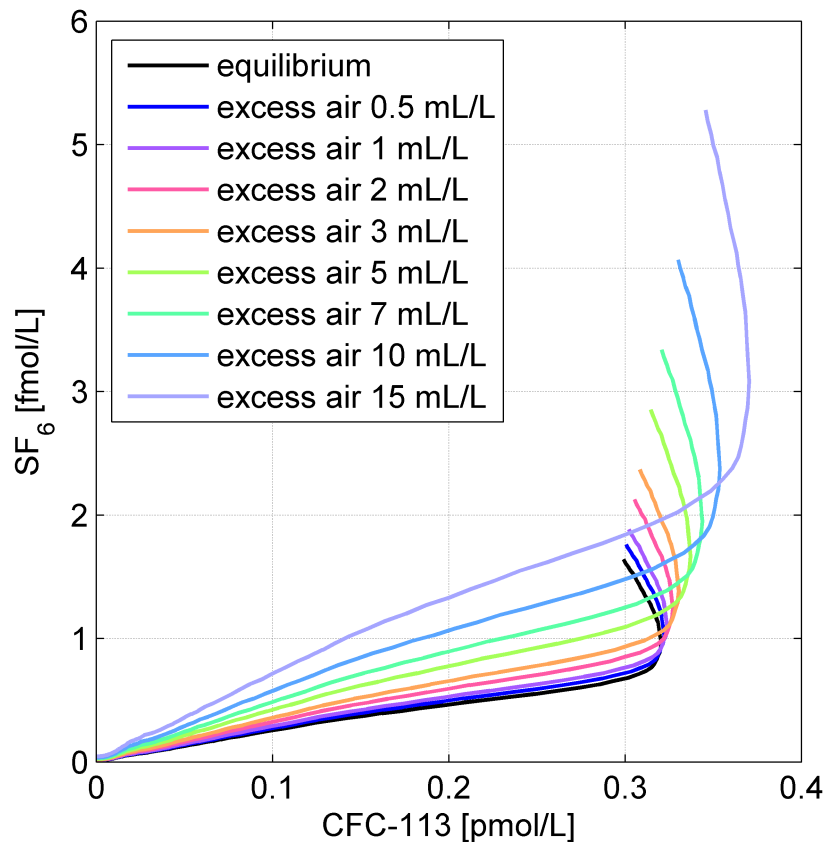
Figure 3.2: CFC-113 and SF$_6$ solubility time series data from 1940 to 2006, including excess air concentrations between 0.5 and 15 mL air/L water. For the calculation atmospheric CFC and SF$_6$ concentrations from [45] were adopted.

that were applied during this study are described:

Piston Flow model (1 degree of freedom): The piston flow model assumes no dispersion along a single flow path. The tracer concentration is only modified by a specified rate for degradation or radioactive decay. This model may have its special applications for instance for the evaluation of tracer migration through an unsaturated soil column. It is frequently used, however, for the interpretation of ^{14}C data. The mean transit time is the free parameter.

Exponential model (1 degree of freedom): As the name suggests the exponential model assumes an exponential distribution of transit times. This implies that the shortest transit time is zero while the longest is infinite. As in the piston flow model there is only one free parameter, which is the mean transit time of the tracer.

Dispersion model (2 degrees of freedom): The dispersion model stands somewhere between an exponential and a piston flow model. Additionally to the mean transit

time parameter like in the other two models it requires the dispersion parameter DP, which is related to but not necessary identical in its meaning to the inverse of the well-known Peclet number. As stated section 4.5, the Peclet number relates the advective to dispersive part of the transport problem.

Common to all of the models are the assumptions, that:

- the flow lines do not mix,

- only the sample is a mixture of all contributing flow lines,

- the system is in steady state, with a constant flow through and a constant volume of mobile water in the system,

- the aquifer is homogeneous.

The models can be coupled in series or in parallel, if the real conditions can not be satisfyingly treated with one of the single models. An example would be the serial coupling of a piston flow with an exponential model to consider the unsaturated zone and the saturated aquifer, respectively. By coupling the two models the whole system comprised two degrees of freedom: the mean transit time for the flow through the unsaturated and saturated zone as well as the proportion of one model with respect to the other. Further application examples are presented for instance in [137] or [171].

4 Methodology

4.1 Selection of the applied tracers

The investigated aquifers of the Cretaceous Judea Group section and the unconsolidated Pleistocene layers in the Jericho area are highly complex with repect to groundwater transite time distributions and potential sources of anthropogenic contamination or salinization. Ideally, to comprehensively describe the systems a set large of tracers could be applied on the one hand. On the other hand, project budgets and duration times, in general, require to select an appropriate set of tracers to approach the key questions with a reasonable effort. Because flow characterization, vulnerability, and salinization processes are of special interest in this study, the focus was on tracers for residence times of years to tens of years such as tritium, CFC, and SF_6, on indicators for different sources of salinity such as general hydrochemistry, hydrochemical tracers ($\delta^{36}S$), helium, and δ^2H and $\delta^{18}O$, as well.

4.2 Sampling

The temporarily insecure situation in the West Bank, and in one case a weeks-long strike of the Israeli customs that prevented the release of the sampling equipment just allowed three field sampling campaigns within the duration of the project. Efforts to sample repeatedly a constant selection of wells were not always successful, in part because several pumps were stopped due to normal well maintenance, low water tables, or elevated water salinities. Often, the water authorities assigned a selection of possible wells on a specific day for sampling according to the remotely controlled pumping regime or other operational reasons. Especially in the Jericho area many wells could not be sampled for gas tracers because the available connection facilities were inadequate to prevent atmospheric contamination.

4.3 Measurements

Part of the hydrochemical data were taken from literature. An exact description of the sampling and the applied analytical procedure can be found there. The samples refering to this study were analysed in the Environmental Laboratory at Al Quds University, Jerusalem. The samples have been transported in iceboxes to the laboratory, stored in refrigerators and analysed within two weeks. Sodium and potassium were flam photometrically determined. Titration was applied for calcium and magnesium against EDTA,

and for hydrogen carbonate against HCl. Chloride, sulfate and nitrate were analysed by ion chromatography. All samples have been taken between 2003 and 2005. Tritium and stable isotopes except for noble gases were measured at the laboratories of the Isotope Hydrology Department of the Helmholtz Centre for Environmental Research – UFZ – in Halle, Germany. Pre-treatment of the Tritium samples with volumes of 0.5 or 1 L was performed depending on their condition. After filtration the samples were distilled – in case of high salinities two times. Subsequently the concentration of Tritium was conducted by electrolytic enrichment starting either with 250 g or 400 g of each sample, which then was followed by activity measurements by means of liquid scintillation counting (LSC). All samples for $\delta^{18}O$ and δ^2H in water were stored in tight 25 mL HDPE bottles. The samples were subsequently equilibrated with CO_2 and H_2 for ^{18}O and ^2H, respectively before analysed using a connected isotope ratio mass spectrometer (IRMS Delta S, Finnigan). The ‰-notation of the measurement values represents the deviation of $^{18}O/^{16}O$ and D/H ratios from the V-SMOV standard in ‰ (parts per thousands). According to the expected sulfate concentration samples destined for determination of $\delta^{34}S$ of sulfate were filled into PE bottles of 1.5 or 2 L in the field and cooled until they were flushed through resin columns (AG1, Bio Rad Laboratories) to adsorb the soluted sulfate. All other steps were performed in the laboratories of the Isotope Hydrology Department of the UFZ in Halle. Here, sulfate was eluted by 3 molar HCl solution and precipitated as $BaSO_4$ by adding $BaCl_2$ solution at 70 °C. After 12 hours, $BaSO_4$ was collected on an ash-free filter (Blue Ribbon 5893, Schleicher and Schuell, Germany) that was completely removed by baking the sample at 800 °C for two hours. The baking procedure also removed any sample-related organic residue that may otherwise interfere with the oxygen isotopic composition of the sulfate. Sulfur isotopic compositions were measured after conversion of $BaSO_4$ to SO_2 using an elemental analyser (continuous flow flash combustion technique) coupled with an isotope ratio mass spectrometer (Delta S, ThermoFinnigan, Bremen, Germany). Sulfur isotope measurements were performed with an analytical error better than $\pm$ 0.3 ‰ and results are reported in delta notation ($\delta^{34}S$) again as part per thousand (‰) deviation relative to the Vienna Cañon Diablo Troilite (V-CDT) standard. For normalizing the $\delta^{34}S$ data, the IAEA-distributed reference materials NBS 127 ($BaSO_4$) and IAEA-S1 (Ag_2S) were used. The assigned values were +20.3 ‰ (V-CDT) for NBS 127 and 0.3 ‰ (V-CDT) for IAEA-S1. Noble gas analysis has been performed at the Institute of Environmental Physics and Oceanography at Bremen University. A description of the analytical procedure can be found in [201]. During sampling in the field continuously pumped groundwater was piped through copper tubes with a geometry of 100 cm x 1 cm. Subsequently the tubes have been clamped at both ends avoiding diffusive gas loss. Part of the He and Ne gas samples [194] were collected in 17 cm^3 stainless steel tubes capped on both ends with Nupro^{TM} valves. The sample holders were connected to the spring orifices through flexible tubings carefully tightened against air. All samples were collected in duplicate. Gas and Water samples were released from the stainless steel tubes on a dedicated extraction and purification system with glass break seals used to transfer the light noble gases to the mass spectrometer (MAP 215E) for isotope analyses at the Freie Universität Berlin. Concentrations and isotope ratios were determined by peak height comparison to a well determined 0.1 cm^3 STP air standard and a Krusvik

Iceland standard (^{3}He/^{4}He $= 1.98 \cdot 10^{-5}$) which were processed in the same way as the samples. The external reproducibility for He ratio was better than 2.5 % (2σ) and for element ratios better than 5 %. The CFC and SF$_6$ measurements were conducted by Spurenstofflabor Dr. Harald Oster in Wachenheim, Germany. The general procedure to separate the gases from the water samples is performed by gas chromatography using an electron capture detection system and is described in [157].

4.4 Realization approach to evaluate the T, CFC, and SF$_6$ samples from the Wadi Qilt springs and the deep wells of the Agur, Herodion, and Ein Samia well fields

The characterization of groundwater sources like springs or wells that relies on just one tracer that even may possess a rising and a falling limb, like tritium, can easily lead to ambiguous results if the number of observations is small and not appropriately distributed over time. If more and different kinds of tracers are considered the number of solutions can be considerably reduced or in the best case a unique solution can be found. For tritium a number of complementary tracers are available, where CFC-11, CFC-12, CFC-113, and SF$_6$ are the most widely used. Theoretical aspects of their application has been described in subsection 3.3.1.

The usual approach using lumped parameter models as described for example in [137] for a combination of different tracers comprises the calculation of theoretical models that are assumed to be valid for an investigated source. Subsequently the samples as well as the theoretical model values for the time of sampling are plottet for two tracers in one diagram. But also plotting of tracer ratios is a common procedure. The points representing the different mean residence times are usually connected by lines for a better visual control when selecting the models that best fits the tracer signature of the sample. This procedure is repeated with different tracer combinations to account for variations in the migration processes for example in the unsaturated zone or problems regarding tracer degradation (see subsection 3.3.1).

The general implementation of the evaluation procedure for the Wadi Qilt springs and the deep wells follows the considerations and scheme listed below:

1. Choosing an appropriate theoretical model configuration for the spring evaluation that would give acceptable solutions for all time series data of the springs, while considering the existence of an old, tracer free and at least one younger groundwater component. The evidence of residing old, tracer free components was shown by low ^{14}C values (e.g. [127] and [125]).

2. Because the deep wells were sampled not more then three times within 12 months the data can not be used in terms of a time series. Therefore, conceptual considerations were essential to select, as for the springs, a reasonable model configuration. Since the basic concept of both, an old, tracer free and at least one younger groundwater

component can be accepted also for the deep wells the same model type like in the spring evaluation could be applied for the wells.

3. Due to the small number of samples from each well ambiguity can not be avoided if more then two parameters control the system. Since in the course of the study of the Wadi Qilt springs a parallely coupled piston flow-dispersion model turned out to be the most appropriate configuration the system possesses three degrees of freedom: the mean transit time and the dispersion parameter of the dispersion model and its proportion with respect to the piston flow model. The mean transit time of the piston flow model was fixed to a large value to simulate the old, residing component.

4. Calculating a series of models with an arbitrary number of parameter combinations and extracting the model output for a time that is close to the sampling. The selected model combinations should cover a range of possible system states that suffices the spectrum of observations.

5. Generating figures with appropriate tracer combinations, the sample data and the model output. The latter is to be corrected with respect to the excess air concentrations that are calculated for the samples beforehand.

6. Extracting the possible parameter ranges for each sample by visual interpretation of the figures and calculating appropriate central tendencies.

To compute all model realizations the Software MULTIS [171], [172] was applied.

4.5 Numerical analysis of parameter sensitivities for ^{4}He accumulation in fractured limestone aquifers using the dual continuum analogon

4.5.1 General considerations

Parameter sensitivity analysis (PSA) can be defined as: technique to study the individual effect of parameter variation or uncertainty on the results of a mathematical model that represents one or more types of processes.

More specifically for the hydrogeological subject this means, that the physical, chemical or biological processes that are going to be modeled to answer specific questions determine the type of mathematical and algorithmic implementation. For simple groundwater flow and transport problems analytical solutions may be suffient to get an overall process understanding. However, many or most real world tasks involve sets of partial differential equations (PDE) and complex model geometries that can not be simplyfied too much without loosing essential information, for instance about important local patterns. Numerical models use specialized discretisation techniques to solve these PDEs for both, space and time.
To follow the above definition for PSA one has to determine the system that is going to

be simulated, the parameters, which are considered, and how the parameter ranges are defined.

With respect to this sensitivity analysis the system is defined as followes:

- steady state flow and transport,

- independend of density and temperature,

- fracture and matrix pore spaces,

- flow boundary conditions: Dirichlet (first kind), Neumann (no-flow, second kind), confined

- transport boundary conditions: Dirichlet (first kind),

- ^{4}He accumulation in groundwater due to ^{4}He production in the rock material with $J_{He} = f(C_{Uranium\,in\,rock}, C_{Thorium\,in\,rock})$.

The varied parameters are:

- four aquifer parameters and the head gradient (see subsection 4.5.4).

Parameter ranges:

- are selected according to the ranges found in the Mountain aquifer itself, as well as other known, natural systems (see subsection 4.5.4)

In the simplest case, the process of in-situ production of ^{4}He from uranium and thorium isotopes under saturated conditions along a particular flow path can be treated and analytically solved as zero order kinetics in 1D using the empirical formulation (Equation 3.7) of [14]. This is due to the fact that one can assume the mass of uranium and thorium in the aquifer rock practically to be constant for the considered time scale. Λ of Equation 3.7 in many cases is set to 1. This assumes that all helium from the in-situ production migrates to the connected pore space. In fact this is valid for rocks in diffusive equilibrium and if the equilibrium set-up time is low. For instants this is especially true for clay and silt sediments because of the large recoil lenghts of the α-particles [13]. The lithium content in the aquifer limestones and dolomites is irrelevant with respect to the production of ^{3}He. However, despite this easy concept of ^{4}He accumulation fractured limestones have at least two types of porosities, a matrix as well as a fracture porosity. Whereas on the one hand the latter usually dominates the flow the matrix porosity, on the other hand, has a very important impact on transport. But most limestones are affected also by karst phenomena to a certain degree. In fact, one may have to deal even with a triple-permeability, which still might not suffice the real aquifer conditions. For larger scale models, however, the computational demand for multi-porosity models is extremely high, as it is already very high for dual permeability aquifers. To describe flow and transport processes more precisely for more then one type of pore spaces the model approach has to be extended.

Potential model approaches for multi-permeability aquifers:

- Discrete (Figure 4.1): Individual fractures or conduits are modeled as discrete features (e.g. [204]). This approach can be further extended to discrete multi structure sets.

- Continuous (Figure 4.1): Finding a continuous porous medium equivalent for the fracture and conduit pore space. This approach can be extended to dual or multi-continuum models, where each continuum is handled separately and special exchange terms in the respective equations control the fluid and mass exchange (e.g. [202], [131], [84]). More simplistic is the concept of a double porosity aquifer, where flow is restricted to the first porosity, while the second one represents an immobile domain. As a result only the tracer mass balance needs to be considered [203].

- Fractal: All considered pores are represented by a pore space of fractal-dimension (e.g. [51]).

As has been emphasized by [182] the applicability of each of the model concepts strongly depends on the length scale of the whole problem, the length scale of the discrete structures if such has to be considered, and on the investigation efforts. While continuum approaches require a smaller investigation effort and thus, are more practicable, discrete model approaches can better handle discrete aquifer heterogenities. In turn, at small scales discrete models are justified. However, today modern groundwater flow and transport simulators like HydroGeoSphere are increasingly capable to combine both, continuum and discrete domains, depending on the focus and progress in the software development process. Although, it is known, that the distribution of many geological features like fractures, faults, or soil pore spaces is often adequately described using fractal approaches their implementations with respect to groundwater flow and transport are still rare. As this concept was not considered in this study its practicable applicability will not be discussed here.

Selection of the model approach for the parameter sensitivity analysis:

The complex groundwater flow pattern in the Upper Judea Group Aquifer in the area of the Agur well field prohibits the application of a simple 2D cross-sectional model along the westnorthwest-eastsoutheast arrangement of the wells Agur 1 to Agur 7 for calibration purposes. Whereas the groundwater gradient is directed west-northwest in the mountain ranges it changes to northwest and north in the Ha'Shefela hill country. The general, regional flow field ([63], [215]) implies that especially in the more western wells part of the groundwater is derived from the south. This makes it impossible to calibrate a numerical flow and transport model using the available data of the Agur wells. Beside the lack of sufficient data, a 3D transport model on the other hand would easily exceed the capacities to run it in appropriate times, for instance using the dual continuum (DC) approach. Additional uncertainty for the interpretation of the measured ^{4}He samples is introduced by strong fault offsets not only in the Agur area. To overcome all these limitations it was decided to conduct a parameter sensitivity analysis along a vertical cross-section (2D) that is detached from the available ^{4}He data of the Agur wells but resembles

Model representations for multi-porous aquifers
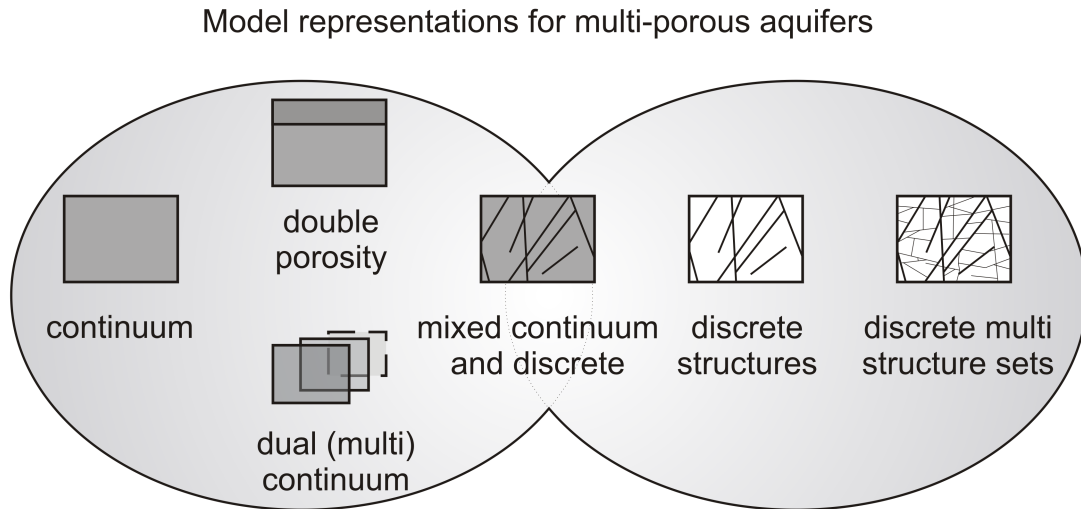
Figure 4.1: Different model approaches to represent aquifers with more then one permeability (modified after [202], [182], [37])

the main geometrical shape of the Upper aquifer (Figure 4.2). This allows to study the process of ^{4}He accumulation and at least to qualitatively compare between the real and the model observations if requested. As the name suggests, the dual continuum analogon for a fractured aquifer translates the discrete nature of fractures, their shape and spatial configuration to a continuous equivalent, which relies on several further assumptions:

- Turbulent flow is neglected, which is justified in many situations where fracture apertures don't significantly exceed 1 cm [221] or the Reynolds number $R_e \not\gg 2300$.

- The discretization of the model respects the concept of the representative elementary volume (REV). Due to the shape and configuration of the fractures we can conclude that $REV_{fracture\,space} \gg REV_{unconsolidated\,soil}$.

- The set of parameters of the dual continuum can not be directly derived from geological field measurements, for instance from a statistical fracture analysis. It rather must be understood as an equivalent, which has to be calibrated on data either of a real or a synthetic fractured aquifer.

Not all of these assumptions can always be perfectly matched as natural systems appear to be manifold. But nevertheless, given the example of karst aquifers many authors have successfully applied to a certain degree dual or multi continuum models [202], [182], [147], [131]. With regard to the previous list of assumptions that is required for most of the available dual continuum implementations the first plan was to closely bind the 2D cross-sectional DC equivalent model to a synthetic, discrete fracture-matrix contiuum (DFMC) model. A similar strategy for a 2D case already was implemented by [37]. Due to the lack of a description of the fracture system in the Agur area data from the Soreq cave [21], north of the Agur well field were adopted. Because of the two documented east-west
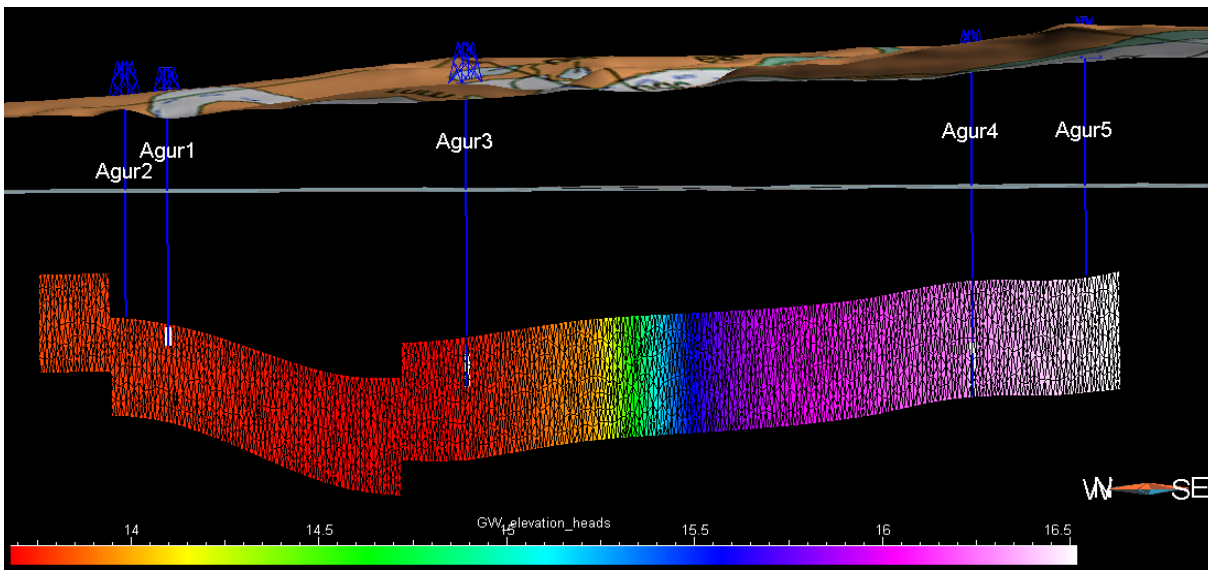
Figure 4.2: Geometry and position of the 10 km ESE-WNW directed 2D cross-section used for the modeling. The color distribution represents the approximate groundwater elevation head distribution (taken from [98]).

and northwest-southeast fracture systems in the cave and the assumed westnorthwestward flow it was possible to set up a small scale double plane-symetric, synthetic DFMC model (DFMC-M, Figure 4.3) using the HydroGeoSphere simulation package (see subsection 4.5.2). However, to suffice the requirements of a comprehensive PSA it became clear that the demand for man power as well as for the numerical computation capacities to loop repeatedly through the whole cycle of:

- determining the REV of the small scale 3D DFMC-M,

- calibrating the 3D DC-M on the 3D DFMC-M using the mass flux across control planes in connection with the inverse modeling software package *Parallel Pest*,

- deriving a 2D cross-sectional DC-M from the 3D DC-M,

- up-scaling the 2D cross-sectional DC-M,

- and running the actual parameter realization on it,

could not be satisfied, although parts of the process were automated using C- and Shell-scripting. The main reason is the contrast between the relative small time stepping to respect the various limiting, numerical criteria and the required simulation time scale to reach steady state conditions for the ^{4}He accumulation. To overcome the computational limits the calibration of the DC analogons with respect to the individual DFMC models was omitted. Instead, parameters for the DC models were selected according to their availability in the literature.
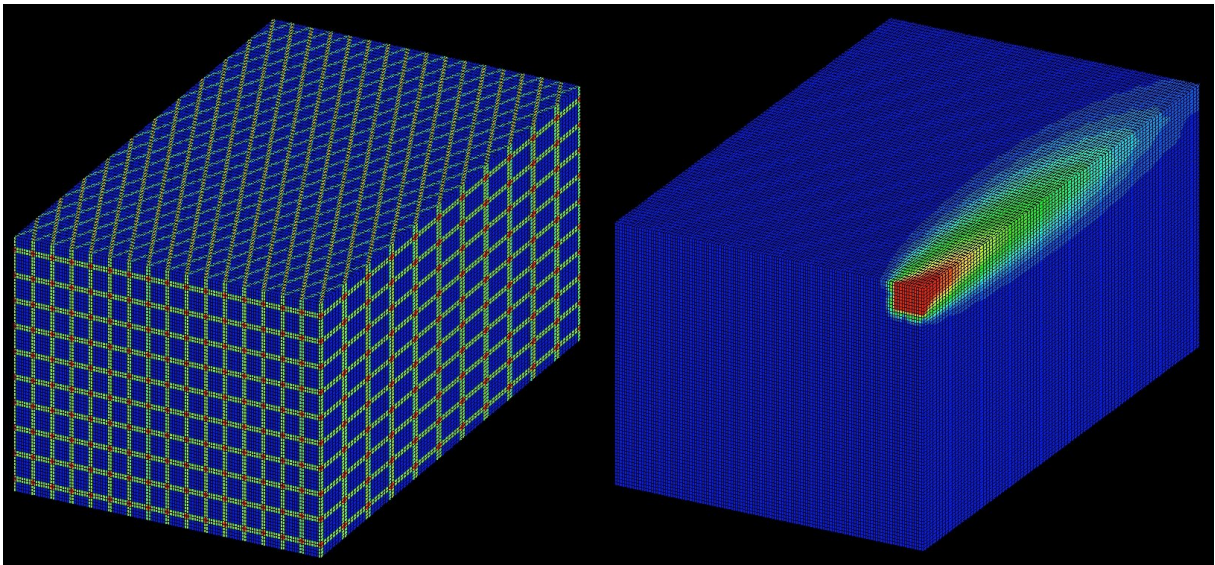
Figure 4.3: Small scale, double plane-symmetric, discrete fracture-matrix contiuum model (DFMC-M) that was originally planed to be used as synthetic aquifer analogon for the larger scale 2D cross-sectional dual continuum model (DC-M).

4.5.2 HydroGeoSphere – the applied flow and transport simulator

In subsection 4.5.1 the requirements for the selection of an appropriate simulation software package were discussed in general and specifically for the process of ^{4}He accumulation in a fractured limestone aquifer. The described considerations led to the HydroGeoSphere (HGS) numerical code [203] as a suitable choice. HydroGeoSphere is a fully-integrated surface-subsurface flow and transport simulator. The subsurface module itself was derived from the FRAC3DVS flow and transport code developed at University of Waterloo and Université Laval, Canada.

HydroGeoSphere implements the control volume finite element method (CVFE-M) to discretize and solve the applied partial differential equations. Thereby, the CVFE-M stands somewhere between the finite difference and finite element methods. It possesses the geometrical flexibility in analogy to the finite element technique, enforces local conservation of mass and energy (and momentum for surface flow) due to the control volume around every "finite element" node, and – because of the latter – can be implemented similar to the finite difference technique. Concerning the requirements for the described parameter sensitivity analysis HydroGeoSphere can handle normal porous media, embedded 2D discrete elements, as well as the dual continuum approach. Since the parameter sensitivity analysis is planned to be extended in future to transient and partially unconfined conditions including well abstraction and distributed infiltration it was important, that the simulation software package in addition has these capabilities. This is all true for HydroGeoSphere. Note that the term dual continuum is used in the HydroGeoSphere manual for the continuum that does not represent the matrix continuum – for example

the fracture porosity. Although this term may be mistakable it is adopted here to keep a direct link to the formulations in the manual.

Governing equations for the model problem

Groundwater flow

Flow in the porous medium:

The derivation of the general flow equation for transient, saturated conditions has been shown by many authors, e.g. [26]. Using the notation from the HydroGeoSphere manual [203] the equation can be written as:

$$\nabla(\mathsf{K}_{ij}\nabla\psi) \pm Q = S_s\left(\frac{\partial\psi}{\partial t}\right) \tag{4.1}$$

with the hydraulic conductivity tensor K_{ij} [L T^{-1}], the volumetric flux Q to a sink (negative) or inflow from a source (positive), the specific storage S_s [dimensionless], and pressure head ψ [L]. Because of its integrated architecture HydroGeoSphere in general applies a modified form of Richard's equation for transient subsurface flow in variably-saturated porous media [203]:

$$-\nabla(w_m\,\mathsf{q}) + \sum\Gamma_{ex} \pm Q = w_m\left(S_w S_s\frac{\partial\psi}{\partial t} + \theta_s\frac{S_w}{\partial t}\right) \tag{4.2}$$

The first term on the left-hand side of Equation 4.2 corresponds to that of Equation 4.1 and is extended for variable-saturated conditions by redefining the fluid flux q [L T^{-1}] as:

$$\mathsf{q} = -\mathsf{K}\cdot k_r\nabla(\psi + z) \tag{4.3}$$

with the hydraulic conductivity tensor K [L T^{-1}], the pressure head ψ [L], the gravitational head z [L], and the dimensionless relative permeability k_r as a function of the dimensionless water saturation:

$$S_w = \frac{\theta}{\theta_w} \tag{4.4}$$

Here, θ stands for porosity and θ_w for the water saturated porosity. To allow K to be a function of density (ρ [M L^{-3}]) and viscosity (μ [M L^{-1} T^{-1}]) of water it is formulated further as:

$$\mathsf{K} = \frac{\rho g}{\mu}\,\mathsf{k} \tag{4.5}$$

where k is the permeability tensor of the porous medium. w_m of Equation 4.2 [dimensionless] is the volumetric fraction of the total porosity of the primary porous medium. The second left-hand side term of Equation 4.2 represents the sum of fluid exchange with other different, but compatible flow domain types, like for instance discrete fractures, the upper surface, or a dual continuum. Finally, Q represents the fluid exchange with the outside of the whole simulation domain. Therefore, $\sum \Gamma_{ex}$, as well as Q of Equation 4.2 correspond to the term Q of Equation 4.1. Γ_{ex} is positive for flow into the porous medium.

The terms on the right-hand side of both, Equation 4.1 and Equation 4.2 describe the storage in the aquifer. Changes of pressure head under saturated conditions entail change in storage, and the specific storage S_s [L^{-1}] itself is derived by compressibility terms for the porous medium and water. In contrary, for the storage under unsaturated conditions only the change in saturation is considered in Equation 4.2.

However, the models of the parameter sensitivity analysis were run under confined conditions in analogy to the conditions in the Agur well field. To always retain maximum performance HydroGeoSphere loads specialized modules to run problems of different kinds, like for instance saturated, unsaturated, or density dependend flow. For that reason there is no need to go further into detail of the terms that control the unsaturated flow conditions.

Flow in the dual continuum:

The dual continuum approach used in HydroGeoSphere is based on [84] and substantially equates to the flow formulation for the porous medium (Equation 4.2). In equivalence to the latter the general modified Richard's equation is written as:

$$-\nabla(w_d\, \mathsf{q}_d) - \Gamma_d \pm Q_d = w_d\Big(S_{wd}S_{sd}\frac{\partial\psi_d}{\partial t} + \theta_{sd}\frac{S_{wd}}{\partial t}\Big) \tag{4.6}$$

Since Γ_{ex} was signed positive for flow into the porous medium, Γ_d must be negative in the dual continuum to respect conservation laws. Due to the analogy it is not necessary to repeat all equations analogous to the formulations for the porous medium.

Porous medium - dual continuum flow coupling:

The linkage between the porous medium and the dual continuum is provided by a fluid exchange term. HydroGeoSphere knows two types of fluid flow coupling between different kinds of flow domains: the common node and the dual node coupling. The common node coupling assumes instantaneous equilibrium of the hydraulic heads of the two domains, whereas the dual node coupling implements a Darcy flux across a virtual layer of porous material. The exchange term between the two continua can be defined according to [84] as:

$$\Gamma_d = \alpha_{wd}K_a k_{ra}(\psi_d - \psi) \tag{4.7}$$

with:

$$\alpha_{wd} = \frac{\beta_d \, \gamma_w}{a^2} \tag{4.8}$$

K_a [L T^{-2}] represents the hydraulic conductivity of the interface and $\psi_d - \psi$ the driving pressure difference between the two flow domains. k_{ra} [dimensionless] is the relative permeability of the interface. The parameter α_{wd} [L^{-1}] is the first order transfer coefficient, β_d a dimensionless geometry coefficient usually ranging between 3 and 15, a the characteristic half-width of a matrix block [L^{-2}], and γ_w a dimensionless scaling factor that was found to approximate to 0.4 ([85], [84]), although [85] also give suggestions based on geometrical considerations for the parameters of Equation 4.8.

Transport

Transport in the porous medium:

The basic advective-dispersive transport equation (ADE) for solutes in incompressible groundwater in saturated porous media incorporates three major processes of transport: advection, molecular diffusion, and mechanical dispersion. It can be extended to consider other processes like chemical reaction and decay through sink and source terms and sorption through a retardation factor describing the partitition of a solute between the liquid and the solid phase by means of linear or non-linear sorption isotherms. Thus, the acronym ADE becomes ADRE. A comprehensive, general definition of transport in saturated porous media using the notation from the HydroGeoSphere manual would be:

$$-\nabla \cdot w_m(\mathsf{q}C - \mathsf{D}\nabla C) + w_m\lambda RC \pm Q_c = w_m \left[R\frac{\partial C}{\partial t} \right] \tag{4.9}$$

where C is the dissolved concentration of a species in water [M L^{-3}], λ its first-order decay constant [T^{-1}] and Q_c [M L^{-3} T^{-1}] the source sink term to describe exchange across the borders of the simulation domain. According to the manual and in equivalence to Equation 4.1 HydroGeoSphere applies the following integrated version for variably-saturated porous media:

$$-\nabla \cdot w_m(\mathsf{q}C - \theta_s S_w \mathsf{D}\nabla C) + [w_m\theta_s S_w\lambda RC]_{par} + \sum \Omega_{ex} \pm Q_c =$$

$$w_m \left[\frac{\partial \theta_s S_w RC}{\partial t} + \theta_s S_w\lambda RC \right] \tag{4.10}$$

where $\sum \Omega_{ex}$ [M L^{-3} T^{-1}] again represents a mass exchange rate, but like in Equation 4.2 only with other supported domain types. R [dimensionless] is a factor refering to the retardation concept, which includes all kinds of non-kinetic sorption processes that may happen across the fluid-solid interface:

$$R = 1 + \frac{\rho_b}{\theta_s S_w}K' \tag{4.11}$$

with the aquifer bulk density ρ_b [M L^{-3}] and the equilibrium partition coefficient K' [L^3 M^{-1}]:

$$K' = \frac{\partial C_{solid,\, immobile}}{\partial C_{fluid,\, mobile}} \tag{4.12}$$

that is evaluated in HydroGeoSphere using a linear Freundlich isotherm. D [L^2 T^{-1}], the hydrodynamic dispersivity tensor (Equation 4.2) can be written according to [26] as:

$$\theta_s S_w \mathsf{D} = \alpha_{ijkl} \frac{\mathsf{q}_k\, \mathsf{q}_l}{|\mathsf{q}_{kl}|} + \alpha_t\, |\mathsf{q}|\, \mathsf{I} + \theta_s S_w \tau D_{free} \mathsf{I} \tag{4.13}$$

where α_l, α_t [L] are the longitudinal and transversal dispersivities, I the identity tensor, D_{free} the free molecular diffusion coefficient, and τ [dimensionless] the porous medium specific tortuosity factor, for which the definition of [146]:

$$\tau = \frac{(\theta_s S_w)^{7/3}}{\theta_s^2} \tag{4.14}$$

is adopted.

Transport in the dual continuum:

Like in the case of groundwater flow the formulation of the ADRE for the dual continuum is similar to that for the porous medium. Only the exchange term describing the mass exchange rate with the porous medium is conversely signed. Thus, we can advance without writing the ADRE again for the dual continuum.

Porous medium - dual continuum transport coupling:

Similar to groundwater flow the transport coupling between the porous medium and the dual continuum is provided by a solute mass exchange rate, which is defined in Hydro-GeoSphere according to [84] as:

$$\Omega_d = -u_m C_m - u_d C_d \tag{4.15}$$

where:

$$u_m = d^* \Gamma_d \phi - \alpha_s w_m \theta_s S_w \tag{4.16}$$

and:

$$u_d = (1 - d^*) \Gamma_d \phi^* + \alpha_s w_m \theta_s S_w \tag{4.17}$$

The mass transfer coefficient α_s [T^{-1}] could be approximated based on approaches provided by [199] or [200] for the double porosity (mobile-immobile) coupling, which according to

the HydroGeoSphere manual seems to be a former implementation in the software. However, the current implementation uses the approach from [85] analogous to Equation 4.8 (communication with T. Graf, Hannover University):

$$\alpha_s = \frac{\beta_d \, D_{eff}}{a^2} \tag{4.18}$$

where β_d and a are the dimensionless geometry factor and the characteristic half-width of a matrix block analogous to Equation 4.8 and D_{eff} [L^2 T^{-1}] is refered to as effective diffusion coefficient analogous to the hydraulic interface conductivity K_a in the fluid flow transfer function (Equation 4.7). Both parameters control the effectivity of the transfer between the matrix and the dual continuum. Due to the definition of α_s and by defining d^* as a dimensionless coefficient that determines the direction of the solute transfer with:

$$d^* = 0.5 \left(1 - \frac{\Gamma_d}{|\Gamma_d|} \right), \quad \Gamma_d \neq 0 \tag{4.19}$$

it appears, that for equal heads $\Gamma_d = 0$ and the solute exchange reduces to diffusion type [85]. To fully account for the saturation conditions in both continua [203] further substitute:

$$\phi = w_m \frac{\theta_s S_w}{\theta_{total}}; \quad \phi = (1 - w_m) \frac{\theta_{sd} S_{wd}}{\theta_{total}}; \quad \theta_{total} = w_m \theta_s S_w + (1 - w_m) \cdot \theta_{sd} S_{wd} \tag{4.20}$$

However, as for the groundwater flow simulation HydroGeoSphere loads specialized transport routines for different conditions to gain maximal performance.

Numerical error control criteria:

Numerical errors are introduced due to spatial and time discretization of the model domain and the simulated time, respectively. They can not be avoided but sufficiently minimized if certain numerical criteria are respected. The critical controls for the simulations perfomed during the study will be explained and formulated using equations from [192]:

The Peclet criterion or cell Peclet number is the ratio of advective to dispersive transport. It conditions the spatial discretization and is generally fomulated as:

$$Pe_{xi} = \frac{v_{xi} \Delta x_{xi}}{D_{xi}} \tag{4.21}$$

where for direction x_i v_{xi} is the velocity, Δx_i the cell size, and D_{xi} the dispersion coefficient. If we empirically define $D_x = v_x \alpha_x$ in x direction, Equation 4.21 may be rewritten as:

$$Pe = \frac{\Delta x}{\alpha_x} \leq 2, \tag{4.22}$$

which more directly shows the connection between Pe and the heterogenity of the aquifer as the cellsize must not be more then two times the dispersivity to avoid negative concentrations.

The Courant criterion is a critical stability control and relates the advective transport to the cell size and time discretization. It limits the maximal timestep to prevent a to high advective mass flux out of the cell for a given time Δt and can be written for a cross-sectional 2D problem as:

$$Co_{x,z} = \left| \frac{\Delta t \, v_{x,z}}{\Delta x_{x,z}} \right| \leq 1 \tag{4.23}$$

The Neumann criterion complements the Courant criterion as it relates the dispersive transport to the cell size and the time discretization. Analogous it limits the maximal timestep to prevent a to high dispersive mass flux out of the cell for a given time Δt and can be written for a cross-sectional 2D problem as:

$$\frac{D_{xx}\Delta t}{\Delta x^2} + \frac{D_{zz}\Delta t}{\Delta z^2} \leq 0.5 \tag{4.24}$$

4.5.3 Preparation of the meshes

To prepare an appropriate mesh for a simulation in HydroGeoSphere the **GridBuilder** program [145] can be utilized, as it provides all necessary tools to determine, for instance, the boundaries, boundary conditions, the internal discretization, and others. However, the capabilities to finely adjust the mesh density is limited, because the first initialization of the mesh also depends on the discretization of the model boundary. After that, only mesh densification by splitting of triangles is possible. Since a local 3D structural model for the Agur area was created using **Gocad** [136], a sophisticated 3D geological modeling software package, it seemed natural to benefit as much as possible from the data handling, vizualization, and mesh adjustment capabilities within the *Gocad* environment. As stated above, the mesh density can be controlled by the node density or the segment lengths of the boundary line. This type of adjustment is integrated in the *Structural Workflow* of *Gocad* to predefine the lateral node density of a triangulated surface that is going to be built.

By following this strategy the triangulated meshes were created in *Gocad* and exported to the *Gocad* text format for *TSurf*-Objects that includes the complete topological information. Afterwards, this format was translated to the text import format (*.imp) of *GridBuilder* using a script that was written in *Python*. A general definition for both formats can be taken from Figure 4.4. Note that the default triangle orientation used in *Gocad* and *GridBuilder* is vise versa. To avoid negative triangle surface areas this is corrected by the Python script, beforehand.

Figure 4.4: *Gocad TSurf* and *GridBuilder* import text formats. Keywords are emphasized.

4.5.4 Model parameterization

The ranges for the parameter variations were selected according to the ranges found in the Mountain aquifer itself, as well as in other known, natural systems. Because of facies changes and due to its karstic and fractured nature the properties of the Mountain aquifer vary considerably throughout the area. It was, however, not the aim of this PSA to investigate the effect of such internal variations on the ^{4}He concentration. Therefore, the same parameters were assigned to all nodes of each model. Because of the long runtimes for the individual models the list of parameters was restricted to a number of 5:

- matrix porosity (primary continuum),

- fracture porosity (dual continuum),

- hydraulic conductivities: $K_x = 10K_z$ (dual continuum),

- dispersivities: $\alpha_l = 10\alpha_{vt}$ (dual continuum),

- distribution of hydraulic head.

All of them have been modified three times. The applied variation of the production rate of ^{4}He refers to its functional dependency on the total porosity (cf. Equation 3.7). Due

Table 4.1: Chosen parameter values for the sensitivity analysis, with the total volumetrical fraction of the matrix (w_m), the total volumetrical fraction (w_d), hydraulic conductivities (K_{xd}/K_{zd}), and dispersivities (α_{ld}/α_{vtd}) of the dual continuum, as well as the total head difference (Δh) between the side boundaries across a total distance of 9970 m.

	w_m [1]	w_d [1]	K_{xd} ($= 10K_{zd}$) [m/s]	α_{ld} ($= 10\alpha_{vtd}$) [m]	Δh [m]
lower limit	0.050	0.009	2.3148e-3	25	1
between lower and upper limit	0.070	0.015	2.6042e-3	45	5
upper limit	0.080	0.021	2.8935e-3	75	10

to their very low decay rate concentrations of uranium and thorium in the rock were assumed to be constant over time. Table 4.1 shows the selected individual parameter values.

An estimation of 0.07 for the effective porosity for the Mountain aquifer based on the time domain electronmagnetic method has been adopted from [112]. [224] also used this estimation for their simulations to investigate the effect of base level changes and geological structures on the location of the groundwater divide. The range of hydraulic conductivities for the Mountain aquifer is very wide and depends much on the degree of karstification, on the type of the local geological structure, faulting, and fracturing. Hydraulic conductivities in the lowlands west of the Judea (Hebron) Mountain range are generally assumed to be very high due to a more mature karstification. Nevertheless, strong karstification is also to be found in some mountaineous areas. Recently, [63] published the results of their calibrated groundwater flow model for the western, i.e. the Yarkon-Taninim aquifer. For the Agur area their calibration assigns hydraulic conductivities between 200 and 250 m/d, which, as they state, is in agreement with other studies like [29], [35], [93], or [95]. Only [29] is publicly available.

Comprehensive data of uranium and thorium rock concentrations for the Judea Group Aquifer are not available. As a rule of thumb the natural uranium background level in limestone will not drop considerably below 2 ppm under most conditions. However, according to the deposition environment, like depth, aeration, or distance to the coast the uranium and thorium concentrations in marine limestones may broadly vary within a range of almost two orders of magnitudes. Thus, on the one hand, a good understanding of the distribution of uranium and thorium in the aquifer material is a crucial factor in the system. Since the Upper Albian transgression on the Arabian shelf established a huge carbonate platform with similar depositional environments it might be appropriate to look for data of neighbouring areas like Jordan or as in this case Lebanon [212]. Under the assumption that the depositional or facial environment is comparable it seems justified

to adopt a comprehensive data set of rock analyses for uranium and thorium from two corresponding geological profiles in the mid-northern part of Lebanon. These are the areas of Nahr Ibrahim and Chekka, between Beirut and Tripoli. From the data published by [4] average uranium and thorium concentrations of 6 ppm and 6 ppm, respectively could be extracted for the whole rock sequence from Upper Albian to Turonian times. On the other hand, the exact helium production rate per kg rock has no effect on any model sensitivities, because the assumed production process is of zero-order. Thus, it is possible to generalise the sensitivities by relating a normalised model output to a normalised model input. In HydroGeoSphere the specification of the fluid and mass exchange between the two continua is adjusted by the hydraulic conductivity of a virtual intermediate layer and the two transfer coefficients. While the first can be reasonably specified with the same hydraulic conductivity as for the matrix the two transfer coefficients may vary broadly according to the density, distribution, orientation, and shapes of the fractures and karst features, which explains that no applicable rule of thumb exist. Thus, the parameters of the two transfer coefficients were chosen in a way, that the required numerical values for the fluid and mass exchange in the input files become 0.6 [m^{-2}] and 0.0235 [s^{-1}], respectively. While the dimensionless geometry factor β_d and the characteristic half-width of the matrix blocks were set to 3 and 1 m, respectively, in the fluid and solute transfer functions, the effective diffusion coefficient D_{eff} (Equation 4.18) was set to $7.83 \cdot 10^{-3}$ [m^{-2} s^{-1}]. The latter value was probably overestimated and enhances the exchange between the two continua. Note, that due to the numerical implementation in HydroGeoSphere the fluid exchange term is to be divided by 2 (communication with Th. Graf, Hannover University). However, the two transfer coefficients are often used as additional calibration parameter or might be estimated by means of column experiments at the laboratory scale, field studies, tracer tests, and detailed mappings of fractures and matrix block sizes. The transfer coefficients could not be considered in the sensitivity analysis, due to the long model run times and because there were no ranges available.

4.5.5 Implementation strategy for the parameter sensitivity analysis

Running a sensitivity analysis for transport even for a simple process like ^{4}He accumulation demands for suffient computation and storage capacity, particularly if embedded discrete elements, or as in this case a dual contiuum are involved. Due to the long runtime of several hours for each individual model, it becomes ineffective above a certain threshold of model cases to run the whole model batch manually, because:

- exept for the program *GridBuilder*, which creates 2D meshes compatible to Hydro-GeoSphere, a rudimentary batch processor **hsbatch**, and **hsplot**, a program that produces formated output for **Tecplot** and **GMS** HydroGeoSphere offers no pre- and postprocessing facilities.

- the exact runtime is not easy to predict for different parameter values, which may lower the utilisation capacity of the computer system;

- each model must be checked to respect the relevant numerical error control criteria;

- an optimally chosen spatial and time discretisation can save computation time;

- suffient storage capacity for instance by compression or uploading to remote file servers must always be ensured to prevent data loss and the need for re-runs;

- individual editing of several text input files can be prone to error;

- checking and postprocessing for many cases and numerous and partially large output files is time expensive;

- it fragments and binds much of the researchers attention to all of the above issues.

To facilitate the whole task, part of the modeling procedure, as well as the listed accessory work therefore was automated using self-developed programs or scripts with respect to:

- Task 1: the creation of the necessary input files for each model;

- Task 2: satisfy a beforehand specified folder and name convention;

- Task 3: run the models for a short time;

- Task 4: selecting a finer discretized mesh, if the Peclet criterion was violated;

- Task 5: adjusting the time stepping;

- Task 6: re-run the model for the whole time period if Peclet criterion was respected;

- Task 7: compressing the project files;

- Task 8: decompressing projects, extract relevant data, raw figures, recompressing;

- Task 9: merging/appending the extracted model outputs of the projects into one data set ready to load by *Octave* or *Matlab*.

The first three tasks were covered by a program written in **C** [44]: **hgsbat**. However, because of the lower abstraction level of the C language compared with other, in general non-compiled languages the rest of the tasks has been implemented using **Python** [3], **Bash** shell [2], and **Octave** [70], [69] scripts. The HydroGeoSphere batch processor (*hsbatch*) has just elementary functionality and could not be integrated into the general simulation workflow, which is presented in Figure 4.5. Beside the fact, that the demo version of *GMS* can be laboriously used to visualize individual problem cases, *Tecplot* and *GMS* were not available for this study. Instead the numerical programing language *Octave* (in part also **Matlab** [1]) was applied for the postprocessing. From Figure 4.5 it can be seen that in fact two programs are involved to control the run of the whole model batch, where *hgsbat* is responsible to enforce the specified name convention, the correct folder structure, the replacement of the parameter values in the template files, as well as the initial model run. It finally calls the self-developed Python script **hgs_criterion**, which in turn ensures the adherence to the considered Peclet, Courant, and Neumann critera, and - if all requirements were met - runs the problem for the whole duration
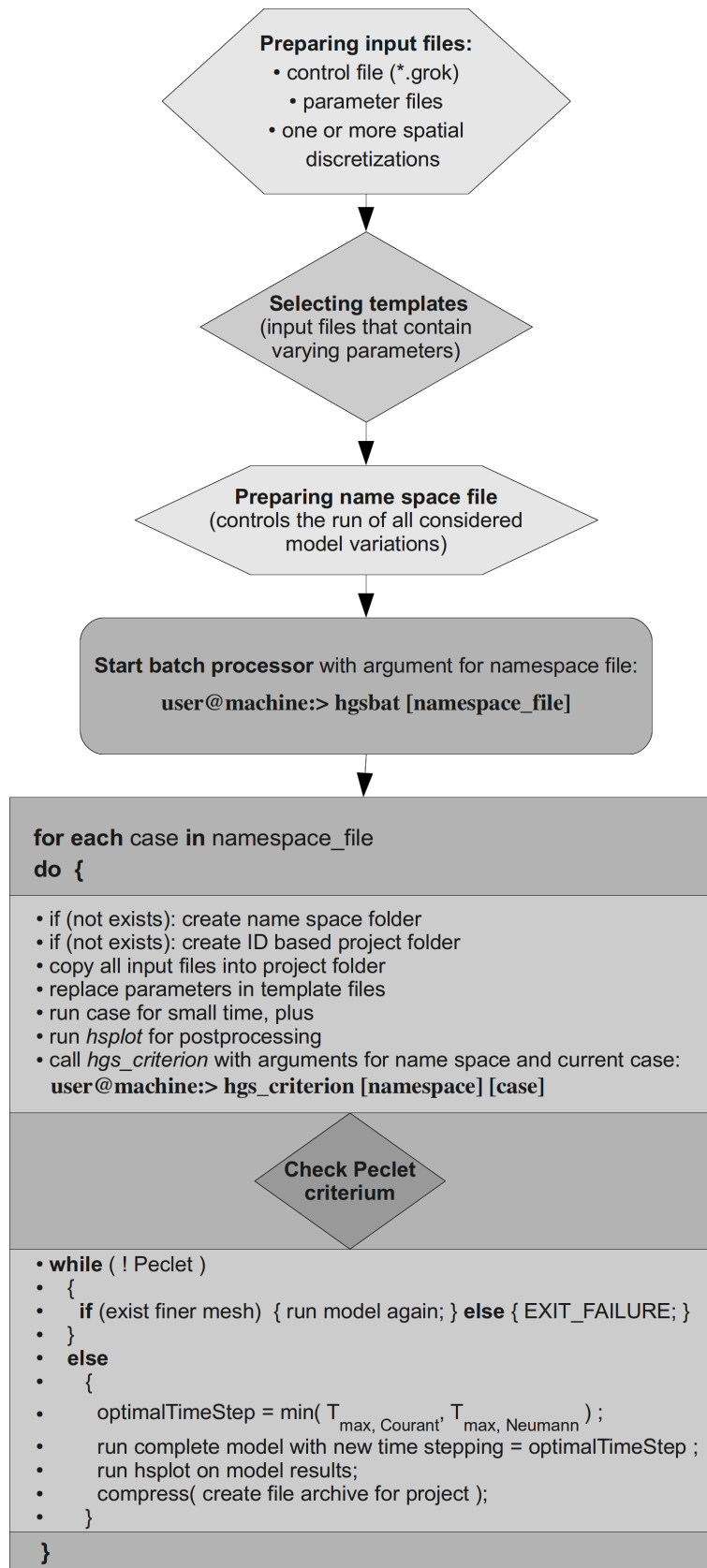
Figure 4.5: General automated workflow for the simulation part of the sensitivity analysis.

time. It also compresses each project to a zipped tar archive, again with respect to the name convention. The latter is specified beforehand in the namespace file. The format of the namespace file was designed to be easily derived from any spread sheet software, to comfortably manage the whole modeling process there. An example for a namespace file to run an arbitrary number of cases is shown in Figure 4.6. The file is structured in sections each starting with a keyword:

- **namespace** - the provided name is assigned to the main folder, in which all case projects are stored. It is further used as prefix for the project file names itself;

- **meshes** - the program *hgs_criterion* may substitute the mesh from the last run with one of the provided mesh files, when necessary. The values after the names of mesh files represent the node distances in x and z direction for a given 2D problem;

- **cases** - limit for major loop: `for( n=0; n<cases; cases++ ) { run case ID }`

- **all files** - files to be copied from the root to the folder of the current case;

- **template** - template file for which parameters must be updated for the current case;

- **vars** - the parameters to be updated correspond to the HydroGeoSphere instructions in the template files;

- **table** - with an arbitrary index of type integer for the current case in the first column and the new parameter values in the following columns (the index provides the second part of the file prefix in each project case)

Thus, the name convention for the directory structure and the project files combine to:

*...any_dir/simulation_root_dir/***namespace/ID/namespace_ID.suffix***.

In the following, this convention could be effectivly exploited to implement the postprocessing scripts using *Bash* shell and *Octave*. According to the namespace and the requested array of case IDs the projects were decompressed and re-compressed afterwards, the model output was read out and saved to more appropriate formats, raw figures were created, and both, the input parameter and the model observations were finally merged into one Octave/Matlab *.m-file to facilitate the interpretation process. In all, the type of name convention has proved to be very effective in terms of automatisation and data management for the whole modeling process.

```
namespace
psa_he4

meshes
2
mesh ../../mesh_20m/aquifer_mesh_20_m_ts 20 20
mesh ../../mesh_15m/aquifer_mesh_15_m_ts 15 15

cases
8

all files
6
batch.pfx
array_sizes.default
prepared_file.grok
matrix.mprops
dualc.dprops
prepared_file.plot.control

template
dual.dprops

vars
2
k anisotropic
longitudinal dispersivity

table
1 5e-4 5e-4 5e-5 15.0
2 5e-4 5e-4 5e-5 30.0
3 5e-3 5e-3 5e-4 15.0
4 5e-3 5e-3 5e-4 30.0
5 5e-4 5e-4 5e-5 15.0
6 5e-4 5e-4 5e-5 30.0
7 5e-3 5e-3 5e-4 15.0
8 5e-3 5e-3 5e-4 30.0

template
matrix.mprops

vars
1
porosity

table
1 0.05
2 0.05
3 0.05
4 0.05
5 0.07
6 0.07
7 0.07
8 0.07
```

Figure 4.6: Example for a namespace file to run an arbitray number of cases.

5 Results

5.1 Jericho - the unconsolidated Plio-Pleistocene to Holocene aquifer

This section will essentially focus on characteristic hydrochemical and isotopic indicators for different sources of salinity based on the data available to this study. As the number of parameters is high, the spatial distribution of sediments, facies, and stratigraphy in the subsurface is poorly known, and the possible chemical interactions in the investigated aquifer are complex, not well studied, and ambiguous with respect to salinization processes, the section is constructed using a sequential chain of evidence approach.

A general assumption for the Shallow Aquifer groundwater of Jericho is that the high salinities especially in the eastern part of Jericho are almost entirely a result of upflow of brines due to heavy groundwater abstraction. The latter is claimed to cause skimming of the freshwater pillow on top of a deeper seated salt water body, which in turn leads to a relevant pressure release and thereby upconing of brines. Other salinization processes frequently suggested refer to a contribution from water-rock interaction, or infiltration of waste water, and agricultural return flow (e.g. [141]). Both may overlap. In the following it will be discussed, how salinization by water-rock interaction can be distinguished from brine admixture, and which arguments speak in favour for or would modify the above assumptions.

5.1.1 Distribution of $\delta^2 H$ and $\delta^{18} O$

The δ^2H/δ^{18}O (H$_2$O) isotope pattern in the Jericho area resembles the groundwater signature of the Mountain Aquifer. Figure 5.1 plots all samples into one chart with different symbols related to the sampling season.

The relative high excess in deuterium in the Eastern Mediterranean region compared to the global isotope pattern in precipitation is related to the Mediterranean Sea itself, since it is a rather closed marine basin with elevated temperatures and lower humidity in the air compared to the open ocean. This causes enhanced kinetic fractionation during evaporation. However, the two isotopes are not suited to prove or disprove mixing with CaCl brines. [124] estimated, that for instance the δ^{18}O signature of Lake Lisan reached maximal values of approximately 7 ‰. Model mixing of Lisan brine (Cl $\approx$ 120000 mg/L) with fresh mountain water (Cl $\approx$ 30 mg/L, δ^{18}O $\approx$ -5.8 ‰) to reach the salinity level of well 19-14/067 (Cl = 1862 mg/L) requires a mixing ratio of 0.015 : 0.985 and would yield a δ^{18}O value of $\approx$ -5.6 ‰. Indeed the samples with the highest Cl concentrations do not distinctly differ from the less saline samples. On the contrary, evaporation is expected to have a

stronger effect on groundwater $\delta^{18}O$ if for instance wadi runoff or contribution of seepage water from the numerous water storage pools and the open canal system in the valley is considered. Depending on the interpretation the data further show either an apparent oscillating deuterium excess between the dry season and spring or a general decrease with time. The first would assume a distinct seasonal effect whos cause is still not easy to explain. [121] interprets the effect according to [58] and [105] as a result of ultrafiltration where the clays act similar like semi-permeable membranes. However, one has to take into account the setup of the experiment of [58], as they applied a water pressure drop of 100 bar and a pressure of 330 bar acting on a few centimeters thick clay disc. Ultrafiltration is one of the processes that produce residual brines in oil shales and is a commonly applied technical desalinization technology. The conditions in the Shallow Aquifer of Jericho are dissimilar to that. With respect to the natural conditions there molecular diffusion seems to be the more likely prevailing process in clay layers. For pure molecular diffusion the slope between $\delta^{18}O$ and δ^2H is ≈ 0.5, and in the ultrafiltration experiments ≈ 3.1. Another theoretical explanation for the oscillating deuterium excesses would be that the well water signature in spring is directly related to the winter runoff that should more correlate to the intensive winter storms in the mountains at cooler temperatures. Consequently this would result in a lower average $\delta^{18}O$ signature as shown by [22], while isotopic enrichment due to evaporation would shift the $\delta^2H/\delta^{18}O$ ratio along a line of a slope less then 8, depending on the ambient humidity downstream in the Wadis. In turn, it would further imply that the isotope pattern between summer and winter reflects the groundwater of the Judea Group Aquifer. However, it is not clear, whether the infiltrating winter runoff could reach the wells within that short time to produce a seasonal effect. Similar to the assumption of a seasonal oscillation of the deuterium excess, the interpretation in terms of a general decrease with time between summer 2003 and spring 2005 is hampered too. Unfortunately no measurements are available for the time between summer 2004 and winter 2004/2005 to give more weight to one or the other interpretation.

5.1.2 Hydrochemical tracing of salinization

All hydrochemical data are presented in Table 5.1 and Table 5.2 except for a few data from sources that are not located inside the study area. For them the literature sources are given instead in the respective table or figure descriptions. As a first assumption, the hydrochemistry in the Shallow Aquifer system of Jericho may be characterised and controlled by the fresh waters originating from the Mountain Aquifer, by waste water of different quality, by upflowing brines, as well as by water-rock interaction in Samra and Lisan formations. Lisan formation embodies an important potential supplier of sulfate and other water soluble salts. For instance [114] found that at the Massada site, some fifty kilometres S of Jericho, the Lisan aragonite layers contain about 50 mg TSS/g (milligram of total water soluble salts per gram of soil) and the detrital layers about 140 mg TSS/g (Lower Lisan). Since on the one hand those water soluble salts obey – except for sulfate – a similar elemental signature like CaCl brines, which are found in the greater vicinity of the Dead Sea, a clear discrimination of both end members is hampered.

Table 5.1: Hydrochemistry of the samples. The sources are: (1) - this study, (2) - data from [121], [120]. Since for source group 2 the sampling dates were given as 'October to November, 2003' the date format '10./11.2003' was used in the table. The spatial coordinates are given as New Israeli Grid.

Object	East	North	Source	Date	Na	K	Ca	Mg	Sr	Cl	Br	SO4	HCO3	NO3	B	$\delta^{34}S$	Group
										meq/L							
Ein Dyouk	240050	644660	2	10./11.2003	1.01	0.06	4.00	2.45	0.003	0.98	0.006	0.35	4.84	0.47	0.0043	6	spring
Ein Sultan	242200	641950	2	10./11.2003	0.99	0.06	3.88	2.47	0.003	0.97	0.013	0.36	4.71	0.68	0.0043	8.7	spring
19-14/026A	242573	641834	2	10./11.2003	2.81	0.16	5.78	5.28	0.012	3.41	0.021	0.47	7.17	0.26	0.1032	10	well, G1
19-14/038	243450	642530	2	10./11.2003	7.66	0.50	6.28	8.40	0.027	15.45	0.077	0.82	6.23	0.12	0.2448	5.9	well, G1
19-14/038	243450	642530	1	12/09/2003	7.22	0.49	6.00	8.00		14.00		1.10	7.50	0.15			well, G1
19-14/062	243380	642630	2	10./11.2003	10.00	0.62	6.90	9.04	0.027	20.56	0.109	0.85	5.97	0.08	0.2456	6.7	well, G1
19-13/069	246950	639250	2	10./11.2003	20.01	2.04	5.72	11.52	0.045	33.09	0.137	2.16	6.86	0.40	0.6810	3.8	well, G1
19-14/052	245680	640980	2	10./11.2003	13.06	0.92	5.98	10.23	0.065	23.44	0.091	1.50	6.23	0.55	0.4125	12.5	well, G1
19-14/067	247010	640560	2	10./11.2003	27.79	2.66	8.20	18.17	0.065	52.52	0.176	3.82	6.01	0.63	1.0990	-2.2	well, G1
19-14/073	247030	641050	2	10./11.2003	15.63	2.04	6.29	13.54	0.042	31.73	0.096	2.00	6.65	0.65	0.8101	6	well, G1
19-14/067	247010	640560	1	01/12/2004	40.81	2.99	8.68	20.51		68.37		3.96	7.40	0.89			well, G1
19-14/020	246490	641020	1	01/12/2004	17.67	2.34	6.36	14.87		42.01		3.24	8.00	0.99			well, G1
19-14/003	243830	641550	1	07/06/2003	12.35	0.87	7.96	9.43		23.78		1.08	6.80	0.15			well, G1
19-14/073	247030	641050	1	01/12/2004	20.64	2.14	6.56	13.31		38.03		2.97	7.60	0.88			well, G1
19-13/069	246950	639250	1	01/12/2004	26.89	2.18	5.19	11.72		29.33		2.25	8.30	0.44			well, G1
19-13/015	246100	639510	2	10./11.2003	9.33	0.98	4.88	8.34	0.040	15.63	0.067	1.27	6.21	0.54	0.3963	9.7	well, G2
19-13/015	246100	639510	1	01/12/2004	11.57	0.85	2.79	6.84		13.91		1.13	7.40	0.53			well, G2
19-13/050A	245810	639380	1	01/12/2004	9.54	0.85	2.63	6.72		12.76		1.78	7.30	0.66			well, G2
19-14/015	245670	640530	1	01/12/2004	10.32	0.47	6.05	10.52		15.64		1.46	9.50	0.93			well, G2
19-13/006	245500	639580	2	10./11.2003	6.90	0.20	8.50	7.69	0.081	12.68	0.031	2.45	6.17	1.17	0.2596	3.5	well, G2
19-13/020	244320	639480	2	10./11.2003	6.45	0.44	4.51	6.04	0.037	7.82	0.031	2.29	5.73	0.80	0.3426	3.6	well, G2
19-13/020	244320	639480	1	07/06/2003	4.22	0.63	3.89	5.03		7.29		2.10	5.60	0.38			well, G2
19-13/047	244850	639880	2	10./11.2003	5.06	0.32	4.59	5.48	0.049	6.53	0.028	1.61	5.70	0.71	0.2224	6.9	well, G2
19-13/048	245310	639660	2	10./11.2003	4.94	0.39	4.49	5.75	0.046	6.95	0.031	1.46	5.82	0.67	0.2136	5.7	well, G2
19-13/052	245880	639670	2	10./11.2003	9.02	0.72	6.26	9.37	0.082	16.65	0.052	3.46	6.05	0.75	0.4126	-5.9	well, G2
19-14/012	245380	640010	2	10./11.2003	4.01	0.29	4.33	5.21	0.043	5.26	0.024	1.23	6.85	0.65	0.1734	4.6	well, G2
19-13/006	245500	639580	1	01/12/2004	11.57	0.20	10.02	6.80		18.21		3.89	7.20	1.22			well, G2
19-13/026A	245600	638456	1	01/12/2004	17.83	0.97	6.37	8.48		21.39		4.69	7.40	0.92			well, G2
19-14/023	245040	640240	1	01/12/2004	6.10	0.36	5.03	5.88		7.66		1.07	8.50	1.41			well, G2
19-14/066	247310	640660	2	10./11.2003	25.10	2.11	9.12	17.58	0.081	45.53	0.197	6.27	7.20	0.48	0.8975	-9.7	well, G2
19-13/052	245880	639670	1	01/12/2004	17.67	0.85	8.96	14.15		28.93		6.48	6.50	0.99			well, G2
19-14/019	246460	640500	1	01/12/2004	17.04	1.45	11.30	15.87		27.61		7.66	8.00	1.15		-7.2	well, G2
19-14/066	247310	640660	1	01/12/2004	34.87	2.30	9.16	15.51		47.72		7.99	9.70	0.72			well, G2
19-13/026A	245600	638456	2	10./11.2003	4.56	0.43	6.37	8.03	0.092	12.44	0.031	1.86	4.25	1.13	0.0639	-5.1	well, G2

Table 5.2: Element ratios of the samples. The sources are: (1) - this study, (2) - data from [121], [120]. Since for source group 2 the sampling dates were given as 'October to November, 2003' the date format '10./11.2003' was used in the table.

Object	Source	Date	SO4/Cl	Na/Cl	Br/Cl	B/Cl	Group
			meq ratio				
Ein Dyouk	2	10./11.2003	0.351	1.023	0.0064	0.0044	spring
Ein Sultan	2	10./11.2003	0.367	1.023	0.0129	0.0044	spring
19-14/026A	2	10./11.2003	0.138	0.823	0.0063	0.0302	well, G1
19-14/038	2	10./11.2003	0.053	0.495	0.0050	0.0158	well, G1
19-14/038	1	12/09/2003		0.516			well, G1
19-14/062	2	10./11.2003	0.041	0.486	0.0053	0.0119	well, G1
19-13/069	2	10./11.2003	0.065	0.605	0.0041	0.0206	well, G1
19-14/052	2	10./11.2003	0.064	0.557	0.0039	0.0176	well, G1
19-14/067	2	10./11.2003	0.073	0.529	0.0034	0.0209	well, G1
19-14/073	2	10./11.2003	0.063	0.492	0.0030	0.0255	well, G1
19-14/067	1	01/12/2004	0.058	0.597			well, G1
19-14/020	1	01/12/2004	0.077	0.421			well, G1
19-14/003	1	07/06/2003		0.519			well, G1
19-14/073	1	01/12/2004	0.078	0.543			well, G1
19-13/069	1	01/12/2004	0.077	0.917			well, G1
19-13/015	2	10./11.2003	0.081	0.597	0.0043	0.0254	well, G2
19-13/015	1	01/12/2004	0.081	0.832			well, G2
19-13/050A	1	01/12/2004	0.139	0.747			well, G2
19-14/015	1	01/12/2004	0.093	0.660			well, G2
19-13/006	2	10./11.2003	0.193	0.544	0.0025	0.0205	well, G2
19-13/020	2	10./11.2003	0.293	0.825	0.0040	0.0438	well, G2
19-13/020	1	07/06/2003	0.288	0.579			well, G2
19-13/047	2	10./11.2003	0.246	0.775	0.0042	0.0341	well, G2
19-13/048	2	10./11.2003	0.210	0.711	0.0045	0.0307	well, G2
19-13/052	2	10./11.2003	0.208	0.542	0.0031	0.0248	well, G2
19-14/012	2	10./11.2003	0.234	0.763	0.0045	0.0330	well, G2
19-13/006	1	01/12/2004	0.213	0.635			well, G2
19-13/026A	1	01/12/2004	0.219	0.833			well, G2
19-14/023	1	01/12/2004	0.139	0.796			well, G2
19-14/066	2	10./11.2003	0.138	0.551	0.0043	0.0197	well, G2
19-13/052	1	01/12/2004	0.224	0.611			well, G2
19-14/019	1	01/12/2004	0.278	0.617			well, G2
19-14/066	1	01/12/2004	0.167	0.731			well, G2
19-13/026A	2	10./11.2003	0.150	0.366	0.0025	0.0051	well, G2
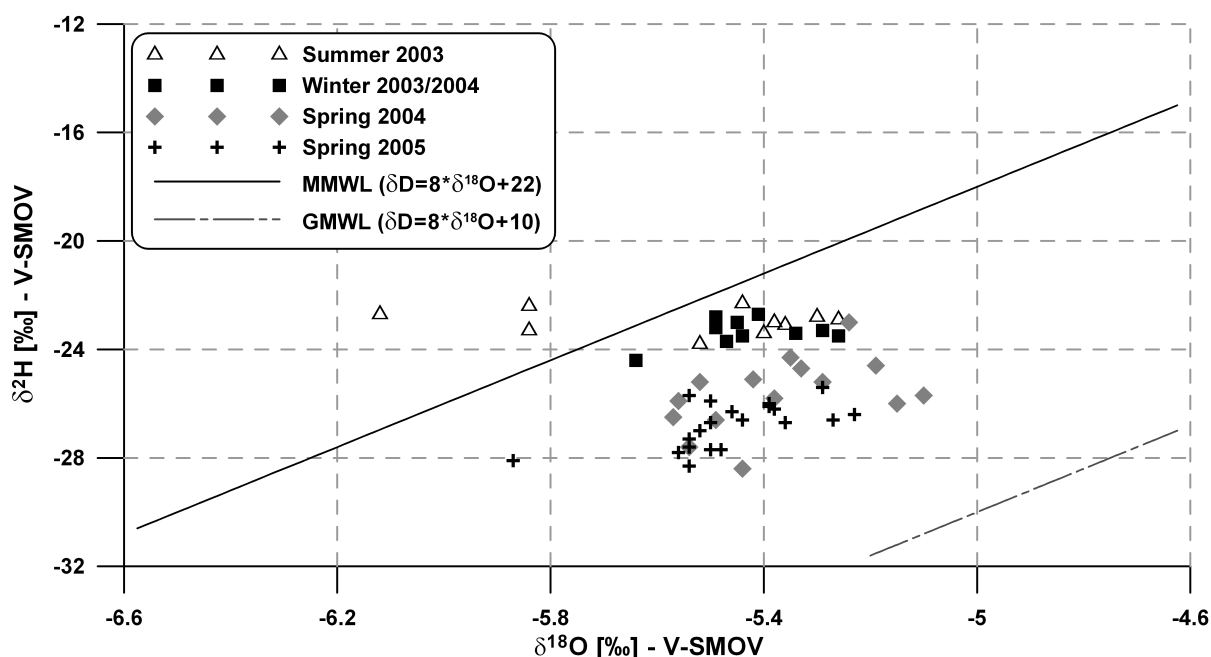
Figure 5.1: $\delta^{18}O$ and δ^2H distribution of groundwater from the Shallow Aquifer, Jericho area (MMWL – Mediterranian Meteoric Water Line, GMWL – Global Meteoric Water Line). The bulk hydrogen and oxygen isotopic signature of groundwater from wells in the Herodion and Ein Samia well fields of the Eastern Basin of the Mountain Aquifer range between -6.0 and -5.5 ‰ in $\delta^{18}O$ and -22.5 and -28 ‰ in δ^2H (compare Figure 5.35 and Figure 5.35).

Sulfate and chloride

On the other hand SO_4/Cl ratios of CaCl brines in general are very low in opposite to mountain derived groundwaters that have a comparatively low salinity.

Therefore the SO_4/Cl ratio appeared to be a potential first approach to group the samples. Because it is obvious that an assumed fresh mountain groundwater, which initially and exclusively mixes with a Ca/Cl brine could take up considerable amounts of sulfate while passing sediments rich in gypsum like the Lisan formation, one can at least clearly identify another group of samples, which is not or only slightly affected by sulfate uptake. In turn, for the complement group this creates a working point to test and discuss arguments concerning the open questions with regard to the two potential paths the observed salinization processes are assumen to follow:

- only mixing of fresh and brine water as well as sulfate uptake by dissolution of gypsum from the Lisan Formation;

- at least part of the salt load is directly derived from the Lisan Formation.

Figure 5.2 shows how SO_4 and Cl are distributed in the samples and indicates that the distinction of two sample groups (G1, G2) according to their SO_4/Cl ratios is appropriate.
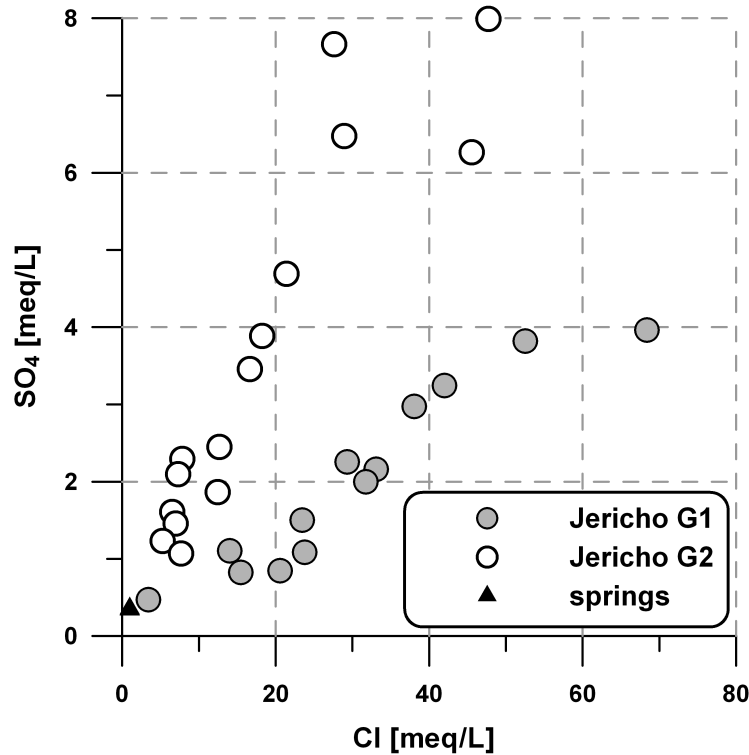
Figure 5.2: Scatter plot showing the distribution of SO_4 and Cl in samples from group 1 and group 2 (G1, G2) as well as from the local springs.

The mean ratios of G1 and G2 are 0.065 and 0.213, respectively. Samples from an intermediate range of the SO_4/Cl ratio (0.08 to 0.14) were not used for the calculation. Even so, these samples are assigned to G2, and are assigned on the map of Fig. 2 to an intermediate group "G2(..G1)". They are limited to lower SO_4 levels of up to 1.78 meq/L and Cl concentrations < 16 meq/L. The locations of the sampled wells according to their grouping are given in Figure 2.4 showing that their distribution is not random. With respect to that grouping of the wells one may notice that many wells of group G2 cluster in the vicinity of Wadi Qilt (Figure 2.4), which suggests a special relation between the two. Substracting two pressure head maps from [222] between autumn 1991 and spring 1992 from each other reveals that the biggest differences in pressure head rather were observed in wells more south in the vicinity of Wadi Qilt (Figure 5.3). This clearly points to a considerable amount of wadi runoff that infiltrates during the rainy season along Wadi Qilt, which is in agreement with the statements made in subsection 2.2.1. It is further likely that along the course of Wadi Qilt higher hydraulic conductivities prevail.

Sodium and chloride

The Na/Cl distribution reveals an apparent bimodality (Figure 5.4a). Less saline water samples fall onto the peak with high Na/Cl ratios. With increasing Cl contents the ratio tends to converge against 0.5 to 0.6, for which two possible explanations apply: (1)
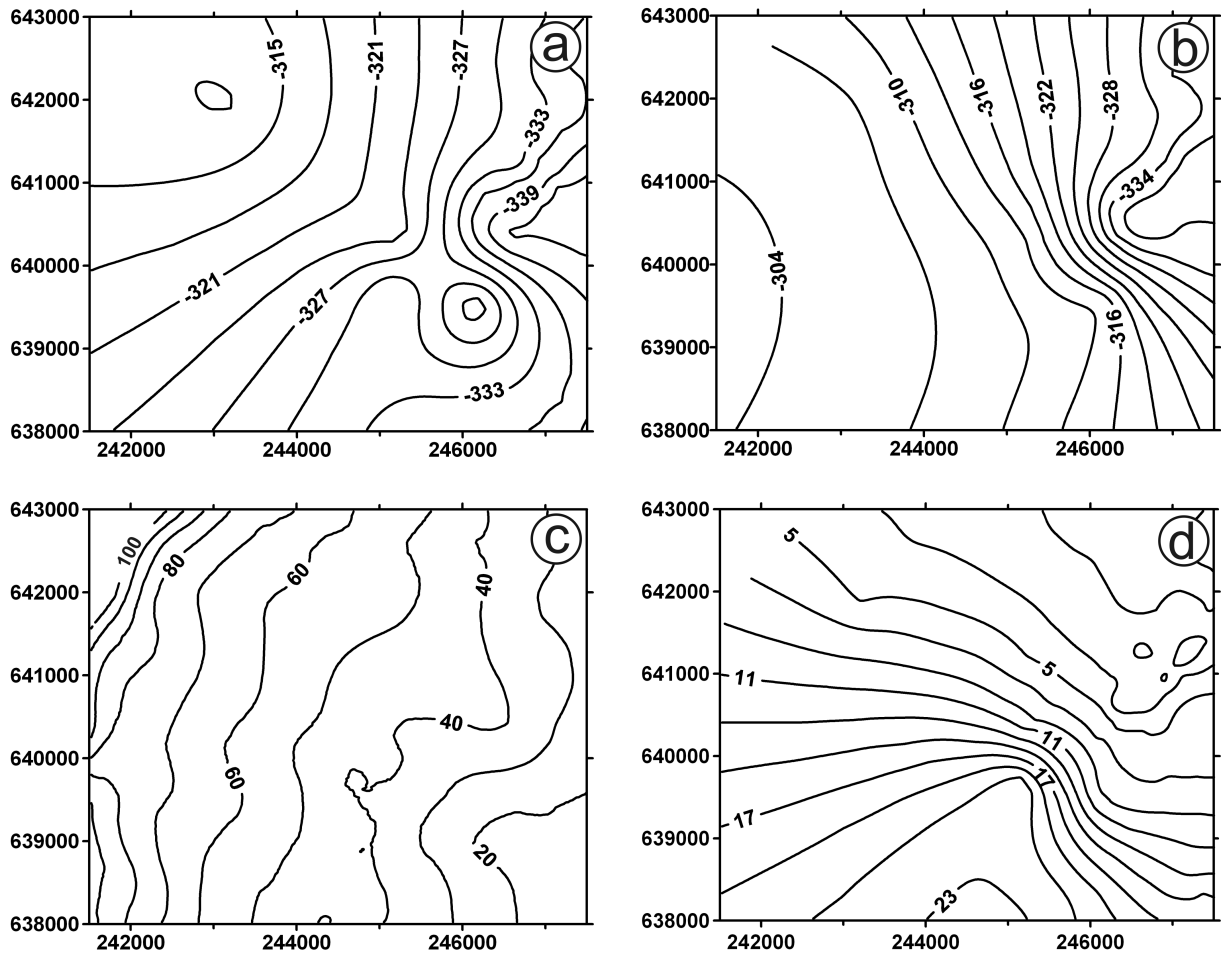
Figure 5.3: Maps modified after [222]: (a) Pressure head distribution in autumn 1991; (b) Pressure head distribution in spring 1992; (c) Mean groundwater level below ground level as taken from (a) and (b); (d) Pressure head difference between autumn 1991 and spring 1992 as taken from from (a) and (b).

Mixture of high Na/Cl water (fresh/sewage sources) with a small fraction of CaCl brine, because such brines have Na/Cl ratios below 0.5; (2) The mentioned range of 0.5..0.6 also mimics the usual ratio of Lisan Formation porewater [18], [114], [180].

Nitrate, bromide, boron, strontium, δ^{34}S of sulfate, and chloride

Salinization in the Jericho area might also be promoted by anthropogenic activities like infiltration of waste water effluents, dissolution of soil precipitates and leaching of sediments in the unsaturated zone. Since the Jericho area is intensively agriculturally used, nitrate can serve as an indicator for percolation water reaching the saturated zone. The samples generally are characterized by high nitrate levels of up to 80 mg/L and a mean of 41.9 mg/L (data set available to the study). One case of waste water disposal by tank trucks has been observed during the sampling. Because, as mentioned above, Jericho

69
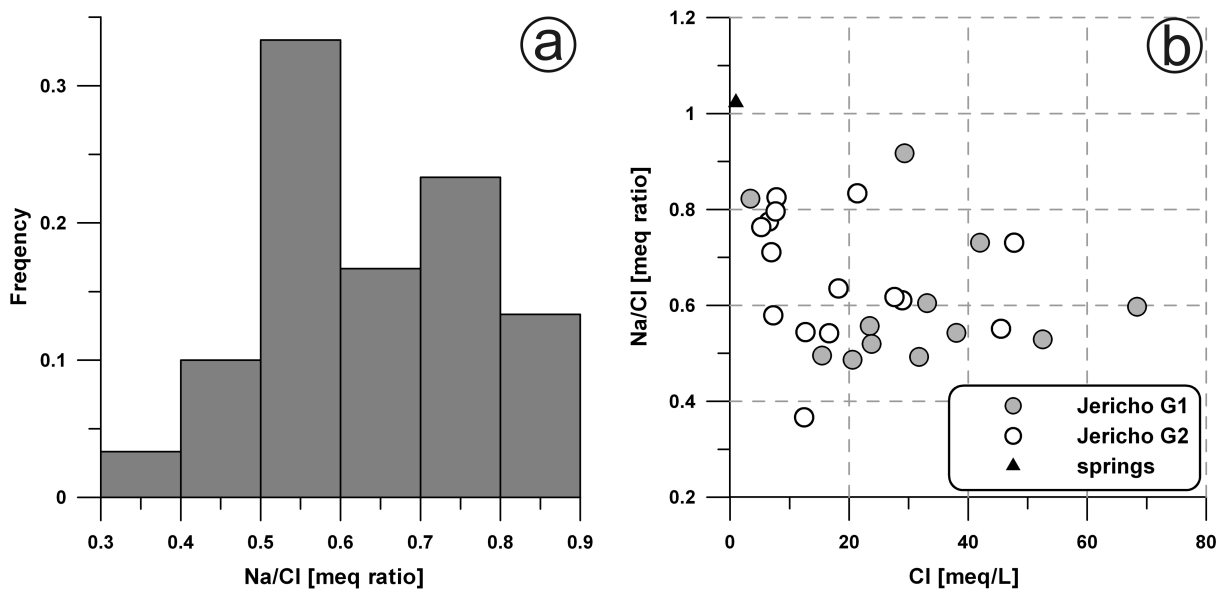
Figure 5.4: (a) Frequency distribution of the Na/Cl ratio of all samples. (b) Scatter plot relating the Na/Cl ratio to the Cl concentration of the same samples. The group membership of the samples is indicated.

lacks appropriate waste water treatment facilities, this should be considered as a probable, common practice rather than an individual case. With respect to waste water disposal into Wadis Jericho is not an exception for an urgent problem in many places of the West Bank. However, the situation has improved in recent years due to a higher awareness about waste water disposal and resulting, probable long term effects on the groundwater sources.

A main nitrate contribution nowadays comes from the major springs itself. For example concentrations in Ein Sultan since the 1980's have risen by a rate of $\approx$ 1.36 mg/L per year, in 2004 reaching the preventive action limit of 50 mg/L defined by World Health Organisation. Because nitrate concentrations drop after the rainy season by about 25 to 33 % it is very likely that nitrate is derived through rapid infiltration of contaminated surface water upstream in the wadis and rapid transport through karst networks to the springs. The expected sources are dumping of waste water into wadis by tank trucks, more or less continuous waste water streams and related deposits as well as infiltration from waste water irrigated soils. Indeed, the springs especially in the wet season discharge a higher amount of young groundwater components [127]. Whatever the souce may be, there is strong indication that water can percolates through the unsaturated zone. Thus infiltration is a potential driving mechanism for groundwater salinization, because it may transport water soluble salts from the soil into the groundwater and it may leach Lisan sediments as well. In order to better understand the processes occurring in the groundwater and soil, trace elements were analyzed and interpreted.

Usually NO_3^- is introduced in agricultural areas by mineral and organic fertilizers, as well as manure and waste water. The only parameters obviously correlating to NO_3^- at the

study site are Sr ($r_{NO_3^-,Sr} = 0.71$), Sr/Ca, Sr/Mg, as wells as Br/Cl ($r_{NO_3^-,Br/Cl} = 0.78$). Br/Cl is a good indicator for different sources or processes like effluents or water-rock interaction and salinization, respectively when it diverges from the ratio of sea water ($\approx$ 1.5..1.7 ‰ – equivalent ratio). Both, the high Br/Cl ratio and the high NO_3^- concentrations in the springs exhibit contribution from effluents upstream in the Wadis as has been described earlier. The distribution of the sample groups in Figure 5.5 indicates at least a three component mixing between a fresh water member that reflects the ratio of sea water, water that is affected by effluents, and water that represents mixing with brine. But also water-rock interaction may lower the Br/Cl ratio as a result of halite dissolution
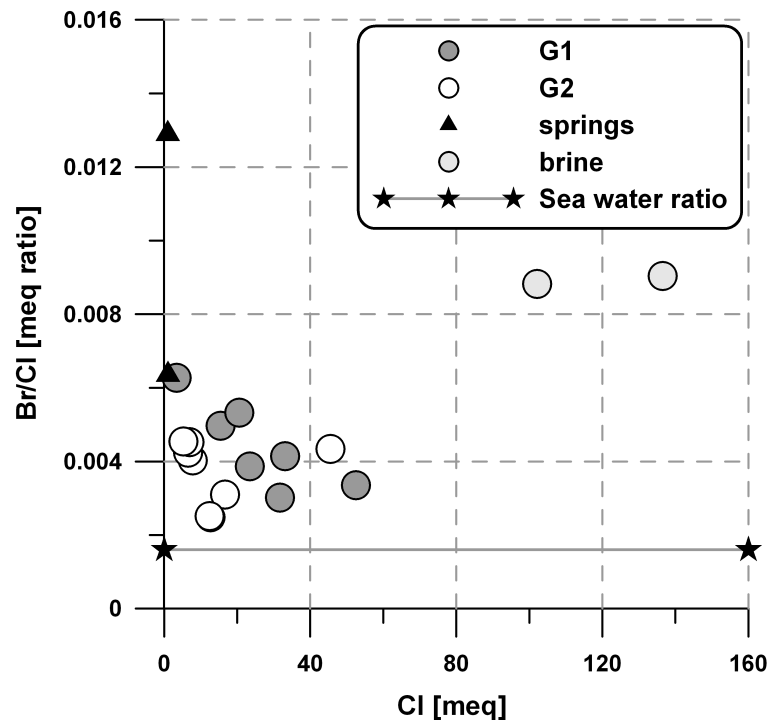
Figure 5.5: Scatter plot showing the distribution of the Br/Cl ratio with respect to Cl concentrations.

in the Lisan formation or mixing with remnant Lisan formation water. But since Br/Cl has a good correlation with NO_3^-, flushing of soil precipitates by agricultural return flow could have an additional effect. In Figure 5.6 Sr/Ca is plotted against Br/Cl. The sample with the lowest Br/Cl and highest Sr/Ca ratios together with a high NO_3^- load, and the lowest Na/Cl ratio of all samples (0.37) at well 19-13/026A could be related to a small iron factory, where according to [121] high amounts of $NaNO_3$ are used in the manfacturing process. If this is the case then the Na footprint was completely altered by the brine Na/Cl signature. But without analyses of such effluents this source can not be rated. Samples with the highest Sr/Ca ratios are assumed, however, to represent enhanced water-rock interaction with the aquifer material, namely dissolution of aragonite, calcite, and gypsum. Again, this would be a pointer to corrosive infiltration waters, like effluents, which is confirmed by a positive correlation to NO_3^-.

Sources and processes for increased concentrations of Sr in Jericho can be summarized as follows:

1. Sr is a valid candidate for tracing water-rock interaction by means of mineral dissolution where percolation waters or groundwaters pass the Lisan formation. For instance, dissolution of Lisan aragonites should be reflected by increasing Sr/Ca ratios since they contain up to 7700 ppm Sr [115], [196].

2. Another likely process is the Sr release due to transformation (recrystallization) of aragonite to calcite ([113], [226]).

3. A third potential Sr source may be provided through the application of mineral - especially phosphorous fertilizers where it can be an important part of the impurities ([149], [39]). Unfortunately phosphate as a cross check is unavailable because it gets fixed in calcareous dominated soils.

In Figure 5.6 the Sr/Ca ratios are cross-plotted together with (a) the Br/Cl ratios and (b) the sulfate concentrations. Both diagrams include typical CaCl brine samples from
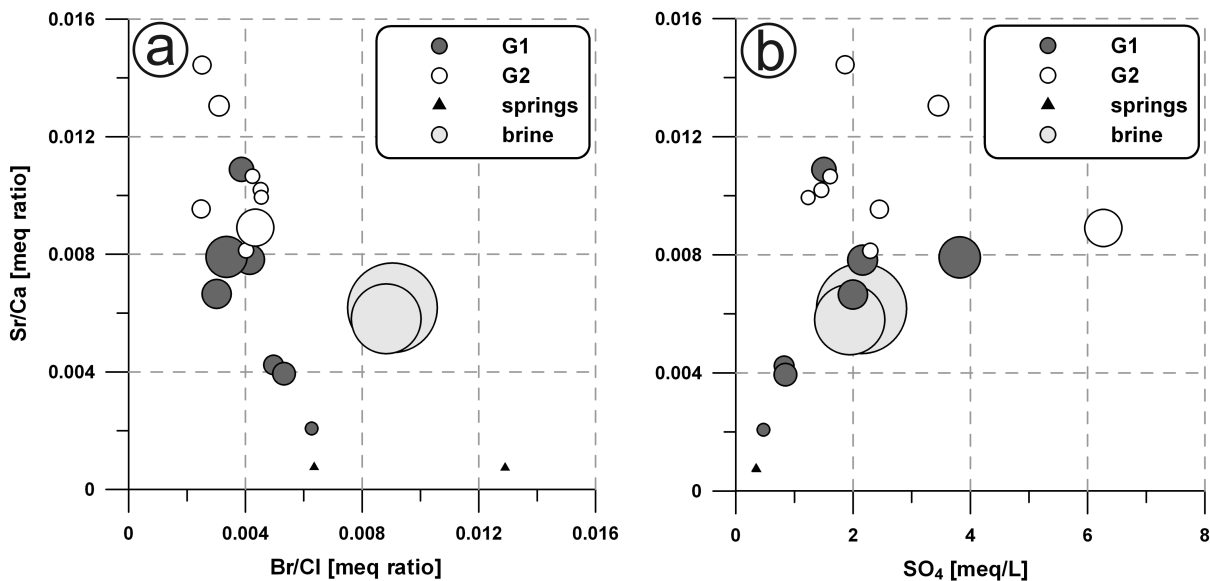
Figure 5.6: (a) Sr/Ca vs. Br/Cl in samples of groups G1 and G2, the local springs, and brines. The symbol size indicates relative Cl concentration. Brine data were obtained from [123]. (b) Sr/Ca vs. SO_4^{2-} in samples of groups G1 and G2, the local springs, and brines. The symbol size indicates relative Cl concentration. Again, brine data were obtained from [123].

springs NW of the Dead Sea [123]. Whereas in Figure 5.6a the degree of anthropogenic deterioration is depicted, Figure 5.6b exposes how this process is related to the sulfate content of the samples. Relative Cl concentrations are indicated by the size of the symbols. What can be taken from the figures is that the Sr/Ca ratio ranges between less then 0.001

in the springs and 0.014, whereas samples with the highest salinities cluster around a ratio of about 0.008. By comparing the latter with the two plotted CaCl brine samples it is shown, that the ratios of the CaCl brines plot around 0.006, and a ratio of 0.008 is likely to be related to water-rock interaction, very probably in connection with Lisan Formation. Both CaCl brine samples also have a significant lower SO_4/Cl ratio than the Jericho samples with the highest salinities. Additionally, the previously made assumption is supported that the SO_4/Cl ratio could be a good indicator for admixture of CaCl brines, even though it is not sufficient. It is obvious, however, that the difference between both, the CaCl brine Sr/Ca ratio and the suggested Sr/Ca ratio from water-rock interaction is not very large and therefore insufficient to value the individual impacts of the two processes on salinization. It has to be noted that the Sr/Ca ratio of the CaCl brine samples already represents a mixture between pure brine and freshwater from the Mountain Aquifer. With increasing salinity these brines would also adopt a Sr/Ca ratio of about 0.008. However, groundwater in the Shallow Aquifer is far from being saline.

If one consideres the surplus in sulfate especially in the G2 samples to be controlled to a great extend by water-rock interaction in the Lisan Formation, then this should be reflected by the $\delta^{34}S(SO_4^{2-})$ signature. All samples are undersaturated with respect to gypsum ($SI_{gypsum} < -1.0$). The sulfur isotope pattern of sulfate clearly indicates that the dominant source is considerably depleted in $\delta^{34}S(SO_4^{2-})$ as shown in Figure 5.7. A similar
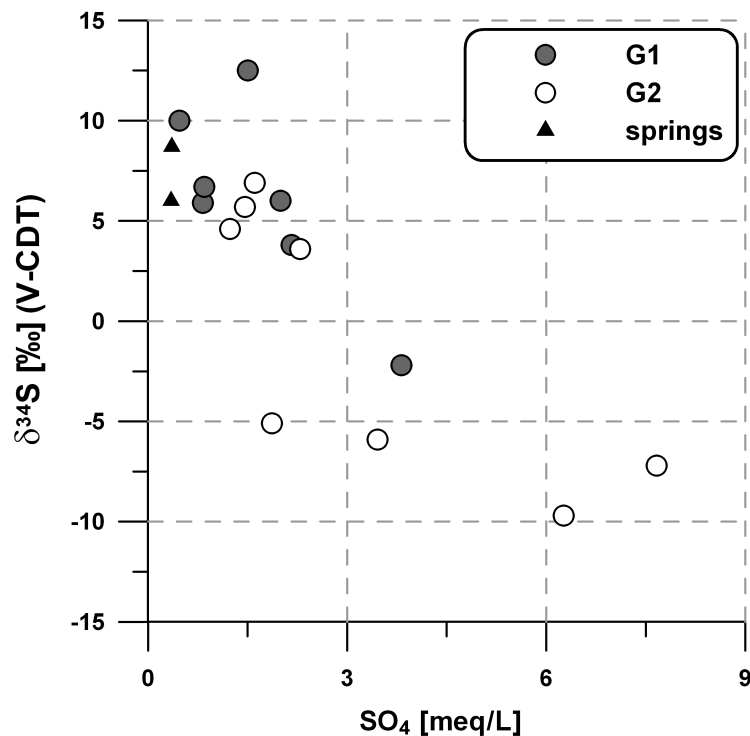
Figure 5.7: $\delta^{34}S(SO_4^{2-})$ vs. SO_4^{2-} in samples of groups G1 and G2 as well as the springs.

trend seems also valid for the G1 samples. But whereas for G2 the depletion of $\delta^{34}S(SO_4^{2-})$ clearly coincides with an increase in Cl concentrations this can not be shown for G1. Only the sample from well 19-14/067, which is situated in the east of the study area, has both,

the highest salinity as well as the lowest $\delta^{34}\text{S}(\text{SO}_4^{2-})$ signature of G1. These observations support the possibility that Lisan formation significantly contributes to salinity, which would be more pronounced in the easternmost wells. They further rule out CaCl brines as the sulfate source, because all known brines in the area exhibit a strongly enriched signature [83]. As has been stated earlier, that in the Lisan Formation disseminated gypsum is the only verified depleted source. However, although metal sulfides in Lisan sediments have not been found in accessible outcrops they are supposedly preserved in presence of interstitial porewater. Both, dissolution of authigenic secondary gypsum and pyrite oxidation result in decreasing $\delta^{34}S$ values. Unfortunately it is impossible to verify the latter process since measured Fe_{total} concentrations in solution in the Shallow Aquifer groundwaters are very low [121], probably because of the carbonate buffered soil (pH $\approx$ 7). Beside gypsum dissolution and pyrite oxidation a third process of H_2S generation by microorganisms from sulfate and organic matter and its back-transformation to SO_4^{2-} under oxic conditions could be possible as well. It is also uncertain, how the described individual processes would modify the Sr/Ca ratio. However, from the $\delta^{34}\text{S}(\text{SO}_4^{2-})$ signature of the samples the main conclusion can be derived that salinization by water-rock interaction is not implausible. It becomes more likely in the easternmost wells of the Jericho area.

The assumption that leaching could represent a major source at least for the eastward increasing sulfate load is supported by boron concentrations since both parameter strongly correlate in G1 as well as G2. [210] showed that the boron adsorption onto the detrital clay fraction of sediments in hypersaline environments indeed can be very effective. However, boron is also a trace supplement of inorganic fertilizers. In Figure 5.8a the $\text{B/Cl} - \text{Na/Cl}$ scatter plot compares samples from this study with brine and freshwater sources related to the Mountain Aquifer. On the one hand, less saline water samples from this study having relevant nitrate concentrations are associated with high Na/Cl and B/Cl ratios. On the other hand samples from wells located near the border fault and remote to Wadi Qilt, i.e. in the northwest of the study area, reveal moderate salinities (TDS between 1000 and 2000 mg/L) but significantly low B/Cl and Na/Cl ratios. It becomes very likely that these wells produce water which represents a mixture of a major fresh and a minor brine component. This fact supports the general assumption that brines, which occur elsewhere along the western border fault, contribute to a certain amount to the groundwater of the Shallow Aquifer of Jericho. The sample that was taken in October/November of 2003 from well 19-13/026A has an odd position in the $\text{B/Cl} - \text{Na/Cl}$ scatter plot. If this position would represent mixing with the indicated potential brine end members a much higher salinity would be expected. Therefore this sample again should be handled with care because the hydrochemistry is assumed to be affected by effluents from the iron factory site. Well 19-13/026A however is situated next to Wadi Qilt, an area potentially highly susceptible to surface infiltration. By reverting to the other samples the question arises whether brine supply might be limited to the border fault zone, because the initial $\text{B/Cl} - \text{Na/Cl}$ and $\text{B/Cl} - \text{Cl}$ pattern becomes completely masked to the east by the infiltration waters as well as probably by the Lisan signature as indicated in Figure 5.8b.
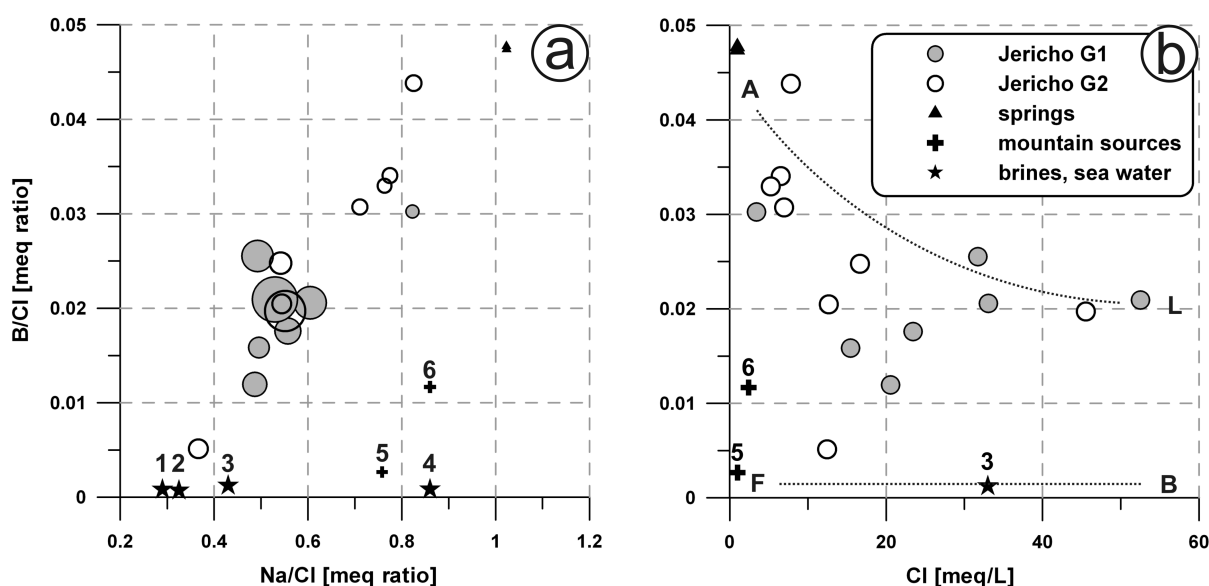
Figure 5.8: (a) $B/Cl - Na/Cl$ scatter plot including wells from the Shallow Aquifer, the local springs, as well as other sources in the area (1 – Dead Sea, 2 – Hamme Mazor (hot spring), 3 – Ein Feshka, 4 – sea water, 5 – Modi'in 4 (deep freshwater well, Mountain Aquifer), 6 – Ein David (freshwater spring W of the Dead Sea). The symbol size indicates chloride concentrations. Data from these other sources in the area were obtained from [210]. (b) $B/Cl - Cl$ scatter plot including the Jericho Shallow Aquifer wells, the local springs, as well as other sources: Modi'in 4 (deep freshwater well, Mountain Aquifer), 6 - Ein David (freshwater spring W of the Dead Sea). Again, data from the other sources in the area were obtained from [210]. End members assigned to the letter index: A – anthropogenically affected (e.g. by effluents), L – Lisan Formation signature, F – anthropogenically unaffected freshwater, B – brine signature.

5.1.3 Noble gases

Due to the chemical inertness of noble gases their evaluation was seperated from subsection 5.1.2. The application of noble gas tracers like helium is a powerful complementary tool to trace processes related to mixing and salinization, deep circulating systems, paleoinfiltration, mantle degassing along fracture systems, or to estimate groundwater age. In his pioneering publication of 1972 [143], Mazor, who was the first to sample springs and wells along the Jordan Valley for noble gases with the intention of using them as climate proxy in terms of paleotemperatures found in contrast to the other analysed noble gases Ne, Ar, Kr, and Xe remarkable helium excess concentrations at many locations, that were subsequently explained by the addition of helium from radiogenic production and by mantle contribution. To recall, the initial noble gas concentrations of groundwaters are set at equilibrium conditions between surface water and atmosphere, which consequently specifies the isotopic ratios of the considered noble gases. The atmospheric ratio of $^3He/^4He$ is

$R_a = 1.384 \times 10^{-6}$ ([53]). Deviations from the initial atmospheric signature in particular affects the helium isotope distribution because ^{3}He and ^{4}He concentrations are modified by in-situ radiogenic production, by the steady crustal He flux, as well as by fluxes originating in the upper mantle. Whereas continental, crustal fluxes as well as in situ radiogenic production lower the ^{3}He/^{4}He ratio (continental, crustal signature: $R_c \approx 2 \times 10^{-8}$ [139]), it is raised in the presence of mantle derived helium ($R_m \approx 1 \times 10^{-5}$ [159]). However, helium from subcontinental lithospheric mantle domains may be associated with ratios considerably lower then R_m (e.g. [68]). In case of in situ production and/or continental, crustal fluxes helium accumulates in the groundwater as it passes the aquifer from the area of infiltration to the area of discharge thus providing valuable information about the residence time of the groundwater. Mantle helium contribution in groundwater sources along the Jordan Valley border faults is not unexpected and has been shown for instance by [194] for the whole western side of the Jordan Valley, by [34], and [33] for the western side of the Sea of Galilee ($R_{sample}/R_a \approx 1.4$) and [71] for the eastern side of the Jordan Valley.

Samples from six Jericho wells were compared with additional data from characteristic brines at the northwestern Dead Sea shore, close to Jericho [194]. The measurement results in Table 5.3 suggest a mixed mantle-terrigenic (crustal and in-situ) helium signature. The noble gas signature in the Jericho area therefore resembles the regional pattern

Table 5.3: Measurement values of the noble gas samples from the Jericho area.

Source	Date	^{22}Ne $\cdot$ 10^{-5}	^{20}Ne $\cdot$ 10^{-4}	^{4}He $\cdot$ 10^{-5}	$\frac{^3\text{He}}{^4\text{He}} \cdot$ 10^{-6}	R_{sample}/R_a
		mL STP/kg				
19-13/018	27/04/2005	2.570	2.513	7.499	1.399	1.016
19-13/018	27/04/2005	2.575	2.519	7.592	1.399	1.015
19-14/024A	26/04/2005	3.201	3.131	9.059	1.400	1.022
19-13/069	26/04/2005	5.395	5.278	20.564	1.394	1.016
19-14/003	27/04/2005	2.116	2.074	29.030	1.354	0.977
19-14/003	27/04/2005	3.541	3.477	34.907	1.317	0.943
19-14/038	27/04/2005	2.065	2.021	14.815	1.411	1.021
19-14/038	27/04/2005	2.051	2.007	14.789	1.414	1.023
19-14/066	26/04/2005	2.484	2.431	10.374	1.390	1.005
19-14/066	26/04/2005	2.502	2.452	10.423	1.390	1.005
Ein Feshka	24/03/1995	NA	0.932	26.000	1.453	1.050
En Zukim	03/01/1997	NA	5.116	220.000	1.024	0.740
Rn-1 15	05/09/1996	NA	3.061	120.000	1.060	0.766
Rn-1 25	05/09/1996	NA	1.250	170.000	1.070	0.773
Rn-1 45	05/09/1996	NA	0.829	400.000	1.050	0.759
Rn-1 54	05/09/1996	NA	0.865	300.000	1.005	0.726
Rn-2 15	05/09/1996	NA	0.868	79.000	1.121	0.810
Rn-2 23	05/09/1996	NA	1.001	68.000	1.118	0.808

indicating that brines have been passing through or at least have been in contact with the border fault. All Jericho samples fall along a mixing line between the Ein Feshka, Ein Zukim, and Radon wells end member on the one hand and water in equilibration with atmosphere on the other hand Figure 5.9. Groundwater that discharges from the

Ein Feshka group of springs has been shown to be a mixture between a high saline end member and fresh groundwater derived from the Mountain Aquifer (e.g. [123], [99]). A
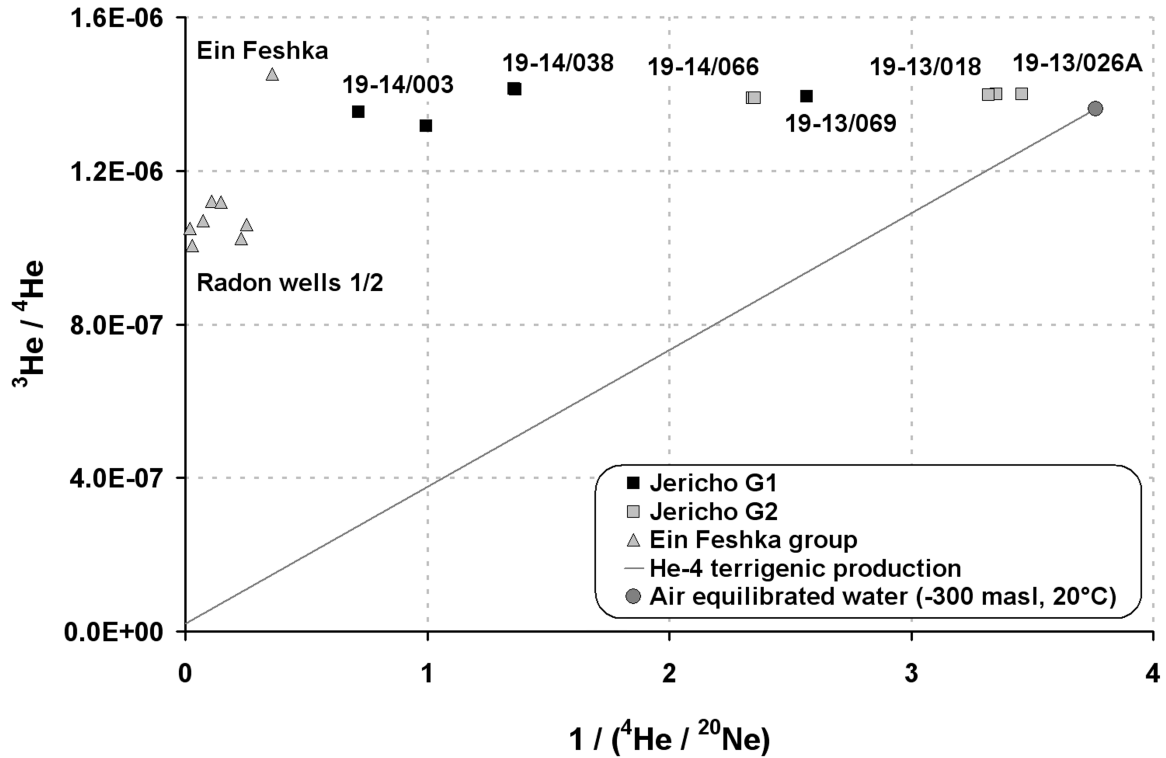
Figure 5.9: ^{3}He/^{4}He ratio plotted versus $1/^4$He/^{20}Ne. Whereas the ^{3}He/^{4}He ratio reflects the He source, the abscissa indicates the amount of ^{4}He that was added to the groundwater. The starting point for a water system is usually represented by water, which is in equilibrium with air. Thus a data point will be shifted left if ^{4}He increases. If the ^{4}He accumulation is related to radiogenic in situ production or/and a continental, crustal flux component a data point would be shifted along the ^{4}He terrigenic production line. Mantle contribution would shift a data point away from the ^{4}He terrigenic production line to a higher ^{3}He/^{4}He ratio.

significant lower ^{3}He/^{4}He ratio is found in the Radon wells and can be interpreted as a result of high Radium activities of up to 400 dpm/L depending on sampling depth, which is responsible for additional radiogenic ^{4}He production.

The ^{20}Ne concentrations of the Radon wells and Ein Feshka samples are considerably lower as would be expected from an air equilibrated originally freshwater source. This could be a strong hint that the brine end member of the Radon wells and Ein Feshka infiltrated the surrounding aquifers as already high saline surface water in the past, maybe Lisan times. In turn it would have been saturated rather with respect to air-equilibrated brine. ^{20}Ne in groundwater is not modified by radiogenic processes and therefore should

represent the initial condition at infiltration. However, correction for salinity according to [189] can not fully explain the low ^{20}Ne values in all samples. The effect of water salinity on the noble gas concentration can be taken from Figure 5.10 and is expressed by
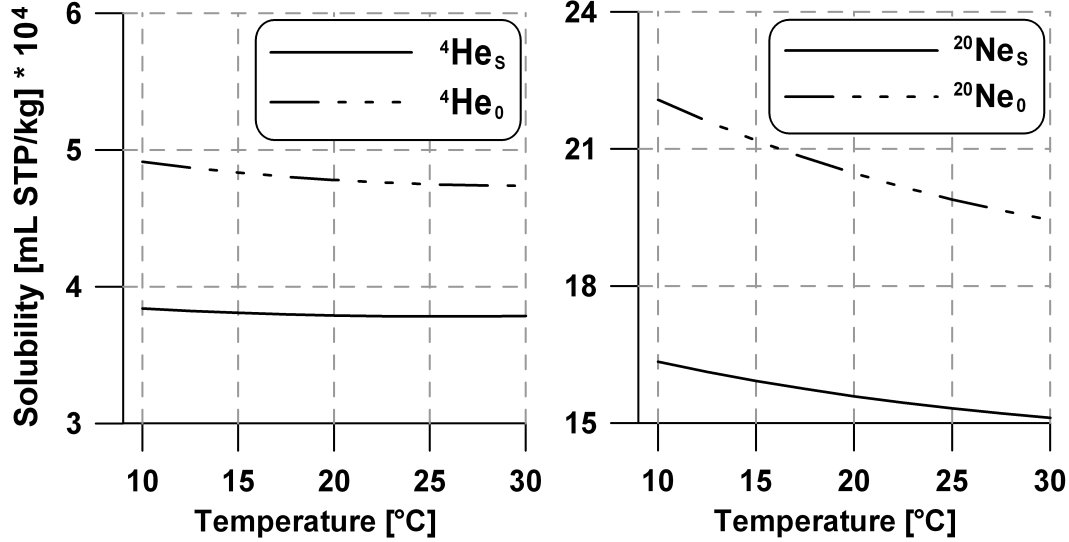
Figure 5.10: ^{4}He and ^{20}Ne solubilities vs. temperature in pure water and 1 molar NaCl solution referring to indices 0 and S, respectively. The solubilities represent the conditions at the elevation level of the Dead Sea (≈ -390 m asl).

the Setchenow equation (Equation 5.1):

$$C_M K_i(T) = ln\left(\frac{\beta_{i,S=0}(T)}{\beta_i(T,S)}\right)$$

(5.1)

where $\beta_{i,S=0}(T)$ and $\beta_i(T,S)$ are the Bunsen solubility coefficients for gas i in freshwater and brine, respectively, C_M is NaCl molarity, and $K_i(T)$ the empirical salting coefficient.

In [219] it was demonstrated that differences in the ionic ratios like between ocean and Dead Sea water have only a moderate impact on K_i, which therefore can be calculated using the existing Setchenow relation by substituting an equivalent sea water salinity in the form of $f \cdot C_M \cdot K_i$ (e.g. $f_{He} \approx 1.08$). Applying this modified correction to the data does not explain the low ^{20}Ne values, which involves partly degassing to be responsible for the loss in Ne of at least the Ein Feshka, Rn-1 45/54 and Rn-2 15/23 samples. But it can be assumed that the other Radon well samples might be affected as well by partial loss of the dissolved gases. It is interesting, however, that the most saline waters, which are found in the east of the Jericho area do not coincide with the highest ^{4}He excess concentrations. Indeed this applies to the wells of G1 in the northwestern vicinity of the border fault (19-14/003, 19-14/038) where already moderate salinities prevail. The G2 wells close to Wadi Qilt (19-13/018, 19-14/024A) show an atmospheric-like helium signature, which is in agreement with regard to the local high infiltration rates expected from the wadi bed in the rainy season. The two easternmost wells that were sampled are also the most saline

wells and belong to G1 (19-13/069) as well as G2 (19-14/066). Both sample signatures lie between the atmospheric-equilibrated and the 19-14/003 and 19-14/038 wells signatures, which consequently supports (1) mixing between these two groups and (2) adding of soluble salts from the surrounding sediments rather than exclusive brine admixture. In turn there is noble gas evidence for different sources of salinization specifically in the eastern Jericho area. Hence the availability of a thick column of Lisan Formation is self-suggesting to have high potential as a contributor to salinization.

5.1.4 Summary and Conclusions

The investigations performed on the groundwater of the Shallow Aquifer of Jericho focused on possible salinization mechanisms that are observed since several decades. A clear discrimination of possible salt pools, which are expected to contribute to the overall salinization is hampered due to the unique situation that upwelling brines as well as leaching of sediments like the Lisan formation are charcterized by a very similar hydrochemical fingerprint. This is caused by the tight genetic relation, which is characteristic for the brines and the Lisan Formation, because they represent the brine and the precipitated solid remnants of Lake Lisan, respectively. Lake Lisan was the Pleistocene precursor of the Dead Sea.

It has been described that the highly unsteady conditions in the Jericho area, its limited lateral extension and the great uncertainty concerning the estimated infiltration volumes, rates, and mechanisms further impede the understanding of the Shallow Aquifer system. For instance estimates of the annual recharge through Wadi Qilt and Wadi Nueima range between 2 and 9 mil. m^3/yr. Further, the annual amount and timing of the winter runoff are expected to be highly variable and depend on the actual precipitation amounts and intensities in the mountains. However, with respect to the size of the investigated area this difference accounts for a huge amount of water, either passing the system or not. In turn this has dramatic implications for the interpretation of the system, like how susceptible the freshwater layer is for brine upwelling or how much irrigation return flow is to be expected. Another self-evident obstacle for the correct interpretation of the hydrochemical pattern of the samples may be related to its potential dependence on the timing of sampling, as the system is highly unsteady.

By using a broad variety of hydrochemical and isotope data from this study and from different literature sources it was possible to work out the mechanisms that are responsible for groundwater salinization. Two general groups of groundwaters were identified by their SO$_4$/Cl ratios, where high ratios (G1) reflect SO$_4$ contribution from the sedimentary column itself (e.g. Lisan formation) and by sewage or soil precipitates due to surface infiltration. The processes that control the addition of SO$_4$ and that may modify the Sr/Ca ratio cannot be specified, because due to the carbonate buffered environment important trace elements like Fe can hardly be detected in solution. Samples with low SO$_4$/Cl ratios (G2) are assumed to be affected to a lower degree by possible leaching from the sedimentary section than the previous group. In turn a possible brine signature is less overprinted, since brines and Lisan formation leachates potentially have the same hydrochemical fingerprint, except for their sulfate signature as well as some trace elements like

boron. The hydrochemical analogy between brines and Lisan formation end members is supported by parameters like the Na/Cl and Sr/Ca ratios.

B/Cl ratios gave initial strong indication for brine admixture in two samples of G1 that are assigned to two wells in the northwest of the study area, but remote from Wadi Qilt. It was approved with the help of the evaluation of He and Ne isotopes. The noble gas isotope signature thereby perfectly matches with the regional context, where R_{sample}/R_a ratios are between ≈ 1 (northwestern Dead Sea shore) and 1.4 (western side of Lake Galilee). All Jericho samples fall along a mixing line between air-equilibrated water and brines from the northwestern Dead Sea shore. The two samples of G1 with the lowest B/Cl and Na/Cl ratios also show the highest ^{4}He excess, whereas the samples with a He signature close to air-equilibrated conditions are assigned to wells in the close vicinity of Wadi Qilt but not too far in the east of the study area. An intermediate position between the two groups is adopted by the most saline and eastern wells, which indicates salt contribution from sources other than upwelling brines. The findings of this study can provide helpful information concerning the implementation of water management schemes in the Jericho area. An important suggestion resulting from the high uncertainty and complexity of the ascertainment of the annual recharge rate and the various recharge paths is a reasonable monitoring system focusing on these two topics. Furthermore, a comprehensive GIS database, which should include continuously collected data about sewage storage in tanks and disposal in cesspits would improve knowledge about the distribution of these practices especially in context of possible occurrences of contaminations, which also applies to former and actual stockyards for hazardous materials. The implementation of an environmental record system would effectively support future investigations and a possible realization of an advanced groundwater management scheme for that highly susceptible Shallow Aquifer system.

The possibility or chance to directly observe changes in the Shallow Aquifer system due to the installation of the new closed-pipe agricultural distribution system in 2006 in exchange for the leaky open canal system by specific tracing tools probably might have been missed.

5.2 Wadi Qilt springs - evaluation of isotope tracer data

5.2.1 Introduction

In this section available tracer data that were published e.g. by [101], [127], [125], [128], and others for the Eastern Aquifer basin are reevaluated with respect to the so far unconsidered younger groundwater components of the major springs of the Wadi Qilt (Fara, Al Fawwar, Ein el Qilt), as well as of Jericho (Ein el Sultan). The latter is located outside of the Wadi Qilt catchment in the northwestern part of Jericho. Tritium as part of the water molecule is well suited to estimate mean transit times (T_M) of young groundwater and to roughly characteristize the groundwater system by means of lumped parameter modeling (chapter 3). The springs were repeatedly sampled between the 1960s and recently. To reveal information about possible old components in the discharged water the above mentioned studies included to a certain extend also the analysis of noble gases and ^{14}C.

The four springs used to be important for the drinking water supply for the local villages as well as in part for Jerusalem. Today, the water from the springs in the Wadi Qilt is to a great extend used for agricultural purposes. However, generally, the demand and importance for a proper characterization and interpretation of a spring source increases with the discharge volume, the size of the spring catchment, the proportion of the spring discharge in the water balance of the catchment, and if the spring contributes to drinking or irrigation water supply. By 1985, when most of the samples of the considered springs were already analysed a possible spring water pollution or the evaluation of the protection level of the spring catchment area was of no real concern. Instead the main focus was to get a first insight on the age structure of the discharging water. Estimation of mean groundwater ages by means of numerical methods like the lumped parameter approach if enhanced by inverse fitting techniques and the ability to couple various basic models with each other was still not available to many reseachers at that time. Also, numerical inverse fitting techniques and testing of many possible parameter realizations to investigate model ambiguity was computatively very costly especially when dispersion and coupled models were involved. Moreover, the knowledge about karst aquifers has tremendously increased during the past 25 years. In this light it may become clear why [127] and [125] did not went beyond a more or less descriptive evaluation of the available data. However, they summarized and conceptualized the results from the water analyses as well as their knowledge then about the possible characteristics of the groundwater drainage systems in terms of a binary mixture of an unspecified "old well water" and an also unspecified "young water" component.

But although [127] and [125] gave an interpretation for the noble gas, tritium and ^{14}C measurements they didn't comprehensively exploited the tritium measurements to characterize the youngest groundwater component. But this would be necessary with respect to the question of vulnerability or how well the discharged groundwater system is protected against short term and longterm antropogenic pollution. Even because of the karstic character of the Wadi Qilt springs including Ein el Sultan and with respect to environmental protection this must be one major concern. Thus, this part of the thesis aims to go beyond the early achievements taking advantage not only of the modern computational capabilities but also of several new post-1985 tritium data that are important to reduce the ambiguity of the applied models, as well as of a more comprehensive understanding of the prevailing conditions in karstic environments.

5.2.2 General description and conceptual model

The average annual discharge of the Wadi Qilt springs is generally estimated to 7.4 mil. m^3 (Table 2.2) for the Fara, Al Fawwar, and Ein el Qilt springs [160]. Since a number of other minor springs also discharge in Wadi Qilt the total volume might be a bit higher [207]. On the other hand the channel that collects the discharge of Al Fawwar and Ein el Qilt can overflow following heavy rainfall in the mountains, and water levels in the wadi bed during

strong runoff events can reach the hight of the channel, both making exact measurements practically impossible. However, the mentioned value will represent about 4.5 % of the Eastern aquifer basins average annual recharge if the estimation of 172 mil. m^3 as statet in the Oslo agreement is assumed to be valid. Adopting from [222] the approximate amount of ca. 9 mil. m^3 as annual infiltration for the Wadi Qilt catchment the spring discharge would represent $\approx 82\%$ of it, which appears to be overestimated. However, it may show, that the subsurface catchment does not match with the surface catchment, which is typical for karstic areas. Other than [222], who completely incorporates also the spring discharge of Ein el Sultan to the water balance of the Wadi Qilt catchment that assignment is not made here because of no tangible evidence. But as one of the main water resources for the Jericho area that has been discussed earlier in this work (section 5.1) the evaluation of the tritium measurements of Ein el Sultan is clearly important as well.

A common pattern for all spring data sets is a large variance in the 1960s and 1970s followed by a significant drop of the variance. The same pattern is reported from other karstic springs in the larger area, e.g. from the Hermon mountains [40]. Generally, large short time variations in the tritium signal of a source are a strong indication for water that has different components with different residence time distributions. This is often related to rapid infiltration during rain events and increased heads in the karst network that prevent the masking of the rapid infiltration by the water stored in the matrix porosity. The majority of the water is stored in the matrix and the non-karstic fissure porosity that - roughly speaking - comprises about 98 % of the whole porosity in a limestone aquifer. But due to the very high conductivity of the karst pore space the flow that happens there clearly dominates the system until the spring outlet, which is not necessarily the case for transport, including tritium. Nevertheless, for that reason it is typical that part of the fast infiltration component reaches the spring outlet within a short time of hours, days or weeks depending on the degree and maturity of the karst system and the distance to the outlet (e.g. [50], [86]). Another important indicator is the coincidence of low ^{14}C and any tritium concentration, which is the case for all of the studied springs. While the first suggests water of very old age the second unequivocally proves that a second component must have been infiltrated later then 1953.

Both, the data patterns as well as the prevailing conditions in karstic systems at different times, suggest the involvement of three main components of changing proportions in the spring discharge:

- old pre-bomb water, which is stored in the matrix porosity (type O),

- mainly advectively transported water whos mean transit time is small enough to have measurable tritium concentrations (type M),

- water from rapid infiltration directly passed through the karst system within an unspecified time of hours to a few years (type R).

A straightforward method to interpret isotope tracers in groundwater is the application of lumped parameter (black box) models. As stated in section 3.4 their clear advantage

is that beside the need for a conceptual understanding of the system it is seen as time-invariant regarding groundwater flow, any spatial variability is neglected and theoretically no pre-knowledge about the specific aquifer characteristics is required. For simple transfer functions and even simple coupled models those parameters can be determined based on the measured data by trial and error or numerical inverse modeling depending on the available software. If appropriate, selecting simpler transfer functions avoid or reduce model ambiguity. The most commonly used basic lumped parameter models are the piston flow (PM), the exponential (EM), and the dispersion (DM) models.

Because a higher complexity behind the tritium signals of the studied springs is expected, it is unjustified to oversimplify the model approach by applying a transfer function that would not consider the coexistance of more then one groundwater component. In those cases two or more of the basic transfer functions may be coupled in a parallel ("||") or serial manner, where parallel coupling often stands for aquifers with more than one porosity and serial coupling simulates a succession of different domains. For the available data sets a common evaluation strategy in 3 steps was developed:

1. Selecting the tritium-^{14}C data pairs with the lowest ^{14}C concentrations assuming that these are the best possible approximation of a water sample that is assumed to be free of rapid infiltration and represents a characteristic two component base flow of the old pre-bomb and the type M water.

2. Using a coupled EM||PM or DM||PM model to estimate the proportion of the type O and type M components, the mean residence time of the type M water component, and the dispersion parameter if the DM||PM combination was chosen. The water component of type O is simulated by the PM, for which a very high transit time (e.g. 5000 years) is set to ensure it is tritium free. This conceptual approach splits up the base flow discharge into a tritium free old and a second component that carries all tritium.

3. To indicate the conceptual mixing of the calculated model output with a fast infiltration and flow component (type R) both are subsequently mixed with the help of an Octave script applying a PM with a transient time of 0 years for the type R component. However, to avoid any misconception it is important to note again that the age structure of the type R component is defined to be unknown, because it is assumed to be highly unsteady. Thus, the instantaneous binary mixing as insinuated in the related figures between the modeled base flow and the non-delayed or zero-age rapid infiltration water does not reflect the real age spectrum of the youngest groundwater component but only the concept of mixing with a fast, karst related groundwater component.

Some of the ^{14}C measurements especially the very low values appeared to be not fully reliable, and not all tritium measurements were accompanied by ^{14}C measurements, which was a limiting factor for step 1. The tritium measurements that were selected to execute step 2 are emphasized everywhere in the respecting spring subsections, where the individual tritium measurement series are evaluated. Since every sample represents an individual

combination of all three components step 3 would have been to applied to each of it, which – to recall – is impossible since the age structure of the type R component is defined as unknown. Instead an arbitrary mixing ratio between type R and the combined type O and type M was set for the diagrams to 0:1 for the summer season and to 0.55:0.45 for the winter or rainy season to somehow accentuate a potential mixing variation. During the inverse modeling procedure the DM||PM model turned out to perform much better as the EM||PM model. For the latter no good fits to the data could be achieved, which is exemplarily shown for Ein el Sultan in Figure 5.14 of subsection 5.2.3. The possible parameter ranges of the DM-T_M, the DP, and the proportion of the DM for all springs that are tabulated in Table 5.4 testify that the solutions for the data fitting for the individual springs are not unique. However, in the course of the discussion in subsections 5.2.6 to 5.2.3 these ranges are reduced. The procedure in order to achieve this, has do respect one or more logical constraints. The constraint that is applied here follows the conceptual model of [127] and [125], that the proportion of the old groundwater ("old well water") decreases from the area of recharge to the Jordan Valley, while the maturity of the karst increases in the same direction (compare Figure 5.11).
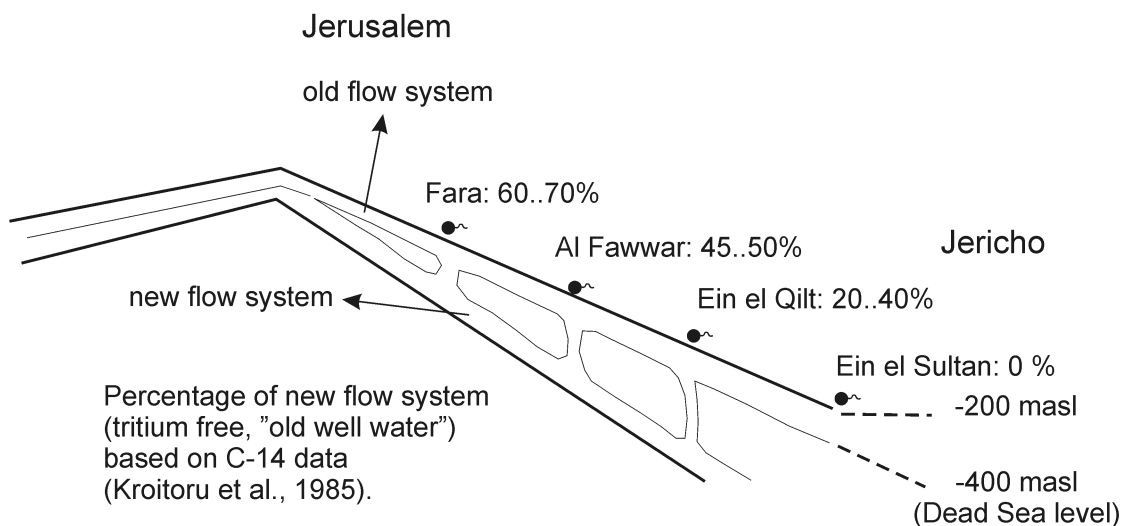
Figure 5.11: Conceptual model of the age structure in the springs of Wadi Qilt and Ein el Sultan based in the evaluation of ^{14}C data by [127].

It is clear that the transit time distribution of the assumed type M component itself is not necessarily stationary and therefore can not be certainly discriminated from type R while the systems slowly returns to base flow conditions. As already stated, the lumped parameter approach also ignores the spatial distribution of rain and the changing contributions from different branches of the karst system. Thus, even the reasonable assumption of three distinguishable and – except for type R – well-defined water components still is a simplification of the system. However, the advantages of the described strategy compared to the fitting of an averaging model to the data is a better understanding of the proportions of the suggested different components and the avoidence of a single mean transit time value of ambigeous meaning. In addition, the results could also be much

Table 5.4: Solution spaces for the DM||PM model parameters for the Wadi Qilt and Ein el Sultan springs.

spring	DM-T_M [years]	DP [-]	proportion of DM [%]
Fara	18.25 .. 63.50	0.100 .. 0.870	21.5 .. 100.0
Al Fawwar	17.50 .. 40.00	0.100 .. 0.700	40.0 .. 100.0
Ein el Qilt	18.00 .. 21.50	0.120 .. 0.225	56.0 .. 74.0
Ein el Sultan	21.00 .. 23.00	0.140 .. 0.175	57.0 .. 66.0

more helpful during the set up and calibration of a numerical groundwater model. It must be considered that the model sensitivity with respect to errors of the input function was not tested. Thus, no error ranges can be assigned to the calculated parameters and parameter ranges.

5.2.3 Ein el Sultan

The inverse modeling of the assumed base flow samples of Ein el Sultan led to the least ambiguous estimations of the three model parameters. Their determined ranges are DM-$T_M = 21.0 .. 23.0$ years, DP $= 0.14 .. 0.175$, and $57.0 ... 66.0\%$ for the proportion of the DM. With respect to the conceptual model of [127] and [125] (compare subsection 5.2.2) the proportion of the old, tritium free (type O) component in the first place seems to be too high and too similar to the calculated solution space for Ein el Qilt. But with regard to the presented ^{14}C data ([127], [125]) there is no distinct discrimination between Ein el Sultan and Ein el Qilt. In addition, considering the beginning of the atomic era in the 1950's it is clear that the ^{14}C concentration is a too unspecific measure with regard to younger ages.

However, as the parameter ranges are not really large there is no need to further reduce the limits of the solution space. Thus, the lower and upper limits are presented in Figure 5.12 and Figure 5.13, respectively.

Examplarily for all springs Figure 5.14 shows for the case of Ein el Sultan, that it is not possible to find any parameter set for the EM||PM model that would give a reasonable fit to the data, neither to the complete data sets nor to the assumed base flow data subsets.

5.2.4 Ein el Qilt

Fitting the DM||PM model to the selected three tritium samples of Ein el Qilt revealed that the possible solution space slightly increased compared to Ein el Sultan. It can be specified as DM-$T_M = 18.0 .. 21.5$ years, DP $= 0.120 .. 0.225$, and $56.0 .. 74.0$ % for the DM fraction. However, the range of the DM fraction fits quite well the suggested proportion range with respect to the conceptual model of [127] and [125] (cf. subsection 5.2.2). In

Figure 5.12: Lower limit of the solution space for possible DM||PM model fits to a subset of the tritium measurements of Ein el Sultan that is assumed to represent conditions similar to the base flow.

Figure 5.13: Upper limit of the solution space for possible DM||PM model fits to a subset of the tritium measurements of Ein el Sultan that is assumed to represent conditions similar to the base flow. This model was further selected as to be the most likely solution with respect to the results for the other springs.
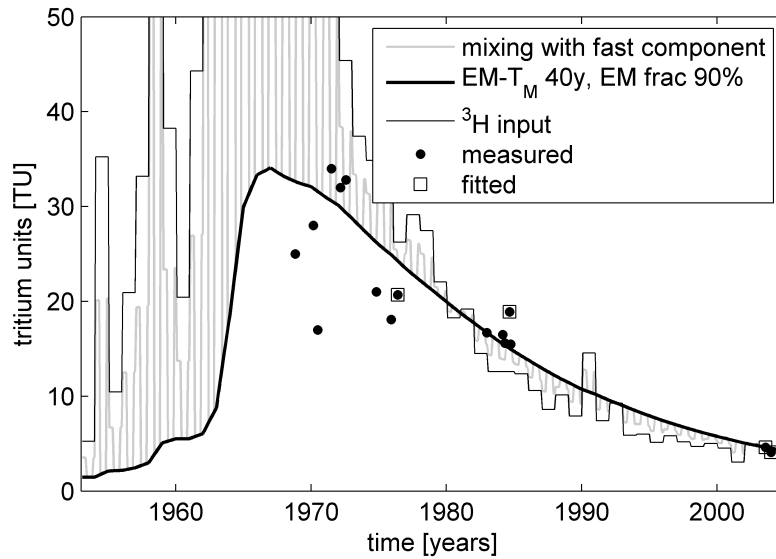
Figure 5.14: Fit for the EM||PM model to a subset of the tritium measurements of Ein el Sultan that is assumed to represent conditions similar to the base flow.

turn, again, there is no logical control to further constrain the solution space for Ein el Qilt. Its lower and upper limits are depicted in Figure 5.15 and Figure 5.16, respectively.

However, the sample from 08.01.1985 has a very low tritium concentration of 5.3 ± 0.3 TU whereby it is unclear whether the measurement is not reliable or the spring was far from the assumed base flow conditions due to the lower than usual amount of precipitation between October and December of 1984. The latter could mean that the second assumption of the conceptual model regarding the water composition (subsection 5.2.2) has to be revised for the case of Ein el Qilt. But without more evidence going too far in speculation should be avoided. Since the tritium concentration of the sample from Mai, 1985 jumped back to 20.4 ± 0.3 TU it is assumed here that the value from January, 1985 is not reliable or represents a rare event of unknown background.

5.2.5 Al Fawwar

The calculated solution space for the spring Al Fawwar is DM-T_M = 17.5 .. 32.5 years, DP = 0.100 .. 0.700, and 40.0 .. 100.0 % with respect to the DM-model fraction. In opposite to the available data for Ein el Sultan and Ein el Qilt data exist neither after the year 2000 nor after the 1980s for Al Fawwar, which increases the solution space significantly. However, the lower limit of the DM-model fraction fits quite good with the suggested lower limit of the conceptual model of [127] and [125] (i.e. their old karst flow system). Adopting also their suggested upper limit with some buffer a model configuration with DM-T_M = 22.0 years, DP = 0.3, and a DM-model fraction of 60.0 % appears to be reasonable. Whereas Figure 5.17 and Figure 5.18 show the lower and upper limits of the solution space for Al Fawwar, Figure 5.19 depicts its most reasonable upper limit with
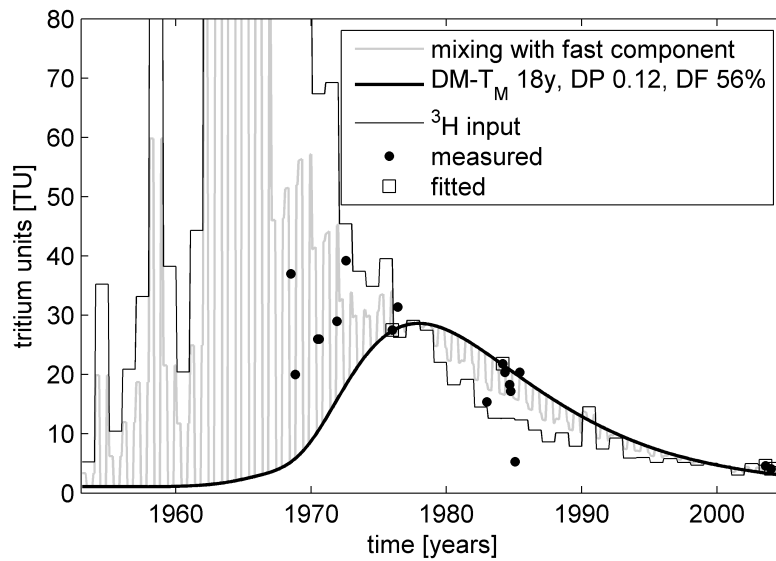
Figure 5.15: Lower limit of the solution space for possible DM‖PM model fits to a subset of the tritium measurements of Ein el Qilt that is assumed to represent conditions similar to the base flow.
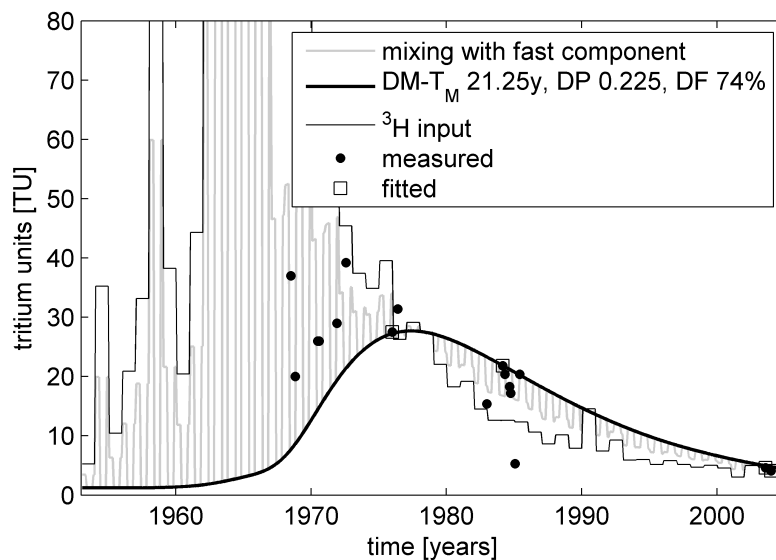
Figure 5.16: Upper limit of the solution space for possible DM‖PM model fits to a subset of the tritium measurements of Ein el Qilt that is assumed to represent conditions similar to the base flow.
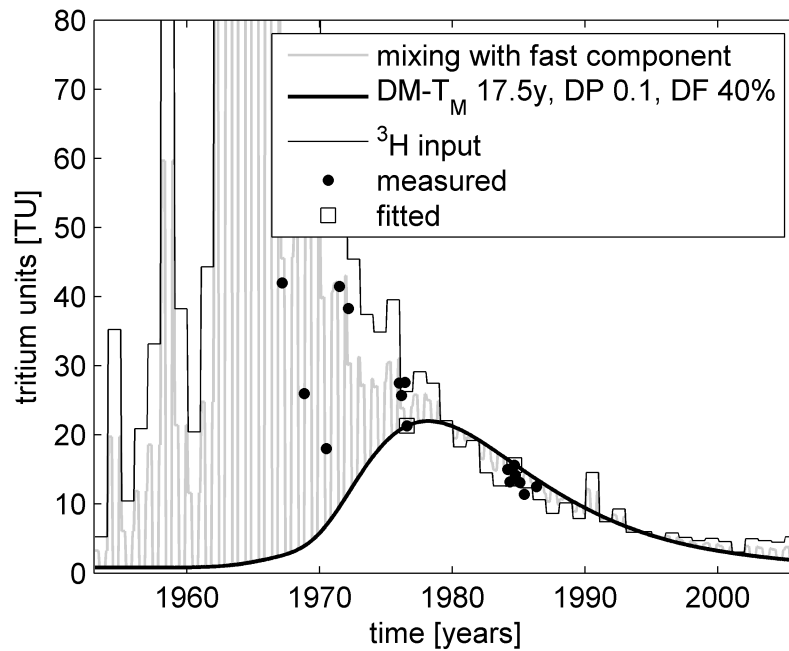
Figure 5.17: Lower limit of the solution space for possible DM||PM model fits to a subset of the tritium measurements of Al Fawwar that is assumed to represent conditions similar to the base flow. This model was selected as to be the most likely solution with respect to the results for the other springs.

respect to the conceptual model of [127] and [125].

5.2.6 Fara

The Fara spring exhibits the lowest tritium concentrations of all springs with a maximum of 18.6 ± 0.4 TU in 1976 on the one hand and the lowest ^{14}C concentration of 5.3 ± 3.8 pmc on the other hand (compare Table 5.5 as taken from [127]). In turn, this would suggest an almost binary mixture of an approximately 15000 years or even older major component with a small contribution from rapidly infiltrated precipitation water. Unfortunately δ^{18}O and δ^2H were not analysed too, because both together could serve as a possible climate proxy to support or reject the existance of such an old water component. Although it is a theoretical possibility, it seems more appropriate to reject that ^{14}C value, since neither in other springs nor in any deep well penetrating the Upper or Lower aquifer of the Eastern basin a similar low value is reported in the available literature ([101], [127], [125], [126], [128], [121]). The sample further was taken during the rainy season in February, which makes base flow conditions rather unlikely. Its measured temperature even was the lowest among all other Fara samples, pointing to a higher portion of recently infiltrated water.

A distinct difference to the other three springs is that all measured tritium values in the 1980s are lower than the tritium values in precipitation. The calculated solution space for the Fara spring is DM-T_M = 18.25 .. 63.50 years, DP = 0.100 .. 0.870, and
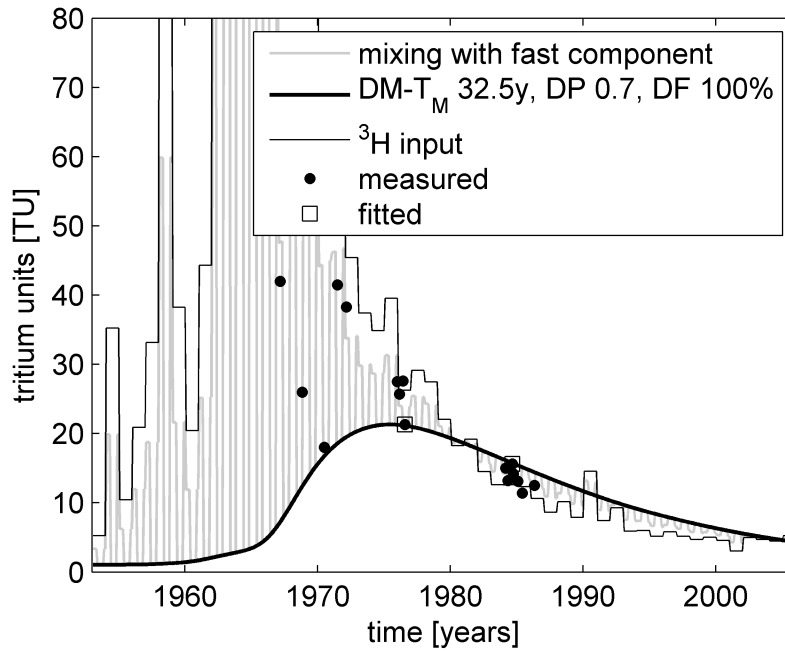
Figure 5.18: Upper limit of the solution space for possible DM||PM model fits to a subset of the tritium measurements of Al Fawwar that is assumed to represent conditions similar to the base flow.

Table 5.5: Tritium and ^{14}C data for Al Fawwar as published by [127]. Note, that the complete data set can be downloaded free of charge from the internet homepage of the International Association of Hydrological Sciences (IAHS).

Date	Temperature [°C]	Tritium [T.U.]	^{14}C [pmc]
04.06.68		14 ± 4	
28.06.70		5.7 ± 1.0	
04.11.71		7.0 ± 1.0	
30.07.72		6.0 ± 1.0	
13.11.75	20.8	11.6 ± 0.4	67.4 ± 1.3
16.02.76	20.5	18.6 ± 0.4	5.3 ± 3.8
09.05.76	21.1	11.1 ± 0.7	21.7 ± 1.2
21.07.76	20.6		56.0 ± 1.0
06.02.84	21.0	12.6 ± 0.4	
30.04.84		11.7 ± 0.3	
25.09.84		11.3 ± 0.4	
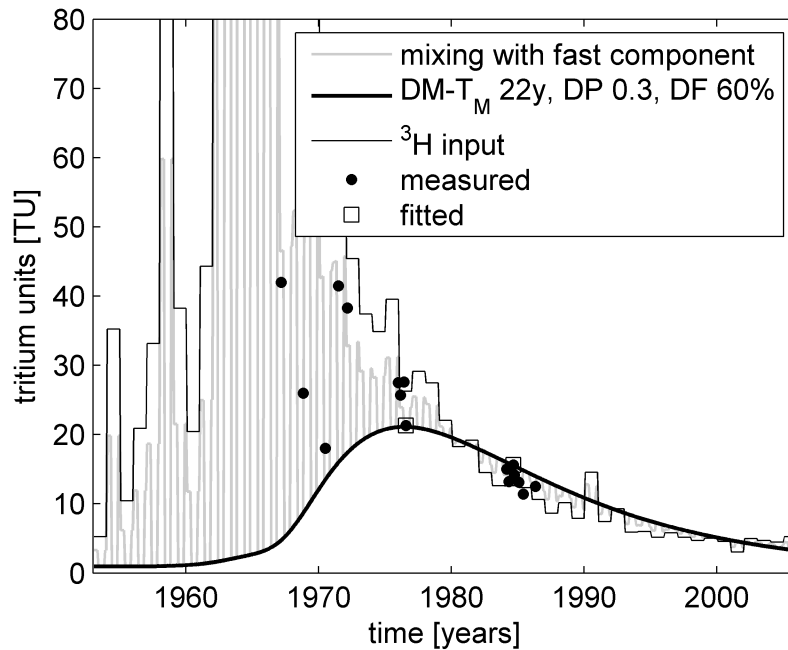
Figure 5.19: Most reasonable upper limit of the solution space for possible DM||PM
model fits to a subset of the tritium measurements of Al Fawwar that is
assumed to represent conditions similar to the base flow with respect to the
results for the other springs and the conceptual model of [127] and [125].
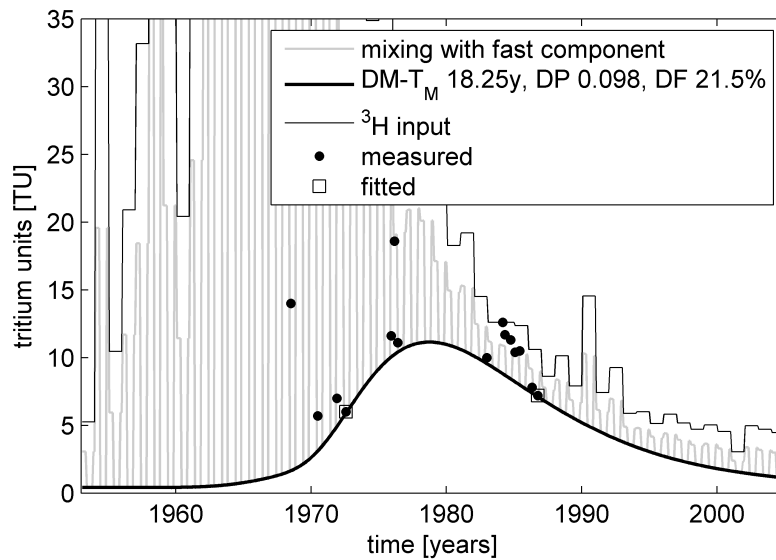
Figure 5.20: Lower limit of the solution space for possible DM||PM model fits to a subset
of the tritium measurements of Fara that is assumed to represent conditions
similar to the base flow.

21.5 .. 100.0 % for the fraction of the DM. Based on the already achieved findings for the other springs and again with respect to the conceptual model of [127] and [125] (subsection 5.2.2) a reduced reasonable solution space would comprise parameter ranges of DM-T_M = 18.25 .. 30.25 years, DP = 0.10 .. 0.32, and 21.5 .. 40.0 %. Note, that the referenced conceptual model predicts an "old well water" or "new flow system" proportion of 60..70 %, which is quite similar to the 60..78.5 % estimated using the tritium observations. However, the lowermost limit of the solution space that could be fitted to the selected tritium measurements is a model configuration of DM-T_M = 16.25 years, DP = 0.056, and 20.45 %. On the one hand, this lowermost limit would be extremely dominated by advective transport and further is in contradiction to base flow conditions as the fitting curve would exceed more observations with respect to the tritium concentration. On the other hand, a higher mean transit time than 30.25 years would increase the DP and thus decrease the proportion of the advective flux in the system, while for the other springs values of DP $\leq$ 0.3 are characteristic. However, although the selected, reasonable boundaries of the solution space are in well accordance with the above mentioned conceptual model and with practical considerations concerning the DP, it can not be logically excluded, that the Fara spring is fed by a system possessing a higher dispersivity reflected by DP > 0.32. While Figure 5.20 and Figure 5.21 show the lower and upper limits of the calculated solution space, respectively with regard to the data, Figure 5.22 represents the suggested realistic upper limit of the solution space.
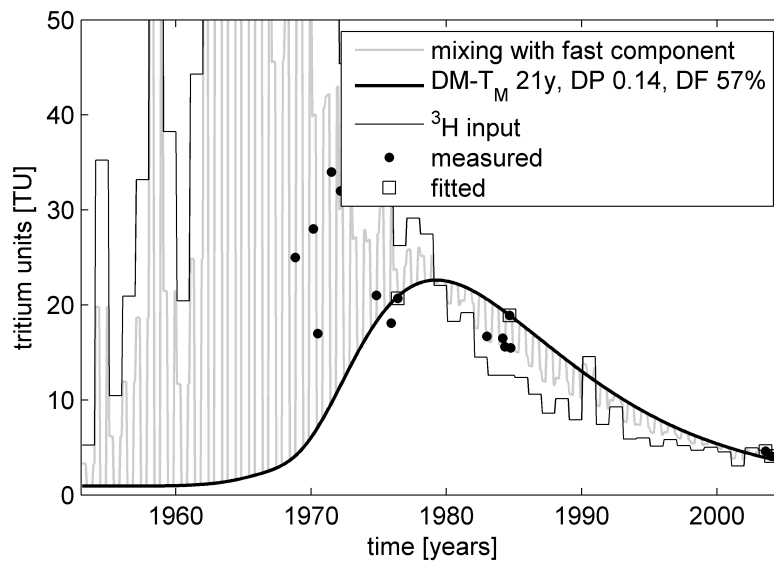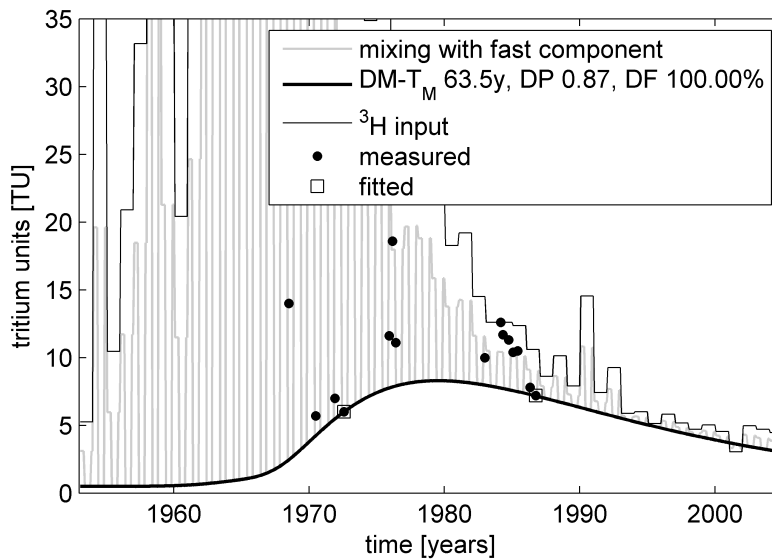

Figure 5.21: Upper limit of the solution space for possible DM‖PM model fits to a subset of the tritium measurements of Fara that is assumed to represent conditions similar to the base flow.

However, as for Al Fawwar, a measurement after the year 2000 that could be used as additional fitting point would make the search for a good model fit more independent from the comparison with the other springs.
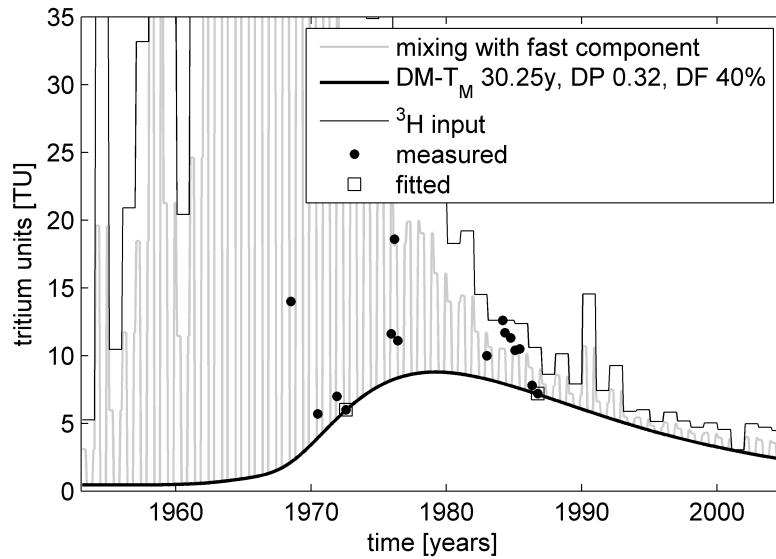
Figure 5.22: Most reasonable upper limit of the solution space for possible DM||PM model fits to a subset of the tritium measurements of Fara that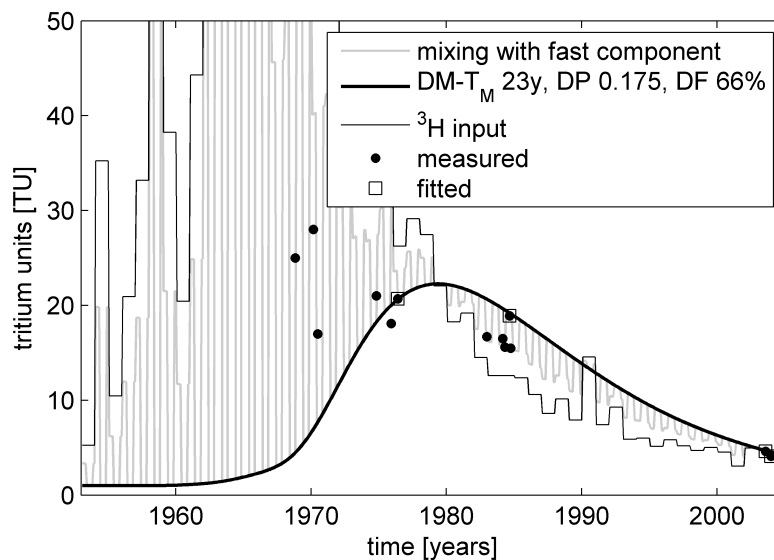 is assumed to represent conditions similar to the base flow with respect to the results for the other springs and the conceptual model of [127] and [125].

5.2.7 Summary of the reevaluation of tracer data of the Wadi Qilt springs

The proposed conceptual model of [127] and [125] (compare subsection 5.2.2) is approved to reasonably reflecting the tritium distributions of the samples from the Fara, Al Fawwar, Ein el Qilt, and Ein el Sultan springs with respect to time. The derived best estimations for the mean transient time, the dispersion parameter, and the proportion of the dispersion model in the parallely coupled DM-PM model are reasonable and consistent for all springs despite the underlying simplifications that the lumped parameter approach requires. Hence, the applied implementation strategy for the conducted data reevaluation was robust and successful.

While Table 5.4 tabulate the calculable solution spaces with respect to the parameter ranges, Table 5.6 lists the suggested parameter ranges after they may were reduced, based on all conceptual considerations as well as logical constraints. It is remarkable that the mean transit times for all springs is about 20 years, except for Fara, which has a larger DM-T_M-range of 18.25..30.25 years. The main differences are limited to the DM and PM proportions, which are consistant with the ideas of [127] and [125].

All considerations that have been made in section 5.2 show that the aquifer or the individual spring catchments are not well protected against antropogenic pollution, which has been shown for example for the spring of Ein el Sultan (section 5.1), where nitrate concentrations become close to the WHO limit for drinking water of 50 mg/L. However, the high nitrate concentrations are correlated to the higher precipitation during the rainy season, which supports effective infiltration of wadi runoff into the ground, flushing the

Table 5.6: Suggested DM‖PM model parameter configurations for the Wadi Qilt and Ein el Sultan springs based on the considerations drawn in subsection 5.2.6 to subsection 5.2.3.

spring	DM-T_M [years]	DP [-]	proportion of DM [%]
Fara	18.25..30.25	0.100..0.320	21.5..40.0
Al Fawwar	17.50..22.00	0.100..0.300	40.0..60.0
Ein el Qilt	18.00..21.50	0.120..0.225	56.0..74.0
Ein el Sultan	21.00..23.00	0.140..0.175	57.0..66.0

waste water residuals in the wadis into the karstified underground. If the base flow proportions of the type O and type M components would be 60 and 40 %, respectively, and in the rainy season the rapid infiltration/fast flow component would for example temporarily account for 25 % of the water discharge, which seems not to be an unrealistic value for the Wadi Qilt and Ein el Sultan springs with respect to the variance of the data, the components of type O and type M would reduce to 30 and 45 %, respectively. Recent investigations conducted at University of Göttingen have veryfied significantly dropping temperatures and increasing nitrate concentrations in Ein el Sultan following heavy rain events. However, the drop in temperature is not very large, and considerations or modeling with respect to heat transport were not made or conducted, respectively, so far. But the tracer results also suggest, that the flow of the young groundwater components is predominantly advective if the dispersion parameter would be interpreted like in distributed numerical models, which in turn would mean that the dispersion of the tracer from the direction of the head gradient is moderate. However, pollutants are retarded to a certain degree in the fine fractures and the matrix pore space. A rehalbilitation of a polluted spring catchment thus depends on the effectivity of this retardation, i.e. the distribution of the pollutants residence times. However, it has to be noted again, that the model results base on the assumption of a binary to tertiary mixture of old tracer free and young groundwater containing all tritium. As already discussed this is a conceptualisation thus simplification of the system in order to evaluate it, but of course, the spectrum of flow velocities is continuous.

5.3 Evaluation of tracers in deep wells of the Judea Group Aquifer

Distributed groundwater flow models in fractured, karstified carbonate aquifers usually can not account for the large aquifer parameter ranges for instance of porosity or hydraulic conductivity. The latter can vary by several orders of magnitudes at very small scales. In case of karst conduits or karstified fractures Darcy's law might not be applica-
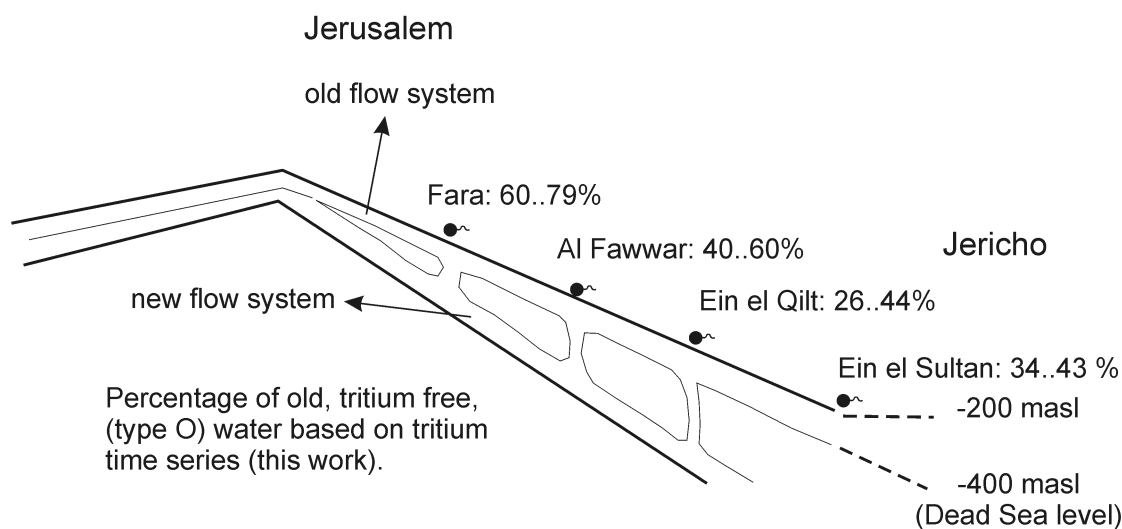
Figure 5.23: Conceptual model of the age structure in the springs of Wadi Qilt and Ein el Sultan based on the evaluation of ^{3}H data of [101], [127], [125], [126], [128], [121]. ^{14}C was used to approximate conditions close to base flow.

ble anymore due to turbulent flow. For most major groundwater drainage basins of the Judea Group Aquifer several distributed flow models were implemented in recent times (e.g. [94], [30], [63]). But although those models are optimized to meet the requirements with respect to water balances or to observed versus modeled groundwater heads they might fail to reproduce the local groundwater age structure for a well, if the flow model would be extended to (reactive) transport. But the local age structure of the groundwater must be known well to assess the potential vulnerability. Nevertheless, it is obvious that the effective vulnerability can only be evaluated if the catchment area and potential or actual sources for pollution are identified. That kind of spatial analysis was not part of this work.

However, if the requirements for the application of lumped parameter models as described in section 4.4 are met, they can be easily applied without the need for spatial aquifer parameterization, since they derive the age structure of a given well due to the provided time input function of the tracer and the selected weighting function. The latter determines the tracer output function in terms of its mean residence time. While the mean transit time is just an aggregate value over the whole age spectrum that is found in the well, the weighting function itself defines the whole spectrum of ages. To characterize the age structure as an indicator for the potential vulnerability of the groundwaters of the Judea Group Aquifer at the specific locations to antropogenic pollution 16 wells of the Agur, Herodion, and Ein Samia well fields have been sampled one to three times each for several stable and radiogenic isotopes and chemical tracers:

- δ^{18}O and δD (stable isotopes)

- ^{3}He, ^{4}He, ^{20}Ne, ^{22}Ne (stable isotopes)

- T (radiogenic isotope)

- CFC-11, CFC-12, CFC-113, and SF_6 (chemical tracers)

Table 5.7 and Table 5.8 list all samples that were analysed for noble gases, tritium, CFC's, and SF_6. While the helium isotopes in this study were used as a qualitative measure for old groundwater components and as an indicator for mantle helium contribution, the CFC's, SF_6, and T were evaluated using lumped parameter models section 4.4. The dissoluted excess air components in the samples were determined by ^{20}Ne.

5.3.1 Evaluation of T, CFC-11, CFC-12, CFC-113, and SF_6

Because of conceptual considerations as well as for consistency and comparability the applied lumped parameter approach generally follows that of the Wadi Qilt spring evaluation in section 5.2:

1. assuming a groundwater component essentially free of any modern tracer,

2. assuming a younger groundwater component that is responsible for the actual tracer concentration.

Both components were again modeled using a coupled piston flow (PM) for the old component and a dispersion model (DM) for the young component. However, in opposite to the Wadi Qilt spring evaluation a fast recharge component was not assumed due to the small observed tracer variations that could be related to either the real nature at the sampling locations or to the sampling time scheme itself.

According to the modeling approach that is described in section 4.4 minimum and maximum values for the well specific mean residence times (T_M) and for the proportions of the DM (DF) were estimated by visual interpretation of 212 figures. In these figures single tracers or ratios of tracers were plottet against each other while the selected lumped parameter is indicated by a color based index. Further 106 figures that aimed to depict the relation between the samples and the possible range of the dispersion parameter of the DM were not suited for that kind of evaluation due to a strong overlapping. However, the dispersion parameter (DP) was kept in analogy to the Wadi Qilt spring evaluation within a resonable range of 0.1 to 0.6 and can therefore also be seen to constrain the possible states the system is allowed to possess. All applied parameter variations are tabulated in Table 5.9. The number of parameter combinations (C_P) is the product of the number of the applied values to each lumped parameter and the selected temperatures (Equation 5.2). For all wells an avarage infiltration elevation of 500 m was assumed although not verified. However, due to the strongly variating topography, the uncertainty about the catchment area for each individual well, and the larger impact of temperature on the solubilty of the CFCs and SF_6 this assumption can be justified as a first approximation.

$$C_P = n_{T_M} \cdot n_{DF} \cdot n_{DP} \cdot n_T \tag{5.2}$$

Table 5.7: CFC-11, CFC-12, CFC-113, and T analyses of samples from deep wells of the Upper and Lower subaquifer.

well	date	T [T.U.]	T$_{error}$ [T.U.]	CFC-11 [pmol/L]	CFC-11$_{err}$ [pmol/L]	CFC-12 [pmol/L]	CFC-12$_{err}$ [pmol/L]	CFC-113 [pmol/L]	CFC-113$_{err}$ [pmol/L]	SF$_6$ [fmol/L]	SF$_6$ err [fmol/L]
Agur 1	25.10.2004	0	0.3	0.02	0.05	0	0.01	0	0.01	0	0.1
Agur 4	05.05.2005	<0.5	0.1	0.22	0.05	0.01	0.05	<0.01		0.1	0.1
Agur 5	23.04.2004	<0.6	0.3	0.12	0.05	0.03	0.05	0.01	0.05	0	0.1
Agur 6	23.04.2004	0.4	0.3	0.7	0.1	0.4	0.05	0.04	0.05	0.5	0.1
Agur 6	05.05.2005	0.4	0.3	0.6	0.1	0.41	0.05	0.04	0.05	0.5	0.1
Agur 7	23.04.2004	1.5	0.4	1.9	0.3	0.34	0.05	0.05	0.05	0.1	0.1
Agur 7	25.10.2004	1.6	0.3	1.4	0.2	0.32	0.05	0.04	0.05	0.1	0.1
Agur 7	05.05.2005	1.6	0.3	1.6	0.2	0.37	0.05	0.04	0.05	0.1	0.1
Agur 8	23.04.2004	2.5	0.4	12	3	0.47	0.05	0.08	0.05	0.1	0.1
Ein Samia 1	03.04.2004	5.4	0.5	3.1	0.4	1.6	0.1	0.26	0.05	0.9	0.1
Ein Samia 1	14.10.2004	5.4	0.5	2.8	0.3	1.4	0.1	0.21	0.05	0.8	0.1
Ein Samia 1	23.04.2005	5.4	0.5	3.3	0.2	1.7	0.10	0.29	0.05	1.1	0.2
Ein Samia 2A	03.04.2004	3.5	0.4	1.8	0.2	1.1	0.1	0.16	0.05	0.6	0.1
Ein Samia 2A	13.10.2004	2.8	0.3	1.6	0.2	1	0.1	0.15	0.05	1	0.2
Ein Samia 2A	23.04.2005	4.3	0.5	1.9	0.2	1	0.10	0.15	0.05	1	0.1
Ein Samia 4	05.04.2004	0.4	0.3	0.05	0.05	0.03	0.05	0.02	0.05	0.3	0.1
Ein Samia 4	13.10.2004	0.1	0.3	0.21	0.05	0.23	0.05	0.02	0.05	0.6	0.1
Ein Samia 6	05.04.2004	3.4	0.4	2	0.2	1.1	0.1	0.17	0.05	1.4	0.2
Ein Samia 6	14.10.2004	3.3	0.3	2	0.2	1.2	0.1	0.17	0.05	1.2	0.2
Ein Samia 6	05.04.2005	3.6	0.5	2.2	0.2	1.3	0.10	0.19	0.05	1.3	0.2
Hebron 1	08.04.2004	0.3	0.3	0.05	0.05	0.01	0.05	0	0.01	0.1	0.1
Hebron 1	12.10.2004	0	0.3	0.06	0.05	0.02	0.05	0	0.01	0.2	0.1
Herodion 1	07.04.2004	1.7	0.4	1.1	0.1	0.9	0.1	0.17	0.05	0.6	0.2
Herodion 1	11.10.2004	1.5	0.3	0.7	0.1	0.39	0.05	0.03	0.05	0.7	0.1
Herodion 1	23.04.2005	1.6		1.7	0.2	1	0.10	0.16	0.05	0.7	0.1
Herodion 2	07.04.2004	0.6	0.3	0.13	0.05	0.07	0.05	0.02	0.05	0.1	0.1
Herodion 2	11.10.2004	0.7	0.3	0.18	0.05	0.11	0.05	0	0.01	0.3	0.1
Herodion 2	23.04.2005	0.65		0.14	0.05	0.09	0.05	<0.01		0.2	0.1
Herodion 3	08.04.2004	0.1	0.3	0.03	0.05	0.03	0.05	0.01	0.05	0.2	0.1
Herodion 3	12.10.2004	0.2	0.3	0.04	0.05	0.03	0.05	0	0.01	0.1	0.1
Herodion 4	08.04.2004	0.3	0.3	0.05	0.05	0	0.01	0.01	0.05	0.1	0.1
Herodion 4	14.10.2004	0.1		0.05	0.05	0.01	0.05	0	0.01	0.1	0.1
Herodion 4	23.04.2005	0.2		0.06	0.05	0.02	0.05	<0.01		<0.1	
Modi'in 2	25.10.2004	2	0.3	1.1	0.2	0.6	0.1	0.07	0.05	0.2	0.1

Table 5.8: Measurement values for noble gas samples of wells of the Agur, Herodion and ein Samia well fields. STP is the common notation for standart temperature, standart pressure.

Well	date	δ^{22}Ne ‰	Ne$\cdot 10^{-4}$	^{4}He$\cdot 10^{-5}$ [mL STP/kg]	$\frac{^3\text{He}}{^4\text{He}}\cdot 10^{-6}$	R_{sample}/R_a
Agur 1	05.05.2005	0.319	2.158	11.710	0.812	0.597
Agur 3	05.05.2005	0.258	2.141	10.564	0.756	0.556
Agur 4	05.05.2005	0.120	2.506	9.161	1.003	0.737
Agur 5	23.04.2004	-0.996	2.090	5.944	1.219	0.896
Agur 6-1	23.04.2004	-0.308	2.135	5.446	1.385	1.017
Agur 6-2	05.05.2005	0.422	2.175	5.448	1.362	1.000
Agur 7-1	23.04.2004	0.261	2.416	6.168	1.439	1.057
Agur 7-2	05.05.2005	-0.206	2.123	5.516	1.405	1.032
Agur 8	23.04.2004	0.080	2.111	5.738	1.396	1.025
Modi'in 2	25.10.2004	0.405	2.270	5.727	1.579	1.160
Ein Samia 1-1	03.04.2004	-0.883	1.968	5.044	1.383	1.016
Ein Samia 1-2	13.10.2004	0.032	1.856	4.784	1.404	1.032
Ein Samia 2 A-1	03.04.2004	0.018	3.304	8.407	1.393	1.024
Ein Samia 2 A-2	13.10.2004	0.204	2.965	7.568	1.397	1.026
Ein Samia 2 A-3	23.04.2005	0.180	3.339	8.767	1.392	1.023
Ein Samia 4-1	05.04.2004	0.110	2.645	7.958	1.198	0.880
Ein Samia 4-2	13.10.2004	0.280	2.781	7.900	1.217	0.895
Ein Samia 6-1	14.10.2004	0.285	3.540	8.794	1.395	1.025
Ein Samia 6-2	23.04.2005	-0.668	8.739	23.570	1.359	0.999
Hebron 1	08.04.2004	0.194	2.653	7.775	1.249	0.917
Herodion 1-1	03.04.2004	0.791	2.087	5.238	1.382	1.016
Herodion 1-2	13.10.2004	0.151	2.171	5.229	1.419	1.043
Herodion 1-3	03.04.2004	0.193	2.375	6.425	1.278	0.939
Herodion 2-1	13.10.2004	-0.171	2.771	7.443	1.329	0.977
Herodion 2-2	23.04.2005	0.288	2.820	7.534	1.345	0.988
Herodion 3-1	05.04.2004	-0.129	2.967	8.146	1.283	0.943
Herodion 3-2	13.10.2004	0.183	3.012	8.142	1.270	0.933
Herodion 4-1	14.10.2004	0.578	2.855	9.234	1.093	0.803
Herodion 4-2	23.04.2005	0.335	2.781	8.935	1.100	0.808

where C_P is the number of parameter combinations, and $n_{Parameter}$ the number of variations of the specified parameter in the index of n.

Table 5.9: Applied lumped parameter ranges for the evaluation of the measured T, CFC-11, CFC-12, CFC-113, and SF_6 values in the groundwater samples of the deep wells of the Agur, Herodion, and Ein Samia well fields.

Lumped parameters of DM	lumped parameter values	infiltration temperatures [°C]
TM [years]	5, 10, 20, 40, 60	
DF [%]	20, 40, 60, 80, 95, 100	16, 18
DP [-]	0.1, 0.35, 0.6	

Thus, the number of calculated theoretical models is 180 for each tracer, except for T, for which only 90 theoretical models were processed, because its concentration is independent of temperature. In total this equals to 810 calculated theoretical models. Due to the expenditure for the model processing, the data post-processing, and the visual evaluation the model outputs for Mai, 2005 were extracted to estimate the minima and maxima of T_M and DF. Because of the expected higher uncertainties due to the application of the lumped parameter models in a multi-porosity aquifer with a very thick unsaturated zone that simplification is justified.

The visual evaluation process is exemplarily shown for the case of the deep well of Ein Samia 2 (Upper subaquifer) for the tracer combination of CFC-12 and SF_6 at an infiltration temperature of 16°C and an infiltration elevation of 500 masl.

In Figure 5.24 the samples are plotted together with the theoretical models for which the corresponding T_M is indicated by an individual color. By visual interpretation the $T_{M,min}$ and $T_{M,max}$ values of the DM can be estimated to 8 years and 20 years, respectively.

In contrary Figure 5.25 depicts the relation of the samples to the proportions of the DM in the coupled PM||DM model. As before, the percentage of the DM that is one of the three varied lumped parameters is indicated using individual colors. Here, minimum and maximum DF values of 52.5 % and 70 %, respectively are suggested from the visual interpretation.

In opposite to the mean residence time and the percentage of the DM no ranges for the DP of the DM can be clearly extracted from Figure 5.26, which in analogy to Figure 5.24 and Figure 5.25 shows the relation of the samples to the computed theoretical models with color indexing based on the three DP.

As implied by the exemplary description of the estimation procedure the tracers were combined with each other in different pairs to study possible ranges for the minimal and maximal T_M and DF. The list of the considered pairs include CFC-11 and CFC-12, CFC-12 and CFC-113, CFC-12 and SF_6, T and CFC-11, T and CFC-12, T and CFC-113, as well as T and SF_6. If the variation between the samples of one well was significantly high,
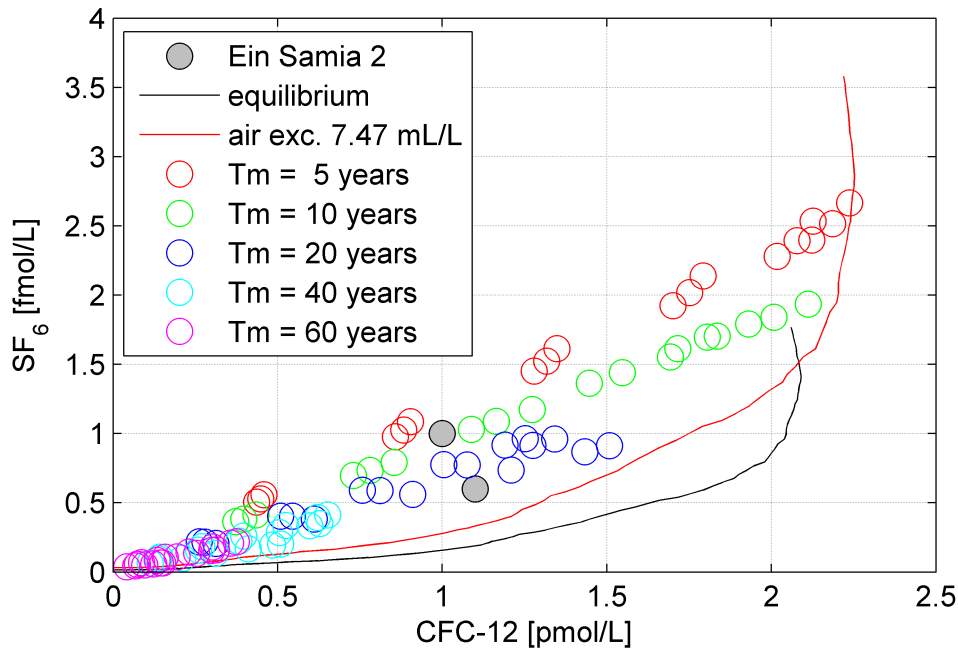
Figure 5.24: Plot of theoretical PM||DM models with DM mean residence times of 5, 10, 20, 40, and 60 years and sample analyses from the well Ein Samia 2 (Upper subaquifer). The amount of excess air was calculated by ^{20}Ne excess.
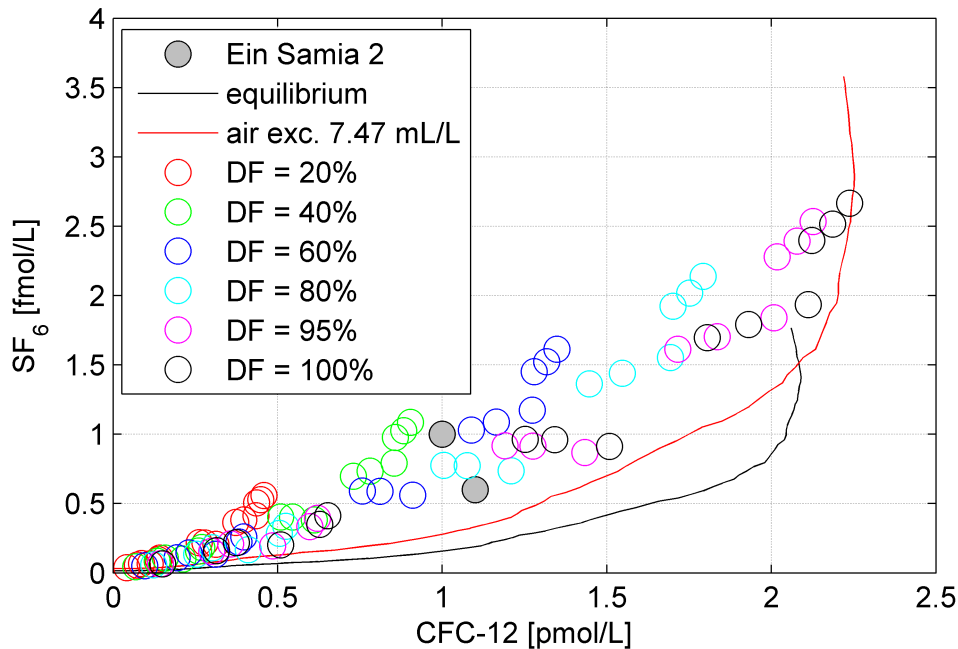
Figure 5.25: Plot of theoretical PM||DM models with proportions of the DM of 20, 40, 60, 80, 95, and 100 % and sample analyses from the well Ein Samia 2 (Upper subaquifer). The amount of excess air was calculated by ^{20}Ne excess.
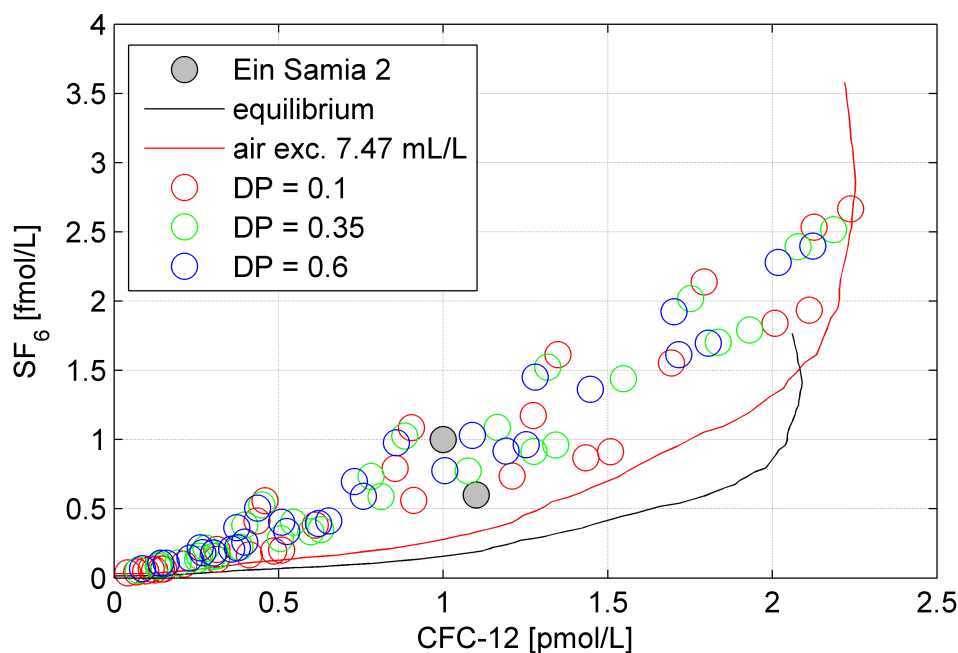
Figure 5.26: Plot of theoretical PM||DM models with DP of 0.1, 0.35, and 0.6 and sample analyses from the well Ein Samia 2 (Upper subaquifer). The amount of excess air was calculated by ^{20}Ne excess.

the samples were split into subgroups like for Herodion 1 and Ein Samia 4.

Figure 5.27 and Figure 5.28 depict the summarized results that were extracted from the ascertained data sets of the Tables 5.10 to 5.13.

Agur well field, Modi'in 2:

In the case of the Agur well field the extracted ranges for the T_M and the DF of the DM are a strong indication for a karstic system. The spatial arrangement of the wells follows the generally westnorthwest directed flow from the mountainous to the Ha'Shefela region. While the estimated minimum and maximum T_M decrease from east to west, the minimum and maximum DF of the DM simultaneously decreases, as well, which only apparently seems contradictory. The most probable interpretation of that pattern is derived from the following conceptual considerations:

- Agur 8 (east, mountainous area): The highest proportion of the DM is accompanied by the highest mean residence time, which suggests a higher non-matrix porosity. Obviously, this is not a contradiction at all. It rather should be interpreted in terms of a more disperse mixture of younger groundwater components, while older components may be less dominant in the unconfined part of the investigated system of the Agur area.
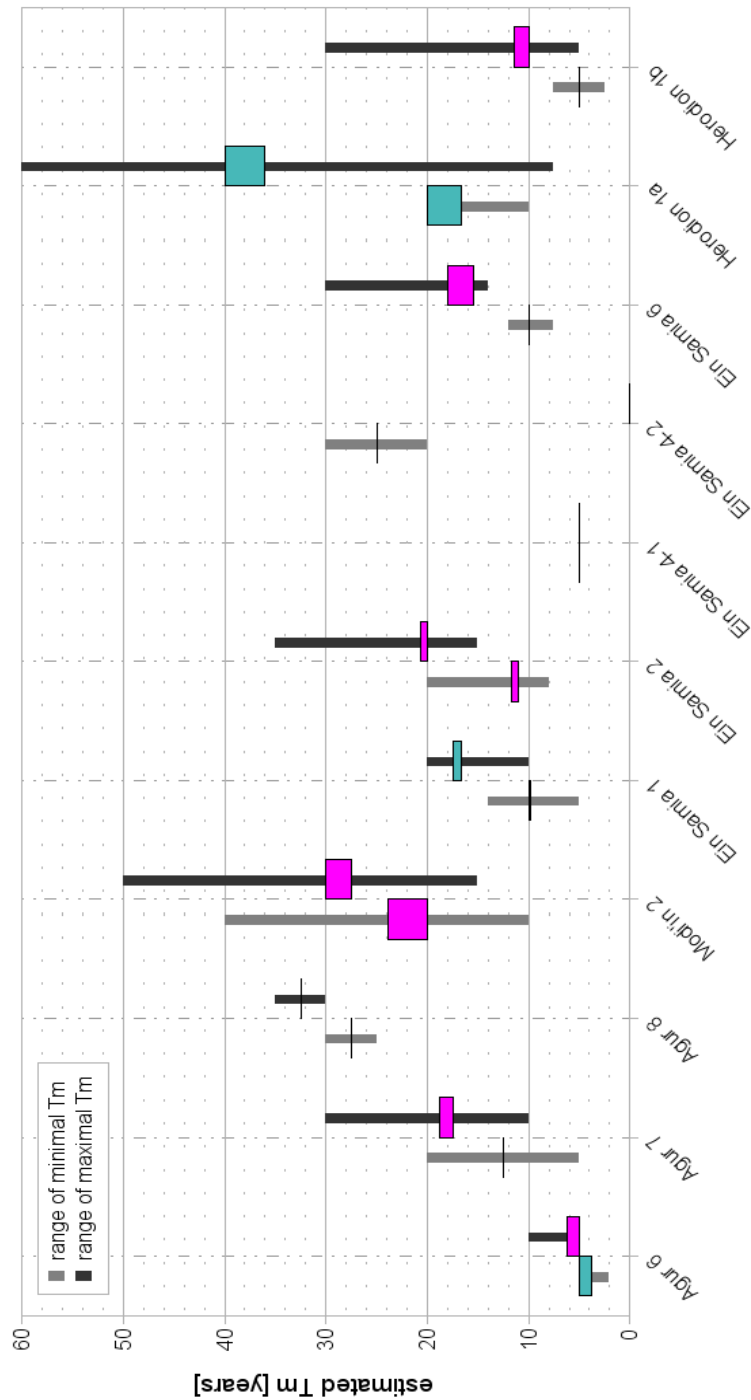
Figure 5.27: Minimal and maximal estimations of T_M for the deep well samples of the Agur, Herodion, and Ein Samia well fields. While lines in light gray represent the range of estimated minimums of T_M, lines in dark gray represent the range of estimated maximums of T_M. The position of and the distance between the mean and the median of the estimates are depicted by the boxes. If mean − median > 0 the boxes are filled with turquoise (cyan) otherwise mangenta.
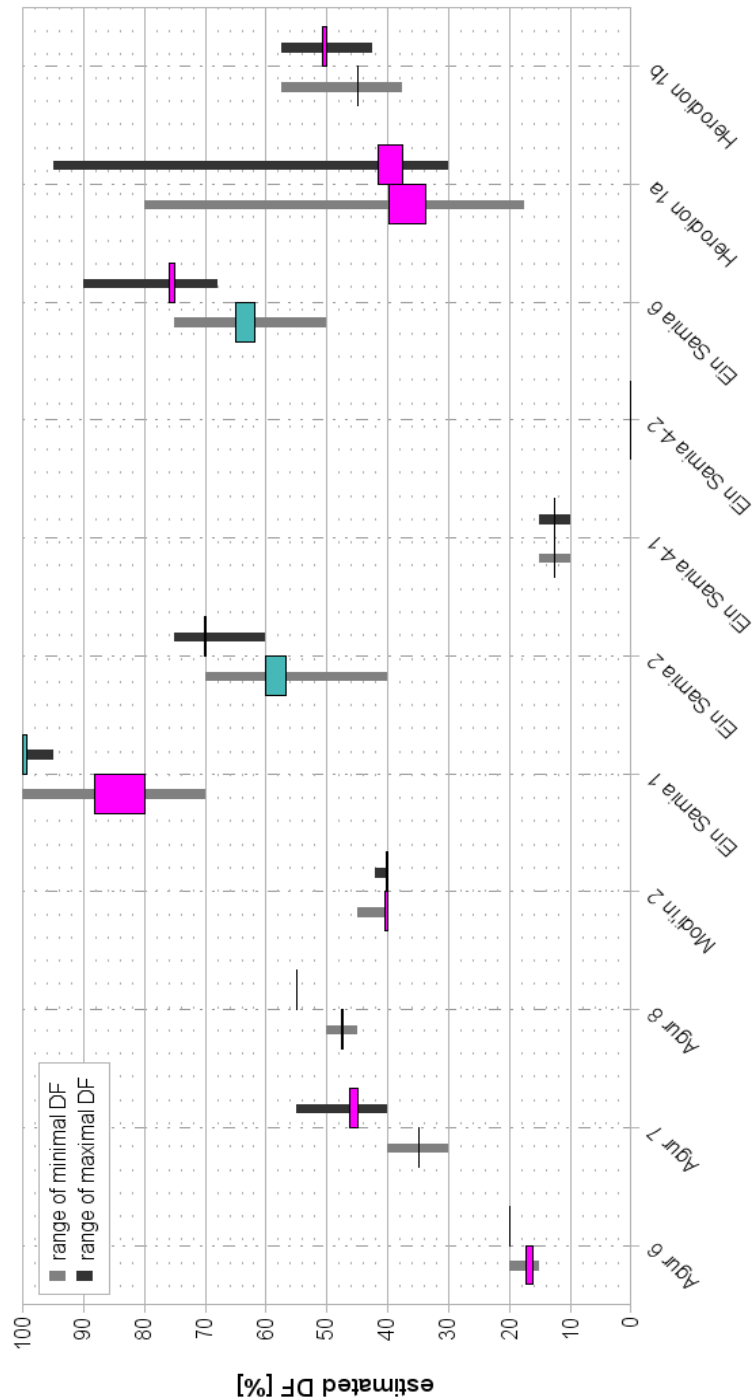
Figure 5.28: Minimal and maximal estimations of the percentage of the DM (DF) for the deep well samples of the Agur, Herodion, and Ein Samia well fields. While lines in light gray represent the range of estimated minimums of DF, lines in dark gray represent the range of estimated maximums of DF. The position of and the distance between the mean and the median of the estimates are depicted by the boxes. If mean − median > 0 the boxes are filled with turquoise (cyan) otherwise mangenta.

- Agur 6 (west, Ha'Shefela area): In contrast, the analyses of samples from Agur 6 indicate, that most of the groundwater is free of modern contributions, i.e. groundwater younger then 1953. Nevertheless, the still existing young groundwater component possess a much younger age structure, which can only be related to a more differentiated karstic system that enables the mixture of very young and old groundwaters.

The evaluation results for the tracer samples from Modi'in 2 are positioned between that of Agur 8 and Agur 7. This fully matches the expectations as the structural position of the well in the steep, to the west dipping layers on the western mountain flank is similar.

Ein Samia well field

The wells of the Ein Samia well field show a different pattern compared to the Agur well field as the PM and DM model proportions are different for Ein Samia 1, Ein Samia 2A, and Ein Samia 6 whereas their DM-T_M are very similar, beside some differences (10..20 years). The individual DF values are between 80 and 100 % for Ein Samia 1, 50 and 70 % for Ein Samia 2A, and 55..80 % for ein Samia 6, which can be interpreted as mixing of a tracer free old component with a young groundwater component that is of identical origin for all three wells. However, the situation meets the expectations for Ein Samia 1 as it is the most shallow well, but it apparently is contradictory for Ein Samia 2A and Ein Samia 6. Because the latter penetrates both, the Lower and Upper subaquifer and Ein Samia 2A solely the Upper subaquifer, the opposite could be expected rather. But the difference is not too large and could be attributed to the visual estimation procedure or to the varying conditions in the karstic system. Ein Samia 4 seems to be decoupled from the other wells, which supports assumptions (oral communications with Jerusalem Water Undertaking company and C. Messerschmidt from the GIZ), that the well is hydraulically seperated by a major fault, causing a head difference of about 100 m between Ein Samia 6 and Ein Samia 4. The DM-T_M/DF pattern of the tracer samples represented by Ein Samia 4-1, on the one hand, are very similar to that of Agur 6 with DM-T_M and DF of only 5 years and 13 %, respectively. Ein Samia 4-2 on the other hand suggest a minimum DM-T_M of 25 years, but it was not possible to estimate any DF. Thus, the evaluation results for Ein Samia 4-2 should be used with caution.

Herodion well field

Because in the Herodion well field only Herodion 1 could be used for the estimations of the T_M and DF no comparison with the Herodion wells was possible. However, the parameter and analysis pattern of the Herodion 1 samples again suggest an elevated proportion of the DM as well as a younger age structure.

5.3.2 Evaluation of the helium and neon isotopes

The data of Table 5.8 tabulate the noble gas analyses of the samples from the deep wells of the Agur, Herodion, and Ein Samia well fields. Some wells were multiply sampled

between spring 2004 and spring 2005, the duration time of the whole study. Sample dublicates were averaged for lucidity. The results of the helium and neon isotope analyses are presented in Figures 5.29 to 5.31.
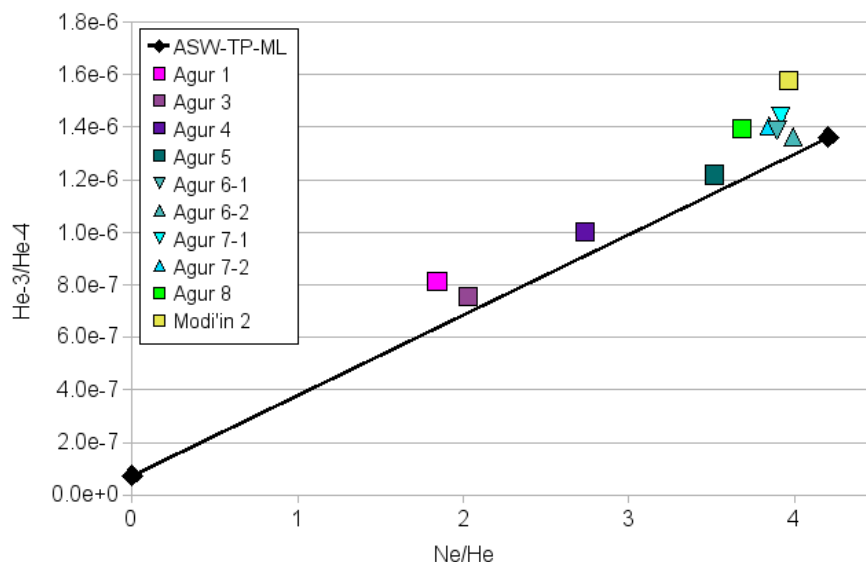
Figure 5.29: Ratios of ^{3}He/^{4}He and Ne/He plottet for the Agur well field. Note that the well Modi'in 2 does not belong to it, since it is located east of the Kefar Uriya well field, northwest of Jerusalem. ASW-TP-ML is the atmospheric saturated water-terrigenic production-mixing line.

While at the abscissa the Ne/He ratio of the samples is applied, the ^{3}He/^{4}He ratio is applied at the ordinate. The Ne/He ratio reflects the increase of the helium concentration in the sampled groundwater over time with respect to neon that is practically assumed to be constant. Conceptually the groundwater is observed as its noble gas signature diverts with time and distance from an equilibrium air saturated water to the signature of the sample. To recall from subsection 3.1.2, the main potential processes for He accumulation are the in-situ He production in the aquifer, the crustal He flux, and a direct contribution from the mantle or lower crustal domains. Further on, the ^{3}He/^{4}He ratio that is applied at the ordinate is the indicator for the two main basic helium sources: radioactive decay of uranium and thorium or mantle helium exhalation possessing a more primordial signature. As stated in subsection 3.1.2, water from aquifer material enriched in Li possess a higher ^{3}He/^{4}He ratio, that could be misinterpreted as mantle contribution. However, the latter does not need to be considered in the investigated study areas since the Judea Group carbonate aquifer is set up of marine platform carbonates, for which increased Li concentrations are unlikely and not reported.

To conduct the estimation of the conceptual model ages (T_M) and proportions of the DM (DF) in the coupled PM||DM model a full dissolution of detected excess air concentrations was presumed, although not verified. But as suggested by several authors and outlined
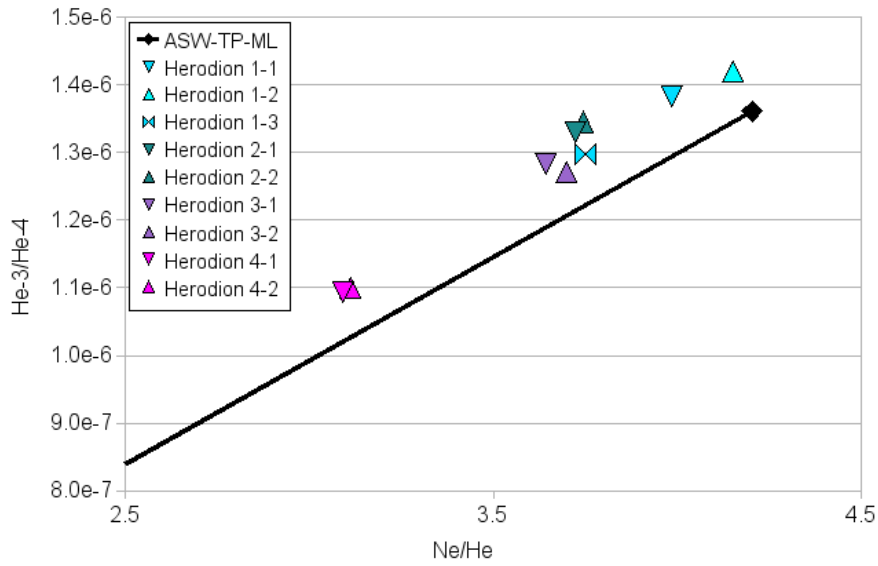
Figure 5.30: Ratios of ^{3}He/^{4}He and Ne/He plottet for the Herodion well field. ASW-TP-ML is the atmospheric saturated water-terrigenic production-mixing line.
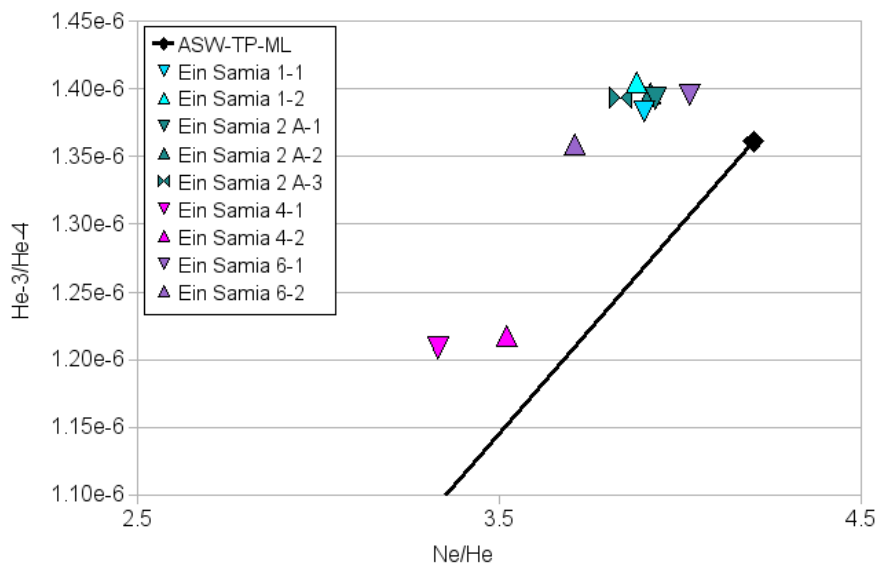
Figure 5.31: Ratios of ^{3}He/^{4}He and Ne/He plottet for the Ein Samia well field. ASW-TP-ML is the atmospheric saturated water-terrigenic production-mixing line.

in subsection 3.1.2 that assumption in many cases may only be restrictedly valid. [106] and [107] provide more experimental and theoretical background to that subject. As indicated in subsection 3.1.2 measurements for preferably all five major noble gasses (He, Ne, Ar, Kr, Xe) would provide the most unambiguous view on the real conditions. With only helium and neon measured several restrictions limit the identification of the real dissolution conditions between the sampled groundwater and a fully or partially dissoluted or reequilibrated excess air component.
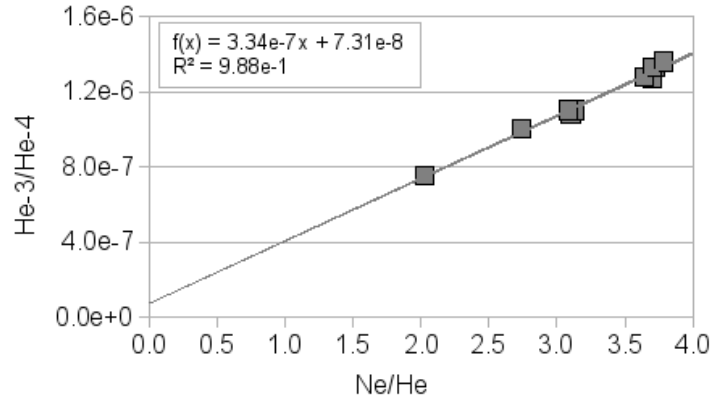
Figure 5.32: ^{3}He/^{4}He versus Ne/He for a subset of the deep wells that is supposedly free of tritiogenic and mantle helium contribution (Agur 3, Agur 4, Herodion 2, Herodion 3, and Herodion 4). The intersection at Ne/He = 0 with the ^{3}He/^{4}He axis can be approximated as the terrigenic ^{3}He/^{4}He production ratio of $\approx 7.3 \cdot 10^{-8}$.

However, if the tritiogenic or mantle derived ^{3}He component can be neglected and the terrigenic ^{3}He/^{4}He ratio can be sufficiently accurate estimated, the atmospheric He component is determined according to [156] by the binary mixing model of Equation 5.3:

$$He_{atmospheric} = He_{measured} \cdot \left(\frac{R_{measured} - R_{terrigenic}}{R_{atmospheric} - R_{terrigenic}} \right) \qquad (5.3)$$

Only a subset of the sampled wells meet these requirements by featuring supposedly negligible amounts of post-1953 tritiogenic helium. Figure 5.29, Figure 5.30, and Figure 5.31 suggest that only the wells of Agur 1, Agur 3, Agur 4, Herodion 2, Herodion 3, and Herodion 4 belong to that group. However, Agur 1 that exposes a similar Ne/He signature as Agur 3 may be slightly affected by a mantle helium component due to an elevated ^{3}He/^{4}He ratio. For that reason Agur 1 was withdrawn from the list. As a result the ^{3}He/^{4}He ratio of the terrigenic production can be determined to $7.3 \cdot 10^{-8}$ (Figure 5.32). By applying Equation 5.3 to all of the considered samples the relation of the atmospheric He and Ne components in the groundwater samples to the theoretical total dissolution or unfractionated air model (UA, e.g. [156]), respectively, can be established. As underlined by Figure 5.33 the validity of the total dissolution model for an infiltration elavation
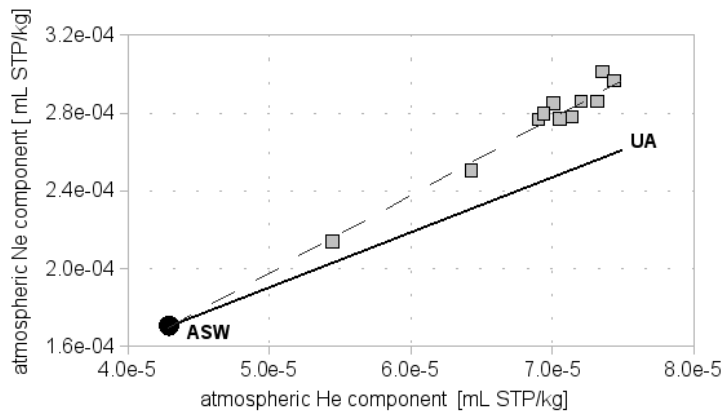
Figure 5.33: ^{3}He/^{4}He versus Ne/He ratios of samples from the wells Agur 3, Agur 4, Herodion 2, Herodion 3, and Herodion 4 that are supposedly free of tritiogenic and mantle helium contribution in comparision to the theoretical dissolution or unfractionated air model (UA) at an infiltration elevation and temperature of 500 m and 17 °C. The position of the samples left of the air saturated water (ASW)-UA line suggests that the assumption of the total dissolution is to be rejected.

and temperature of 500 m and 17 °C, respectively is to be rejected for the tested wells. However, for all other wells including those that were suited for the lumped parameter modeling (subsection 5.3.1) the question concerning the correct dissolution model remains unsolved. Hence, the possible effect on the estimated DM ages and DM proportions can not be quantified.

Because the suited well samples were already evaluated with respect to their age structure in subsection 5.3.1 the tritiogenic ^{3}He was not further exploited for additional, similar calculations. Regarding the old, essentially tracer free groundwater components the data clearly indicate that:

1. in the Agur well field its proportion follows an increasing tendency along the flowpath from east to west. Nevertheless this trend discontinues between Agur 3 and Agur 1, which can be related to the northbound direction of flow in the Ha'Shefela region.

2. in the Herodion well field that is located in or very close to the recharge area the increase in terrigenic helium is related to the abstracted aquifer and very likely to both, the depth of the well and the local aquifer characteristics. All wells are located close to each other.

3. in the Ein Samia well field the general age structure is much more shifted to an overall younger age spectrum except for Ein Samia 4, which is hydraulically separated from the other wells by a major fault that acts as an effective flow barrier.

The different interpretations for the well fields are fully consistent with the results of the lumped parameter modeling in subsection 5.3.1. Only at Agur 1 and Modi'in 2a

significantly elevated ^{3}He/^{4}He ratios could be an indication for a small contribution from mantle helium. Thus, with respect to the young components of the Modi'in 2 sample mantle and tritiogenic ^{3}He may not be discriminated unambiguously.

Beside the approved valuable information that was extracted from the noble gas data, important limitations can be drawn with respect to the age structure of the old groundwater component, and possible links to mixing processes, which potentially could be derived from the accumulated, dissolved ^{4}He. The reason is not only related for example to uncertainties with respect to the distinct flow paths that must be known in order to apply any analytical or empirical equation, like that of Equation 3.7. The main obstacle is the multi-porosity character of the studied Judea Group Aquifer, a phenomenon, which is common also to other aquifer types like fractured sandstone or chalks and that distinctively affect the spatial distribution of flow velocities, the variation of flow paths, as well as the transport of ^{4}He (e.g. [132]). For the simple case that the vertical helium crustal flux component is neglegted and the uranium and thorium rock concentrations are known it is still impossible to use the terrigenic, in-situ helium production rate for age estimations if the dependencies on important aquifer parameters with respect to the multi-porosity character are unknown. Further, beside the antropogenic induced stress on the aquifer, changes in the head distribution were likely to happen during time spans of hundreds or thousands of years. All of those effects have still not been studied comprehensively so far. In section 5.4 the results of a sensitivity analysis that was conducted for a simple aquifer configuration are presented.

Table 5.10: Estimated minimum mean residence times for the deep wells of the Agur, Herodion, and Ein Samia well fields. Central tendencies are provided as mean (m) and median (md). NSD is the normalised standart deviation. The RDM is the percentage of |mean-median| with respect to the range of estimates. If |mean-median| = 0, RDM is set to 0.

well	CFC-11/12 16 C	CFC-11/12 18 C	CFC-12/13 16 C	CFC-12/13 18 C	CFC-12/SF6 16 C	CFC-12/SF6 18 C	T/CFC-11 16 C	T/CFC-11 18 C	T/CFC-12 16 C	T/CFC-12 18 C	T/CFC-113 16 C	T/CFC-113 18 C	T/SF6 16 C	T/SF6 18 C	min	max	m	md	NSD [1]	RDM [%]
															\[min Tm [years]\]					
Agur 6						5	5	5	2	2					2	5	3.8	5	0.43	-40.0
Agur 7							5	5	20	20					5	20	12.5	12.5	0.69	0.0
Agur 8									30	25					25	30	27.5	27.5	0.13	0.0
Modïin 2			40	40	40	40	10	10	15	10	25	17	20	20	10	40	23.92	20	0.53	13.1
Ein Samia 1			5	5	5	10	13	12	14	13	11	10	10	10	5	14	9.83	10	0.33	-1.9
Ein Samia 2			10	12	8	20	15	12	12	10	12	10	10	10	8	20	11.75	11	0.27	6.3
Ein Samia 4-1											5	5	5	5	5	5	5	5	0.00	0.0
Ein Samia 4-2	20	30													20	30	25	25	0.28	0.0
Ein Samia 6			10	10	7.5	7.5	12	10	10	10	12	10	10	10	7.5	12	9.92	10	0.14	-1.9
Herodion 1a							20	20	20	20	10	10			10	20	16.67	20	0.31	-33.3
Herodion 1b			2.5	2.5	7.5	7.5	5	5	5	5	5	5	5	5	2.5	7.5	5	5	0.30	0.0

Table 5.11: Estimated maximum mean residence times for the deep wells of the Agur, Herodion, and Ein Samia well fields. Central tendencies are provided as mean (m) and median (md). NSD is the normalised standart deviation. RDM is the percentage of |mean-median| with respect to the range of estimates. If |mean-median| = 0, RDM = 0.

well	CFC-11/12 16 C	CFC-11/12 18 C	CFC-12/13 16 C	CFC-12/13 18 C	CFC-12/SF6 16 C	CFC-12/SF6 18 C	T/CFC-11 16 C	T/CFC-11 18 C	T/CFC-12 16 C	T/CFC-12 18 C	T/CFC-113 16 C	T/CFC-113 18 C	T/SF6 16 C	T/SF6 18 C	min	max	m	md	NSD [1]	RDM [%]
									max Tm [years]											
Agur 6					5	5	10	10	5	5			5	5	5	10	6.25	5	0.37	25
Agur 7							10	10	25	30					10	30	18.75	17.5	0.55	6.25
Agur 8									35	30					30	35	32.5	32.5	0.11	0
Modi'in 2	50	40	40	40	40	40	20	20	20	15	20	20	30	25	15	50	30	27.5	0.38	7.14
Ein Samia 1	20	20	15	15	10	10	20	19	20	19	19	16	15	16	10	20	16.71	17.5	0.21	-7.86
Ein Samia 2	35	35	20	17	20	20	20	18	17	15	17	15	20	20	15	35	20.64	20	0.31	3.21
Ein Samia 4-1																				
Ein Samia 4-2													5	5	5	5	5	5	0	0
Ein Samia 6	30	30	20	20	15	15	17	15	17	15	16	14	14	14	14	30	18	15.5	0.3	15.63
Herodion 1a	60	60	40	40	60	60	20	20	20	20	50	40	7.5	7.5	7.5	60	36.07	40	0.55	-7.48
Herodion 1b	30	30	10	7.5	7.5	10	12.5	10	10	10	7.5	5	5	5	5	30	11.43	10	0.72	5.71

Table 5.12: Estimated minimum proportions of the DM in the PM‖DM for the deep wells of the Agur, Herodion, and Ein Samia well fields. Central tendencies are provided as mean (m) and median (md). NSD is the normalised standart deviation. The RDM is the percentage of |mean−median| with respect to the range of estimates. If |mean−median| = 0, RDM is set to 0.

Values for the ratio columns are given as min DF [%].

well	CFC-11/12 16 C	CFC-11/12 18 C	CFC-12/13 16 C	CFC-12/13 18 C	CFC-12/SF6 16 C	CFC-12/SF6 18 C	T/CFC-11 16 C	T/CFC-11 18 C	T/CFC-12 16 C	T/CFC-12 18 C	T/CFC-113 16 C	T/CFC-113 18 C	T/SF6 16 C	T/SF6 18 C	min	max	m	md	NSD [1]	RDM [%]
Agur 6					17.5	20	15	15	15	15			20	20	15	20	17.19	16.25	0.14	18.8
Agur 7							40	40	30	30					30	40	35	35	0.16	0.0
Agur 8					45	50			50	45					45	50	47.5	47.5	0.07	0.0
Modi'in 2			40	40	45	40	40	40	40	40	40	40	40	40	40	45	40.42	40	0.04	8.3
Ein Samia 1	70	80	80	80	80	80			100	100	100	100	100		70	100	88.18	80	0.13	27.3
Ein Samia 2	40	45	60	60	52.5	52.5	55	60	60	60	60	60	60	70	40	70	56.79	60	0.13	-10.7
Ein Samia 4-1													10	15	10	15	12.5	12.5	0.28	0.0
Ein Samia 4-2																				
Ein Samia 6	50	50	50	50	55	60	65	70	65	70	67	70	68	75	50	75	61.79	65	0.15	-12.9
Herodion 1a	17.5	20	80	80	37.5	37.5	30	30	30	30			42.5	42.5	17.5	80	39.79	33.75	0.51	9.7
Herodion 1b	45	50	40	40	37.5	57.5	37.5	37.5	45	45	45	50	42.5	42.5	37.5	57.5	45	45	0.29	0.0

Table 5.13: Estimated maximum proportions of the DM in the PM∥DM for the deep wells of the Agur, Herodion, and Ein Samia well fields. Central tendencies are provided as mean (m) and median (md). NSD is the normalised standart deviation. The RDM is the percentage of |mean−median| with respect to the range of estimates. If |mean−median| = 0, RDM is set to 0.

well	CFC-11/12		CFC-12/13		CFC-12/SF6		T/CFC-11		T/CFC-12		T/CFC-113		T/SF6		min	max	m	md	NSD	RDM
	\<--- max DF [%] ---\>																		[1]	[%]
	16 C	18 C	16 C	18 C	16 C	18 C	16 C	18 C	16 C	18 C	16 C	18 C	16 C	18 C						
Agur 6							20	20	20	20			20	20	20	20	20	20	0	0.0
Agur 7							50	55	40	40					40	55	46.25	45	0.16	8.3
Agur 8							55	55	55	55					55	55	55	55	0	0.0
Modi'in 2						40	40	40	40	42			40	40	40	42	40.29	40	0.02	14.3
Ein Samia 1					95	100	100	100	100	100				100	95	100	99.29	100	0.02	-14.3
Ein Samia 2					70	70	65	70	72	75	75	75	60	70	60	75	70.2	70	0.07	1.3
Ein Samia 4-1													10	15	10	15	12.5	12.5	0.28	0.0
Ein Samia 4-2																				
Ein Samia 6					80	90	70	75	75	78	70	75	68	78	68	90	75.9	75	0.08	4.1
Herodion 1a				95			30	30	30	30	37.5	37.5	42.5	42.5	30	95	41.67	37.5	0.50	6.4
Herodion 1b	57.5			57.5	55	57.5	47.5	50	45	50	50	52.5	42.5	45	42.5	57.5	50.83	50	0.10	5.6

5.3.3 Evaluation of δ^2H and δ^{18}O

δ^{18}O and δ^2H in precipitation

Although the spread of the isotopic signature in rain water in the area of the Judea Mountains ranges for δ^{18}O between -12 and 4 ‰ and for δ^2H between -80 and 60 ‰ [22], it is limited to a very small range in the groundwaters of the Judea Group Aquifer. The bulk falls into a narrow range between -6.0 and -5.0 ‰ and -30 and -20 ‰, respectively. [22] provide a functional relationship for the amount effect at the location of the Soreq Cave (northwest of Jerusalem) relating annual rainfall and the weighted, cumulative δ^{18}O signature (Equation 5.4).

$$\delta^{18}O = -0.004 \cdot (annual\ rainfall) - 3.7 \qquad (5.4)$$

Although this relation is valid for the Soreq Cave it provides a good indirect measure for the amplitude of the relation if one assumes the slope to be comparable with that for the Jerusalem area. Due to the monotoneous kind of the δ^{18}O-δ^2H pattern in the groundwater and the restriction of the major infiltration volume to the crestal area of the mountains the content of extractable information is limited, for instance with respect to the discrimination of different groundwater sources. The same limitation applies to the identification of possible salinization processes as a result of admixing brines, which are characterized by isotope patterns that can significantly diverge from that of fresh water (e.g. [105]), if they are not refered to dissolution processes. On the one hand the three sampled well fields show no clear evidence for such mixtures with respect to the δ^{18}O signature. On the other hand salinity gradually increases in the Agur well field from east to west. But the quantity of salinity surplus there is still too small to confirm either of these processes with certainty. This also has been shown for the Jericho well field in section 5.1.

However, despite the mentioned narrow isotope ranges the analysed samples obey spatial trends and local finger printings that reflect different infiltration conditions, different catchments as well as specific topographical characteristics. Figure 5.34, Figure 5.36, and Figure 5.35 suggest two main groups, that can be discriminated by their δ^{18}O distributions:

- a mountaineous group with values between -6.0 and -5.5 ‰

- and a group that is characteristic for the wells in the Ha'Shefela southwest of Jerusalem with values between -5.5 and -5.0 ‰.

According to [22] the elevation effect between the Soreq Cave (400 masl) and Jerusalem ($\approx$ 800 masl) is reflected by a lower δ^{18}O value of 0.5 to 1.0 at the sampling location in Jerusalem. This is in good agreement with an average lapse rate of $\approx$ -0.28 ‰/100 m valid for most areas at elevations below 5000 masl and moderate temperatures [164]. This opens a range for elevation differences between $\approx$ 200 and 350 m. Thus, since the wells of the Ha'Shefela group are located further west of the Soreq cave at lower elevations between
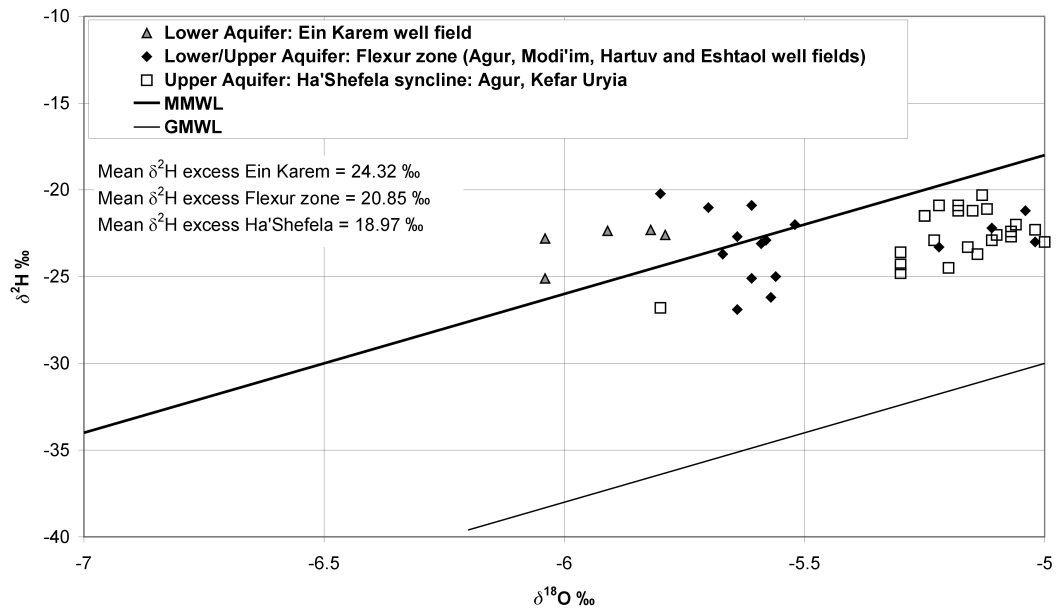
Figure 5.34: $\delta^{18}O$ and δ^2H distribution in the Agur, Kefar Uryia, Modi'in, Hartuv, and Eshtaol well fields. MMWL and GMWL are abbreviations for the mediterranean and the global meteoric water lines, respectively. Data are compiled from the GAPI-Project, [126], and [82].

about 200 and 300 m and there is no relevant infiltration in areas with a post-Turonian cover the groundwaters would have been derived from areas with elevations between 400 and 800 m, which would not contradict the available data.

Further, applying Equation 5.4 to the data set an annual precipitation of more then 500 mm and less than 400 mm could be expected for the mountaineous group and the Ha'Shefela group, respectively. According to for example [186], [89] the average annual precipitation in the area of the sampled wells exceeds 500 mm. Only approximately south of the line of 590000 N (New Israeli Grid), which is approximately south of Hebron the average annual precipitation starts to drop below 400 mm. Indeed, the general northbound flow from north of Beer Sheva to further north of the region of the Ha'Shefela well group can coherently explain the isotope pattern of the latter. It would be additionally in agreement to the similar helium composition of Agur 1 and Agur 3 (subsection 5.3.2).

However, both alternatives can not be discriminated and probably overlap each other.
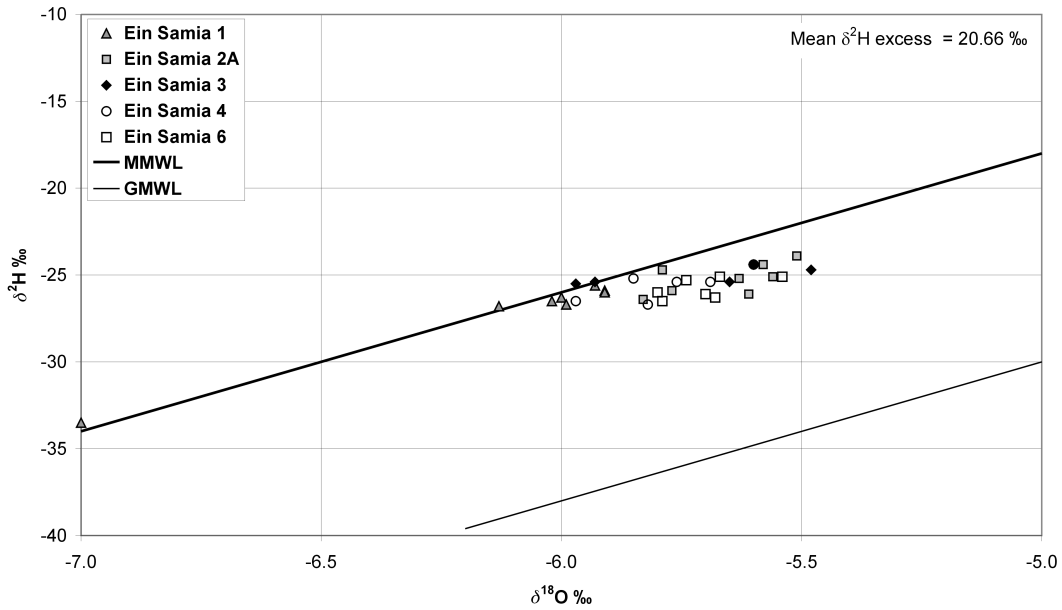
Figure 5.35: δ^{18}O and δ^2H distribution in the Ein Samia well field. MMWL and GMWL are abbreviations for the mediterranean and the global meteoric water lines, respectively.
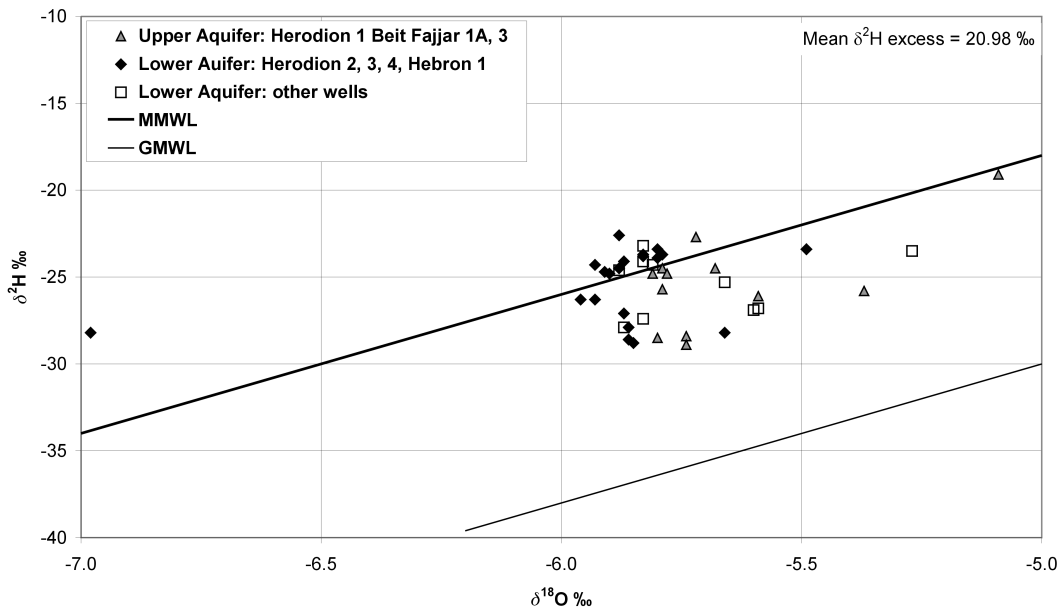
Figure 5.36: δ^{18}O and δ^2H distribution in the Herodion well field. MMWL and GMWL are abbreviations for the mediterranean and the global meteoric water lines, respectively.

5.4 Parameter sensitivities for ^{4}He accumulation in a dual continuum numerical transport model

In subsection 5.3.2 limitations regarding the extractable information from the noble gas data with respect to the age structure of the old groundwater component or possible mixing processes in the deep well samples from the Judea Group Aquifer are taken up and are adressed with an initial study about the sensitivities of the helium accumulation in groundwater to several, important aquifer parameters. Only a few studies were conducted to actually model the helium accumulation and transport in groundwater by means of distributed, numerical models, e.g. [198], [48], [36], [47], [46]. All of these publications in general deal with large scale, regional models - the Carrizo aquifer in Southwest-Texas, USA, the Paris, the Great Hungerian, and the Great Artesian Basin in Australia. At this areal extent small scale variations have less effect on the whole system.

However, to evaluate the sensitivity of the simulated system to parameter changes all major system variables describing its state have to be identified beforehand. For the considered case of helium accumulation in a dual continuum aquifer with the given geometry, boundary conditions, and the other uniformly distributed parameters as described in section 4.5 these state variables are the tracer mass fluxes across a specified area, preferably across the entire aquifer thickness close to the flow outlet boundary, in both, the matrix as well as dual continuum or fracture continuum, respectively.

In turn, the two state variables or mass fluxes can only be evaluated once the system is in steady state. To find steady state conditions for the applied parameter sets the model has to be initialized with specified concentrations and to run until the mass flux in the two continua converge to a value that is characteristic for the system. The input signal for the system that is studied here, actually is transduced in the form of a Heaviside or step function at time $t_0 = 0$, representing the switchover of the rate of helium production in the aquifer material from 0 to J_{He}. According to the selected parameter set the system answers with a response function that specifically lags behind the Heaviside event. The time lag represents the transition between the initial and the final steady state.

The mass fluxes of both, the matrix and dual continuum are a function of all varied parameters (Equation 5.5). Therefore, the system is underdetermined because the number of the varied parameters is greater than the number of state variables and only the individual contribution can be evaluated.

$$J_{He;\,Matrix,DC} = f(\Delta h, \Delta \alpha_{l,vt;Matrix,DC}, \Delta \theta_{Matrix,DC}, \Delta K_{X,Z;\,Matrix,DC}) \tag{5.5}$$

An obstacle for most parameter sensitivity analyses is the restricted comparability between the different parameters. Parameters usually comprise different scales, orders of magnitudes, or units. Further, in fact there are three kinds of objectives for a sensitivity analysis:

- uncertainty analysis – studies the sensitivity of the system state variables to the

uncertainty of the parameters

- test for uniqueness for a given solution – or how well defined is a system by a certain number of observations and a given set of known and unknown or estimated parameters

- system analysis – studies the possible states a system can possess within predefined parameter ranges

The latter is not the classical objective of the sensitivity analysis and often is refered to as parameter study. With the propagation of the parallel and distributed computing paradigm this might change in the future. The presented study is rather a mixture of all of the above types of objectives. Table 4.1 contains the predefined parameter ranges. Each of it is represented by three discrete values, which are not necessarily equidistant. The reason is to provide one parameter set, that is similar to parameter sets suggested by other authors (e.g. [63]) for the Agur well field, to have a kind of a real parameter set.

5.4.1 Evaluation of the sensitivities

To recall, while the accumulation of ^{4}He is modeled as a zero-order production rate (Equation 3.7), the exchange term between the matrix continuum and the DC follows a linear relationship too. From that follows, that the sensitivities are all independent from the actual uranium and thorium concentrations per unit rock mass and thus from the actual in-situ production rate per unit rock mass. But however, the production rate was corrected with respect to the porosity of the rock. The results of this study are presented as listed below:

- All sensitivities reflect the relation of the percentage change of the model output to the percentage change of the model input.

- Normalisation of the parameter change is calculated twofold with one using the absolute change of the parameter Equation 5.6:

$$\Delta P_{norm} = \frac{P_{new} - P_{reference}}{P_{reference}} \cdot 100\%, \quad with: \ P_{new} > P_{reference} \tag{5.6}$$

and the other using the relative change of the parameter within the given parameter range (Equation 5.7 and Equation 5.8):

$$\Delta P_{norm, \ lower \ limit \Rightarrow between} = \frac{P_{between \ lower/upper \ limit} - P_{lower \ limit}}{P_{upper \ limit} - P_{lower \ limit}} \cdot 100\% \tag{5.7}$$

and

$$\Delta P_{norm, \ between \Rightarrow upper \ limit} = \frac{P_{upper \ limit} - P_{between \ lower/upper \ limit}}{P_{upper \ limit} - P_{lower \ limit}} \cdot 100\% \tag{5.8}$$

- Direct plotting of model output versus model input was omitted and substituted by diagrams reflecting the different system states. The distribution of the parameter values, however, is indicated by color indexing.

- The range of the different system states is provided by normalised system state variables (model output like tracer flux) with respect to the maximum values of all model runs. A range between 0 and 100 % thus applies.

Exemplarily the Jacobian matrix around the model case, where all parameters are between their minimum and maximum values (Table 4.1) is depicted in Table 5.14 and Figure 5.37 with respect to the percentage of absolute parameter change, it is depicted in Table 5.15 and Figure 5.38 with respect to the percentage of relative change within the given parameter ranges.

Table 5.14: Parameter sensitivities (Jacobian matrix) with respect to the normalized absolute change around the model case, where all parameters are between their minimum and maximum values (Table 4.1), with kdc±: Δ DC conductivity, ndc±: Δ DC porosity, ddc±: Δ DC longitudinal dispersivity, nm±: Δ matrix porosity, gh±: Δ head gradient, $\Delta t_{transition}$: time of model convergence, $\Delta C_{matrix, DC}$: ^{4}He concentration, and $\Delta J_{^4He, matrix/DC}$: ^{4}He flux in the matrix and DC, respectively. The model output parameter were observed close to the outlet border.

	$\Delta t_{transition}$	$\Delta C_{matrix, DC}$	$\Delta J_{^4He, matrix}$	$\Delta J_{^4He, DC}$
kdc−	−9.93e−1	−9.41e−1	−1.00e+0	−1.00e+0
kdc+	−8.94e−1	−8.47e−1	−9.00e−1	−9.00e−1
ndc−	−8.23e−1	−9.56e−1	−1.03e+0	−9.53e−3
ndc+	−5.85e−1	−6.83e−1	−7.36e−1	−1.55e−2
ddc−	7.56e−2	7.30e−4	−5.37e−1	−5.37e−1
ddc+	1.23e−1	1.51e−3	−5.79e−1	−5.79e−1
nm−	5.83e−1	6.43e−6	7.14e−1	−2.17e−5
nm+	8.15e−1	9.06e−6	1.00e+0	−3.24e−5
gh−	−9.93e−1	−9.41e−1	−8.08e−1	−8.08e−1
gh+	−4.95e−1	−4.71e−1	−5.00e−1	−5.00e−1

Both sensitivity diagrams indicate that the sensitivities to the individual parameter changes are not linear with respect to their considered ranges as well as to their absolute values, except for the matrix porosity of the range plot (Figure 5.38), which is positively and linearly correlated over the whole considered range. For all other parameters the same general trend applies to both, the relative change in the considered ranges and the absolute change.

As expected, the fluid flux in the system has the highest impact on mass fluxes and concentrations, but also on the time of transition. Due to a constant ^{4}He production rate in the aquifer material the correlation is negative for increasing fluid flux. As already mentioned, although the transition time is not a state variable on its own, it is
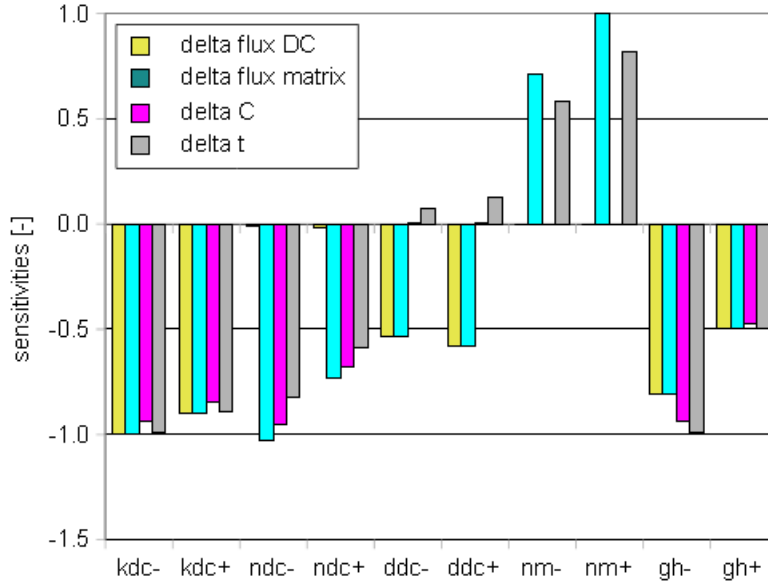
Figure 5.37: Parameter sensitivities (Jacobian matrix of Table 5.14) with respect to the normalized absolute change around the model case, where all parameters are between their minimum and maximum values (Table 4.1). The notation for the parameters in the first column is to be taken from Table 5.14. The model output parameter were observed close to the outlet border.

Table 5.15: Parameter sensitivities (Jacobian matrix) with respect to the normalized relative change in the range of interest around the model case, where all parameters are between their minimum and maximum values (Table 4.1), with kdc±: Δ DC conductivity, ndc±: Δ DC porosity, ddc±: Δ DC longitudinal dispersivity, nm±: Δ matrix porosity, gh±: Δ head gradient, $\Delta t_{transition}$: time of model convergence, $\Delta C_{matrix, DC}$: ^{4}He concentration, and $\Delta J_{^4He, matrix/DC}$: ^{4}He flux in the matrix and DC, respectively. The model output parameters were observed close to the outlet border.

	$\Delta t_{transition}$	$\Delta C_{matrix, DC}$	$\Delta J_{^4He, matrix}$	$\Delta J_{^4He, DC}$
kdc−	−2.48e−1	−2.35e−1	−2.50e−1	−2.50e−1
kdc+	−1.99e−1	−1.88e−1	−2.00e−1	−2.00e−1
ndc−	−1.10e+0	−1.27e+0	−1.37e+0	−1.27e−2
ndc+	−4.68e−1	−5.46e−1	−5.89e−1	−1.24e−2
ddc−	1.51e−1	1.46e−3	−1.07e+0	−1.07e+0
ddc+	1.37e−1	1.67e−3	−6.43e−1	−6.43e−1
nm−	3.50e−1	3.86e−6	4.29e−1	−1.30e−5
nm+	3.49e−1	3.88e−6	4.29e−1	−1.39e−5
gh−	−7.15e+0	−6.77e+0	−5.81e+0	−5.81e+0
gh+	−1.11e+0	−1.06e+0	−1.13e+0	−1.13e+0

considered in the derivative matrix because it is a characteristic value for the ability of the system to respond with a certain speed. Thus, it is valuable information with respect to the interpretation of helium measurements when the state of an investigated aquifer has to be assessed: transition or steady. Groundwater flow will adjust much faster to new constraints on the system, for example in the curse of climatic changes, compared to the steady stated distribution of helium concentrations, which will lag behind considerably depending on the aquifer parameters. In turn, this question is important in terms of estimating groundwater residence times, additional contributions of other than in-situ sources, or the liability to parameter uncertainty. These considerations support the already assumed importance of the duration time of the transition state to thoroughly understand the whole system behavoir within the limits of the parameter ranges.
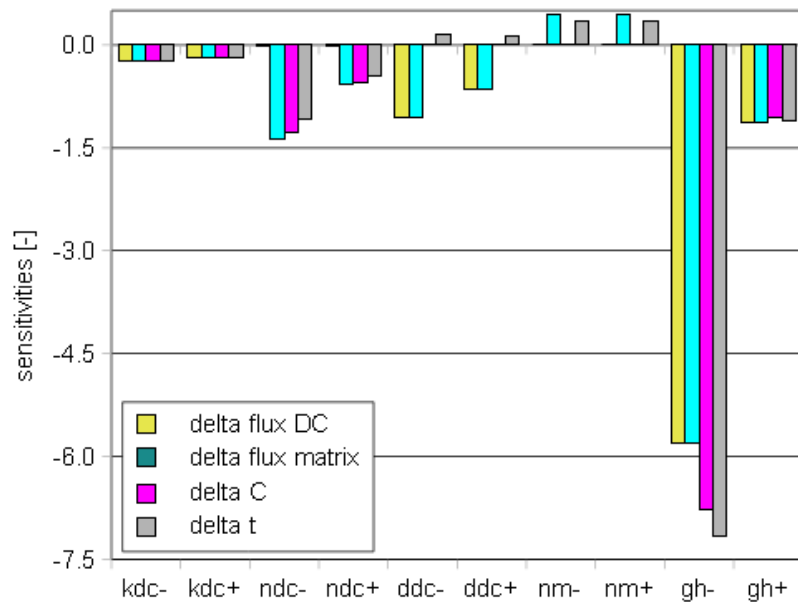
Figure 5.38: Parameter sensitivities (Jacobian matrix of Table 5.15) with respect to the normalized relative change in the range of interest around the model case, where all parameters are between their minimum and maximum values (Table 4.1). The notation for the parameters in the first column is to be taken from Table 5.15. The model output parameter were observed close to the outlet border.

In opposite to the usual visualization technique of plotting individual Δ *model outputs* versus individual Δ *parameters*, for example $\partial J_{^4He}/\partial K_{X,DC}$ it appears more elucidative to introduce the visualization of the state variables to each other in a way similar to a phase space diagram, with color indexing based on the parameter distributions. The different steady states with respect to the mass fluxes in both continua the simulated system can possess are shown in Figures 5.39 to 5.43, where the colors are indicative for the parameter values.
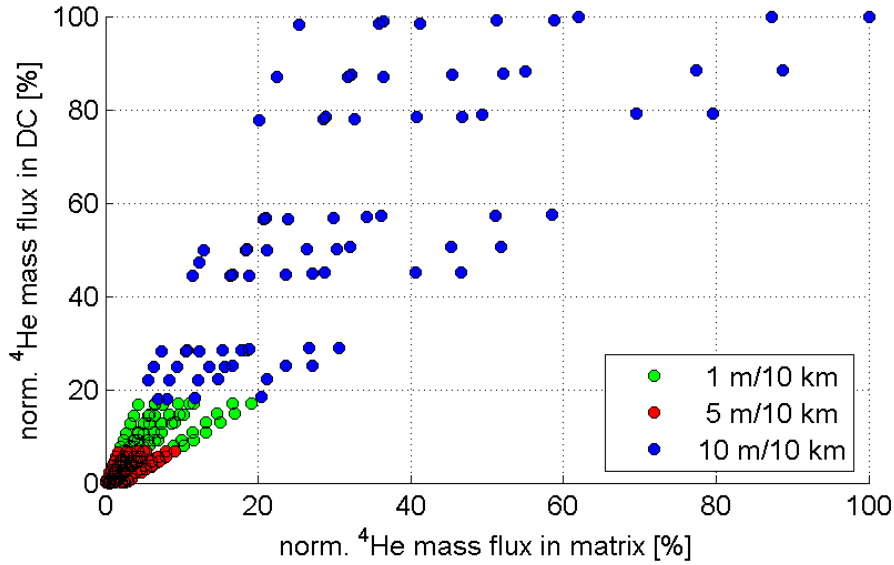
Figure 5.39: Range of possible system states reflected by the mass fluxes at the model outlet and defined by the chosen parameter ranges (Table 4.1). The color index represents the considered head gradients. Normalization to 100 % is done with respect to the maximum output values of all model runs.
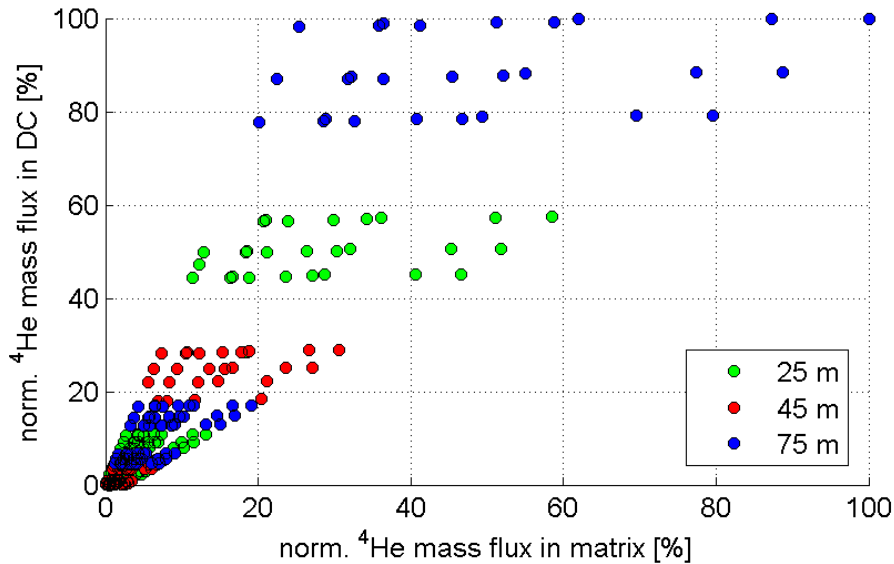
Figure 5.40: Range of possible system states reflected by the mass fluxes at the model outlet and defined by the chosen parameter ranges (Table 4.1). The color index represents the considered DC longitudinal dispersivities. Normalization to 100 % is based on the range of the state variable between zero and the maximum of all model runs.
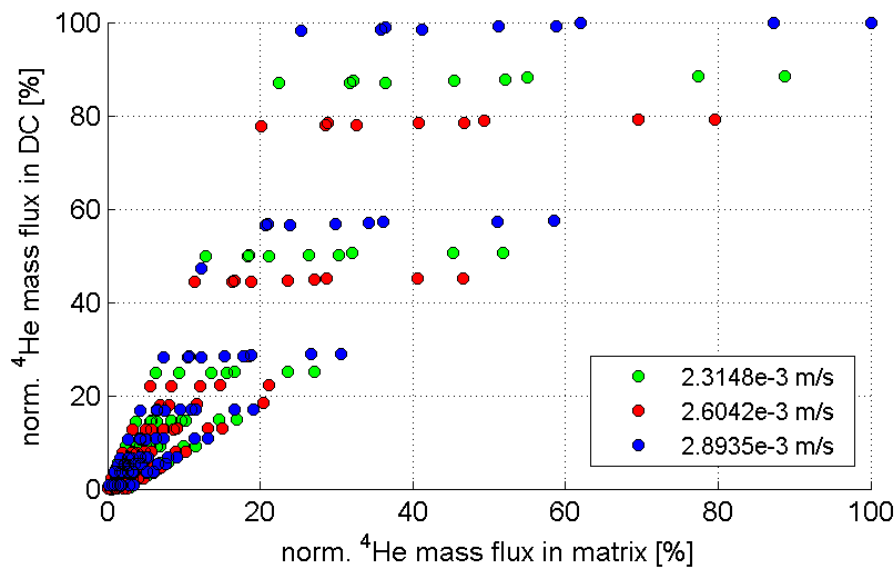
Figure 5.41: Range of possible system states reflected by the mass fluxes at the model outlet and defined by the chosen parameter ranges (Table 4.1). The color index represents the considered DC hydraulic condactivities. Normalization to 100 % is based on the range of the state variable between zero and the maximum of all model runs.
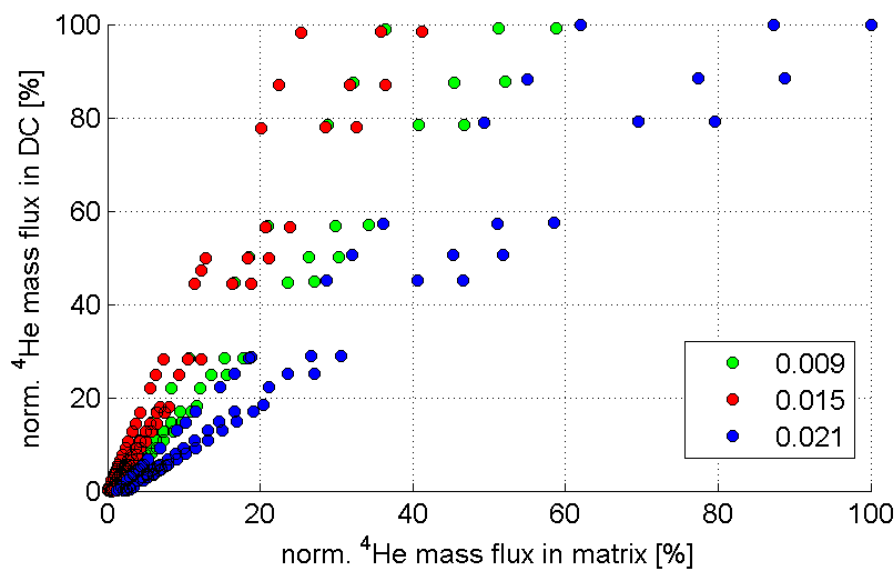
Figure 5.42: Range of possible system states reflected by the mass fluxes at the model outlet and defined by the chosen parameter ranges (Table 4.1). The color index represents the considered DC porosity. Normalization to 100 % is based on the range of the state variable between zero and the maximum of all model runs.
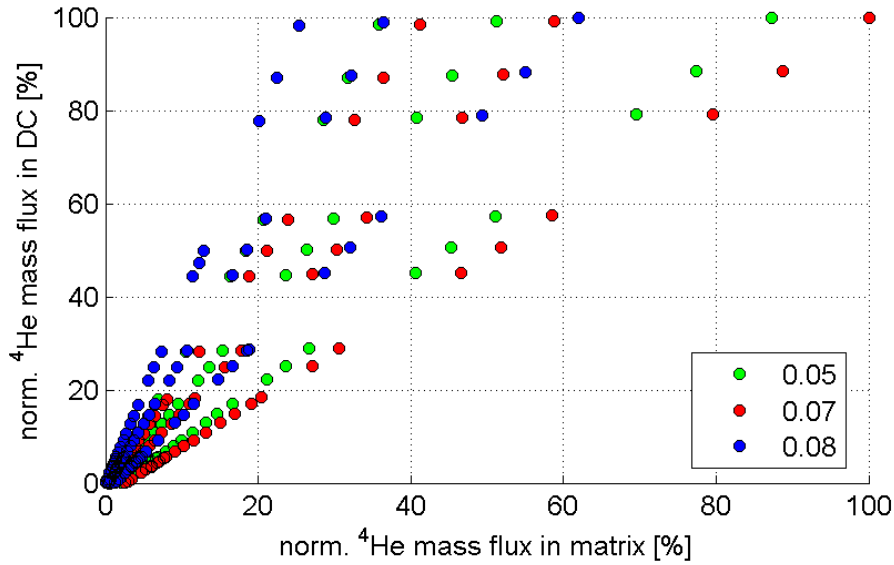
Figure 5.43: Range of possible system states reflected by the mass fluxes at the model outlet and defined by the chosen parameter ranges (Table 4.1). The color index represents the considered matrix porosity. Normalization to 100 % is based on the range of the state variable between zero and the maximum of all model runs.

From the presented data and with respect to the given parameter ranges the following can be concluded:

- The head gradient is the strongest force on the system, followed by the DC dispersivity.

- Much smaller, but still not negligible is the effect on the system imposed by the change of the DC hydraulic conductivity.

- While the head gradient, the DC dispersivities, and the DC hydraulic conductivities each affect the helium flux in the matrix as well in the DC equally or in similar way, the porosities of the DC and the matrix have a much higher effect on the helium mass flux in the matrix than in the DC. The difference is about one order of magnitude, respectively for the DC porosity and about four orders of magnitudes, respectively for the matrix porosity.

- The effect of the DC and matrix porosity on the system is vice versa. While the matrix mass flux is negatively correlated to the DC porosity it is positively correlated to the matrix porosity.

- A relevant positive correlation between the parameters and the state or quasi-state variables prevails only between matrix porosity and both, matrix mass flux and transition time, as well as between the DC dispersivities and the transition time.

- The transition time is positively correlated only to the matrix porosity and the DC dispersivities, but negatively to the other parameters.

The documented system behavior is related to the effects, which the individual parameters impose. Parameters that increase the fluid flux (hydraulic gradient and hydraulic conductivity) will consequently decrease the mass fluxes and the transition time. Mechanical dispersion, that solely modifies the transport velocity spectrum of the solute increase the systems transition time, while again the mass fluxes drop, which is in accordance to the definition of the hydrodynamic dispersion term in the advectiv-dispersive transport equation (Equation 4.9). Increasing the matrix or DC porosity raises the mobile volumetric water content in the system. As the associated mass fluxes in the two continua additionally are a function of the fluid and mass transfer coefficients to account for the exchange between the two, the effect of the different porosities can not be generalised. For this study and parameter configuration the effects have been adressed in the above list.

To elucidate the whole system behavior also with respect to its characteristic response or transition time, the latter is introduced, again in normalized way, in the diagramm of the state variables represented by the z-direction of the coordinate system (Figures 5.44 to 5.48).

Figure 5.44: Extended version of Figure 5.39 including the transition time from intial to steady state - normalized with respect to the maximum transition time.
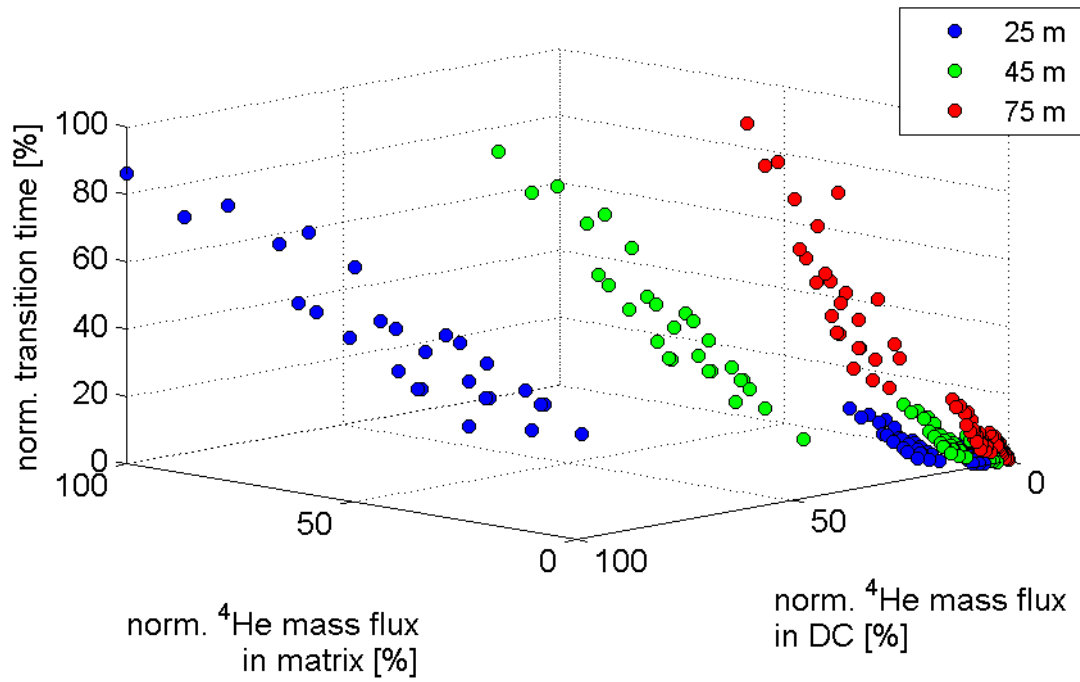
Figure 5.45: Extended version of Figure 5.39 including the transition time from intial to steady state - normalized with respect to the maximum transition time.
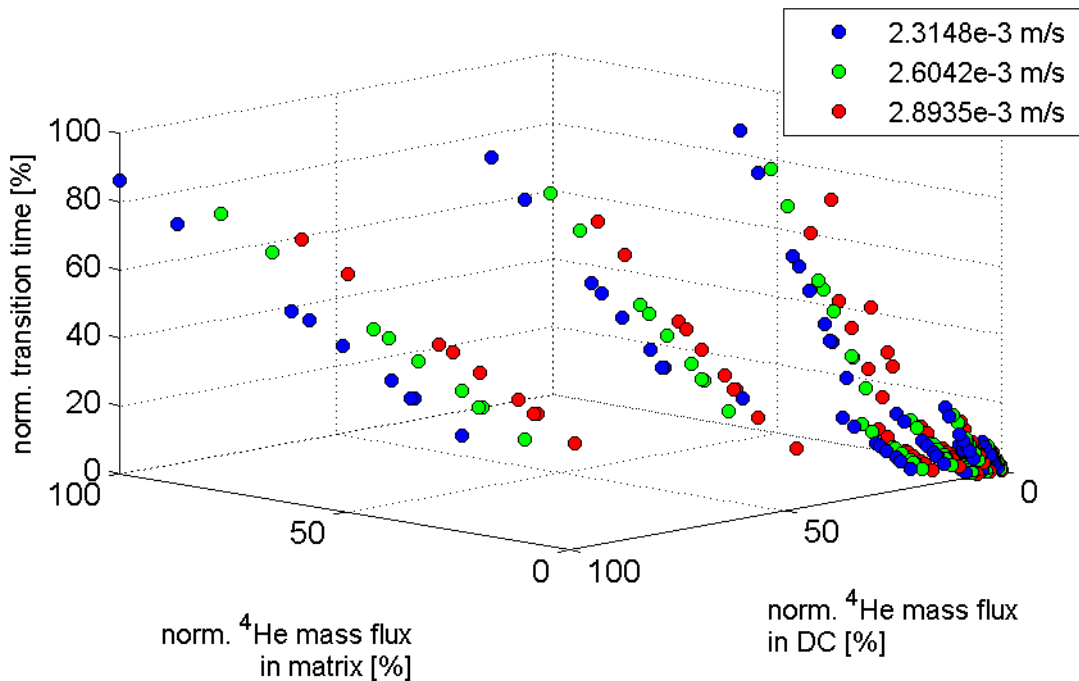
Figure 5.46: Extended version of Figure 5.41 including the transition time from intial to steady state - normalized with respect to the maximum transition time.
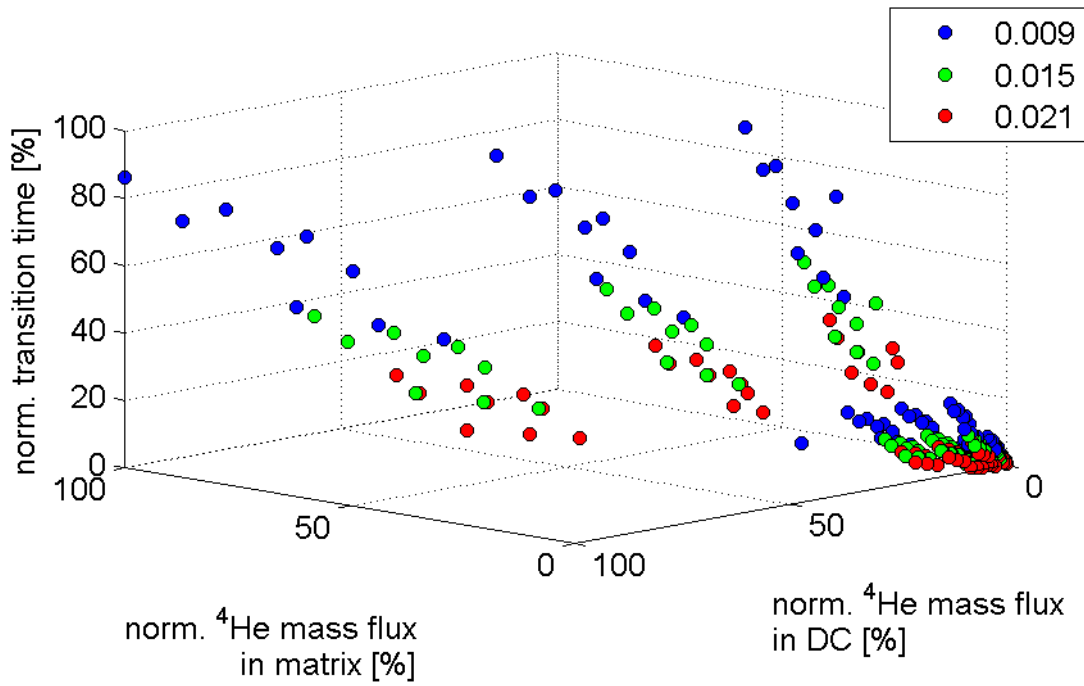
Figure 5.47: Extended version of Figure 5.42 including the transition time from intial to steady state - normalized with respect to the maximum transition time.

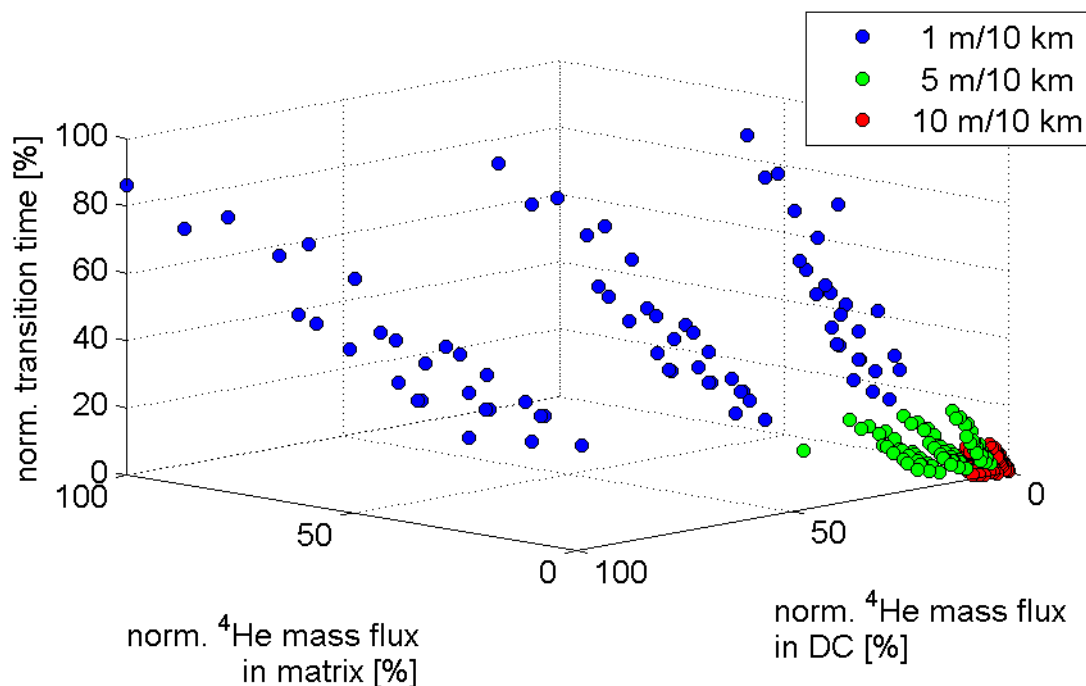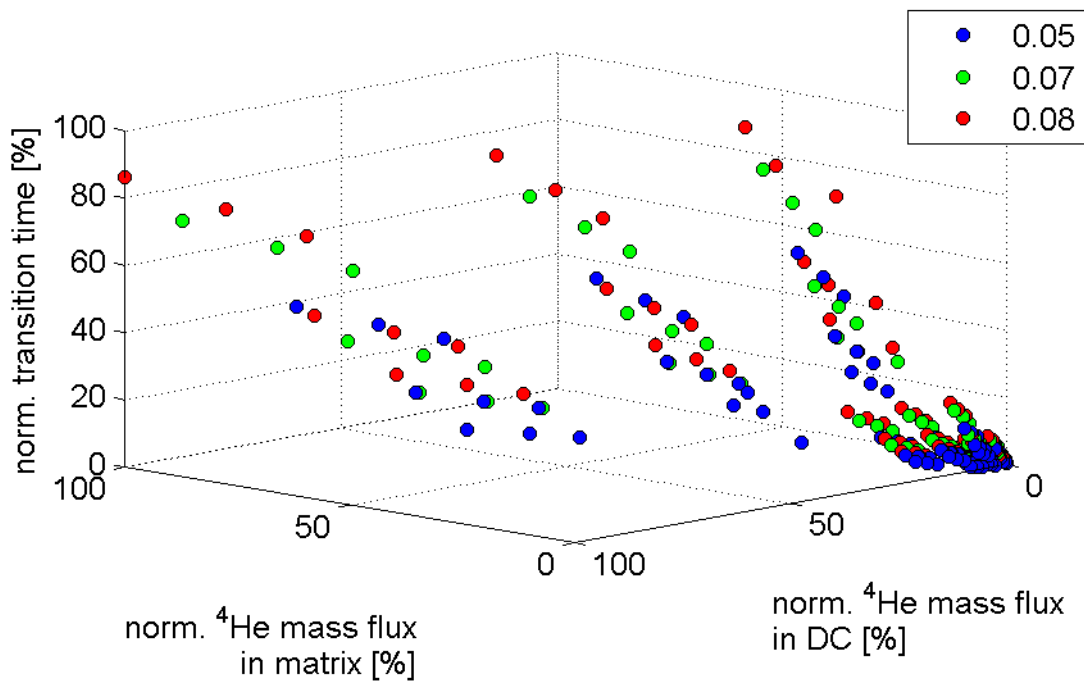**Figure 5.48:** Extended version of Figure 5.43 including the transition time from intial to steady state - normalized with respect to the maximum transition time.

6 Summary

Five study areas in Israel and Palestine were selected to trace flow processes and salinization mechanisms using multi-tracer approaches. With focus on the young components the age structures of the sampled groundwater from wells of the Agur (Israel), Herodion, and Ein Samia (Palestine) well fields and four major springs in Wadi Qilt and Jericho (Palestine) were evaluated. While the wells in the Agur, Herodion, and Ein Samia well fields are generally several hundred meters deep and abstract water from the karstified Cretaceous carbonate aquifer, the wells in the Jericho area are drilled into the unconsolidated Shallow Aquifer to depths of less than 100 m. In addition to the evaluation of real measurements, a sensitivity analysis was conducted with respect to the accumulation of helium in groundwater by in-situ production in a dual continuum aquifer. The sensitivity of that process was investigated with respect to five varied parameters (head gradient, dual continuum dispersivities, dual continuum hydraulic conductivity, matrix and dual continuum porosities). Thus, the results are summarized with respect to the above mentioned main topics.

(A) Age structures of groundwaters in the Judea Group Aquifer (deep wells and springs):

The Agur well field in Israel, the Herodion and Ein Samia well fields, and four springs of Wadi Qilt and Jericho in Palestine were investigated to unveil the age structure especially of the young groundwater components of the sampled wells and to derive information with respect to their vulnerability. The applied strategy was to use a lumped parameter approach and to split up the sampled groundwater into two major components. One was defined as old and free any of the tritium, CFC, or SF_6 tracers while the other component was defined as young and to contain all of the tracers. Conceptually, this is reflecting the simultaneous existance of very old groundwater as verified by many ^{14}C measurements in the past and young tracers like tritium, CFCs, and SF_6. Because of the highly variable temporal tritium pattern of the Wadi Qilt springs a base flow component was discriminated based on specific ^{14}C and tritium observations and defined as continuous volumetric flow in order to respect the requirements of the lumped parameter approach. Tritium observations diverting from the assumed base flow component were defined as much faster, thus again younger components, but of unknown mean transit time distribution. This fast component is related to a non-steady flow that happens during or after intensive precipitation events in the karst porosity and therefore can not be treated using the applied lumped parameter approach. However, it still provides valuable information about the probable proportions of the fast flow component in the spring water. As for the

fast component the distribution of the transit times of the old component was considered to be unknown.

The results of the evaluation of the individual groundwater age structures can be summarized as follows:

1. In the Agur well field the proportion of the dispersion model on the coupled piston flow-dispersion model positively correlated to the mean transit time of the dispersion model. This is indicative for a karstic system. On the one hand, a higher karst porosity (epikarst) is characteristic for the infiltration area of the Judea Group or Mountain aquifer, respectively and responsible for a wider spectrum of flow velocities (Agur 7 and Agur 8). On the other hand, west of the infiltration area, in the confined part of the aquifer, a smaller but more mature karst porosity is developed (Agur 6).

2. Also, the Ein Samia well field produces water from a karstified aquifer. But in contrast to the Agur well field the proportion of the dispersion model is very high, i.e. 55..70 % in Ein Samia 2A, 62..76 % in Ein Samia 6, and 80..100 % in Ein Samia 1. At the same time the mean transit times are generally low and similar for these three wells, i.e. 10..20 years. This is an indication, that the young groundwater component, that is represented by the dispersion model is probably of the same origin and only its proportion due to mixing with the old component changes, which would suggest a mature karst system in the Upper as well as the Lower subaquifer, where the wells abstract their water from. Ein Samia 4 stands out due to its location east of a major fault that acts as a flow barrier. With respect to the age distribution and the proportion of the dispersion model it may be compared to Agur 6 although there is indication for a certain variability. However, the productivity of the Agur wells is much higher than that of Ein Samia 4.

3. Similar to the Ein Samia well field the groundwater from the well Herodion 1 possesses a high proportion of the dispersion model of 35..50 % accompanied by a relatively small mean transit time of 5..20 but maximal 40 years.

4. The fitted dispersion model parameters for the Wadi Qilt springs do not contradict but support the conceptualized findings of [127] and [125] although the covered time scales of the ^{14}C and tritium methods are very different. The proportion of the dispersion model representing the defined base flow components increases between the Fara (21.5..40 %) and Ein el Qilt (57..66 %) in the lower Wadi Qilt. A mean transit time of the dispersion model of about 20 years is characteristic for all springs except for Fara, where the upper limit may be around 30 years. Advective transport dominates the system with respect to the reduced solution spaces.

(B) Salinization processes in the Shallow Aquifer of Jericho:

The conducted study in the Jericho area focused primarily on the mechanisms of groundwater salinization that is observed to increase in eastern direction and thus is maximal in the easternmost wells. Of special interest was the question, whether salinization is

fully attributed to brine admixture due to the overexploitation of the Shallow Aquifer or whether some contribution may be derived from leachates from the Lisan formation. The second question is derived from the first and refers to what the most indicative tracers are.

The results of the Jericho study can be summarized as follows:

1. Due to the expected strong hydrochemical similarities of the remnant brines in the Jericho area and the possible salt contribution from leachates from the Lisan formation a distinct discrimination of both is hampered.

2. Strong indications for water-rock interaction in the Lisan formation is provided especially by the SO_4/Cl ratio, the isotopic sulphure signature of SO_4, and the B/Cl, Na/Cl, and Sr/Ca ratios. A potential key indicator to trace the salinization mechanism is the boron concentration with respect to Cl and the Na/Cl ratio. It is expected that boron and strontium isotopes would provide even more insight with respect to the sources and the salinization mechanisms. The $^3He/^4He$ ratio turned out to be a valuable indicator for the residing brines that are linked to the precurser of the Dead Sea, Lake Lisan. The helium isotope signature of the samples from wells close to the border fault thereby clearly corresponds to the regional signature alongside the western border fault of the Jordan graben structure.

3. However, the highest uncertainty for the groundwater characterization in the Jericho area is related to the little detailed knowledge about the local geology, the water balance of this small scale area, as well as the poorly understood migration of the water network leakage, of the agricultural return flow, or of the winter runoff in Wadi Qilt as well as Wadi Nueima with respect to the spatial distribution of the infiltration velocities and the consequences that are related to hydrochemistry or the distribution of tracers like tritium and comparable.

(C) Parameter sensitivities for ^4He accumulation in a dual continuum aquifer equivalent:

The evaluation of parameter sensitivities for the ^4He accumulation in a dual continuum numerical transport model was conducted to provide an insight into the main driving forces with respect to the selected parameters. This study can only be seen as an inital investigation in order to understand the helium accumulation in multi-porosity aquifers and to extract as much as possible information from this valuable tracer. The helium concentrations in groundwater are strongly correlated to the prevailing residence time distribution in the aquifer, which may be multimodal with respect to the different porosities. Thus, changing environmental conditions on larger time scales will result in different system responses depending on the aquifer parameters.

The results of the sensitivity analysis can be summarized as follows:

1. The imposed head gradient, dual continuum dispersivity, and the dual continuum hydraulic conductivity are the forces that affect the helium mass fluxes in the matrix

and in the dual continuum similarly, but with a very different amplitiude. The amplitude decreases in above mentioned order, meaning the head gradient is the dominant force with respect to the considered parameter ranges.

2. The porosities of the dual continuum and the matrix have a much higher effect on the helium mass flux in the matrix than in the dual continuum. The difference is about one order of magnitude, respectively for the dual continuum porosity and about four orders of magnitudes, respectively for the matrix porosity. However, the helium mass flux in the matrix correlates vise versa with the matrix and dual continuum porosity, i.e. positively and negatively, respectively.

3. The transition time from inital to steady state conditions is positively correlated only to the matrix porosity and the dual continuum dispersivities. For all other parameters an increase is synonymous with a shorter response time of the groundwater system with respect to the ^{4}He accumulation due to in-situ production.

7 Conclusions

From the achieved results concerning the three main investigated topics with respect to (A) the characterization of the young groundwater components in the Agur, Herodion, and Ein Samia well fields, and four major springs in Wadi Qilt and Jericho, (B) the salinization mechanisms in the Jericho area, as well as (C) the sensitivity of the helium accumulation in groundwater to five selected parameters the derived conclusions again are presented for every topic separately.

The characterization and quantification of the young groundwater components of the different study locations were conducted in order to obtain practical measures to evaluate the potential vulnerability or protection level that can be attributed to the different well and spring objects. As the strategy to split up the sampled water into an old, distinct tracer free and a young groundwater component containing all of the tracer was successfully applied for all well and spring objects in the same or similar way, it should be considered as an easy and practical way to categorize specific objects or locations with respect to its protection level. If one speaks about potential vulnerability the considered time scale becomes an important factor. Generally, the main parameter is the proportion of the young groundwater component on the whole volume that passes the system. The smaller the proportion is, the lesser effect any contaminant will have due to its dilution by the old, presumedly contamination free groundwater component. However, it is obvious, that the strength of the contamination source is relevant too. Thus, a strong contaminant source may also significantly affect a well or spring object, that indeed has a smaller proportion of a young groundwater component, but at the same time possesses a low mean residence time of the young component. The logical consequence is to create a potential vulnerability map based on appropriate tracers like tritium, CFCs, SF_6, or others. To limit costs, initial tritium measurements should be used as indicators, whether the approach is expected to provide valuable results. Consequently, objects that possess very low tritium concentrations could be treated as well protected. However, due to the applied simplifications with respect to the lumped parameter approach, the once calculated or fitted model parameters might not be straightaway applicable as a measure for the potential vulnerability. Therefore, that kind of results have to be related to or verified based on real cases of contamination in a way similar to a calibration process. Based on that but also based on the local and practical experiences of the involved experts local or catchment based regulations could be implemented with respect to agriculture, waste water disposal into wadis etc. Commonly, the definition of groundwater protection zones in connection with other investigations should be the prefered outcome.

Based on the findings of the Jericho area study with respect to salinization processes

the applied strategy to descriminate the two possible mechanisms of brine admixture and contributions from leachate from the Lisan formation should be optimized, again also with regard to the costs for the hydrochemical analyses. The most important hydrochemical parameters that are suggested from the results of the presented thesis are Na, Cl, Sr, B, SO_4, $\delta^{34}S(SO_4)$, and the helium isotope signature. Isotope analyses for B and Sr are suggested as these are potential tools in order to trace hydrochemical mechanisms that take place in the course of groundwater salinization. Due to the large fluctuations of the annual groundwater recharge in the small area of Jericho the relation between the spatial distribution and intensity of rainfall in the mountains and the runoff in the Wadis should be determined with reasonable accuracy. Together with other water balance measures like water network losses or abstracted groundwater volumes an integrated, model based water management tool must be developed and calibrated to react on time. In turn, that kind of management tool is suggested to be an integral part of the Jericho Water Master Plan, that currently is developed. As a final recommendation, the geological information about the subsurface in the Jericho area needs to be updated, because it is an important key to understand the Shallow aquifer system and thus, is one of the major foundations for any model that involves groundwater flow or transport.

As the results of the sensitivity analyses for the ^{4}He acculumation in the dual continuum aquifer suggest, the total helium concentrations in the well or spring discharge can not be evaluated without a basic understanding of the real conditions in a karstic, or multi-porosity aquifer. Although studies have been conducted on large scale and regional aquifers, no study until now considers possible effects related to multi-porosity or to important environmental changes in the past. In order to extract all possible information from helium or noble gas analyses, whose costs are not negligible, it is therefore important to proceed and advance to unveil the most important dependencies of the accumulation process. In order to handle the computation demand for parameter sensitivity analyses with an arbitrary number of parameters and variations tools as has been developed in the course of this study are necessary, as well as the exploitation of parallelized code and hardware infrastructure.

Bibliography

[1] *MATLAB 2008a.* The MathWorks Inc., 2008.

[2] *BASH*, 2010. `http://www.gnu.org/software/bash/`.

[3] *Python*, 2010. `http://www.python.org/`.

[4] Abdel-Rahman, A.F.M. and F.H. Nader: *Characterization of the Lebanese Jurassic-Cretaceous carbonate stratigraphic sequence: a geochemical approach.* Geological Journal, 37(1):69–91, 2002.

[5] Aeschbach-Hertig, W., H. El-Gamal, M. Wieser, and L. Palcsu: *Modeling excess air and degassing in groundwater by equilibrium partitioning with a gas phase.* Water Resources Research, 44:W08449, 12 PP, 2008.

[6] Aeschbach-Hertig, W., F. Peeters, U. Beyerle, and R. Kipfer: *Interpretation of dissolved atmospheric noble gases in natural waters.* Water Resources Research, 35(9):2779–2792, 1999.

[7] Aeschbach-Hertig, W., F. Peeters, U. Beyerle, and R. Kipfer: *Palaeotemperature reconstruction from noble gases in ground water taking into account equilibration with entrapped air.* Nature, 405:1040–1044, 2000.

[8] Al-Jayyousi, O.R.: *Rehabilitation of Irrigation Distribution Systems: The Case of Jericho City.* Water Resources Management, 13(2):117–132, April 1999.

[9] Aldrich, L.T. and A.O. Nier: *The Abundance of He^3 in Atmospheric and Well Helium.* Phys. Rev., 70(11-12):983–984, Dec 1946.

[10] Aldrich, L.T. and A.O. Nier: *The Occurrence of He^3 in Natural Sources of Helium.* Phys. Rev., 74(11):1590–1594, Dec 1948.

[11] Aliewi, A., B. Sawalhi, and C. Messerschmidt: *Ein Samia # 6 – Executive Summary Report.* Report, Jerusalem Water Undertaking, 1999.

[12] Allègre, C.J., P. Sarda, and T. Staudacher: *Speculations about the cosmic origin of He and Ne in the interior of the Earth.* Earth and Planetary Science Letters, 117(1-2):229 – 233, 1993.

[13] Andrews, J.N.: *Radiogenic and inert gases in groundwater.* In *Proceedings of the Second International Symposium on Water-Rock Interaction, Strasbourg, 1977*, pp. 334–342, 1977.

[14] Andrews, J.N., I.S. Giles, R.L.F. Kay, D.J. Lee, J.K. Osmond, J.B. Cowart, P. Fritz, J.F. Barker, and J. Gale: *Radioelements, radiogenic helium and age relationships for groundwaters from the granites at Stripa, Sweden.* Geochimica et Cosmochimica Acta, 46(9):1533–1543, Sept. 1982.

[15] Applied Research Institute Jerusalem: *Environmental Profile for the West Bank Volume 2: The Jericho District.* Pdf, Applied Research Institute Jerusalem, 1995. `http://www.arij.org/pub/Jericho-Profile.pdf`.

[16] Applied Research Institute Jerusalem: *Localizing Agenda 21 in Palestine*, 2001. `http://www.arij.org/Agenda-21/l_o_c_a_l_i_z_i_n_g.htm`.

[17] Arad, A. and A. Michaeli: *Hydrogeological Investigations in the Western Catchment of the Dead Sea.* Israel Journal of Earth Sciences, 16:181–196, 1967.

[18] Arkin, Y. and A. Starinsky: *Lisan sediment porosity and porewater as indicators of original Lake Lisan composition.* GSI Current Research, pp. 83–84, 1981. Kopie vorhanden.

[19] Atkins, P.W.: *Physikalische Chemie.* Wiley-VCH, 2002.

[20] Avisar, D., E. Rosenthal, A. Flexer, H. Shulman, Z. Ben-Avraham, and J. Guttman: *Salinity sources of Kefar Uriya wells in the Judea Group aquifer of Israel. Part 1— conceptual hydrogelogical model.* Journal of Hydrology, 207:27–38, 2003. Mountain Aquifer, Israel, groundwater, wells, deep, Kefar Uriya, Kefar Uriyya, Kefar Uria, Eshtaol, salinization, chemistry, infiltration, karst, structural geology, faults, foothills, Hashephela Syncline.

[21] Ayalon, A., M. Bar-Matthews, and E. Sass: *Rainfall-recharge relationships within a karstic terrain in the Eastern Mediterranean semi-arid region, Israel: $\delta^{18}O$ and δD characteristics.* Journal of Hydrology, 207(1-2):18–31, 1998. precipitation, recharge, karst, Israel, groundwater, isotopes, stable.

[22] Ayalon, A., M. Bar-Matthews, and B. Schilman: *Rainfall isotopic characteristics at various sites in Israel and the relationships with unsaturated zone water.* Geological survey of israel reports GSI/16/04, The Ministry of National Infrastructures, Jerusalem, 2004.

[23] Bakalowicz, M., M. El Hakim, and A. El-Hajj: *Karst groundwater resources in the countries of eastern Mediterranean: the example of Lebanon.* Environmental Geology, 54(3):597–604, 2008. `http://dx.doi.org/10.1007/s00254-007-0854-z`.

[24] Bar-Yosef, O.: *The PPNA in the Levant – an overview.* Paléorient, 15:57–63, 1989.

[25] Bauer, S., C. Fulda, and W. Schäfer: *A multi-tracer study in a shallow aquifer using age dating tracers 3H, 85Kr, CFC-113 and SF6 – indication for retarded transport of CFC-113.* Journal of Hydrology, 248(1-4):14–34, July 2001.

[26] Bear, J.: *Dynamics of fluids in porous media.* American Elsevier Publ. Co., Inc., 1972.

[27] Begin, B., A. Ehrlich, and Y. Nathan: *Lake Lisan – the Pleistocene precursor of the Dead Sea.* Geological Survey of Israel Bulletin, 63:30, 1974.

[28] Begin, Z.: *The Geology of the Jericho Sheet.* Geological Survey of Israel Bulletin, 67:35, 1975.

[29] Ben-Itzhak, L.L.: *Groundwater Flow Modeling in the Eastern Jud Group Aquifer, Israel.* Master's thesis, The Hebrew University of Jerusalem, February 2003.

[30] Ben-Itzhak, L.L. and H. Gvirtzman: *Groundwater flow along and across structural folding: an example from the Judean Desert, Israel.* Journal of Hydrology, 312(1-4):51–69, October 2005.

[31] Benson, B.B. and D. Krause: *Empirical laws for dilute aqueous solutions of nonpolar gases Bruce B. Benson and Daniel Krause.* Journal of Chemical Physics, 64(2):689–709, 1976.

[32] Benson, B.B. and D. Krause: *Isotopic fractionation of helium during solution: A probe for the liquid state.* Journal of Solution Chemistry, 9:895–909, 1980.

[33] Bergelson, G., R. Nativ, and A. Bein: *Assessment of hydraulic parameters of the aquifers around the Sea of Galilee.* Ground Water, 36:409–417, 1998.

[34] Bergelson, G., R. Nativ, and A. Bein: *Salinization and dilution history of ground water discharging into the Sea of Galilee, the Dead Sea Transform, Israel.* Applied Geochemistry, 14:91–118, 1998.

[35] Berger, D.: *Hydrological Model for the Yarqon-Taninim Aquifer (in Hebrew).* Techn. rep., Mekorot Ltd., 1999.

[36] Bethke, C.M., X. Zhao, and T. Torgersen: *Groundwater flow and the ^{4}He distribution in the Great Artesian Basin of Australia.* Journal of Geophysical Research, 104(B6):12999–13011, 1999.

[37] Beyer, M. and U. Mohrlok: *Parameter estimation for a double continuum transport model for fractured porous media.* In *Calibration and Reliability in Groundwater Modelling: From Uncertainty to Decision Making (Proceedings of ModelCARE'2005, The Hague, The Netherlands, June 2005)*, p. 80–86, 2005.

[38] Bigeleisen, J.: *Chemistry of Isotopes.* Science, 147(3657):463–471, 1965.

[39] Böhlke, J.K.: *Groundwater recharge and agricultural contamination.* Hydrogeology Journal, 10:153–179, 2002, ISSN 1431-2174. `http://dx.doi.org/10.1007/s10040-001-0183-3`, 10.1007/s10040-001-0183-3.

[40] Brielmann, H.: *Recharge and discharge mechanism and dynamics in the mountainous northern Upper Jordan River Catchment, Israel.* Ph.d., Ludwig-Maximilians-Universität, München, January 2008.

[41] Bu, X. and M.J. Warner: *Solubility of chlorofluorocarbon 113 in water and seawater.* Deep Sea Research Part I: Oceanographic Research Papers, 42(7):1151–1161, 1995.

[42] Buchbinder, B.: *Turonian 'Pisolites' from the Judean Hills and Northern Negev: Storm Rip-Ups of carbonate mud sediments in a back-shoal lagoonal setting.* Geological Servey of Israel Current Research, 12:150–154, 2000.

[43] Bullister, J.L., D.P. Wisegarver, and F.A. Menzia: *The solubility of sulfur hexafluoride in water and seawater.* Deep Sea Research Part I: Oceanographic Research Papers, 49:175–187, 2002.

[44] Burgess, M. and R. Hale-Evans: *The Gnu C Programming Tutorial.* Gnu Software Manuals Series. Free Software Foundation, 2003.

[45] Busenberg, E. and L.N. Plummer: *USGS spreadsheet program for preliminary evaluation of CFC data (CFC-2005-2a)*, 2005. `http://water.usgs.gov/lab/`.

[46] Castro, M.C.: *Helium sources in passive margin aquifers–new evidence for a significant mantle 3He source in aquifers with unexpectedly low in situ 3He/4He production.* Earth and Planetary Science Letters, 222(3-4):897–913, June 2004.

[47] Castro, M.C. and P. Goblet: *Calibration of regional groundwater flow models: Working toward a better understanding of site-specific systems.* Water Resources Research, 39:1172, 25 pp., 2003.

[48] Castro, M.C., P. Goblet, E. Ledoux, S. Violette, and G. de Marsily: *Noble gases as natural tracers of water circulation in the Paris Basin: 2. Calibration of a groundwater flow model using noble gas isotope data.* Water Resources Research, 34:2467–2483, 1998.

[49] CDM/Morganti and Palestinian Authority: *Water Resources Program, Task 18: Study of the Sustainable Yield of the Eastern Aquifer Basin – Priliminary Conceptual Model and Initial Estimate of the Sustainable Yield (USAID Contract No. 294-0021-00-6560-00).* Unpublished report, Palestinian Water Authority, 1997.

[50] Charlier, J.B., J. Mudry, and C. Bertrand: *Use of Dissolved Organic Carbon to Characterize Infiltration in a Small Karst System in the French Jura Mountains (Fertans, France).* In LaMoreaux, J.W., B. Andreo, F. Carrasco, J.J. Durán, and J.W. LaMoreaux (eds.): *Advances in Research in Karst Media*, Environmental Earth Sciences, pp. 151–156. Springer Berlin Heidelberg, 2010.

[51] Chon, B. and Y.S. Choi: *Modeling of three-dimensional groundwater flow using the method to calculate fractal dimension.* Korean Journal of Chemical Engineering, 18(3):382–386, 2001.

[52] Clark, I. and P. Fritz: *Environmental isotopes in hydrogeology.* Lewis Publishers (CRC Press) , Boca Raton, New York, 1997.

[53] Clarke, W.B., W.J. Jenkins, and Z. Top: *Determination of tritium by mass spectrometric measurement of* ^{3}He. The International Journal of Applied Radiation and Isotopes, 27(9):515–522, September 1976.

[54] Cook, P., L. Plummer, D. Solomon, E. Busenberg, and L. Han: *Effects and processes that can modify apparent CFC age: Use of Chlorofluorocarbons in Hydrology: A Guidebook*, ch. 4, pp. 31–58. International Atomic Energy Agency (IAEA), 2006.

[55] Cook, P.G. and D.K. Solomon: *Transport of Atmospheric Trace Gases to the Water Table: Implications for Groundwater Dating with Chlorofluorocarbons and Krypton 85.* Water Resources Research, 31(2):263–270, 1995.

[56] Cook, P.G. and D.K. Solomon: *Recent advances in dating young groundwater: chlorofluorocarbons, 3H/3He and 85Kr.* Journal of Hydrology, 191(1-4):245–265, 1997.

[57] Cook, P.G., D.K. Solomon, L.N. Plummer, E. Busenberg, and S.L. Schiff: *Chlorofluorocarbons as tracers of groundwater transport processes in a shallow, silty sand aquifer.* Water Resources Research, 31(3):425–434, 1995.

[58] Coplen, T.B. and B.B. Hanshaw: *Ultrafiltration by a compacted clay membrane–I. Oxygen and hydrogen isotopic fractionation.* Geochimica et Cosmochimica Acta, 37(10):2295 – 2310, 1973.

[59] Craig, H.: *Isotopic Variations in Meteoric Waters.* Science, 133(3465):1702–1703, 1961.

[60] Craig, H. and D. Lal: *The Production Rate of Natural Tritium.* Tellus, 13(1):85–105, 1961.

[61] Craig, H. and J. Lupton: *Primordial neon, helium, and hydrogen in oceanic basalts.* Earth and Planetary Science Letters, 31(3):369–385, 1976.

[62] Dachsbacher, C., T. Bolch, and M. Stamminger: *Procedural Reproduction of Terrain Textures with Geographic Data.* In T. Aach, L.K. amd T. Kuhlen amd and R. Westerman (eds.): *Vision, Modeling, and Visualization 2006: Proceedings, November 22 - 24, 2006, Aachen, Germany*, pp. 105–112. IOS Press, Amsterdam, 2006.

[63] Dafny, E., A. Burg, and H. Gvirtzman: *Effects of Karst and geological structure on groundwater flow: The case of Yarqon-Taninim Aquifer, Israel.* Journal of Hydrology, In Press, Accepted Manuscript, 2010.

[64] DÁns, J. and E. Lax: *Makroskopische Physikalisch-Chemische Eigenschaften*, vol. 1. Springer-Verlag, Berlin, 1967.

[65] Dansgaard, W.: *Stable isotopes in precipitation.* Tellus, 16(4):436–468, 1964.

[66] Davis, B.M., J.D. Istok, and L. Semprini: *Push-pull partitioning tracer tests using radon-222 to quantify non-aqueous phase liquid contamination.* Journal of Contaminant Hydrology, 58(1-2):129–146, 2002.

[67] Divine, C.E., E.W. Sanfordb, and J.E. McCray: *Helium and Neon Groundwater Tracers to Measure Residual DNAPL.* Vadose Zone Journal, 2(2):382–388, 2003.

[68] Dodson, A., D. J., DePaolo, and B.M. Kennedy: *Helium isotopes in lithospheric mantle: evidence from tertiary basalts of the western USA.* Geochimica et Cosmochimica Acta, 62(23-24):3775–3787, December 1998.

[69] Eaton, J.W.: *Octave,* 2010. `http://www.octave.org`.

[70] Eaton, J.W., D. Bateman, and S. Hauberg: *GNU Octave Manual Version 3.* Network Theory Limited, 2008.

[71] Eraifej, N.: *Gas geochemistry and isotopic signatures in the deep thermal waters in Jordan.* Wissenschaftliche Mitteilungen des Instituts für Geologie, Freiberg, 32:256, 2006.

[72] Eriksson, E.: *The possible use of tritium for estimating groundwater storage.* Tellus, 10(4):472–478, 1958.

[73] Farley, K. and R. Poreda: *Mantle neon and atmospheric contamination.* Earth and Planetary Science Letters, 114(2-3):325 – 339, 1993.

[74] Fleischer, L. and R. Gafsou: *Top Judea Group – Digital Structural Map of Israel (Appendix C and Plate IV).* In Hall, J.K., V.A. Krasheninnikov, F. Hirsch, C. Benjamini, and A. Flexer (eds.): *Geological framework of the Levant, Volume II: the Levantine Basin and Israel.*, pp. 745–753. Historical Productions-Hall, 2005. Plate IV.

[75] Flexer, A., A. Gilat, F. Hirsch, A. Honigstein, A. Rosenfeld, and T. Reuffer: *Late Cretaceous evolution of the Judean Mountains as indicated by ostracodes.* Terra Nova, 1:349–358, 1989.

[76] Freund, R., Z. Garfunkel, I. Zak, M. Goldberg, T. Weissbrod, and B. Derin: *The shear along the Dead Sea rift.* Philosophical Transaction of the Royal Society London, Series A, 267:107–130, 1970.

[77] Frumkin, A. and H. Gvirtzman: *Cross-formational rising groundwater at an artesian karstic basin: the Ayalon Saline Anomaly, Israel.* Journal of Hydrology, 318(1-4):316–333, March 2006.

[78] Galewsky, J.: *Orographic precipitation isotopic ratios in stratified atmospheric flows: Implications for paleoelevation studies.* Geology, 37(9):791–794, 2009.

[79] Garfunkel, Z. and B. Derin: *Permian - early Mesozoic tectonism and continental margin formation in Israel and its implications for the history of the Eastern Mediterranean.* In Dixon, J.E. and A.H.F. Robertson (eds.): *The Geological Evolution of the Eastern Mediterranean*, Geological Society Special Publications, pp. 87–201. Blackwell, Oxford, 1984.

[80] Gat, J.R.: *Oxygen and hydrogen isotopes in the hydrologic cycle.* Annual Review of Earth and Planetary Sciences, 24(1):225–262, 1996.

[81] Gat, J.R., E. Mazor, and Y. Tzur: *The stable isotope composition of mineral waters in the Jordan Rift Valley, Israel.* Journal of Hydrology, 7(3):334–352, 1969.

[82] Gavrieli, I., A. Burg, and J. Guttman: *Transition from confined to phreatic conditions as the factor controlling salinization and change in redox state, Upper sub-aquifer of Judea Group.* Hydrogeology Journal, 10:483–494, 2002. groundwater, salinization, israel, kefar uriyya, wells, judea group, israel, deep.

[83] Gavrieli, I., Y. Yechieli, L. Halicz, B. Spiro, A. Bein, and D. Efron: *The sulfur system in anoxic subsurface brines and its implication in brine evolutionary pathways: the Ca-chloride brines in the Dead Sea area.* Earth and Planetary Science Letters, 186:199–213, 2001.

[84] Gerke, H. and M. van Genuchten: *A dual-porosity model for simulating the preferential movement of water and solutes in structured porous media.* WATER RESOURCES RESEARCH, 29(2):305–319, 1993.

[85] Gerke, H.H. and M.T. van Genuchten: *Evaluation of a First-Order Water Transfer Term for Variably Saturated Dual-Porosity Flow Models.* WATER RESOURCES RESEARCH, 29(4):1225–1238, 1993.

[86] Geyer, T., S. Birk, R. Liedl, and M. Sauter: *Quantification of temporal distribution of recharge in karst systems from spring hydrographs.* Journal of Hydrology, 348(3-4):452 – 463, 2008.

[87] Goff, J.A. and S. Gratch: *Low-pressure properties of water from -160 to 212 F.* In *Proceedings of the 52nd annual meeting of the American society of heating and ventilating engineers*, Transactions of the American Society of Heating and Ventilating Engineers, pp. 95–122, New York, 1946. American Society of Heating and Ventilating Engineers.

[88] Golani, A.: *Water resources in the Jericho area (in Hebrew).* Report HR/72/016, Tahal Consulting Engineers Ltd., Tel Aviv, Israel, 1972.

[89] Goldreich, Y.: *The spatial distribution of annual rainfall in Israel — a review.* Theoretical and Applied Climatology, 50:45–59, 1994. 10.1007/BF00864902.

[90] Gonfiantini, R.: *Environmental isotopes in lake studies.* In Fritz, P. and J.C. Fontes (eds.): *Handbook of Environmental Isotope Geochemistry*, vol. 2, pp. 113–168. Elsevier, Amsterdam, 1986.

[91] Gooddy, D.C., W.G. Darling, C. Abesser, and D.J. Lapworth: *Using chlorofluorocarbons (CFCs) and sulphur hexafluoride (SF6) to characterise groundwater movement and residence time in a lowland Chalk catchment.* Journal of Hydrology, 330:44–52, 2006.

[92] Guttman, J.: *Multi-Lateral Project - Project 02WT9719 within the framework of the German-Israeli-Jordanian-Palestinian Joint Research Program for the Sustainable Utilization of Aquifer Systems, Final Report 1997-2000, Sub Project B: Hydrogeology of the Eastern Aquifer in the Judea Hills and Jordan Valley.* internal report 468, Mekorot Israel National Water Co., 2000.

[93] Guttman, J. and L. Kronbuter: *The southern coastal plain of the Carmel-affects of increasing exploitation upon local flow regime (in Hebrew).* Report 1291, Mekorot Ltd., Tel-Aviv, 2007.

[94] Guttman, J. and J. Kronfeld: *Tracing interaquifer connections in the Kfar Uriyya-Agur region (Israel), using natural uranium isotopes.* Journal of Hydrology, 55:145–150, 1982.

[95] Guttman, J. and H. Zukerman: *Yarqon-Taninim – Beer Sheva groundwater basin: setting and calibrating flow model (in Hebrew).* Report 01/95/72, Tahal Ltd., Tel Aviv, 1995.

[96] Gvirtzman, G. and G. Steinitz: *The Asher Volcanics - an Early Jurassic event in Northern Israel.* Geological Servey of Israel Current Research 1982, 3:28–33, 1983.

[97] Gvirtzman, G. and T. Weissbrod: *The Hercynian Geanticline of Helez and the Late Paleozoic history of the Levant.* In Dixon, J. and A. Robertson (eds.): *The Geological Evolution of the Eastern Mediterranean*, vol. 17 of *Geological Society Special Publications*, p. 177–186. Blackwell, Oxford, 1985.

[98] Gvirtzman, H.: *Israel Water Resources, Chapters in Hydrology and Environmental Sciences (in Hebrew).* Yad Ben-Zvi Press, Jerusalem, 2002.

[99] Hasan, J.A.: *Nature and the Origin of Ein Feshcha Springs (NW Dead Sea).* Dissertation, Karlsruher Institut für Technologie (KIT), Universität Karlsruhe, 2009.

[100] Heaton, T. and J. Vogel: *"Excess air" in groundwater.* Journal of Hydrology, 50(1-3):201–216, 1981.

[101] Herzberg, O. and E. Mazor: *Hydrological applications of noble gases and temperature measurements in underground water systems: Examples from Israel.* Journal of Hydrology, 41(3-4):217–231, 1979.

[102] Hess, K.M., J.A. Davis, D.B. Kent, and J.A. Coston: *Multispecies reactive tracer test in an aquifer with spatially variable chemical conditions, Cape Cod, Massachusetts: Dispersive transport of bromide and nickel.* Water Resources Research, 38(8):1161–1178, 2001.

[103] Hinsby, K., A.L. Højberg, P. Engesgaard, K.H. Jensen, F. Larsen, L.N. Plummer, and E. Busenberg: *Transport and degradation of chlorofluorocarbons (CFCs) in the pyritic Rabis Creek aquifer, Denmark.* Water Resources Research, 43:W10423, 2007.

[104] Ho, D.T., P. Schlosser, W.M. Smethie, and H.J. Simpson: *Variability in Atmospheric Chlorofluorocarbons (CCl3F and CCl2F2) near a Large Urban Area: Implications for Groundwater Dating.* Environmental Science and Technology, 32(16):2377–2382, 1998.

[105] Hoefs, J.: *Stable Isotope Geochemistry.* Springer Berlin Heidelberg, 4th ed., 1997.

[106] Holocher, J., F. Peeters, W. Aeschbach-Hertig, M. Hofer, M. Brennwald, W. Kinzelbach, and R. Kipfer: *Experimental investigations on the formation of excess air in quasi-saturated porous media.* Geochimica et Cosmochimica Acta, 66(23):4103 – 4117, 2002.

[107] Holocher, J., F. Peeters, W. Aeschbach-Hertig, W. Kinzelbach, and R. Kipfer: *Kinetic Model of Gas Bubble Dissolution in Groundwater and Its Implications for the Dissolved Gas Composition.* Environmental Science & Technology, 37(7):1337–1343, 2003.

[108] IFAD: *Modernizing an ancient oasis - Jericho's Ain Al-Sultan spring project*, 2007. `http://www.ruralpovertyportal.org/english/regions/asia/pse/voices/oasis.htm`.

[109] International Atomic Energy Agency/World Meteorological Organisation: *The GNIP database*, 2005. `http://isohis.iaea.org`.

[110] Issar, A.S.: *Recharge and salination processes in the carbonate aquifers in Israel.* Environmental Geology, 21(3):152–159, June 1993.

[111] Japan International Cooperation Agency, JICA: *The feasibility study on water resources and management in the Jordan River Rift Valley - Final Report - Volume I, Main Report.* Report, Ministry of Agriculture and Palestinian Water Authority and Palestinian National Authority, December 2008.

[112] Kafri, U. and M. Goldman: *The use of the time domain electromagnetic (TDEM) method to delineate saline groundwater in granular and carbonate aquifers and to evaluate their porosity.* Journal of Applied Geophysics, 57(3):167–178, 2005.

[113] Kahle, C.F.: *Strontium in oolitic limestones.* Journal of Sedimentary Research, 35(4):846–856, December 1965.

[114] Katz, A. and N. Kolodny: *Hypersaline diagenesis and evolution in the Dead Sea-Lake Lisan system (Israel).* Geochimica et Cosmochimica Acta, 53(1):59–67, January 1989.

[115] Katz, A., Y. Kolodny, and A. Nissenbaum: *The geochemical evolution of the Pleistocene Lake Lisan-Dead Sea system.* Geochimica et Cosmochimica Acta, 41:1609–1611, 1977.

[116] Kaufman, A.: *U-series dating of the Dead Sea Basin carbonates.* Geochimica et Cosmochimica Acta, 35:1269–1281, 1971.

[117] Kaufman, A., M. Bar-Matthews, A. Ayalon, and I. Carmi: *The vadose flow above Soreq Cave, Israel: a tritium study of the cave waters.* Journal of Hydrology, 273(1-4):155–163, 2003.

[118] Kaufman, S. and W.F. Libby: *The Natural Distribution of Tritium.* Physical Reviews, 93(6):1337–1344, Mar. 1954.

[119] Kawaguchi, T. and A.W. Decho: *A laboratory investigation of cyanobacterial extracellular polymeric secretions (EPS) in influencing CaCO3 polymorphism. – Journal of Crystal Growth.* Journal of Crystal Growth, 240:230–235, 2002.

[120] Khayat, S., H. Hötzl, S. Geyer, and W. Ali: *Hydrochemical investigation of water from the Pleistocene wells and springs, Jericho area, Palestine.* Hydrogeology Journal, 14(1-2):192–202, January 2006.

[121] Khayat, S.K.: *Hydrochemistry and Isotope Hydrogeology in the Jericho Area/ Palestine.* Dissertation, University of Karlsruhe, Germany, Nablus, Palestine, December 2005.

[122] Kirshenbaum, I.: *Physical properties and analysis of heavy water*, vol. III of *National nuclear energy series.* McGraw-Hill, New York, London, 1951.

[123] Klein-BenDavid, O., E. Sass, and A. Katz: *The evolution of marine evaporitic brines in inland basins: The Jordan-Dead Sea Rift valley.* Geochimica et Cosmochimica Acta, 68(8):1763–1775, April 2004.

[124] Kolodny, Y., M. Stein, and M. Machlus: *Sea-rain-lake relation in the Last Glacial East Mediterranean revealed by $\delta^{18}O$-$\delta^{13}C$ in Lake Lisan aragonites.* Geochimica et Cosmochimica Acta, 69:4045–4060, 2005.

[125] Kroitoru, L.: *The characterisation of flow systems in carbonate rocks defined by ground waterparameters: Central Israel.* PhD thesis, Feinberg Graduate School of the Weizman Institute, 1987.

[126] Kroitoru, L., I. Carmi, and E. Mazor: *Groundwater ^{14}C activity as affected by initial water-rock interactions in the Judean Mointains, Israel.* Chemical Geology, 79:259–274, 1989. groundwater, wells, deep, israel, judea group, judean mountains, 14C,

13C, T, isotopes, radio, stable, noble gases, Ein Karem, Eshtaol, Modi'im, mass balance, 14C-initial activity, Weizmann, Rehovot, karst.

[127] Kroitoru, L., E. Mazor, and D. Gilad: *Hydrological characteristics of the Wadi Kelt and Elisha spring.* In IAHS (ed.): *Scientific Basis for Water Resources Management — Proceedings of the Jerusalem IAHS Symposium, September 1985*, vol. 153 of *IAHS Publications*, pp. 207–218. IAHS, 1985.

[128] Kronfeld, J., J.C. Vogel, and A. Rosenthal: *Natural isotopes and water stratification in the Judea Group aquifer (Judean Desert).* Isr. J. Earth Sci., 39:71–76, 1992.

[129] Kuss, J. and M. Bachmann: *Cretaceous paleogeography of the Sinai peninsula and neighbouring areas.* Comptes Rendus de l'Académie des Sciences, Serie IIa, Sciences de la Terre et des Planetes, 322:915–933, 1996.

[130] Landmann, G., G.M.A. Qudaira, K. Shawabkeh, V. Wrede, and S. Kempe: *Geochemistry of the Lisan and Damya Formations in Jordan, and implications for paleoclimate.* Quaternary International, 89:45–57, 2002.

[131] Lang, U.: *Simulation regionaler Strömungs- und Transportvorgänge in Karstaquiferen mit Hilfe des Doppelkontinuum-Ansatzes: Methodenentwicklung und Parameterstudie.* Dissertation, Institut für Wasserbau, Universität Stuttgart, 1995.

[132] Lange, T., T. Graf, and M. Sauter: *Parameter sensitivies for helium-4 accumulation in groundwater due to in-situ production in dual porosity aquifers.* In Union, E.G. (ed.): *Geophysical Research Abstracts, EGU General Assembly 2011, Vienna*, vol. 13 of *Geophysical Research Abstracts*, pp. EGU2011–14035, 2011.

[133] Lenda, A. and A. Zuber: *Tracer dispersion in groundwater experiments.* In *Isotope Hydrology*, pp. 619–641. IAEA, Vienna, 1970.

[134] Lippmann, F.: *Sedimentary carbonate minerals*, vol. 6 of *Theoretical and Experimental Studies*. Springer, Berlin, 1973.

[135] M. Beinhorn, M., J. Guttman, and O. Kolditz: *Groundwater flow and transport model of the Jericho area.* Technical report 2004-30, Center for Applied Geosciences, University of Tübingen, 2004.

[136] Mallet, J.L.L.: *Geomodeling.* Applied geostatics series. Oxford University Press, Inc., New York, NY, USA, 2002.

[137] Maloszewski, P. and A. Zuber: *Determining the turnover time of groundwater systems with the aid of environmental tracers : 1. Models and their applicability.* Journal of Hydrology, 57(3-4):207 – 231, 1982.

[138] Maloszewski, P. and A. Zuber: *Tracer experiments in fractured rocks: Matrix diffusion and the validity of models.* Water Resources Research, 29(8):2723–2735, 1993.

[139] Mamyrin, B.A. and I.N. Tolstikhin: *Helium Isotopes in Nature*, vol. 3 of *Developments in Geochemistry*. Elsevier, Amsterdam, 1984.

[140] Mandell, A.H., D.G. Zeiton, and G. Dagan: *Salinity sources of Kefar Uria wells in te Judea group aquifer of Israel. Part 2 - quantitative identification model*. Journal of Hydrology, 270:39–48, 2003.

[141] Marie, A. and A. Vengosh: *Sources of Salinity in Ground Water from Jericho Area, Jordan Valley*. Ground Water, 39(2):240–248, March 2001.

[142] Mariner, P.E., M. Jin, J.E. Studer, and G.A. Pope: *The First Vadose Zone Partitioning Interwell Tracer Test for Nonaqueous Phase Liquid and Water Residual*. Environmental Science & Technology, 33(16):2825–2828, 1999.

[143] Mazor, E.: *Paleotemperatures and other hydrological parameters deduced from noble gases dissolved in groundwaters; Jordan Rift Valley*. Geochimica et Cosmochimica Acta, 36:1321–1336, 1972.

[144] McCulloch, A., P. Midgley, and D. Fisher: *Distribution of emissions of chlorofluorocarbons (CFCs) 11, 12, 113, 114 and 115 among reporting and non-reporting countries in 1986*. Atmospheric Environment, 28(16):2567 – 2582, 1994, ISSN 1352-2310.

[145] McLaren, R.G.: *Grid Builder - A pre-processor for 2D, triangular element, finite-element programs*. University of Waterloo, Groundwater Simulation Group, April 2009.

[146] Millington, R.J. and J.P. Quirk: *Permeability of porous solids*. Transactions of the Faraday Society, 57:1200–1206, 1961.

[147] Mohrlock, U.: *Parameter-Identifikation in Doppel-Kontinuum-Modellen am Beispiel von Karstaquiferen*. No. 31 in *Tübinger Geowissenschaftliche Arbeiten (TGA), Reihe C*. Institut und Museum für Geologie und Paläontologie der Universität Tübingen, 1996.

[148] Molina, M.J. and F.S. Rowland: *Stratospheric sink for chlorofluoromethanes: chlorine atomc-atalysed destruction of ozone*. Nature, 249:810–812, 1974.

[149] Mortvedt, J.J. and J. Beaton: *Heavy metal and radionuclide contaminants in phosphate fertilizers*. In Tiessen, H. (ed.): *Phosphorus in the global environment: transfer, cycles and management*, pp. 93–106. Wiley, New York, 1995.

[150] Moustafa, A. and M. Khalil: *The geology of Egypt*, ch. Geology of selected areas: Structural characteristics and tectonic evolution of north Sinai fold belts, pp. 381–392. Rotterdam, 1990.

[151] Neupauer, R.M. and J.L. Wilson: *Numerical Implementation of a Backward Probabilistic Model of Ground Water Contamination*. Ground Water, 42(2):175–189, 2004.

[152] Niemann, H.B., S.K. Atreya, G.R. Carignan, T.M. Donahue, J.A. Habermann, D.N. Harpold, R.E. Hartle, D.M. Hunten, W.T. Kasprzak, P.R. Mahaffy, T.C. Owen, N.W. Spencer, and S.H. Way: *The Galileo probe mass spectrometer: Composition of Juptiter's atmosphere.* Science, 272:846–855, 1996.

[153] Nir, A.: *On the Interpretation of Tritium 'Age' Measurements of Groundwater.* Journal of Geophysical Research, 69(12):2589–2595, June 1964.

[154] NOAA Earth System Research Laboratory, March 2011. `http://www.esrl.noaa.gov/gmd/hats/insitu/cats/`.

[155] Nottebohm, M., T. Licha, I. Ghergut, K. Nödler, and M. Sauter: *Development of Thermosensitive Tracers for Push-Pull Experiments in Geothermal Reservoir Characterization.* In *Proceedings World Geothermal Congress 2010 Bali, Indonesia, 25-29 April 2010*, 2010.

[156] Osenbrück, K., S. Stadler, J. Sültenfuß, A.O. Suckow, and S.M. Weise: *Impact of recharge variations on water quality as indicated by excess air in groundwater of the Kalahari, Botswana.* Geochimica et Cosmochimica Acta, 73(4):911–922, 2009.

[157] Oster, H.: *Datierung von Grundwasser mittels FCKW:Voraussetzungen, Möglichkeiten und Grenzen.* Dissertation, Institut für Umweltphysik, Universität Heidelberg, 1994.

[158] Oster, H., C. Sonntag, and K.O. Münnich: *Groundwater Age Dating with Chlorofluorocarbons.* Water Resources Research, 32(10):2989–3001, 1996.

[159] Ozima, M. and F. Podosek: *Noble gas geochemistry.* Cambridge University Press, Cambridge, 2nd ed., 2002.

[160] Palestinian Authority and Palestinian Water Authority: *Summary of Palestinian Hydrologic Data, Volume 1: West Bank.* Data compilation report, Palestinian Authority, Palestinian Water Authority, 2000.

[161] Palestinian Hydrology Group and Mairie de Paris: *Master plan report.* 2011.

[162] Peeters, F., U. Beyerle, W. Aeschbach-Hertig, J. Holocher, M.S. Brennwald, and R. Kipfer: *Improving noble gas based paleoclimate reconstruction and groundwater dating using* ^{20}Ne/^{22}Ne *ratios.* Geochimica et Cosmochimica Acta, 67(4):587–600, 2002.

[163] Pérez, A., A. Luzón, A.C. Roc, A.R. Soria, M.J. Mayayo, and J.A. Sánchez: *Sedimentary facies distribution and genesis of a recent carbonate-rich saline lake: Gallocanta Lake, Iberian Chain, NE Spain.* Sedimentary Geology, 148:185–202, 2002.

[164] Poage, M.A. and C.P. Chamberlain: *Empirical Relationships Between Elevation and the Stable Isotope Composition of Precipitation and Surface Waters: Considerations for Studies of Paleoelevation Change.* American Journal of Science, 301(1):1–15, 2001.

[165] Pruess, K.: *Numerical simulation of multiphase tracer transport in fractured geothermal reservoirs.* Geothermics, 31(4):475–499, 2002.

[166] Qannam, Z., B. Merkel, and T. Lange: *Herodion-Beit Fajjar well field of high quality and resource-productivity groundwater endangered by severe over-pumpage.* In Zereini, F. and W. Jaeschke (eds.): *Water in the Middle East and in North Africa – resources, protection and management*, pp. 75–86. Springer Verlag, Berlin, 2004.

[167] Quennel, A.: *The structure and evolution of the Dead Sea rift.* Quarternary Journal of the Geological Society, 64:1–24, 1958.

[168] Quennel, A.: *The Western Arabia rift system.* In Dixon, J. and A. Robertson (eds.): *The Geological Evolution of the Eastern Mediterrean*, pp. 775–788. The Geological Society, London, 1984.

[169] Rayleigh, J.W.S.: *Theoretical considerations respecting the separation of gases by diffusion and similar processes.* Philosophical Magazine, 42:493–593, 1896.

[170] Reches, Z., D. Hoexter, and F.Hirsch: *The structure of a monocline in the Syrian Arc system, Middle East - surface and subsurface analysis.* Journal of Petroleum Geology, 3:413–425, 1981.

[171] Richter, J. and P. Szymczak: *MULTIS: Ein Computerprogramm zur Auswertung isotopenhydrologischer Daten auf Grundlage gekoppelter konzeptioneller Boxmodelle.* TU Freiberg, Lehrstuhl für Hydrogeologie.

[172] Richter, J., P. Szymczak, T. Abraham, and H. Jordan: *Use of combinations of lumped parameter models to interpret groundwater isotopic data.* Journal of Contaminant Hydrology, 14:1–13, 1993.

[173] Risi, C., S. Bony, and F. Vimeux: *Influence of convective processes on the isotopic composition ($\delta^{18}O$ and δD) of precipitation and water vapor in the tropics: 2. Physical interpretation of the amount effect.* Journal of Geophysical Research, 113:D19306, 12 pp., 2008.

[174] Rivadeneyra, M.A., G. Delgado, A. Ramos-Cormenzana, and R. Delgado: *Biomineralization of carbonates by Halomonas eurihalina in solid and liquid media with different salinities: crystal formation sequence.* Research in Microbiology, 149:277–287, 1998.

[175] Robertson, A.: *Mesozoic-Tertiary tectonic-sedimentary evolution of a south Tethyan ocean basin and its margins in southern Turkey.* In Bozkurt, E., J. Winchester, and J. Piper (eds.): *Geological Society Special Publication – Tectonics and Magmatism in Turkey and the Surrounding Area*, pp. 177–186. The Geological Society, London, 2000.

[176] Roether, W.: *Estimating the tritium input to groundwater from wine samples: groundwater and direct runoff contribution to central European surface waters.* In IAEA (ed.): *Isotopes in Hydrology (Proc. Symp. Vienna, 1966)*, pp. 73–91, Vienna, 1967. IAEA, IAEA.

[177] Rofe and Raffety: *Jerusalem District water supply, Geological and Hydrological Report.* Unpublished report, Hashemite Kingdom of Jordan Central Water Authority, 1963.

[178] Roth, I.: *The geology map of israel 1:50000, sheet 12: Wadi qilt.* Techn. rep., Geological Survey of Israel.

[179] Roth, I.: *The geology of the Wadi Qilt region (in Hebrew).* Master of science thesis, Hebrew University, 1969.

[180] Salameh, E.: *Sources of Water Salinities in the Jordan Valley Area/Jordan.* Acta hydrochimica et hydrobiologica, 29(6-7):329–362, 2001.

[181] Sandler, A.: *A Turonian Subarial Event in Israel: Karst, Sandstone and Pedogenesis.* Geological Survey of Israel Bulletin, (85):1–52, 1996.

[182] Sauter, M.: *Quantification and forecasting of regional groundwater flow and transport in a karst aquifer (Gallusquelle, Malm, SW. Germany).* No. 13 in *Tübinger Geowissenschaftliche Arbeiten (TGA), Reihe C.* Institut und Museum für Geologie und Paläontologie der Universität Tübingen, 1992.

[183] Sebol, L., W. Robertson, E. Busenberg, L. Plummer, M. Ryan, and S. Schiff: *Evidence of CFC degradation in groundwater under pyrite-oxidizing conditions.* Journal of Hydrology, 347(1-2):1 – 12, 2007.

[184] Sengör, A. and Y. Yilmaz: *Tethyan evolution of Turkey: A plate tectonic approach.* Tectonophysics, 75(3-4):181–241, June 1981.

[185] Shadeed, S.: *Up to date hydrological modeling in arid and semi-arid catchment, the case of Faria catchment, West Bank, Palestine.* Dissertation, Institut für Hydrologie, Universität Freiburg, 2008.

[186] Sharon, D. and H. Kutiel: *The distribution of rainfall intensity in Israel, its regional and seasonal variations and its climatological evaluation.* International Journal of Climatology, 6(3):277–291, 1986.

[187] Singer, A.: *The Soils of Israel.* Springer Verlag, 2007.

[188] Singer, A., E. Ganor, S. Dultz, and W. Fischer: *Dust deposition over the Dead Sea.* Journal of Arid Environments, 53:41–59, 2003.

[189] Smith, S.P. and B.M. Kennedy: *The solubility of noble gases in water and in NaCl brine.* Geochimica et Cosmochimica Acta, 47(3):503–515, March 1983.

[190] Sneh, A., Y. Bartov, T. Weissbrod, and M. Rosensaft: *Geological Map of Israel, 1:200,000 - Sheet Judea.* Israel Geological Survey, 1998.

[191] Sonier, D.N., N.L. Duran, and G.B. Smith: *Dechlorination of trichlorofluoromethane (CFC-11) by sulfate-reducing bacteria from an aquifer contaminated with halogenated aliphatic compounds.* Applied and Environmental Microbiology, 60(2):4567–4572, 1994.

[192] Spitz, K. and J. Moreno: *A Practical Guide to Groundwater and Solute Transport Modeling.* John Wiley, New York, 1996.

[193] Starinsky, A.: *Relationship between Ca-chloride brines and sedimentary rocks in Israel.* Ph.d. thesis, Hebrew University Jerusalem, 1974.

[194] Starinsky, A. and H. Friedrichsen: *Radioactivity and noble gases along the Dead Sea rift.* Unpublished report to the German Israeli Foundation, 1997.

[195] Stein, M.: *The sedimentary and geochemical record of Neogene-Quaternary water bodies in the Dead Sea Basin – inferences for the regional paleoclimatic history.* Journal of Paleolimnology, 26:271–282, 2001.

[196] Stein, M., A. Starinsky, A. Katz, S.L. Goldstein, M. Machlus, and A. Schramm: *Strontium isotopic, chemical, and sedimentological evidence for the evolution of Lake Lisan and the Dead Sea.* Geochimica et Cosmochimica Acta, 61(18):3975–3992, 1997.

[197] Stute, M., M. Forster, H. Frischkorn, A. Serejo, J.F. Clark, P. Schlosser, W.S. Broecker, and G. Bonani: *Cooling of tropical Brazil (5 C) during the last glacial maximum.* Science, 269:379–383, 1995.

[198] Stute, M., C. Sonntag, J. Deák, and P. Schlosser: *Helium in deep circulating groundwater in the Great Hungarian Plain: Flow dynamics and crustal and mantle helium fluxes.* Geochimica et Cosmochimica Acta, 56(5):2051–2067, May 1992.

[199] Sudicky, E.A.: *The Laplace transform Galerkin technique for efficient timecontinuous solution of solute transport in double-porosity media.* Geoderma, 46:209–232, 1990.

[200] Sudicky, E.A. and R. McLaren: *The Laplace transform Galerkin technique for large-scale simulation of mass transport in discretely-fractured porous formations.* WATER RESOURCES RESEARCH, 28(2):499–415, 1992.

[201] Sültenfuß, J., M. Rhein, and W. Roether: *The Bremen Mass Spectrometric Facility for the measurement of helium isotopes, neon, and tritium in water.* Isotopes in Environmental and Health Studies, 45(2):1–13, 2009.

[202] Teutsch, G. and M. Sauter: *Groundwater modelling in karst terranes: scale effects, data provision and model validation.* In *EPA/NWWA International Syposium on Environmental Problems in Karst Terranes (Nashville, December 1991)*, pp. 17–35, 1991.

[203] Therrien, R., R.G. McLaren, E. A.Sudicky, and S.M. Panday: *HydroGeoSphere - A threedimensional numerical model describing fully-integrated subsurface and surface flow and solute transport.* Manual, Université Laval and University of Waterloo, Canada, 2010.

[204] Therrien, R. and E.A. Sudicky: *Three-dimensional analysis of variably-saturated flow and solute transport in discretely-fractured porous media.* Journal of Contaminant Hydrology, 23(1-2):1–44, 1996.

[205] Toll, M.: *An integrated approach for the investigation of unconsolidated aquifers in a brackish environment - A case study on the Jordanian side of the lower Jordan Valley.* Dissertation, Georg-August-Universität Göttingen, 2001.

[206] Toll, M.: *Hydrogeological characterization of the Uppermost Aquifer in the Wadi Qilt area.* Diploma thesis, Department of Applied Geology, Universität Tübingen, 2001.

[207] Toll, M., C. Messerschmid, J. Wolfer, H. Hötzl, W. Ali, and M. Sauter: *Uppermost aquifer in Wadi Qilt.* In Hötzl, H., P. Möller, and E. Rosenthal (eds.): *The Water of the Jordan Valley - Scarcity and Deterioration of Groundwater and its Impact on the Regional Development*, pp. 265–286. Springer Berlin, Heidelberg, 1st ed., 2009. hartkopie vorhanden.

[208] Torfstein, A., I. Gavrieli, and M. Stein: *The sources and evolution of sulfur in the hypersaline Lake Lisan (paleo-Dead Sea).* Earth and Planetary Science Letters, 236(1-2):61–77, July 2005.

[209] Unterweger, M.P., B.M. Coursey, F.J. Schima, and W.B. Mann: *Preparation and calibration of the 1978 National Bureau of Standards tritiated-water standards.* The International Journal of Applied Radiation and Isotopes, 31(10):611 – 614, 1980.

[210] Vengosh, A., A. Starinsky, Yehoshua, Kolodny, and A.R. Chivas: *Boron isotope geochemistry as a tracer for the evolution of brines and associated hot springs from the Dead Sea, Israel.* Geochimica et Cosmochimica Acta, 55(6):1689–1695, 1991.

[211] Visser, A., J.D. Schaap, H.P. Broers, and M.F. Bierkens: *Degassing of ^{3}H/^{3}He, CFCs and SF6 by denitrification: Measurements and two-phase transport simulations.* Journal of Contaminant Hydrology, 103(3-4):206 – 218, 2009.

[212] Walley, C.D.: *The Lithostratigraphy of Lebanon: A Review.* Lebanese Science Bulletin, 10(1):81–108, 1997.

[213] Wang, J.L., C.J. Chang, and Y.H. Lin: *Concentration distributions of anthropogenic halocarbons over a metropolitan area.* Chemosphere, 36(10):2391–2400, 1998.

[214] Warner, M.J. and R. Weiss: *Solubilities of chlorofluorocarbons 11 and 12 in water and seawater.* Deep Sea Research, 32(12):1485–1497, 1985.

[215] Weinberger, G., E. Rosenthal, A. Ben-Zvi, and D.G. Zeiton: *The Yarkon-Taninim groundwater basin, Israel hydrogeology: case study and critical review.* Journal of Hydrology, 161(1-4):227–255, September 1994.

[216] Weiss, R.: *The solubility of nitrogen, oxygen and argon in water and seawater.* Deep Sea Research and Oceanographic Abstracts, 17(4):721 – 735, 1970.

[217] Weiss, R.: *Carbon dioxide in water and seawater: the solubility of a non-ideal gas.* Marine Chemistry, 2(3):203 – 215, 1974.

[218] Weiss, R.F.: *Solubility of helium and neon in water and seawater.* Journal of Chemical & Engineering Data, 16(2):235–241, 1971.

[219] Weiss, R.F. and B.A. Price: *Dead Sea gas solubilities.* Earth and Planetary Science Letters, 92(1):7–10, February 1989.

[220] Weissbrod, T.: *The Late Palaeozoic geanticlines in the Near East and North Africa.* In Yugan, J. and L. Chun (eds.): *Compte Rendu 11e Congres International de Stratigraphie et de Géologie du Carbonifère (Beijing 1987)*, vol. 4, p. 334–343. Nanjing University Press, 1991.

[221] White, W.B. and E.L. White: *Groundwater flux distribution between matrix, fractures, and conduits: constraints on modeling.* Speleogenesis and Evolution of Karst Aquifers, 3(2):3, 2005.

[222] Wolfer, J.: *Hydrogeological investigatios along the Jerusalem – Jericho Transect (Wadi el Qilt) Israel/West Bank.* Master's thesis, Universität Karlsruhe, 1998.

[223] Yechieli, Y., U. Kafri, S. Wollman, V. Lyakhovsky, and R. Weinberger: *On the Relation between Steep Monoclinal Flexure Zones and Steep Hydraulic Gradients.* Ground Water, 45(noch nicht erschienen):1745–6584, May 2007. `http://dx.doi.org/10.1111/j.1745-6584.2007.00327.x`.

[224] Yechieli, Y., U. Kafri, S. Wollman, E. Shalev, and V. Lyakhovsky: *The effect of base level changes and geological structures on the location of the groundwater divide, as exhibited in the hydrological system between the Dead Sea and the Mediterranean Sea.* Journal of Hydrology, 378(3-4):218–229, Nov. 2009.

[225] Yechieli, Y., D. Ronen, B. Berkowitz, W.S. Dershowitz, and A. Hadad: *Aquifer characteristics derived from the interaction between water levels of a terminal lake (Dead Sea) and an adjacent aquifer.* Water Resources Research, 31(4):893–909, 1995.

[226] Yoshioka, S., S. Ohde, Y. Kitano, and N. Kanamori: *Behaviour of magnesium and strontium during the transformation of coral aragonite to calcite in aquatic environments.* Marine Chemistry, 18(1):35–48, February 1986.

[227] Zagana, E., M. Obeidat, C. Kuells, and P. Udluft: *Chloride, hydrochemical and isotope methods of groundwater recharge estimation in eastern Mediterranean areas: a case study in Jordan.* Hydrological Processes, 21(16):2112–2123, March 2007.

[228] Zhang, T.F. and Q. Chen: *Identification of contaminant sources in enclosed environments by inverse CFD modeling.* Indoor Air, 17(3):167–177, 2007.